N DIV. LIB.

JOURNAL OF THE Electrochemical Society

106, No. 5 May 1959

แผนกห้องสมุด กรมวิทยาศาสตร์
กระทรวงอุตสาหกรรม

LOS ALAMOS
SCIENTIFIC LABORATORY

MAY 12 1959

LIBRARIES
PROPERTY

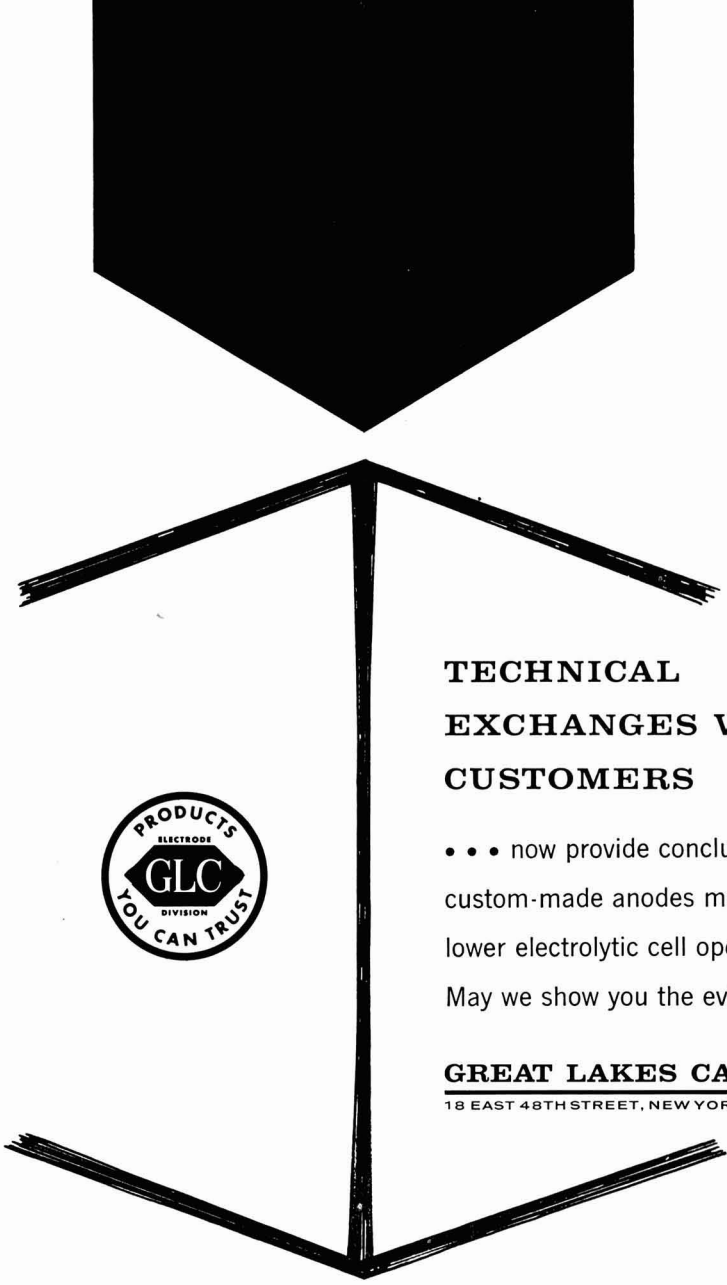

PRODUCTS ELECTRODE GLC DIVISION YOU CAN TRUST

TECHNICAL EXCHANGES WITH CUSTOMERS

• • • now provide conclusive proof that custom-made anodes materially lower electrolytic cell operating costs. May we show you the evidence?

GREAT LAKES CARBON CORPORATION

18 EAST 48TH STREET, NEW YORK 17, N.Y. OFFICES IN PRINCIPAL CITIES

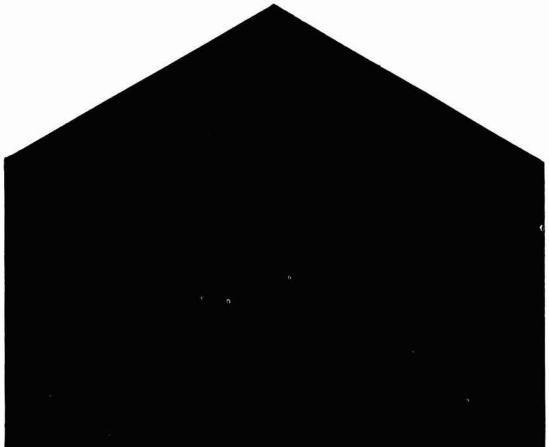

EDITORIAL STAFF

H. H. Uhlig, Chairman, Publication Committee

Cecil V. King, Editor

Norman Hackerman, Technical Editor

Ruth G. Sterns, Managing Editor

U. B. Thomas, News Editor

H. W. Salzberg, Book Review Editor

Natalie Michalski, Assistant Editor

DIVISIONAL EDITORS

W. C. Vosburgh, Battery

Milton Stern, Corrosion, I

R. T. Foley, Corrosion, II

T. D. Callinan, Electric Insulation

Seymour Senderoff, Electrodeposition

H. C. Froelich, Electronics

Ernest Paskell, Electronics—Semiconductors

Sherlock Swann, Jr., Electro-Organic, I

Stanley Wawzonek, Electro-Organic, II

John M. Blocher, Jr., Electrothermics and Metallurgy, I

A. U. Seybolt, Electrothermics and Metallurgy, II

N. J. Johnson, Industrial Electrolytic

C. W. Tobias, Theoretical Electrochemistry, I

A. J. deBethune, Theoretical Electrochemistry, II

ADVERTISING OFFICE

ECS
1860 Broadway, New York 23, N. Y.

ECS OFFICERS

Sherlock Swann, Jr., President
University of Illinois, Urbana, Ill.

W. C. Gardiner, Vice-President
Olin Mathieson Chemical Corp., Niagara Falls, N. Y.

R. A. Schaefer, Vice-President
Cleveland Graphite Bronze Div., Clevite Corp., Cleveland, Ohio

Henry B. Linford, Vice-President
Columbia University, New York, N. Y.

Lyle I. Gilbertson, Treasurer
Air Reduction Co., Murray Hill, N. J.

I. E. Campbell, Interim Secretary
National Steel Corp., Weirton, W. Va.

Robert K. Shannon, Executive Secretary
National Headquarters, The ECS, 1860 Broadway, New York 23, N. Y.

Journal of the Electrochemical Society

MAY 1959 **VOL. 106 • NO. 5**

CONTENTS

Published monthly by The Electrochemical Society, Inc., from Manchester, N. H., **Executive Offices, Editorial Office** and **Circulation Dept.,** and **Advertising Office** at 1860 Broadway, New York 23, N. Y., combining the JOURNAL and TRANSACTIONS OF THE ELECTROCHEMICAL SOCIETY. Statements and opinions given in articles and papers in the JOURNAL OF THE ELECTROCHEMICAL SOCIETY are those of the contributors, and The Electrochemical Society assumes no responsibility for them. Nondeductible subscription to members $5.00; subscription to nonmembers $18.00. Single copies $1.25 to members, $1.75 to nonmembers.

Copyright 1959 by The Electrochemical Society, Inc.

Entered as second-class matter at the Post Office at Manchester, N. H., under the act of August 24, 1912.

Keithley electrometers for every dc laboratory test

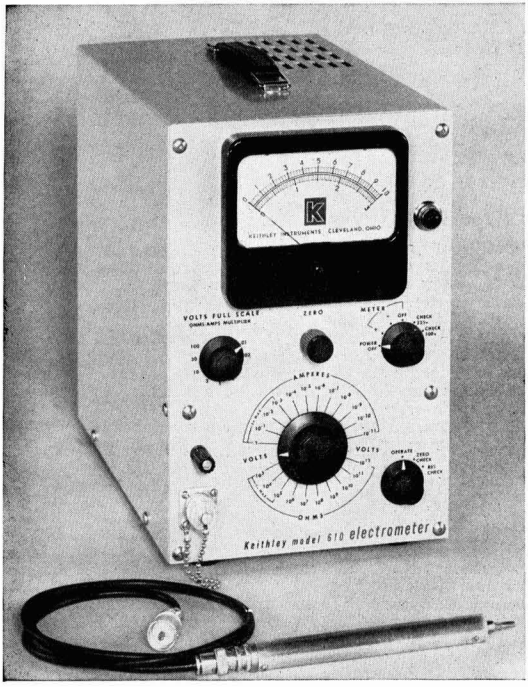

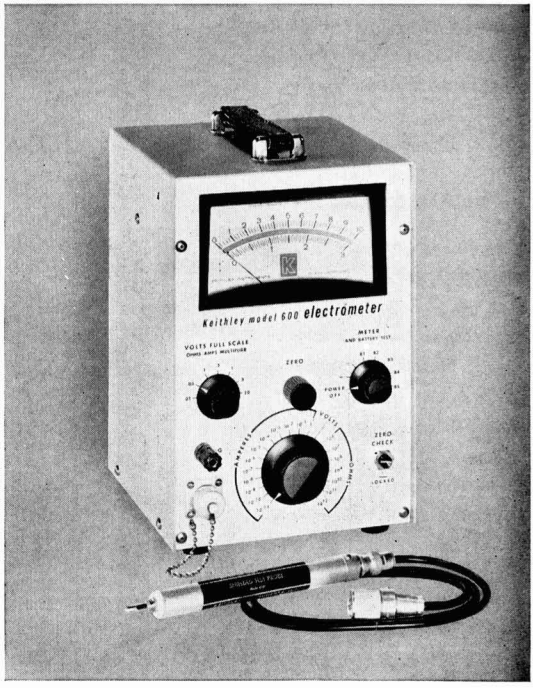

Model 610, line-operated, 59 ranges

The Keithley 610 Electrometer is a laboratory workhorse, doing the work of several instruments. It covers the extreme spans of dc voltage, current, and resistance tabulated below, and is a useful preamplifier as well. It has precise gains to 1000, a dc to 500 cps bandwidth, and 10-volt and 1-ma outputs. Input resistance of the 610 is selectable from one ohm to over 10^{14} ohms. It checks its own resistance and voltage supply standards. Zero drift is comfortably within 2 millivolts per hour after warmup.

Model 600, battery-operated, 53 ranges

The Model 600 is a small, portable, battery-operated sister of the 610. Its many ranges also are tabulated below. Like the 610, its input resistance may be varied from one ohm to over 10^{14} ohms, permitting an optimum balance of low circuit loading versus minimum pick-up. Output is sufficient to drive potentiometric recorders directly, with a dc to 100 cps band-width, and zero drift is within 2 millivolts per hour. The 600 will check its own batteries; minimum battery life is 500 hours.

Need a few specials?

Recent Keithley developments include instruments for the Navy's Vanguard, for Army research balloons, and for Air Force research missiles. Your special problem will receive a prompt reply.

MODEL	FULL SCALE RANGES			PRICE
	VOLTAGE	CURRENT	RESISTANCE	
610	10 mv to 100 volts	10^{-13} amp. to 3 amperes	10 ohms to 10^{14} ohms	$465.00
600	10 mv to 10 volts	10^{-13} amp. to 3 amperes	10,000 ohms to 10^{13} ohms	$380.00

THREE ACCESSORY probes are available to facilitate measurements and extend the measuring range to 30 kv (Model 610) or 10 kv (Model 600). A convenient accessory test shield permits rapid checks of small components. Write today for more details.

KEITHLEY INSTRUMENTS, INC.

12415 EUCLID AVENUE • CLEVELAND 6, OHIO

GRACE SILICON

(ultra-high-purity)

Minute instruments in the nose cones of American space explorers record vital phenomena beyond the pull of earth's gravity. The phenomena: the unknowns of outer space including bands of radiation, cosmic rays, temperatures, etc. The data recorders: complex electronic devices packed with transistors, diodes, rectifiers and other subminiature signal transmitters.

It wasn't possible ten years ago. It wouldn't be possible today if it weren't for ultra-high-purity silicon. Purity such as is produced by the Pechiney process used in the manufacture of Grace Silicon.

May we suggest that wherever silicon of top quality is required—for semiconductor devices in research, military, industrial and entertainment uses—call or write GRACE ELECTRONIC CHEMICALS, INC., PL 2-7699, 101 N. Charles Street in Baltimore.

GRACE ELECTRONIC CHEMICALS, INC.

101 N. Charles St., Baltimore, Maryland

Subsidiary of W. R. Grace & Co.

แผนกพัฒนาอุตสาหกรรม กรมวิทยาศาสตร
117C
กระทรวงอุตสาหกรรม

Editorial

Basic Research

THE definitions of Research and Development and the appraisal of research projects are important to all scientists. Much soul-searching on these matters is apparent in both popular and technical literature. With the vast expansion of "research" carried out with government funds, are we getting our money's worth? I read with a great deal of interest Dr. Hans Selye's article "What makes Basic Research Basic?" ("Adventures of the Mind 19," *Saturday Evening Post*, January 24, 1959). Dr. Selye directs the Institut de Medècine et de Chirurgie Expèrimentales, Universitè de Montrèal, Montreal, Canada, and is credited with the discovery that the human organism has innate defenses against fatigue, pain, and disease. His findings have been ranked beside those of Pasteur, Koch, and Ehrlich.

Dr. Selye defines basic research as the study of natural laws for their own sake, irrespective of *immediate* practical applicability. The kind of research designated as "basic" is true *discovery*. What follows is *development*. Basic research appears impractical and the work haphazard because original observations cannot be planned in advance. Most of the complete new leads are accidental discoveries made by men with the rare talent of noticing the totally unexpected.

There is an important difference between observing and discovering. The Indians and the Vikings saw America but Christopher Columbus discovered it for the benefit of mankind. A German physiologist had produced diabetes in dogs by removing their pancreas in 1889 but he did not realize that the disease resulted from a lack of pancreatic insulin. Banting and his co-workers extracted insulin and showed that it would cure diabetes, thus applying his observations to the use of mankind. This is discovery.

A great need is to be able to distinguish between greater and lesser research projects. The distinction is immensely important to both the investigator and the organization supporting the research. The future welfare of humanity depends on the recognition of first-rate basic research in its earliest stages.

Dr. Selye offers three criteria for great basic discoveries: (a) They are true not only as facts but in the way that they are interpreted; (b) they are generalizable; (c) they are surprising in the light of what was known at the time of discovery. All of these characteristics are illustrated by the observation by Alexander Fleming that penicillin can kill varieties of disease-producing microbes at dose levels tolerated by man. This is true not only in the fact itself but by the inference that penicillin can cure an infection. It is generalizable since other investigators have derived other useful drugs from mold. It was surprising that molds could have curative value since they are generally regarded as contaminators.

The basic scientist must have a peculiar type of intuition. He must be able to look at "self-evident facts" without necessarily accepting them, and let his imagination play with most unlikely possibilities. He requires serendipity, the gift of finding unsought treasures. He must have the power of abstract thinking and be able to dream and have persistence or faith in his dream to make it come true. Yet he must have the proper balance between these qualities. He must have faith in his dream and yet continue his experiments. He is obviously a unique person. His work is hard to recognize and support. An enviable accomplishment is to recognize him early and to be able to support him in the proper atmosphere for carrying on his research.

Dr. Selye has done both the public and the scientist a service.

—W. C. GARDINER[1]

[1] Electrochemical Society President 1959-60; Olin Mathieson Chemical Corp., Niagara Falls, N. Y.

WE'RE LEARNING WHY TWO EARS ARE BETTER THAN ONE

Which speaker is making the sound? In echoless chamber at Bell Labs, Robert Hanson measures test subject's ability to localize sounds – observes how two ears operate in partnership. This and other tests may point the way to better telephone instruments.

In listening to stereophonic music, how is it that our ears and brain construct a picture of the entire orchestra with but two samples (the sounds from two speakers) to work with?

How is it that our ears and brain are able to pinpoint *one* voice in a roomful of talkers—to listen to it alone and ignore the rest?

What makes *two* ears better than one?

Bell Telephone Laboratories scientists are searching for the answers. For in finding them, better telephone instruments and better ways of transmitting sound will surely result.

Our hearing performs feats that no electronic system can yet duplicate. How? Laboratories scientists believe the secret lies in the way our two ears function in partnership and in the way our neural network connects them with our brain. *The problem:* to discover what functions the network performs and to see whether electronic duplication might enhance understanding.

The work is under way. Electronic circuits that simulate the operation of nerve cells have already been created—and conceptual models of the neural network are being constructed.

Alexander Graham Bell's interest in deafness and hearing led to the invention of the telephone. Bell Laboratories' current explorations in binaural sound may well lead to important new advances in the transmission of speech and music.

BELL TELEPHONE LABORATORIES
World center of communications research and development

GET *ALL* THE ANSWERS TO *YOUR* FINISHING PROBLEMS

at the
FIFTH INDUSTRIAL FINISHING EXPOSITION!

(Held in conjunction with the
GOLDEN JUBILEE CONVENTION
of the
AMERICAN ELECTROPLATERS' SOCIETY)

The finishing experts will all be under one roof next June. In Detroit, at the Detroit Artillery Armory, from June 15 to 19, at the Fifth Industrial Finishing Exposition!

Take your problems to them. Get expert help . . . at the largest display of finishing equipment, materials and processes ever assembled under one roof.

Make a list of your plating problems. Take it to Detroit with you. See the men who man the booths. The experts with professional, up-to-date help for you. They'll be there to demonstrate the right way to solve your problems.

If you want more information on the Fifth Industrial Finishing Exposition *now*, ask the exposition chairman: ● ● ● ● ● ● ● ● ●

HOWARD J. McALEER
3171 BELLEVUE AVE.
DETROIT 7, MICHIGAN

Precision-formed Sylvania ingots yield more single-crystal Germanium...

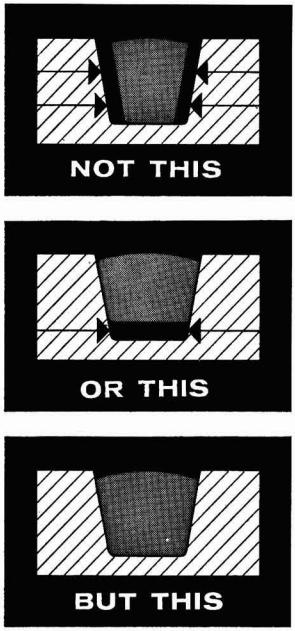

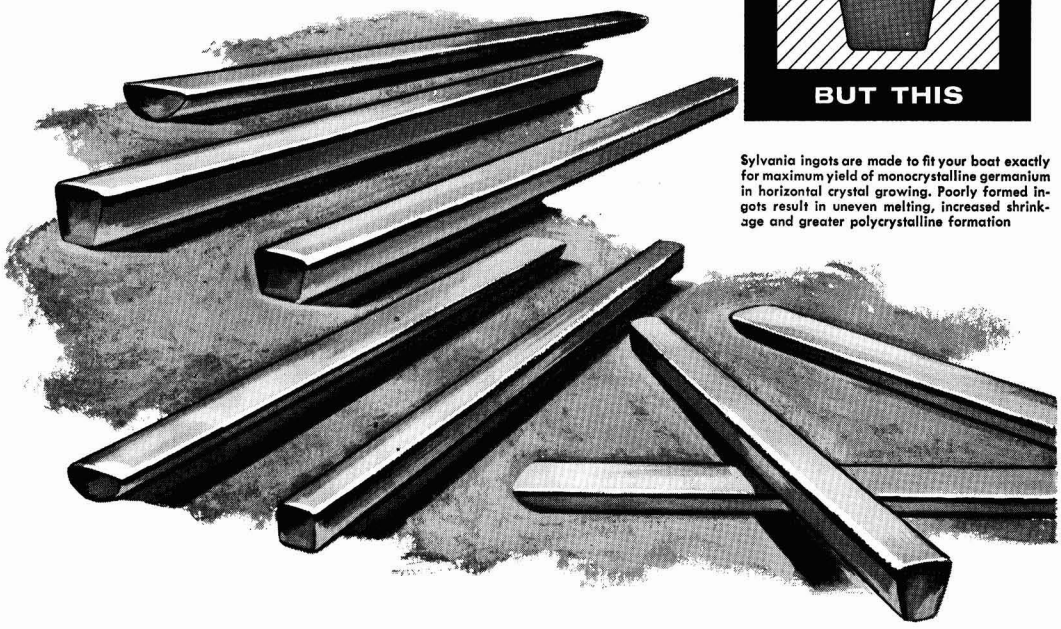

Sylvania ingots are made to fit your boat exactly for maximum yield of monocrystalline germanium in horizontal crystal growing. Poorly formed ingots result in uneven melting, increased shrinkage and greater polycrystalline formation

SEMICONDUCTOR device manufacturers can rely on a greater yield of monocrystalline germanium when they specify Sylvania ingots. The size and shape of Sylvania ingots are held to tolerances within 0.005 inch on base and radius dimensions, 0.1 inch on height, and ½ degree on taper. As a result a Sylvania ingot will fit your horizontal crystal growing boat precisely, and deter polycrystalline formation. Melting is even, surface drop is held to a minimum and shrinkage is reduced. You get a greater yield of doped single crystals and lower unit costs.

Sylvania germanium ingots are available in any one of seven standard cross sections or in designs made to your specifications. Whatever form you specify, you can count on a maximum yield from Sylvania germanium ingots. Contact your Sylvania representative for further information on precision-formed germanium or write the Chemical and Metallurgical Division directly.

SYLVANIA

Subsidiary of
GENERAL TELEPHONE & ELECTRONICS

GENERAL SYSTEM

SYLVANIA ELECTRIC PRODUCTS INC.
Chemical & Metallurgical Div.
Towanda, Penna.

FUTURE MEETINGS OF
The Electrochemical Society

Philadelphia, Pa., May 3, 4, 5, 6, and 7, 1959

Headquarters at the Sheraton Hotel

Sessions will be scheduled on

Electric Insulation, Electronics (Including

Luminescence, Semiconductors, Thermionics, and Devices), Electrothermics and Metallurgy,

Industrial Electrolytics, and Theoretical Electrochemistry

★ ★ ★

Columbus, Ohio, October 18, 19, 20, 21, and 22, 1959

Headquarters at the Deshler-Hilton Hotel

Sessions probably will be scheduled on

Batteries, Corrosion (including a joint Corrosion–Electronics-Semiconductors session),

Electrodeposition (including symposia on "Electrodeposition from Organic Solvents"

and "Electro- and Chemical-Polishing"),

Electronics (Semiconductors), Electro-Organics,

and Electrothermics and Metallurgy

★ ★ ★

Chicago, Ill., May 1, 2, 3, 4, and 5, 1960

Headquarters at the Lasalle Hotel

★ ★ ★

Houston, Texas, October 9, 10, 11, 12, and 13, 1960

Headquarters at the Shamrock Hotel

★ ★ ★

Papers are now being solicited for the meeting to be held in Columbus, Ohio, October 18-22, 1959. Triplicate copies of each abstract (*not exceeding 75 words in length*) are due at Society Headquarters, 1860 Broadway, New York 23, N. Y., *not later than June 1, 1959* in order to be included in the program. *Please indicate on abstract for which Division's symposium the paper is to be scheduled, and underline the name of the author who will present the paper.* Complete manuscripts should be sent in triplicate to the Managing Editor of the JOURNAL at 1860 Broadway, New York 23, N. Y.

CHEMISTRY

Expanding the Frontiers of Space Technology

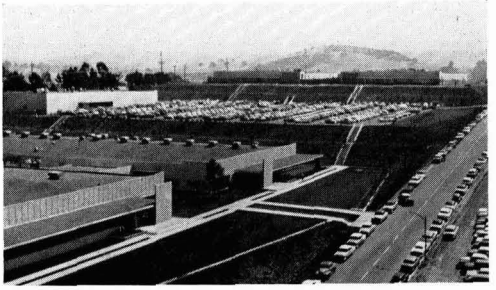

Research and Development facilities in the Stanford Industrial Park at Palo Alto, California, provide the latest in technical equipment.

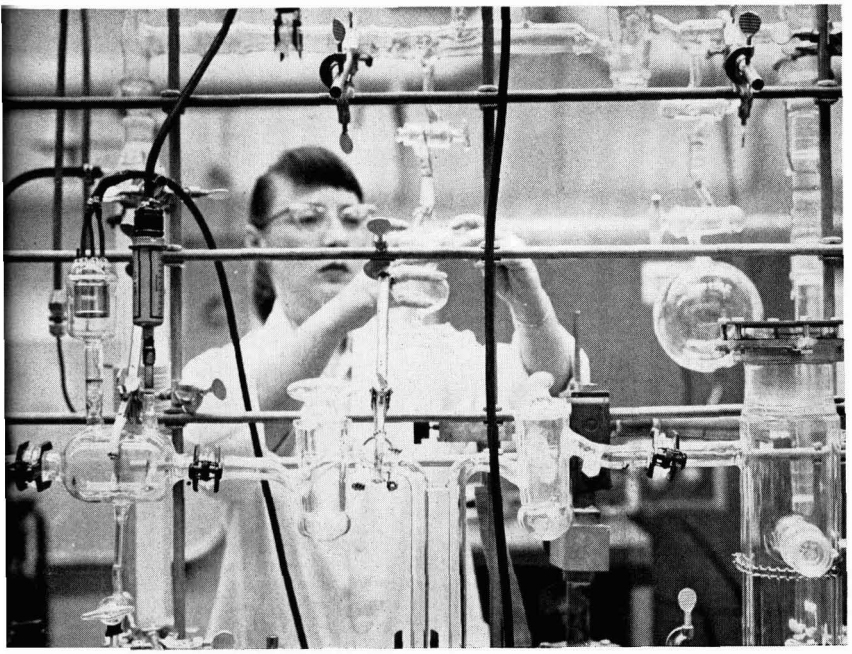

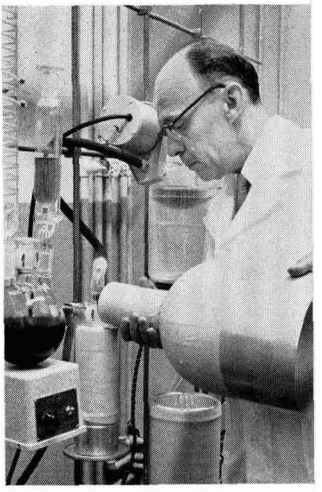

(above) Synthesizing high-energy propellant in development of new and exotic fuels in propulsion chemistry laboratory.

(left) Vacuum systems used in study of gas metal reactions at elevated temperatures – one of many studies in materials research program.

At Lockheed, chemistry plays a highly important role in materials, research, metallurgy, solid state electronics, ordnance, propulsion and test. Applications are for advanced missile, spacecraft and nuclear projects.

Special programs include: research in high and low temperature materials; radio-active and toxic materials; pure metals; properties of beryllium and the alloys and the development of refractory and special-purpose metals, cermets and ceramics.

Other chemical studies embrace reaction kinetics and thermodynamics, and the development of new and exotic fuels, high-energy batteries and fuel cells, and explosives. In electrochemistry, solid state work is directed to related fuel research in electrode reaction kinetics and materials synthesis by electrochemical methods and vacuum deposition.

The test laboratories assay raw materials, evaluate materials and components and assist in design and development.

Scientists and engineers of outstanding talent and inquiring mind are invited to join us in the nation's most interesting and challenging basic research programs. Write: Research and Development Staff, Dept. E-26, 962 W. El Camino Real, Sunnyvale, California. U.S. Citizenship required.

"The organization that contributed most in the past year to the advancement of the art of missiles and astronautics." NATIONAL MISSILE INDUSTRY CONFERENCE AWARD

Lockheed / **MISSILES AND SPACE DIVISION**

Weapons Systems Manager for Navy POLARIS FBM; DISCOVERER SATELLITE; Army KINGFISHER; Air Force Q-5 and X-7.

SUNNYVALE, PALO ALTO, VAN NUYS, SANTA CRUZ, SANTA MARIA, CALIFORNIA
CAPE CANAVERAL, FLORIDA • ALAMOGORDO, NEW MEXICO • HAWAII

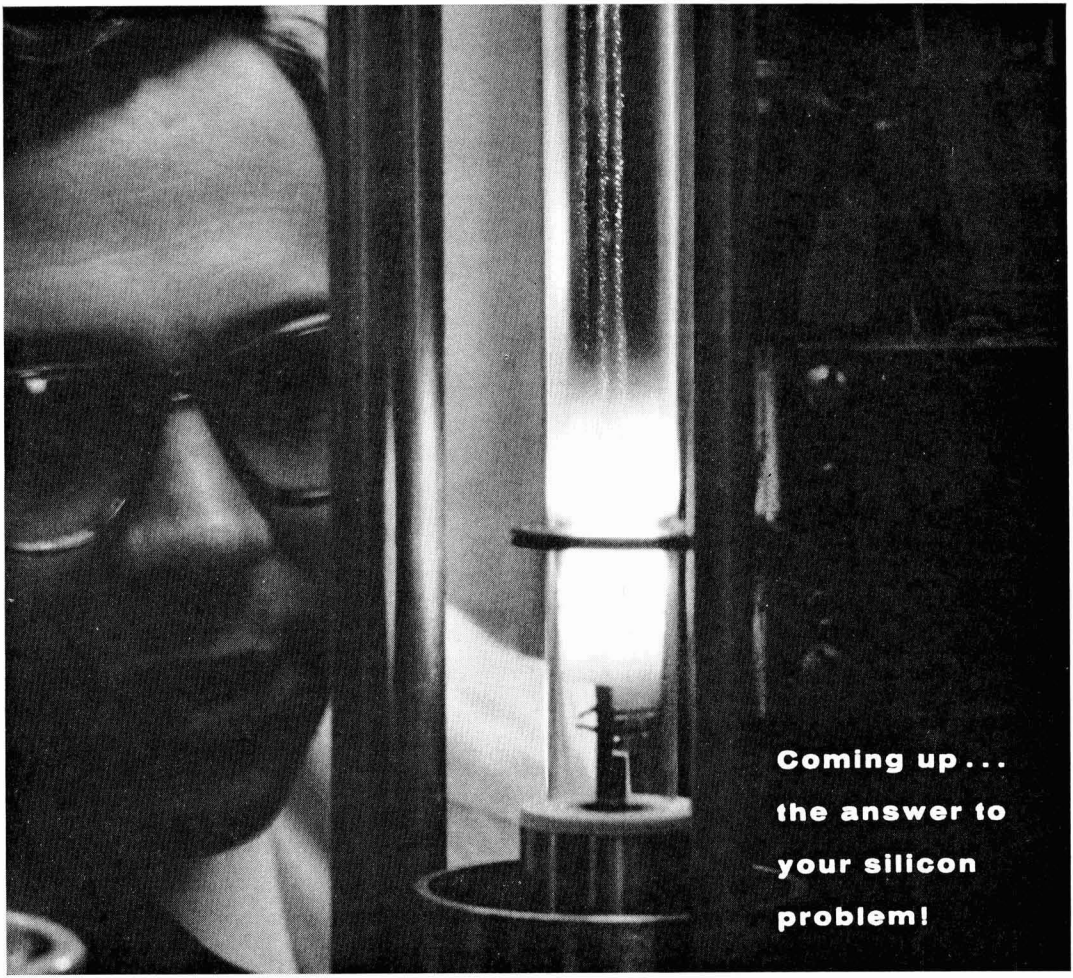

Du Pont . . . manufacturer of Hyperpure Silicon offers the services of technical specialists

When you specify Du Pont HYPERPURE Silicon, you get a product of highest dependability as well as expert technical assistance, when needed. Experienced Du Pont Technical Specialists will gladly discuss techniques of crystal growing and materials processing with you. What's more, you can take advantage of Du Pont's new $3,000,000 Technical-Service Laboratory designed for researching customer problems.

Floating zone single crystals of Du Pont HYPERPURE Silicon are available in a wide range of resistivities. Du Pont HYPERPURE Silicon is also supplied in densified cut rods . . . and rods suitable for float zone refining. They're offered in several grades with carefully controlled purity levels.

Here's more news: Du Pont's new Brevard, N. C., plant has a capacity of 70,000 lbs. of HYPERPURE Silicon per year. That means you're assured of a prompt supply of high-purity silicon in the form you need. For more information, write Du Pont . . . pioneer producer of semiconductor-grade silicon.

Free booklet is available upon request. It describes the manufacture, properties and uses of HYPERPURE Silicon. E. I. du Pont de Nemours & Co. (Inc.), Pigments Dept., Silicon Development Group, Wilmington 98, Delaware.

HYPERPURE SILICON

DU PONT
REG. U.S. PAT. OFF.

BETTER THINGS FOR BETTER LIVING
. . . *THROUGH CHEMISTRY*

The Anodic Oxides of Lead

Jeanne Burbank

U. S. Naval Research Laboratory, Washington, D. C.

ABSTRACT

The anodic oxides formed on lead under varying potential and *p*H were identified by x-ray and electron diffraction. Pure lead specimens were anodized at selected constant potentials to develop anodic coatings of sufficient thickness to give strong x-ray patterns. The domains of occurrence of: α and β PbO_2, yellow and red PbO, and the intermediate oxides, Pb_3O_4, and PbO_x were determined for acid and alkaline electrolytes. The intermediate oxides are not believed to be direct anodic oxides, but to represent chemical reaction products. The occurrence of certain of the oxides may be attributable to an initial electrochemical oxidation of water. The identifications have been presented in potential-*p*H phase diagrams.

Coincident with a study of the positive grid corrosion of the lead-acid storage cell, the anodic oxides formed on lead at various potentials in H_2SO_4 were identified by x-ray and electron diffraction (1, 2). Considered in the light of the potential-*p*H phase diagrams for the system (3), it became evident that certain aspects of the diagrams could be verified by application of diffraction techniques to anodic products formed on lead under controlled conditions of potential and *p*H. Furthermore, it was of interest to know which of the many oxides of lead occur as direct anodic products.

The potential-*p*H diagram is an isothermal phase diagram showing the various valence states of a metal, solubilities of oxides and salts, areas of thermodynamic stability of solid phases, ionic species, and their homogeneous and heterogeneous equilibria. The original presentation of the diagrams for the lead system (3) was based on available thermodynamic information. This present study was undertaken to identify the solid oxide phases appearing on lead as anodic products and to expand the usefulness of the diagrams by verification of the stable and metastable equilibria. In addition, it was desired to clarify the apparent thermodynamic anomaly of the simultaneous occurrence of the two crystallographic modifications of PbO_2 and of tetragonal PbO as anodic products on lead in acid solutions, and relate the known corrosion domains to those predicted on the basis of the diagrams.

Lead forms a number of oxides and Table I presents selected references (4-24) and the designations used in this report. An exhaustive listing has not been attempted. The hydrated lead monoxides have not been included because these materials are not well-established crystallographic identities. Bystrom (25) has presented a survey of the sterochemistry of the lead oxides.

Previous studies have indicated that the corrosion processes on the lead anode in H_2SO_4 at selected positive potentials included a group of reactions quite distinct from the reversible PbO_2, $PbSO_4$ and Pb, PbSO, electrode reactions (1, 2, 26-28). In order to clarify further the anodic corrosion reactions on lead, this detailed identification of the anodic products was undertaken.

Experimental

The anodic deposits formed on lead at controlled potential and *p*H were determined by polarizing pure lead sheet under fixed conditions and identifying the anodic products by x-ray and electron diffraction patterns taken by reflection from the anodized surfaces. The standard diffraction patterns used for identification are found in the X-ray Powder Data File (29) or in one or more of the references cited for each oxide in Table I.

The electrolytes used in this study were made from C. P. chemicals and distilled water. In the solutions near neutral limited amounts of CO_2 did not interfere with the observations. In order to check this a few experiments were carried out with freshly boiled distilled water and KOH very low in CO_2, in a closed cell. The results of these anodic tests were identical with those obtained in fresh solutions with nominal concentrations of CO_2. Fresh KOH solution was prepared for each run in which it was used. Values of reference electrode potentials were taken from the literature (30-33).

A Beckmann *p*H meter using a glass electrode, saturated calomel reference electrode, and standard buffer solutions were used to monitor the *p*H of the electrolytes. Solutions were made with C. P. reagents to approximate values and their actual *p*H's determined. Whenever feasible, the reference electrodes were used in the same solutions during anodization to eliminate liquid junctions. In sulfuric acid solutions, the electrode was Hg_2SO_4, Hg and in KOH solutions, HgO, Hg. Potentials were converted to the standard hydrogen electrode for this report.

Anodizations were carried out in glass cells, and usually only a few hours were required to develop coatings sufficiently heavy to give excellent x-ray diffraction patterns. Some specimens were anodized for longer periods of time, and as much as one week. The constant potential regulator described by Work and Wales (34) was used as the source of polarizing potential. A negative electrode of Pb or Pt gauze

Table I. Some known oxides of lead

	Formula*	Lattice	Other designations	Reaction with Acids	References
	PbO_y*	Orthorhombic	Litharge, yellow		(4, 5)
	PbO_t*	Orthorhombic-pseudotetragonal	Distorted PbO, yellow, brown, red	$PbO + 2H^+ = Pb^{++} + H_2O$	(6)
	Red PbO	Tetragonal	Massicot, red		(7, 8)
	PbO	Hexagonal	Yellow Litharge		(9)
$PbO_x \cdot xPbO_2$* or PbO_x*	Pb_3O_4*	Tetragonal	Minimum-orange Red lead	$Pb_3O_4 + 4H^+ = 2Pb^{++} + \beta PbO_2 + 2H_2O$	(6, 9-11)
	Pb_7O_{11}	Orthorhombic-pseudotetragonal	Black minium		(6, 12-17)
	Pb_2O_3		$PbO_{1.33-1.51}$ maroon to	$PbO_x + 2H^+ = Pb^{++} + \alpha PbO_2 + H_2O$	
	Pb_2O_3	Orthorhombic-pseudocubic	$PbO_{1.47-1.57}$ black	$1.33 \leqq x \leqq 1.57$	
		Monoclinic			(16, 18, 19)
	βPbO_2*	Tetragonal	Beta; $PbO_{1.87-2.02}$	Insoluble or dissolves as divalent Pb	(6, 13, 20, 21)
	αPbO_2*	Orthorhombic	Alpha; $PbO_{1.94-2.02}$		(22-24)

* Symbols used in this report.

was of such area that a constant positive polarization potential was obtained.

C. P. lead sheet to be anodized was annealed at 100°C for six weeks, cleaned of its air-formed oxide film by washing in saturated ammonium acetate solution, rinsing in water and inserting into the electrolyte while wet. Anodic polarization was begun simultaneously with insertion into the electrolyte, and the first few minutes of polarization was monitored carefully with a bench potentiometer and reference electrode to determine that the desired anodic potential was applied to the positive electrode.

At the termination of polarization, the electrode was removed from the solution, and rinsed in water, blotted dry on tissue, and placed immediately in the diffraction apparatus. The patterns were recorded as soon as possible after mounting.

GE-XRD-5 x-ray diffraction equipment was used with copper and iron targets, and electron diffraction examination was carried out with the diffraction attachment of an RCA-EMU-2 electron microscope.

In order to determine whether the two polymorphic forms of PbO_2 were readily interconvertible by crystallization from alkaline or acid media several tests were made on C. P. βPbO_2. Beta PbO_2 was dissolved in KOH solution, in concentrated HNO_3 solutions, and filtered with water aspiration. Water was added dropwise to the filtrates and, when sufficient material had hydrolyzed, it was collected on a filter and identified by x-ray diffraction examination.

C.P. βPbO_2 was treated with solid KOH and sufficient water to form a slurry. After several days' digestion at room temperature, large water-clear crystals formed up to 2 cm in diameter. These were washed free of excess PbO_2 with distilled water, and then placed in contact with a few drops of *N* KOH solution. They were slowly converted to dark brown powder which was examined by x-ray diffraction. The residual unconverted PbO_2 was also examined by diffraction.

Large clear crystals up to 6 mm in diameter formed from C.P. PbO_2 when treated with concentrated HNO_3. These were washed free of excess PbO_2, and placed in contact with dilute HNO_3 at room temperature. They were converted gradually to a brown powder that was examined by x-ray diffraction.

Essentially identical potential arrests are reported in many polarization studies of lead anodes in alkalies and only a few are cited here (35-38). Consider-

Table II. Electrolytes and anodic potentials used in this study

pH	Electrolyte Composition	Potential in volts with respect to standard hydrogen electrode — Anodic lead specimens			
−0.63	3.5*N* H_2SO_4	2.08	1.87	1.62	1.30
		2.07	1.86	1.59	1.10
		1.90	1.70	1.56	1.06
2.5	*N* $NaSO_4$	1.85	1.19	0.32	
	H_2SO_4*	1.57	1.17	0.02	
7	M K_2SO_4	1.33	1.05	1.00	
	N Na_2SO_4	1.4	1.00	0.51	
		1.20	0.80	−0.30	
12	*N*/1000 KOH	0.85	0.45	−0.41	
14.5	3*N* KOH	1.03	0.67	0.38	0.27
		0.98	0.45	0.36	−0.57
		0.85	0.43	0.33	−0.66
		Platinum anode potentials			
2.5	0.1M $Pb(NO_3)_2$	2.3	1.47	1.32	
8	0.1M $Pb(NO_3)_2$ KOH*	1.8	1.30	1.1	
14.5	3*N* KOH PbO**	1.06	0.34		

* Sufficient quantities of these reagents were added to adjust the pH to the indicated values.
** Excess solid PbO was present in the cell during electrolysis.

ation of such reports enabled judicious choice of the potentials used for the anodic treatments of this study.

Table II is a list of the electrolytes, and the potentials, employed in these anodization studies. Certain experiments were rerun many times in order that the identification should be conclusive. Certain other areas, where there seemed no possibility of question, were identified with only a few runs. The anodic products formed on lead in H_2SO_4 solutions have been reported earlier (1,2).

Some anodic coatings were laminated, and the material at the solution interface was removed by wiping the electrode with dry tissue, or by scoring around the edge of the electrode and lifting off the outer layer.

By using spot tests (39) it was possible to detect the appearance of a highly oxidizing material on the electrode surface considerably below the potentials where PbO_2 or the intermediate oxides became apparent in the x-ray diffraction patterns from specimens anodized in the strong acid range. Sheet lead specimens were anodized in H_2SO_4 solutions at carefully monitored potentials within a range ± 0.1 v to the theoretical reversible O_2,H_2O potential. After anodizations as long as 24 hr, the electrodes were removed from the electrolyte and dropped into the selected reagent: acetic acid when the benzidine test was used and starch-KI solution when this was used.

In order to verify the reported deposition of α and β PbO_2 as residues from the intermediate oxides, Pb_3O_4 and PbO_x were extracted with H_2SO_4, $NH_4C_2H_3O_2$ (saturated solution), HNO_3, and $HC_2H_3O_2$. The residues were rinsed in water, sucked dry on a filter, and the diffraction patterns recorded.

Neutral, acid and alkaline solutions of lead were electrolized between platinum electrodes. The potentials at which lead dioxide first deposited on the anode were observed, and the initial and final deposits were examined by x-ray diffraction.

αPbO_2 was heated in air at temperatures between 150° and 400° and the decomposition followed by x-ray diffraction examination of the products. The temperature range between 290°-305° was examined in steps of 2° with heating times of 48 hr. The decomposition was compared with that reported and verified for C.P. βPbO_2 (6, 13, 17).

Results and Discussion

The solid anodic products formed on lead at fixed pH and potential are divided into two categories: (a) the product of the anodic reaction at the solution interface; and (b) the product of the anodic reaction at the metal interface. These may be the same or different reactions, and there may or may not be other reactions between cell components. Thorough familiarity with the potential-pH diagram originally published (3) for the system is assumed, and this report deals mainly with the solid oxide phases associated with certain conditions of potential and pH at room temperature, but does not include solubility data.

Free energy values have been used to calculate the equilibrium potentials of this report in conformity with the original presentation of the potential-pH diagram; however, the free energy of formation of PbO_2 used by Delahay, Pourbaix, and Van Rysselberghe was only −50.86 kcal. Latimer gives a value of −52.34 kcal (40).

The domain of thermodynamic stability of metallic lead may approach that of PbO_2, and the equilibrium expected between the metal and this oxide has been calculated (28)

$$\beta PbO_2 + 4H^+ + 4e^- = Pb + 2H_2O \qquad [1]$$
$$E = 0.6775 - 0.0591\ pH$$

However, it is known that metallic lead usually tends to dissolve in the presence of PbO_2 and will be oxidized in a mixture containing excess higher oxide; or if metallic lead is in excess, the higher oxide will be discharged (41, 42). The electrochemical instability of PbO_2 in strong H_2SO_4 solutions at potentials below the reversible $PbSO_4$, PbO_2 electrode has been discussed by Lander (28). But at the potential of reaction [1], metallic lead is thermodynamically stable in the presence of PbO_2. However at this potential PbO_2 is not thermodynamically stable with respect to PbO_t or Pb^{++}. Therefore when the potential of a lead anode is raised above that of reaction [1], any formation of PbO_2 from metallic lead would tend to undergo the reaction

$$PbO_2 + 2H^+ + 2e^- = PbO_t + H_2O \qquad [2]$$
$$E = 1.107 - 0.0591\ pH$$

until the reversible potential for this reaction is exceeded. At potentials above those of reaction [1], metallic lead is unstable with respect to both PbO_t and PbO_2.

Anodic oxides at the solution interface.—It has been reported and was verified in this study that electrolysis of Pb^{++} solutions between platinum electrodes develops deposits largely of βPbO_2 from acid and αPbO_2 from alkaline solutions. Either or both polymorphs may be deposited from certain solutions depending on current density (potential) (23, 24).

Figure 1 shows the anodic oxides identified in this study at the electrode-solution interface on lead polarized in solutions of varying pH at several potentials. The lines for the oxidation of water to ozone and H_2O_2 have been added for reference. The effect of anions other than sulfate has not been indicated on the diagram; however, the corresponding salts will precipitate at the solution interface. The accumulations of solid products on the anode surfaces appear as oxides or hydrated oxides intermixed with the salts owing to depletion of the anolyte in anions.

The areas designated as PbO_y, βPbO_2, and the hydrous oxides (43) indicated on the diagram, Fig. 1, are not at thermodynamic equilibrium. Lead dissolves in solutions of pH less than 9.4 as the divalent Pb^{++} to form a saturated solution adjacent to the electrode, and when the rate of solution exceeds the rate of diffusion of anions from the bulk of the electrolyte the oxide crystallizes as a chemical deposit from this solution. The deposits designated in Fig. 1 of the hydrous oxides and the yellow glistening crystals of orthorhombic PbO_y are in this category and form normal and basic salts with anions present.

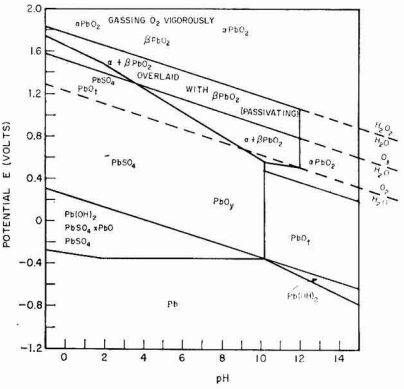

Fig. 1. Anodic oxides on lead at the solution interface. This diagram indicates the areas of occurrence of the solid oxide phases identified by x-ray and electron diffraction, and obtained on anodization of lead metal at fixed pH and potential. The lines for the following equilibria have been added

$$O_3 + 6H^+ + 6e^- = 3H_2O$$
$$E = 1.51 - 0.0591\ pH \qquad P_{O_3} = 1\ atm$$
$$H_2O_2 + 2H^+ + 2e^- = 2H_2O$$
$$E = 1.77 - 0.0591\ pH \qquad a_{H_2O_2} = 1M$$

Anions present in the electrolytes will form normal and basic salts with the lower oxides as indicated in the original potential -pH diagram of the system (3).

The open-circuit potential of the lead electrode is controlled by the amount of Pb^{++} in solution and is independent of *p*H. Above *p*H of 9.4 lead passes into solution as biplumbite ion, and the reaction has a slope 0.089 vs. *p*H. By impressing anodic potential on the system, more and more salt and oxide will be deposited unless a uniform coherent coating forms on the surface (passivation). These phenomena have been described in detail by Wolf and Bonilla for a large number of anions (44).

The crystals of PbO_y deposit in platelets shown by x-ray diffraction to be parallel to the c_o face typical of solution-grown crystals of this material. It does not form dense passivating films but grossly crystalline deposits. It is an anodic oxide in the sense that it is the solid deposited from saturated lead ion solutions.

At more elevated potentials such an electrode becomes covered with a layer of PbO_t in which the crystals of PbO_y are embedded. The domains of solubility of the two polymorphs of PbO_2 intrude into this area at higher *p*H, and a mixture of the four oxides is obtained. It is in this area that the intermediate oxides Pb_3O_4 and PbO_x as chemical reaction products will form after a time, but the electrode does not passivate. Only above the line indicated in Fig. 1 corresponding to the theoretical reversible O_3/H_2O reaction does passivation appear. The corrosion reaction of the metal surface is primarily a divalent one up to a potential corresponding to the reversible ozone reaction, while the deposition of tetravalent oxide takes place at the solution interface, resulting in a mixture of di- and tetravalent products.

In solutions of *p*H 12 and higher, a lead anode becomes covered with a deposit of hydrated lead oxide designated as $Pb(OH)_2$ in Fig. 1, and subsequently with a tetragonal oxide designated as PbO_t. If the potential is increased, plumbate ion is formed in the solution, and the surface of the electrode becomes covered with a layer of αPbO_2. There is an underlying layer of PbO_t which may react with the αPbO_2 formed at the solution interface to produce the intermediate oxides.

It may be possible to limit the deposition of αPbO_2 from alkaline solutions to a rate comparable to its chemical reaction rate with PbO_t and thereby obtain a deposit at the solution interface of the intermediate oxides, but such a condition was not observed in this work during anodization. Self-discharge may also produce such a surface. These intermediate oxides do not appear to be deposited directly from oxidation-reduction reactions, but from chemical combinations, i.e.

$$\left.\begin{aligned} PbO + PbO_2 &= Pb_2O_3 \\ 2PbO + PbO_2 &= Pb_3O_4 \end{aligned}\right\} \text{designated } PbO_t \cdot xPbO_2$$

An infinitude of stoichiometries is possible in such anodic products.

X-ray diffraction examination shows that βPbO_2 is obtained by hydrolysis of both acid and alkaline solutions of tetravalent lead ion, and is the main product deposited electrolytically from acidic Pb^{++} solutions at elevated potentials. Anodization of metallic lead, however, produces a mixture of α and βPbO_2 at elevated potentials. The anodic deposition of βPbO_2 in alkaline solutions occurs simultaneously with the evolution of O_2 gas. It therefore probably deposits by hydrolysis at the local areas on the anode where alkalinity is reduced by the gassing reaction.

Anodic oxides at the metal interface.—The x-ray and electron diffraction examination of the anodic products developed on Pb at various *p*H and potential conditions showed that the metal-coating interface exhibited the same oxides throughout the *p*H range, at the same potentials relative to the reversible hydrogen electrode in the same solutions (not the standard electrode). This means that the anodic reactions have slopes of 0.059 vs. *p*H. The solid phases identified in this study are indicated in Fig. 2.

When the potential of a lead surface exceeds the line bounding the lower extent of the area designated as $Pb(OH)_2$, a film of the solid hydrous oxide forms on the metal surface.

When the potential of a lead anode is raised above the line representing the reaction:

$$PbO_t + 2H^+ + 2e = Pb + H_2O \qquad E_o = 0.248$$

in Fig. 2, the lead becomes covered by a layer of PbO_t. This oxide has a tetragonal lattice showing a characteristic combination of sharp and diffuse lines in its diffraction patterns (6,13, 14). It is considered more reactive than either of the normal monoxides, and it appears on a lead anode in both acid and alkaline media. Katz described this as orthorhombic pseudotetragonal PbO (6). In alkaline solutions heavy coatings of this material appear yellow when wet with electrolyte, but are pale peach in color when dry and may form beautiful glossy coatings on a lead electrode. It has been described as a yellow

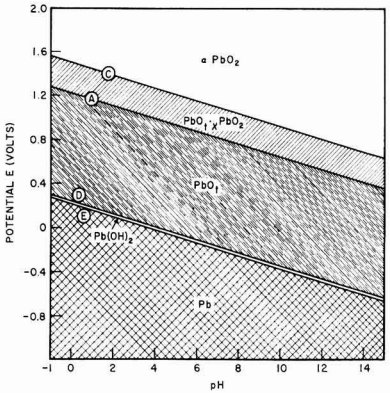

Fig. 2. Anodic oxides of lead at the metal interface. This diagram indicates the areas of occurrence of the solid oxide phases obtained at the metal-coating interface on anodization of lead at fixed potential and pH. The reactions represented by the lines D and E bounding Pb and the phases $Pb(OH)_2$ and PbO_t will be recognized from the original diagram (3), and were found to occur at essentially their reversible potentials throughout the pH range. The exception is the boundary between PbO_t and PbO_2. The intermediate region labeled $PbO \cdot xPbO_2$, representing oxides and mixtures of oxides of di- and tetravalent lead, was found to appear between the reversible oxygen and ozone potentials, lines A and C. Above line C, αPbO_2 is the principal anodic oxide at the metal interface. The reactions are represented as follows

(A) $O_2 + 4H^+ + 4e^- = 2H_2O$
$E = 1.228 - 0.0591\ pH \qquad P_{O_2} = 1\ atm$

(C) $O_3 + 6H^+ + 6e^- = 3H_2O$
$E = 1.51 - 0.0591\ pH \qquad P_{O_3} = 1\ atm$

(D) $PbO_t + 2H^+ + 2e^- = Pb + H_2O$
$E = 0.258 - 0.0591\ pH$

(E) $Pb(OH)_2 + 2H^+ + 2e^- = Pb + 2H_2O$
$E = 0.242 - 0.0591\ pH$

scum (37). Thermodynamically this oxide is stable up to a potential described by the reaction:

$$PbO_2 + 2H^+ + 2e = PbO_t + H_2O \qquad E_o = 1.107$$

The area associated with PbO_t is one of rapid corrosion of the anode unless there is a passivating layer of salt at the solution interface that permits establishment of metastable equilibrium. In sulfuric acid $PbSO_4$ serves this purpose, but in alkaline solutions no passivation occurs and the anode continues to corrode at high rates.

The area designated in Fig. 2 as $PbO \cdot xPbO_2$ is determined by both diffraction examination and spot tests. In this area PbO_2 as such is not detected by diffraction examination at the metal interface. In acid solutions the product is PbO_t giving a spot test for a highly oxidizing material after polarization above a potential corresponding to the theoretical reversible oxygen potential. The highly oxidizing material is considered in this report to be tetravalent lead. It appears immediately above the O_2/H_2O electrode potential and is not observed in the area where H_2O_2 could form from O_2 reduction. In neutral and alkaline solutions a mixture of the oxides Pb_3O_4, PbO_x, and PbO_t is observed. The reason for the difference in anodic materials developed in highly acid and in neutral or alkaline solutions is that PbO_2 varies in solubility with the pH at the solution interface. It is discharged in strong acid solutions, preventing accumulation of significant amounts of tetravalent lead. Both forms of PbO_2 are formed at the solution interface at higher pH so that larger amounts of tetravalent material do accumulate. In the alkaline solutions of $pH > 9.4$, the electrode is covered with a gray or black film of PbO_2 which is loose and may be lifted off the electrode revealing a layer colored bright orange, yellow, and peach giving the diffraction patterns for PbO_t, Pb_3O_4, and PbO_x. Lead is corroding under these conditions by a divalent mechanism (26, 28, 35, 36) forming PbO_t, part of which is being oxidized to PbO_2, and acted on at the solution interface by plumbate ion. The anodic products designated $PbO_t \cdot xPbO_2$ at the metal interface represent the mixture obtained by chemical reaction of these materials.

The existence of this area is belived to be caused by the relative rates of these several reactions

$$Pb + H_2O = PbO_t + 2H^+ + 2e^-$$

$$2H_2O = 2(O)_{aq} + 4H^+ + 4e^-$$

$$PbO_t + (O)_{aq} = PbO_2$$

$$\left.\begin{aligned} PbO_t + PbO_2 &= Pb_2O_3 \\ 2PbO_t + PbO_2 &= Pb_3O_4 \end{aligned}\right\} \text{Designated } PbO_t \cdot xPbO_2$$

The following mechanism is suggested: The anodic current may take two paths: (*a*) it corrodes Pb to form PbO_t or divalent products; (*b*) it oxidizes H_2O to $O_{2(aq)}$ which reacts with PbO_t to form the intermediate oxides (6, 13). Lander (26, 28) showed that within experimental limits all the current went to a divalent corrosion mechanism up to a potential of 1.58 v in acid solutions, and only above that potential did a tetravalent corrosion mechanism become significant. Grube and Glasstone (35, 36) showed a similar divalent corrosion mechanism in NaOH solutions up to a corresponding potential. It is suggested that the kinetics of the electrochemical reactions determine the anodic corrosion rate, and above potentials expressed by line C, Fig. 2, PbO_2 is present directly on the metallic surface. Line C corresponds to the reversible oxidation potential of water to ozone.

$$O_3 + 6H^+ + 6e^- = 3H_2O \qquad E_o = 1.51$$

The fact that the passivation of Pb in both acids and alkalies occurs just above this potential, that the reaction has a slope of 0.059 vs. pH, that it exceeds the potentials for formation of PbO_2 from Pb and PbO_t indicates that the corrosion reactions occurring at this potential may be related to water oxidation reactions.

The kinetic analyses of Lander (26) show that when lead is polarized above the potential for oxidation of water to O_2, the reaction mechanism changes. It was further determined that the anodic corrosion rates were related to the square of the water activity up to a potential corresponding to the maximum in the rate. Above this potential the relationship of the corrosion rate to water activity has values "ranging between two and four" (27). The water oxidation reactions to give O_2 and O_3 depend on the square and cube of the water activity, respectively.

The steps in the over-all water oxidation mechanisms are not known at the present time. The relation of the oxidation processes of the lead anodes to the water activity does not prove that $O_2(aq)$ or $O_3(aq)$ is liberated in these reactions; however, it does suggest that the anodic processes depend on the simultaneous reaction of two and more water molecules. It is possible that Pb or PbO_t catalyzes the water oxidation reaction, and that the subsequent step is reaction of Pb and PbO_t with the water oxidation product to form the intermediate oxides rather than molecular gas evolution.

If the lead anode in alkaline solutions is disturbed while in the laminated condition, before polarization above line C, Fig. 2, so that PbO_2 is mechanically brought into physical contact with the base lead metal, oxygen gas begins to be evolved at a potential lower than it will be from an undisturbed electrode. This effect, described by earlier workers (35), was verified in this study. With this positive identification of the anodic materials, it is concluded that PbO_2 must be in direct contact with the metal surface for the oxygen gas liberation reaction to take place and that the reaction may be associated with oxidation of H_2O or $(OH)^-$ to H_2O_2.[1]

It should be emphasized that this is a study of the dynamic anodization of lead under the potential and pH conditions indicated. Polarization of lead within the area designated $PbO \cdot xPbO_2$ does not establish a passivating coating on the surface, and anodic corrosion rates are high. Deposition of PbO_2 at the solution interface does not comprise a protective coating.

The area indicated at αPbO_2 in Fig. 2 is characterized by a heavy deposit of this material directly on the electrode, providing other reactions do not interfere. This material has not been well characterized chemically, and is probably the low-temperature polymorph (45).

X-ray diffraction examination of the residues obtained on air ignition of αPbO_2 at temperatures corresponding to those reported for thermal degradation of βPbO_2 (6, 17) showed evidence that prior to decomposition α converted to βPbO_2. The conversion temperature lies between 296° and 301°C. Subsequent thermal decomposition, determined by x-ray diffraction examination, follows the same path as βPbO_2.

It may be concluded from this examination of the oxides occurring at the metal-coating interface on anodic lead specimens that the oxides formed are: $Pb(OH)_2$; PbO_t and αPbO_2. The potentials for these reactions have a slope of 0.0591 vs. pH and are believed to represent the electrochemical reactions of lead with water and its oxidation products.

The reaction of metallic lead with water to form PbO_t takes place near the calculated reversible potential. Arrests appear near the theoretical potential in both acid and alkaline solutions on both anodic and cathodic treatment, and PbO_t is observed by diffraction examination of the surface. This indicates that the oxidation proceeds by direct reaction with water molecules or hydroxyl ions at the electrode interface and that no preliminary oxidation of water occurs in this reaction. But the reaction forming PbO_2 at the metal interface should probably be written to indicate that water is first oxidized to an oxygen species and the solid anodic products result from secondary reactions. This suggests that the anodic studies of lead may offer a method for kinetic analysis of the water, oxygen electrodes.

Anions and passivation.—As pointed out previously and discussed extensively by Wolf and Bonilla (44) anions present in the solutions will react with the lead ion and/or the lower oxides, and the corresponding salt will be deposited at the solution interface. If the anion is suitable, a tight passivating film is deposited on the anode surface [i.e., $Pb_3(PO_4)_2$, PbI_2, $PbSO_4$] (44, 46), and continued polarization of the electrode will result in the characteristic anodic oxide at the metal-coating interface. If the lead salt of the anion is not passivating, the electrode process may be changed by only very high current densities or cell potentials (47).

A picturization of a cross section of an anodic lead surface is shown in Fig. 3. This indicates the reaction products identified on the anode surface at $pH = 0$, and the reference potentials are presented in the left margin. The cross section is schematic;

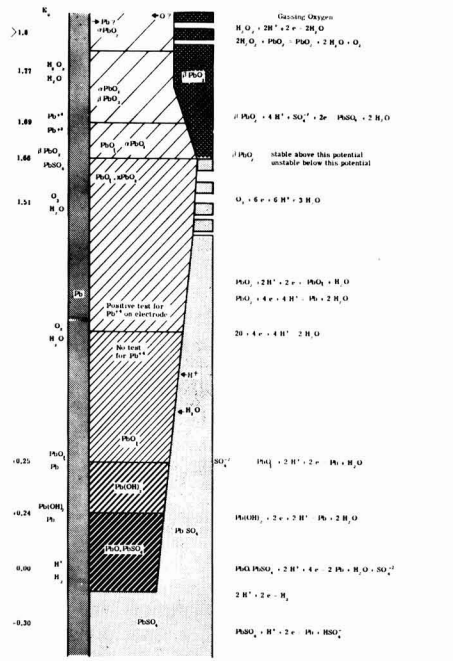

Fig. 3. Schematic cross-section of an anodic lead surface in H_2SO_4 at $pH = 0$. Anodic products identified by diffraction techniques on a lead surface held at constant potential in sulfuric acid are indicated. Electrochemical reactions are shown at the right within the areas where they were observed to occur. Some E_0 values are indicated at the left for orientation purposes. At the potential 1.8 v oxygen gas is evolved, and a hydrogen peroxide reaction mechanism is indicated as suggested by the potential. At this potential lead is represented as corroding by either migration of Pb or O in the film. The mechanism of this corrosion process is not known at the present time.

[1] The reactions in alkaline solution may be written with $(OH)^-$ rather than H^+, and the HO_2^- reactions have different slopes, but for simplicity these are not included in this discussion.

however, it indicates that as the potential is increased the $PbSO_4$ coating appears to become thinner while the PbO_t layer becomes increasingly thicker. Some suggested reactions are indicated at the right of the drawing. The solid phases identified by diffraction examination are indicated within the potential ranges where they were observed. Areas corresponding to high corrosion rates are indicated as porosity in the outer coating. These rates were determined by Lander under constant potential anodization (26, 28). Several reactions appear near their reversible potentials, exhibiting little polarization, and it is thought that the superficial $PbSO_4$ coating is permeable to H^+ ion and water, but not to SO_4^- ion (26, 44). The action of this passivating film is to permit establishment of pseudo equilibrium in an electrochemical reaction in an environment where the reaction would normally be driven in a destructive direction. This, of course, describes the condition called metastable equilibrium.

As the potential is increased, the lead sulfate present on the surface may be converted to βPbO_2. Electron diffraction examination of the anodic products indicates that the βPbO_2 is a polycrystalline coating at the solution interface. Beneath this is a thin layer of a mixture of the two polymorphs of PbO_2 (1, 2). These materials are believed to arise from two reactions forming PbO_2, one from the base lead and PbO_t and the other from $PbSO_4$.

The oxygen gassing reaction at elevated potentials has been indicated as going by way of the formation of H_2O_2 (possible at these potentials) and being decomposed catalytically by the PbO_2. This is merely a representation and suggestion of a possible oxygen liberation mechanism which potential appears to be related to the peroxide reaction in both acid and alkaline solutions (48, 49). The lead metal is represented as corroding by migration of an oxygen species in and lead outward through an αPbO_2 coating at very elevated potentials. Lead exhibits an increased corrosion rate (26, 28), and αPbO_2 comprises the major portion of the anodic product at these potentials, but it is not known whether the mechanism involves attack of the lead through fissures in the coating or migration through a continuous film.

Conclusions

The areas of occurrence of the anodic lead oxide phases are indicated on the potential-*p*H phase diagrams of Fig. 1 and 2. There appear to be two sets of anodic reactions, producing different anodic products. Some of the observed oxides are believed to be electrode species, and some deposits from saturated solutions and chemical reactions.

The occurrence of αPbO_2 as an anodic product on lead in acid solutions has been attributed to oxidation of PbO_t and lead metal by the preliminary oxidation of water.

It is suggested that the corrosion rate of lead depends on the kinetics of these water reactions, and that inhibition of corrosion depends on the imposition of a "corrosion" current and potential that results in a steady-state condition in which PbO_2 is maintained in direct contact with the base metal. Upon anodic polarization of a clean lead surface, it is necessary to "overshoot" the steady-state potential and current in order to generate the required materials, but once the materials are formed in the solution and on the electrode surface then only a minimal current is required to maintain passivation. The low corrosion rate of telephone battery service (50) is believed to be a reflection of this requirement.

The passivation domains originally outlined to correspond to the domains of thermodynamic stability of PbO_2 and $PbSO_4$ (3) should be modified to indicate two areas of passivation: one where the composite coating of $PbSO_4$ and PbO_t is protective below line A in Fig. 2; and the other above line C. These passivation domains are separated by an area of intense corrosion believed to be caused by the electrochemical oxidation of water at the metal interface at a rate insufficient to maintain a passivating coating of PbO_2 on the metal surface.

X-ray diffraction examination of calcined αPbO_2 suggests that it is the low-temperature polymorph and is converted to βPbO_2 at approximately 300°C in air.

The potentials associated with gassing oxygen from a PbO_2 electrode indicate that the reaction may go by way of peroxide in both acid and alkaline media.

Manuscript received Mar. 24, 1958. This paper was prepared for delivery before the Buffalo Meeting, Oct. 6-10, 1959.

Any discussion of this paper will appear in a Discussion Section to be published in the December 1959 JOURNAL.

REFERENCES

1. J. Burbank, *This Journal*, **103**, 87 (1956).
2. J. Burbank, *ibid*, **104**, 693 (1957).
3. P. Delahay, M. Pourbaix, and P. Van Rysselberghe, *ibid.*, **98**, 57 (1951).
4. A. Bystrom, *Arkiv. Kemi. Min. Geol.*, **17B**, No. 8 (1943).
5. F. Halla and F. Pawlek, *Z. Phys. Chem.*, **128**, 49 (1927).
6. T. Katz, *Ann. Chim.*, **5**, 5 (1950).
7. R. G. Dickinson and J. G. Friauf, *J. Am. Chem. Soc.*, **46**, 2457 (1924).
8. W. J. Moore and L. Pauling, *ibid.*, **63**, 1392 (1941).
9. P. E. Jensen and E. J. Ritchie, Paper presented at the Buffalo Meeting, Electrochemical Society, Oct. 7-10, 1957.
10. S. T. Gross, *J. Am. Chem. Soc.*, **65**, 1107 (1943).
11. A. Bystrom and A. Westgren, *Arkiv. Kemi. Min. Geol.*, **16B**, No. 14 (1943).
12. M. LeBlanc and E. Eberius, *Z. Phys. Chem.*, **160A**, 69 (1932).
13. A. Bystrom, *Arkiv. Kemi. Min. Geol.*, **20A**, No. 11 (1945).
14. G. L. Clark and J. Rowan, *J. Am. Chem. Soc.*, **63**, 1302 (1941).
15. C. Holtermann, *Ann. Chim.*, **14**, 121 (1940).
16. G. L. Clark, N. C. Schieltz, and T. T. Quirke, *J. Am. Chem. Soc.*, **59**, 2305 (1937).
17. G. Butler and J. L. Copp, *J. Chem. Soc.*, **1956**, 725.
18. S. T. Gross. *J. Am. Chem. Soc.*, **63**, 1168 (1941).
19. A. Bystrom, *Arkiv. Kemi. Min. Geol.*, **18A**, No. 23 (1944).
20. A. E. Van Arkel, *Physica*, **5**, 162 (1925).
21. A. Ferrari, *Rend. d. Acc. Nag. d. Lincei*, **2**, 186 (1925).
22. J. A. Darbyshire, *J. Chem. Soc.*, **1932**, 211.
23. A. I. Zaslavskii, J. D. Kondrashov, and S. S. Toklachev, *Doklady Akad. Nauk. S.S.S.R.*, **75**, 559 (1950).

24. A. I. Zaslavskii and S. S. Toklachev, *J. Phys. Chem. S.S.S.R.*, **26**, 743 (1952).
25. A. Bystrom, *Arkiv. Kemi. Min. Geol.*, **25A**, No. 13 (1947).
26. J. J. Lander, *This Journal*, **98**, 213 (1951).
27. J. J. Lander, *ibid.*, **98**, 220 (1951).
28. J. J. Lander, *ibid.*, **103**, 1 (1956).
29. X-Ray Powder Data File, Amer. Soc. Testing Mat., Philadelphia, 1950-1957.
30. Ming Chow, *J. Am. Chem. Soc.*, **42**, 488 (1920).
31. W. C. Vosburgh and D. N. Craig, *ibid.*, **51**, 2009 (1929).
32. H. S. Harned and W. J. Hamer, *ibid.*, **57**, 27 (1935).
33. H. S. Harned and W. J. Hamer, *ibid.*, **57**, 9 (1935).
34. G. W. Work and C. P. Wales, *This Journal*, **104**, 67 (1957).
35. S. Glasstone, *J. Chem. Soc. Trans. II*, **121**, 2091 (1922).
36. G. Grube, *Z. Elektrochem.*, **28**, 273 (1922).
37. N. P. Fedotieff, B. P. Artamonoff, and N. J. Rasmerova, J. Electrodepositors' Tech. Soc., **12**, 26 (1937).
38. P. Jones, H. R. Thirsk, and W. F. K. Wynne-Jones, *Trans. Faraday Soc.*, **52**, 1003 (1956).
39. F. Feigl, "Qualitative Analysis by Spot Tests," Nordeman Publishing Co., New York (1939).
40. W. M. Latimer, "Oxidation States of the Elements and Their Potentials in Aqueous Solutions," 2nd ed., Prentice-Hall, New York (1952).
41. S. Glasstone, *J. Chem. Soc. Trans. II*, **121**, 1469 (1922).
42. L. V. Andrews and D. J. Brown, *J. Am. Chem. Soc.*, **56**, 388 (1934).
43. G. L. Clark and W. P. Tyler, *ibid.*, **61**, 58 (1939).
44. E. F. Wolf and C. F Bonilla, *Trans. Electrochem. Soc.*, **79**, 307 (1941).
45. H. Bode and E. Voss, *Z. Elektrochem.*, **60**, 1053 (1956).
46. J. Kamecki, Z. Zembura, and J. Trau, *Roczniki Chem.*, **30**, 261 (1956).
47. R. Piontelli and G. Poli, *Z. Elektrochem.*, **62**, 320 (1958).
48. M. Pourbaix, "Thermodynamics of Dilute Aqueous Solutions," Trans. by J. N. Agar, Edward Arnold and Co., London (1949).
49. P. Delahay, M. Pourbaix, and P. Van Rysselberghe, *Ind. Chim. Belge.*, **16**, 396 (1951).
50. U. B. Thomas, F. T. Forster, and H. E. Haring, *Trans. Electrochem. Soc.*, **92**, 322 (1947).

Evidence for a Logarithmic Oxidation Process for Stainless Steel in Aqueous Systems

Milton Stern

Metals Research Laboratories, Union Carbide Metals Company, Division of Union Carbide Corporation, Niagara Falls, New York

ABSTRACT

Upon immersion of a passive stainless steel electrode into an oxidizing ferrous-ferric aqueous solution, the mixed potential of the electrode gradually approaches the reversible redox potential of the solution. During this period, an oxidation process occurs, the rate of which decreases with time. The process is most likely oxidation of metal since the potential range over which it occurs is more active than the estimated reversible oxygen potential for the system, and no other oxidation reaction is likely. The kinetics of oxidation of stainless steel are similar to kinetics reported for anodic oxidation of metals which form thin amorphous oxides. Therefore, it is believed that evidence has been obtained for growth of a similar type of oxide on stainless steel. At constant potential, the oxidation process can be described closely by a logarithmic oxidation equation. Also, the kinetics are consistent with equations which describe ion current through thin oxides as a function of the field across the oxide.

A study of ferrous-ferric electrode kinetics on stainless steel surfaces has been reported (1). The data supported theoretical equations which describe potential-current relationships for such a system. All rate measurements were conducted on electrodes whose potential, with no applied current, was very close to the reversible ferrous-ferric potential. However, it was also shown that stainless steel does not exhibit this potential immediately after immersion in the oxidizing solution. The electrode is initially more active than a platinum electrode in the same solution and slowly approaches the platinum potential over a period of several thousand minutes in a manner already illustrated (1). No effort was made to explain the processes occurring during this time interval; however, pertinent data were obtained which, at that time, were not particularly clear. A better understanding of the nature of the system now provides a reasonable explanation of this initial potential-time dependence, and the purpose of this discussion is to describe the kinetics of the processes which occur.

Experimental

The experimental procedure was described earlier (1, 2) and only pertinent details are repeated. The environment was either a mixture of ferrous and ferric sulfate in water or a mixture of ferrous and ferric chloride containing sodium nitrate as a pitting inhibitor. Solutions were oxygen-free. Platinized platinum was used as reference and as auxiliary electrodes during polarization. The material was commercial Type 304 stainless steel. Sample preparation involved thorough degreasing, activation in concentrated HCl until hydrogen evolution was ob-

served, a rinse in distilled water, brief (approximately 5 sec) immersion in concentrated HNO_3, a second rinse, and immediate introduction into the cell. This treatment produces a passive surface prior to immersion in the electrolyte. The initial potential-time behavior was recorded using a L&N pH meter which drove an appropriate potential recorder. Since platinized platinum was used as a reference, the approach of the stainless steel electrode to the reversible potential could be observed readily by watching the approach of the recorder indication to zero. During this time interval, a measurement not reported earlier was conducted. It involved periodic anodic polarization of the sample to the platinum potential and determination of the current required to do this. The procedure required a maximum of about 10 sec and did not affect the normal potential-time behavior significantly. To minimize the time during which the sample was polarized, an anodic current was applied to produce a zero recorder reading, after which the polarizing circuit was opened. The value of current required to polarize to the platinum potential was determined by substituting a shunt for the cell in the series polarizing circuit and measuring current through the series circuit without the presence of the cell. Values of resistance in the circuit were high so that the current was not significantly affected by introduction or removal of the effective resistance represented by the cell. This procedure was repeated periodically from the first few minutes after the electrode was introduced into the solution to the time when the potential was essentially stationary.

These measurements were not conducted with a view toward interpretation in the manner presented below. Rather, they were done to determine whether it was possible to measure the instantaneous corrosion rate of the material by a method described by Vetter (3). He reported that the corrosion rate of passive iron in concentrated nitric acid can be determined electrochemically by polarizing the surface anodically to the potential of platinum in the same solution. The current required to polarize is equivalent to the corrosion current. Measurements of this type were discontinued when it was realized that very special electrochemical conditions, described elsewhere (4), are required for the method to work. A sufficient number of experiments of this type were conducted to provide convincing evidence that the observations described below are correct for stainless steel. Since, qualitatively, similar potential-time behavior was observed for other materials, it is possible that the analysis presented below could well apply to the various other surfaces which were used to study ferrous-ferric oxidation-reduction kinetics. However, data for these other metals are not available.

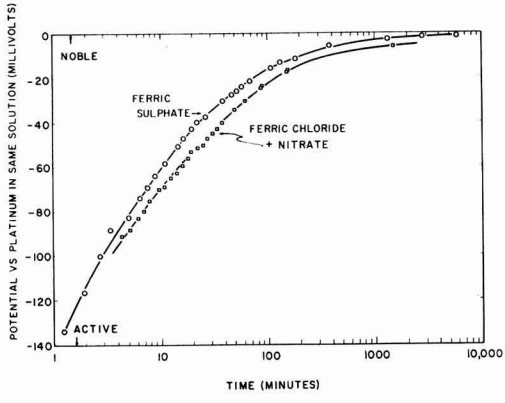

Fig. 1. Potential as a function of time for stainless steel

Time-Potential Measurements

Figure 1 illustrates the potential-time behavior described above. The circles represent data in ferric-ferrous sulfate and are the data reported earlier (1) without explanation. The squares apply to a ferrous-ferric chloride system containing nitrate. Kinetic data for oxidation and reduction of ferrous and ferric ions have already been reported for these systems. In the sulfate solution with a ferrous-ferric reversible potential of +0.770 v, the exchange current, i_o, is 0.045 μamp/cm^2; the Tafel slope for reduction of ferric ions, β_c, is 0.123 v; the Tafel slope for oxidation of ferrous ions, β_a, 0.102 v. For the chloride system (2) with a reversible potential of +0.824 v, i_o, is 0.063 μamp/cm^2; β_c is 0.146; β_a is 0.165. These measurements were made after the electrodes had come to a steady-state potential very close to the reversible ferrous-ferric potential.

Anodic Polarization Measurements

It is assumed that the above kinetic parameters apply to the system very soon after the electrode is immersed and that they do not change during the time the potential approaches that of platinum. Justification for this important assumption is presented later. If this assumption is correct, another oxidation reaction, in addition to oxidation of ferrous ions, must be occurring during this time. According to the theory of the mixed potential, the system must satisfy the following relation:

$$\overleftarrow{i_{Fe^{++}}} + \overleftarrow{i_m} = \overrightarrow{i_{Fe^{+++}}} \qquad [1]$$

where $\overleftarrow{i_{Fe^{++}}}$ (μamp/cm^2) is the rate of oxidation of ferrous ions; $\overleftarrow{i_m}$ is the rate of oxidation of a second oxidation process, and $\overrightarrow{i_{Fe^{+++}}}$ is the rate of reduction of ferric ions. Equation [1] simply states that there can be no net oxidation or reduction in the system and holds at any time where no external current is applied. The most likely process represented by $\overleftarrow{i_m}$ is oxidation of metal, particularly since potentials involved are more active than the reversible oxygen potential and oxygen evolution is not likely.

Upon anodic polarization to the potential of platinum ($\eta = o$), with an applied current, $\overleftarrow{i_p}$, the equation satisfied is:

$$\overleftarrow{i_p} = (\overleftarrow{i_{Fe^{++}}} + \overleftarrow{i_m}) - \overrightarrow{i_{Fe^{+++}}} \qquad [2]$$

but at $\eta = o$, $\overleftarrow{i_{Fe^{++}}} = \overrightarrow{i_{Fe^{+++}}} = i_o$, so that

$$\overleftarrow{i_m} = \overleftarrow{i_p} \qquad [3]$$

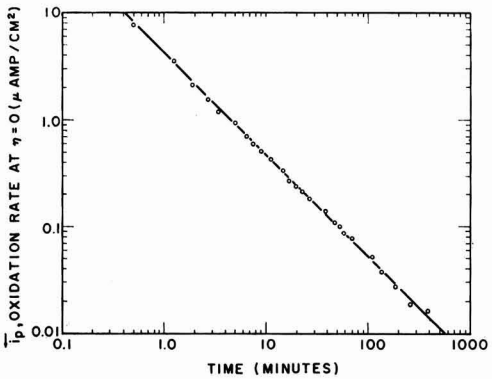

Fig. 2. Oxidation rate at zero overvoltage as a function of time for stainless steel in a ferric-ferrous sulfate solution with reversible potential of +0.770 v.

As described above, $\overleftarrow{i_p}$ was measured as a function of time. Consequently, the kinetics of metal oxidation *at constant potential* can be described in considerable detail solely from this type of measurement. Since the data range over three orders of magnitude, it is convenient to plot them on logarithmic scales. Data for sulfate solution are given in Fig. 2. The points fall on a good straight line, the slope of which is close to minus one. This means that $\overleftarrow{i_m}$ is inversely proportional to time.

$$\overleftarrow{i_m} = \frac{k'}{t} \qquad [4]$$

Consider that $\overleftarrow{i_m}$ represents the rate of oxidation of metal to form an oxide of some type in accordance with a process similar to $M + H_2O \rightarrow MO + 2H^+ + 2e$. Then $\overleftarrow{i_m}$ is proportional to the rate of growth of oxide thickness

$$\overleftarrow{i_m} = \frac{k''dx}{dt} \qquad [5]$$

where x is the oxide film thickness. Therefore,

$$\frac{dx}{dt} = \frac{k}{t} \qquad [6]$$

and upon integration a logarithmic oxidation equation is obtained

$$x = A + B \log t \qquad [7]$$

Whether one considers x an oxide film thickness or simply the weight of metal oxidized, it is quite clear that the kinetics of the process at constant potential closely approximate the general logarithmic oxidation equation.

Generally, Eq. [7] applies to oxidation at low temperatures when thin films are formed.

Relation to Other Work on Oxidation of Metals

Considerable work has been reported on oxidation kinetics of metals such as aluminum, tantalum, columbium, and zirconium, where amorphous oxide films are formed. Much of the experimental work has been directed toward determination of the applicability of the Mott and Cabrera (5) type of equation which relates ionic current through an oxide film with the field, F, across the film.

$$i = \alpha e^{\beta F} \qquad [8]$$

For example, Charlesby has worked with aluminum (6) and zirconium (7) and reports general agreement with Eq. [8]. Van Rysselberghe and co-workers (8) extended work with zirconium to much thinner films than those investigated by Charlesby and also found Eq. [8] valid. Young (9) reports that results for columbium may be expressed by this equation. Vermilyea (10) has conducted extensive studies on the formation of anodic oxide films on tantalum and finds that at constant temperature results are described by an equation similar in form to [8]. However, detailed work has shown that the Mott and Cabrera theory is not adequate for describing all observed phenomena, and efforts to provide modifications or new theories have appeared (11-14).

It is not the purpose of this work to evaluate any of these detailed descriptions. Rather, an effort will be made to show that observed kinetics of stainless steel anodic oxidation are very similar in form to observed kinetics for anodic oxidation of aluminum, columbium, tantalum, and zirconium where amorphous oxide films are produced.

At constant potential, Eq. [8] [where i is proportional to dx/dt and $F = E/x$] may be put in the form of the so-called inverse logarithmic equation by making suitable approximations (5).

$$\frac{1}{x} = a - b \log t \qquad [9]$$

It is particularly difficult to distinguish experimentally between Eqs. [7] and [9]. Measurements over better than two orders of magnitude in time are required. This is described clearly by Vermilyea and illustrated by his data for anodic oxidation (10) and dry oxidation (15) of tantalum. Thus, it is possible that the thickness-time relation observed here for stainless steel could also fit the inverse logarithmic equation and be consistent with Eq. [8].

Charlesby (6) in work with anodized aluminum tried to determine whether his data best fit Eq. [8] or whether they are best described by the strong field emission formula of Fowler and Nordheim (16).

$$i = \alpha F^2 e^{(-B/F)} \qquad [10]$$

He also illustrates the difficulty involved and further reports that the Guntherschulze and Betz' (17) data for tantalum fit Eqs. [8] and [10] equally well. Charlesby's data of particular interest here involve decay of current with time at constant potential, exactly the experimental conditions used for stainless steel in Fig. 2. He shows mathematically that for systems described by Eq. [8], $(d \log i)/(d \log t)$ varies with βF. Over a range of βF values from 10 to 50, which should cover many real systems, $(d \log i)/(d \log t)$ varies from −0.87 to −0.96. For Eq. [10], with B/F values from 10 to 30, $(d \log i)/(d \log t)$ varies from −0.984 to −0.998. These values are closer to −1 than the corresponding values for Eq. [8] and may serve to distinguish between the

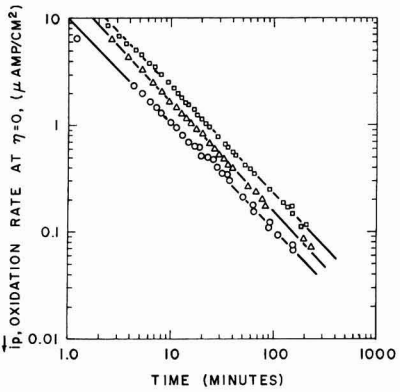

Fig. 3. Oxidation rate at zero overvoltage as a function of time for stainless steel in ferric-ferrous chloride solutions containing nitrate with reversible potentials of +0.824 v (circles), +0.823 v (triangles), and +0.809 v (squares).

two. Charlesby favored Eq. [8] for his data, but reported the results as inconclusive.

The line drawn through the points on Fig. 2 has a slope, $(d \log i)/(d \log t)$, of −0.96. Although values of B and F are not known for the stainless steel system, these data alone indicate that Eq. [8] may apply. However, similar data for three chloride systems are shown in Fig. 3. The circles are for the ferrous-ferric chloride system illustrated in Fig. 1. The squares and triangular points are for stainless steel in a similar solution with reversible ferrous-ferric potentials of +0.809 and +0.823 v, respectively. The straight lines drawn through the three sets of data have slopes of −1.0 (circles), −1.0 (squares), and −0.97 (triangles).

It is evident from the above discussion that the oxidation kinetics observed for stainless steel at constant potential in the oxidizing aqueous environments investigated can be considered to comply reasonably well with either the logarithmic or inverse logarithmic oxidation equations. Also, the data can be considered reasonably consistent with either Eqs. [8] or [10] describing ion current as a function of field across an oxide.

Dependence of Metal Oxidation Rate on Potential

For Eq. [8], which is favored by most work on anodic oxidation, $dF/(d \log i)$, is a constant[1] which is often referred to as the Tafel slope by Dewald (11) and Young (9). Thus, at constant film thickness, $dE/(d \log i)$ is a constant. The rapid (~10-sec) anodic polarization measurements described above for determination of $\overleftarrow{i_p}$ may be considered polarization at constant film thickness. Thus, one would expect a straight line relation between potential and log $\overleftarrow{i_m}$ at any time t. While extensive data showing the variation of $\overleftarrow{i_m}$ with potential at constant time cannot be obtained by the methods used, two points at any time have been measured. This is best described with the aid of a schematic

[1] There is now evidence that β in Eq. [8] is not strictly independent of field (14, 18). However, for the situation described, the change in field is quite small, and this relation may be considered to apply.

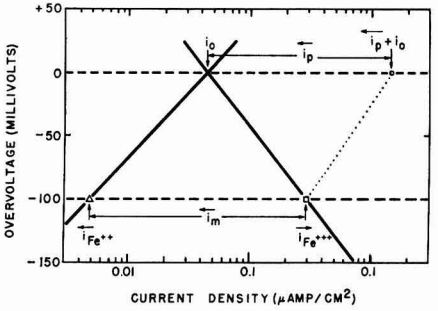

Fig. 4. Schematic polarization diagram showing the position of partial currents during the approach to a steady-state potential.

polarization diagram using the assumption (described above) that the ferrous-ferric oxidation-reduction kinetics are constant with time. With the measured kinetic parameters in sulfate solution used as an example, Fig. 4 illustrates the relation between the various partial currents during the approach to a steady state. Potentials are referred to platinized platinum in the same solution. The two solid Tafel lines represent the rate of oxidation and reduction of ferrous and ferric ions as a function of potential. Since these do not vary at any time (t) during the approach to the platinum potential, the magnitudes of $\overleftarrow{i_{Fe^{++}}}$ and $\overrightarrow{i_{Fe^{+++}}}$ are known from a knowledge of the mixed potential. For example, when the potential is −100 mv, $\overleftarrow{i_{Fe^{++}}}$ is about 0.005 μamp/cm^2 and $\overrightarrow{i_{Fe^{+++}}}$ is about 0.30 μamp/cm^2. These values are shown as the triangles and squares on Fig. 4. From Eq. [1], $\overleftarrow{i_m}$ is the difference between these values or approximately 0.30 μamp/cm^2. Therefore, the point representing $\overrightarrow{i_{Fe^{+++}}}$ also represents $\overleftarrow{i_m}$ when $\overleftarrow{i_{Fe^{++}}}$ is negligible and, in any case, represents the total anodic current.

Upon rapid anodic polarization to the potential of platinum, another value of $\overleftarrow{i_m}$ is determined as shown by Eqs. [2] and [3]. At this potential, $\overleftarrow{i_m} + \overleftarrow{i_{Fe^{++}}}$ represents the total anodic current. Since $\overleftarrow{i_m} = \overleftarrow{i_p}$ and $\overleftarrow{i_{Fe^{++}}} = i_o$, $\overleftarrow{i_p} + i_o$ also represent the total anodic current. Therefore, the dotted line on Fig. 4 connecting $\overleftarrow{i_p} + i_o$ with $\overrightarrow{i_{Fe^{+++}}}$ represents the total anodic polarization curve of the system when the mixed potential is −100 mv. As described above, when the potential is far from the reversible potential, $\overleftarrow{i_{Fe^{++}}}$ is negligible and the dotted line represents the change of $\overleftarrow{i_m}$ with potential. At longer times, when η is small, $\overleftarrow{i_{Fe^{++}}}$ can no longer be neglected, and an analogous dotted line would represent the sum of two logarithmic curves which, over the small potential increment considered, may also be represented by a single Tafel line (19).

As described above, $\overleftarrow{i_p}$ was measured periodically during the approach of the sample potential to that

of platinum in the same solution. The exchange current and Tafel lines were measured after the electrode had reached a steady potential value. Constructing a similar plot to Fig. 4, the data for the sulfate system are shown in Fig. 5. The square points which lie along the Tafel line for ferric reduction are measured potentials at various times during the approach to zero overvoltage. They are the same points illustrated in Fig. 1 and are placed on this figure using the assumption that ferrous-ferric kinetics are independent of time. The circles are values of $\overleftarrow{i_p} + i_o$, where $\overleftarrow{i_p}$ is also measured during the approach to zero overvoltage. The solid lines connecting circles and squares represent data obtained at the same time (within about 10 sec), the time after immersion in the cell being indicated along the appropriate line. The lines are not exactly parallel, those at the shorter times exhibiting a higher slope. The lines at short times should more nearly represent $\overleftarrow{i_m}$ as a function of potential since $\overleftarrow{i_{Fe^{++}}}$ is insignificant, while the lines at long times are influenced by $\overleftarrow{i_{Fe^{++}}}$. Unfortunately, for short times, the interval during which the sample is anodically polarized is significant in respect to the total time, so that these data cannot be considered as accurate as those for which the sample has been immersed for long times.

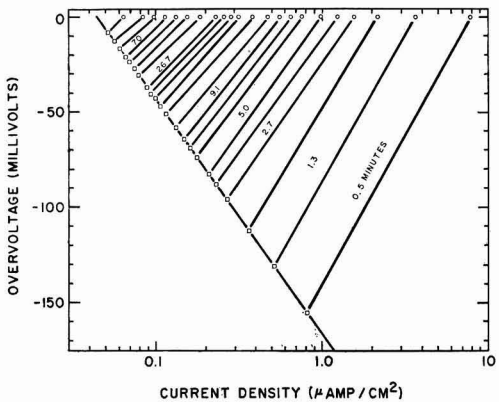

Fig. 5. Total anodic polarization curve for stainless steel as a function of time during the approach to a steady-state potential in ferric-ferrous sulfate with a reversible potential of +0.770 v.

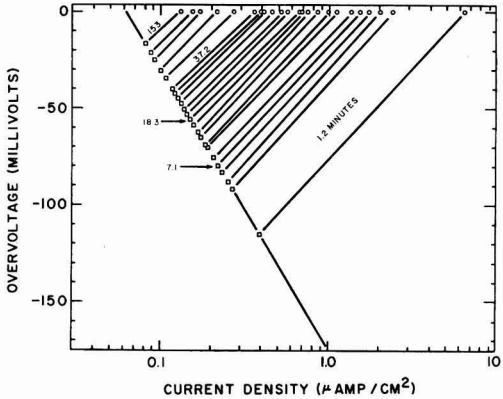

Fig. 6. Total anodic polarization curve for stainless steel as a function of time during the approach to a steady-state potential in ferric-ferrous chloride containing nitrate with a reversible potential of +0.824 v.

Figure 6 shows a similar plot for the chloride system. Here the total polarization lines are all more nearly parallel.

Regardless of whether one considers the family of total polarization curves parallel or not (and one would not expect them necessarily to be parallel since two different processes, $\overleftarrow{i_m}$ and $\overleftarrow{i_{Fe^{++}}}$, with possibly different β values are involved), it is evident that $\overleftarrow{i_m}$ appears to be a logarithmic function of potential as required by Eq. [8].

Potential-Time Behavior

The initial potential-time behavior is explained readily in terms of the processes described above. The potential decreases in the manner shown in Fig. 1 because an anodic Tafel line (representing $\overleftarrow{i_m}$ as a function of E) sweeps from right to left across the polarization curves of $\overleftarrow{i_{Fe^{++}}}$ and $\overrightarrow{i_{Fe^{+++}}}$. The mixed potential at any time is that value at which the sum of all the rates of oxidation ($\overleftarrow{i_{Fe^{++}}} + \overleftarrow{i_m}$) equals the rate of reduction ($\overrightarrow{i_{Fe^{+++}}}$). At short times, $\overleftarrow{i_{Fe^{++}}}$ is negligible and the potential is determined primarily by $\overleftarrow{i_m}$ which is changing rapidly. When $\overleftarrow{i_m}$ approaches $\overleftarrow{i_{Fe^{++}}}$, the potential is determined by the sum of these two currents. In this interval, $\overleftarrow{i_m}$ is changing less rapidly. Finally, when $\overleftarrow{i_m}$ becomes negligible in comparison to $\overleftarrow{i_{Fe^{++}}}$, the total anodic current is essentially $\overleftarrow{i_{Fe^{++}}}$. In this condition, $\overleftarrow{i_{Fe^{++}}} = \overrightarrow{i_{Fe^{+++}}}$ (or the exchange current), and the metal exhibits the reversible ferrous-ferric potential of the solution where $\eta = o$. The potential no longer changes with time.

Oxide Film Thickness

The oxidation kinetics observed for stainless steel during the approach of its mixed potential to that of platinum in ferric-ferrous solutions are similar to kinetics observed for anodic oxidation of metals which are known to form thin amorphous films. This is evidence that similar films are formed on the iron-chromium-nickel alloy.

An estimate of the thickness of the film formed at constant potential may be made by determining the number of coulombs involved in the observations reported in Fig. 2. Integrating the current-time relationship between 1 min and 400 min produces a value of 1.3 (10^{-3}) coulombs/cm^2. Considering the relationship applies from 1 sec to 1000 min increases this value to 2.5 (10^{-3}) coulombs/cm^2. Using 2 (10^{-4}) g/coulomb for the electrochemical equivalent for oxidation of the alloy, gives a value of approximately 5 (10^{-7}) g/cm^2 for the weight of metal oxidized after 1000 min. Assuming the oxide has the formula M_2O_3 with average molecular weight of 150 and metal atomic weight of 55, the weight of oxide

produced is approximately 7 (10^{-7}) g/cm² or 0.7 μg/cm². With a surface roughness factor of 2.5, this value is reduced to 0.3 μg/cm². This may be compared with Rhodin's (20) values of 0.5 to 1.0 μg/cm² obtained by weighing oxides stripped from stainless steels. Assuming an oxide density of 5 g/cm³, the oxide thickness grown in the oxidizing solution after passivation in nitric acid is 6Å, a value which could easily be in error by a factor of two, considering the assumptions which are involved.

The calculation is made primarily to show that experimental values of current are consistent with a process involving logarithmic growth of thin oxide films.

General Discussion

The important assumption made in this entire analysis is that the ferrous-ferric kinetics remain constant with time during the approach of the potential to the reversible redox value of the solution. No absolute proof for the validity of this assumption can be presented. However, it appears quite reasonable, and the entire kinetic description based on this assumption is quite self-consistent.

It should perhaps be mentioned that construction of Fig. 5 and 6 to produce a family of curves which are so nearly parallel provides a very severe test of both the assumption involved and the experimental data. Note, for example, the points along the platinum potential are values of $\overleftarrow{i}_p + i_o$, where i_o is quite significant in respect to $\overleftarrow{i}_p$ for an appreciable fraction of the total anodic curves shown. If i_o or β_c for the ferric-ferrous system were to change appreciably with time, it would be highly unlikely that construction of Fig. 5 and 6 would have produced such a parallel array of anodic curves. This perhaps provides some justification for the assumption. Further, the assumption is consistent with a redox process occurring on an oxide surface, since one would not necessarily expect redox kinetics to change as the oxide becomes thicker provided the rate is not limited by the rate of electron transfer through the oxide.

Perhaps anodic oxidation kinetics for stainless steel, similar to that described here, have not been heretofore reported because stainless steel exhibits a transpassive potential region. That is, at relatively noble potentials, stainless steel dissolves rapidly, whereas oxides on other metals can support much higher fields. Also, overvoltages for oxygen evolution on metals like tantalum, zirconium, columbium, and aluminum are relatively high in comparison to the overvoltage for the process on stainless steel. Thus, the potential range where such kinetics can be observed for stainless steel is much more limited than that which exists for metals which can be anodized readily. Since the oxide on stainless steel apparently cannot support high fields, the thickness cannot readily be built up to the interference color range.

In most work on anodic oxide films, the field required to produce growth is applied externally, whereas here the redox system is considered to provide the field. This is consistent with considerations of Young (9), Dewald (11), Vermilyea (10), and Van Rysselberghe (8), who all have taken into account the field produced by electrochemical processes in solution as well as the field created by an applied potential.

Acknowledgments

The author would like to acknowledge critical discussions with Drs. N. D. Greene, A. C. Makrides, and H. Wissenberg. Dr. Makrides pointed out that the kinetics observed at constant potential can be described by a logarithmic oxidation equation. This led to the interpretation presented here.

Manuscript received Nov. 18, 1958.

Any discussion of this paper will appear in a Discussion Section to be published in the December 1959 JOURNAL.

REFERENCES

1. M. Stern, *This Journal*, **104**, 559 (1957).
2. M. Stern, *ibid.*, **104**, 600 (1957).
3. K. J. Vetter, *Z. Elektrochem.*, **56**, 814 (1952).
4. M. Stern, *This Journal*, **105**, 638 (1958).
5. N. Mott and N. Cabrera, *Repts. Prog. in Phys.*, **12**, 163 (1949).
6. A. Charlesby, *Proc. Phys. Soc. London*, **B66**, 317 (1953).
7. A. Charlesby, *Acta Met.*, **1**, 340 (1953).
8. G. B. Adams, N. Maraghini, and P. Van Rysselberghe, "Proc. 6th Meeting, International Committee for Electrochemical Thermodynamics and Kinetics," p. 249, Butterworths Scientific Publications, London (1955).
9. L. Young, *Trans. Faraday Soc.*, **50**, 159 (1954); **52**, 502 and 515 (1956).
10. D. A. Vermilyea, *Acta Met.*, **1**, 282 (1953).
11. J. F. Dewald, *This Journal*, **102**, 1 (1955); *J. Phys. Chem. Solids*, **2**, 55 (1957).
12. C. P. Bean, J. C. Fisher, and D. A. Vermilyea, *Phys. Rev.*, **101**, 551 (1956).
13. H. H. Uhlig, *Acta Met.*, **4**, 541 (1956).
14. P. Winkel, C. A. Pistovius, and W. Ch. van Geel, *Philips Res. Repts.*, **13**, 277 (1958).
15. D. A. Vermilyea, *Acta Met.*, **6**, 166 (1958).
16. R. H. Fowler and L. Nordheim, *Proc. Royal Soc. A*, **119**, 173 (1928).
17. A. Güntherschulze and H. Betz, *Z. Physik*, **92**, 367 (1934).
18. D. A. Vermilyea, *This Journal*, **102**, 655 (1955).
19. M. Stern, *ibid.*, **104**, 645 (1957).
20. T. N. Rhodin, *Ann. N. Y. Acad. Sci.*, **58**, 855 (1954).

Role of Thiourea in the Electrodeposition of Copper

Bacon Ke, John J. Hoekstra,[1] Bienvenido C. Sison, Jr.,[2] and Dan Trivich

Department of Chemistry, Wayne State University, Detroit, Michigan

ABSTRACT

Single crystal spheres of copper were used to study the effect of thiourea on the plating of copper from an acid bath and the adsorption of thiourea on copper. By x-ray diffraction methods, it was found that instead of the normal tendency of copper to receive single-crystal deposits on the (111) regions from the acid bath, the presence of thiourea caused a uniform bright polycrystalline deposit to be received over the entire sphere. By the use of thiourea labelled with S-35, it was found that thiourea was strongly but fairly uniformly adsorbed on the spheres. It is concluded that the adsorption of thiourea is general with no preference for any crystal face of copper and that the adsorbed thiourea interferes with the crystal growth of the copper electrodeposit.

During the development of modern electroplating practice, it was found that the inclusion of small amounts of the proper addition or brightening agent in the plating bath results in marked changes in the nature of the deposit obtained from the bath. In most cases addition agents are used to obtain smooth bright deposits although they also may be used in some cases to improve other properties. In some cases addition agents permit the use of higher current densities and, as is the case particularly with some bright nickel baths, produce a leveling action, whereby the plated surface is smoother than the original surface. The amount of addition agent required to produce these effects is surprisingly small, and the action of the addition agent is often specific for a particular bath.

The advent of bright plating represents a considerable commercial advance in the field of electrodeposition. In particular, substantial savings in cost and effort have been made since a good deal of the hand finishing previously used can be eliminated.

The early history of bright plating has been reviewed by Rubinstein (1) and by Henricks (2). The discovery of the brighteners used in the various plating baths was accidental in some cases, and in others was the result of painstaking experimentation, almost invariably by means of repeated test platings on a small scale. However comparatively little research effort has been devoted to incisive inquiry into the mechanism of bright plating. Henricks (2) reviewed several theories proposed for the mechanism of bright plating. The most prominent of these theories are the reducing menstruum theory of Kern (3), the adsorption theory of Bancroft (4) [cf. Blum (5)], the complex theory of Mathers (6), and the cathode interference theory of Hunt (7). Each of these proposed theories explains some of the phenomena associated with brightener action, but none of these completely explains all of the facts observed. While the explanations of the mechanism of bright plating are still obscure, the prevalent opinion among more recent workers (8) is that some form of adsorption is involved. The development of a satisfactory theory of bright plating will be of importance in bringing about the development of further bright baths of commercial utility.

A successful theory of bright plating must explain most or all of the following aspects of bright plating: the refinement of the deposit in regard to crystal size and the production of bright, smooth surfaces; the frequent accompaniment by leveling action; the extension of the current density range; the specific nature of the structure of the brightener; inclusion of the brightener or its reaction products in the deposit; the accompaniment of polarization; and the possible change of orientation in deposits.

The specific action of particular agents in certain baths is one of the characteristics that is hardest to explain. It is puzzling that some small variations in the structure of a brightener can ruin its brightening ability and that often there is little carry-over of the brightening power of a particular compound from one bath to another. This suggests that a proper theory of brightening should take into account this specificity in the nature of the brightener and its relation to the metal being plated.

In the face of these facts, we agree with the prevalent hypothesis that brightening is primarily the result of some form of adsorption. Our assumption of this point of view is based particularly on the fact that the molar concentration of the brightener is always much less than the molar concentration of the metal ion. Clearly then it is not possible for a small amount of brightener to form a complex with any substantial fraction of a large amount of metal ion. The most plausible mechanism in which such small amount of brightener can control the disposition of a large amount of metal must require that its action be localized principally at a surface. While it is possible that a brightener is carried into the cathode film in the form of a complex, or that it may exist at or near the electrode surface as a complex, this appears to us to be incidental to the real mechanism.

One could postulate several variations of adsorption mechanisms. One we shall call "structure-sen-

[1] General Motors Fellow at Wayne University, 1954-5.

[2] General Motors Fellow at Wayne University, 1954.

sitive," i.e., the adsorption of the brightener is selective, so that only molecules of a certain size, shape, and chemical structure can be adsorbed on the metal surface. This corresponds to something like chemisorption and may require a suitable spacing between metal atoms on the surface of the electrodeposit to hold the organic molecules. To test this, single crystals of copper were used in this investigation to carry out the adsorption studies. Plating tests were also made with the single crystals, and x-ray studies were made of the deposits on the various faces of the crystal obtained in the absence as well as in the presence of the brightening agent.

Another type of adsorption that could be postulated might be called "current density sensitive," or better "shape sensitive," i.e., the adsorption of the brightener molecules on the cathode surface occurs under electrolysis conditions regardless of the nature of the crystalline structure of the cathode but dependent on the surface contour of the electrode. Here primary consideration is given to the leveling action in certain bright baths, in which the expected low current density areas grow faster than the high current density areas, suggesting the possibility that the high current density areas are blocked preferentially by these compounds. It should be mentioned here that leveling is a microscale phenomenon and that the high and low current density areas being referred to here are micro protrusions and recesses. Relatively less attention was given to the leveling aspect of the subject in the present work. Some investigations of this aspect are in progress and will be reported later. The subject of leveling has recently been reviewed by Leffler and Leidheiser (19).

These types of adsorption may be viewed as physically independent but not necessarily always separate. There could be situations where one type of mechanism operates to the entire exclusion of the others and *vice versa,* but it would be more likely that any real situation would show some contribution from each. The degree to which each mechanism would be represented will probably vary from case to case. It should be mentioned that these postulated variations of an adsorption mechanism are not original with the present authors and that suggestions reminiscent of them can be found in the work of a number of other authors [e.g. (8, 19-24)].

The bath chosen for initial investigation was the acid copper bath using thiourea as a brightener, since this bath appeared to be simpler than others which might have been chosen. Typical compositions for bright acid copper baths are given by Blum (8a), Clifton and Phillips (9), and Beaver (10).

Electrodeposition Studies on Copper Single Crystal Spheres from the Acid Copper Bath

In the structure-sensitive hypothesis, it was suggested that adsorption processes might be operative in which a particular match would occur between the interatomic distances in the brightener molecule and those in the metal crystals of the surface of the electrodeposit. It appeared that such processes could be studied to good advantage by the use of large single crystals of metals.

The desirability of using metal single crystals in any studies in which the metal surface is concerned has been well demonstrated by Gwathmey, Leidheiser, and co-workers (11). Since an ordinary metal specimen is composed of many small crystallites which may have random orientations, the value of a measured surface property of such a specimen is a composite and variable average value of contributions due to exposed crystallite surfaces of many orientations. Such a surface is not readily reproducible and is not suitable for incisive studies of adsorption and other surface phenomena on metals. For such investigations metal single crystals can provide a more readily reproducible surface of better known character and can allow one to choose surfaces parallel to particular crystal planes for study. Single crystal spheres are useful in metal surface studies because a sphere permits all possible crystal faces to be exposed for study in any given experiment and under competitive conditions.

In the present research, two types of studies employing copper single crystals were made. The first type was the electrodeposition of copper on single crystal spheres from plain acid copper plating baths and from acid copper baths containing thiourea as a brightener. The second type was the study of the adsorption of the brightener, thiourea, on copper crystal spheres by means of radiotracer techniques. Plating studies are presented in this section and the radiotracer adsorption studies are presented later. The object of both types of experiments was to determine the relation between crystal structure of the copper metal and brightener action.

Experimental

Copper single crystal rods were grown by the Bridgman method in a resistance furnace which is a modification of one described by Gwathmey and Benton (11a) and also by a method using an induction heated stationary graphite crucible, developed here (12). The copper used was Baker's C.P. shot and also "high-purity" rods.[3] The single crystal rods obtained were machined into spheres by means of a lathe attachment and method developed here (13). Following the machining operation the spheres were first polished mechanically with abrasive papers and then electropolished until etching showed that all worked material had been removed. In general, the procedure followed was that outlined by Gwathmey and Benton (11a). The crystal spheres were further annealed at 1000°C in a nitrogen atmosphere for approximately 12 hr using a Lindberg CF-1 tube furnace. The area of the spheres was determined from micrometer measurements for current density calculations.

Plating experiments were conducted in 1-liter beakers which were immersed in a 25°C thermostat. The experimental electrolyte used was a standard acid copper bath: 205g/l $CuSO_4 \cdot 5H_2O$ and 50 g/l conc. H_2SO_4 (sp gr 1.84).[4] Trace organic impurities which had been found to cause poor results were removed by stirring some activated charcoal[5] into the

[3] Obtained from the American Smelting and Refining Co.

[4] Both chemicals were Baker and Adamson Reagent Grade.

[5] Darco Red Label Grade.

solution at 60°C, allowing the solution to stand a short time, and filtering to remove the carbon. The anodes were thin, high-purity copper rods.[3] The single crystal sphere as cathode was immersed in the center of the cell.

Two series of plating experiments were performed; one series in a plain acid copper bath and the other in a bright acid copper bath, run at a fixed current density of 5 amp/dm^2 at 25°C for plating times of 1, 5, 10, and 20 min, corresponding to approximate deposit thicknesses of 1, 5, 10, 20 μ. The bright plating bath was the same as the plain bath, but contained 0.01 g/l of thiourea (Matheson, further purified by recrystallization from alcohol) in addition. At the beginning of a plating experiment the sphere was again electropolished for 5 min to remove oxide films; then the sphere was rinsed with water and immediately placed in the plating bath. Plating was begun at the current calculated to give the desired current density. The plating bath was agitated by bubbling filtered air through it. Immediately after plating, the spheres were rinsed with water, dried carefully with tissue paper, and then lacquered by dipping in a 4% solution of Saran F-120 in methyl ethyl ketone. The lacquer coating was advisable to preserve the deposit from oxidation to allow subsequent examination by x-ray diffraction. The appearance of the deposit was observed and in some cases photographed.

X-ray diffraction photographs were taken of the deposits on various crystal faces using the back reflection technique. Some early experiments were done with a General Electric XRD-3 x-ray diffraction unit but most of the work reported here was done with a North American Phillips model 5001 unit, using a copper target tube and one of the pin-hole ports. The camera was a Sachs type back reflection camera consisting of a cassette and pinhole system.

The crystal sphere was mounted in a two-circle goniometer which enabled positioning the desired crystal face normal to the beam and 3 cm from the film. The white radiation necessary for the examination of single crystal structures was obtained by running the copper tube at 48 kv, 16 ma. In the case of polycrystalline deposits, usually two x-ray diffraction patterns were taken, one with white radiation and one with monochromatic radiation which accentuate the single crystal and the polycrystalline structures, respectively. The monochromatic radiation was the copper K-α line, which was obtained by running the tube at 30 kv, and 24 ma and using a 0.00075-in. nickel filter at the window of the x-ray tube. The film used was Eastman Kodak "No Screen" medical x-ray film and the exposure time was 1-1½ hr.

Results

It should be mentioned that the single crystal spheres before plating were bright and uniform in appearance following the polishing and electropolishing procedures. Plating these spheres with copper from the plain acid bath resulted in the development of characteristic patterns of striking symmetry [as first observed by Gwathmey and co-workers (11c)]. The deposit in the (100) region consisted of a matte area in the form of a square, while the deposit in the (111) region consisted of a bright triangle. There were six such square areas parallel to the faces of a cube and eight such triangles perpendicular to the body diagonals of a cube. Further we have found that this same pattern was obtained over a substantial range of temperatures and current densities (14). As a matter of fact, the patterns are so characteristic of copper electroplates on good single crystals from a pure bath that they may be used as a test of good procedures. The adequacy of the preparation, handling, cleaning, and plating conditions could be judged by the distinctness of the electroplated patterns obtained. For example, electropolishing insufficient to remove worked surface would result in an irregularly patterned deposit. The annealing treatment of the single crystals and the activated carbon treatment of the plating baths were instituted because such plating tests indicated their advisability. Many plating tests were made and the ones quoted are representative.

The structure of the electrodeposits on the single crystal bases plated in the plain acid copper bath is shown by the x-ray diffraction patterns in Fig. 1. In the bright (111) region, the patterns characteristic of a single crystal structure were obtained for plating times up to 10 min. Even a 20-min plate showed strong preferred orientation. In the matte (100) region, the structure is shown to be polycrystalline at a much earlier stage in the course of plating.

In contrast to the patterned deposits from the plain bath, the bright deposit obtained from a bath containing thiourea was bright and uniform over the entire sphere with no indication of the structure of the underlying single crystal base. Also, x-ray

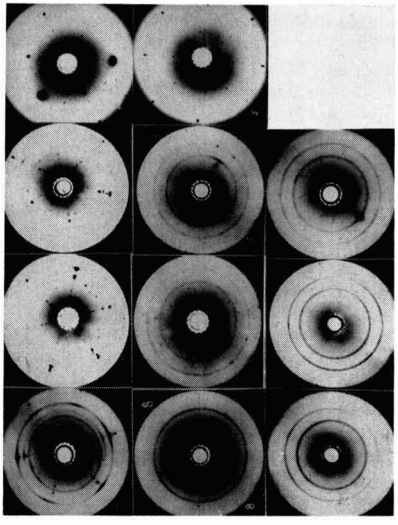

Fig. 1. X-ray diffraction patterns for copper electrodeposits of various thicknesses on copper single crystal spheres plated in an acid copper bath. First column is for white radiation on (111) face; second, white radiation on (100) face; and third, monochromatic radiation on (100) face. Plating times at 25°C at 5 amp/dm^2 from top to bottom: 1, 5, 10, and 20 min.

diffraction studies showed the deposit to have the same structure over the entire sphere. In this case the bright deposit was found to have a polycrystalline structure even in very thin deposits, in contrast to the single crystal bright deposit obtained on the (111) region from a plain acid bath.

Discussion of Plating Results

These results show that under normal plating conditions electrodeposition from the acid copper bath has the greatest tendency to continue the structure of the base crystal on the (111) faces. On the (100) faces, the process is sufficiently less favorable that a polycrystalline deposit is obtained. In a related study by Leidheiser and Gwathmey (11e), it was found in the electrodeposition of nickel from a Watts bath on copper single crystals that the favored direction for continuation of the single crystal structure was on the (100) face. The preferential direction of growth of metal crystals in electrodeposition is probably a composite effect of the influence of a number of variables, including the base crystal, bath composition, and plating conditions. It is well known that this same tendency for the electrodeposit from some baths to continue the structure of the base metal exists even in the case of polycrystalline metal bases when properly prepared [cf. (8a) p. 89].

Under the usual plating conditions on a polycrystalline base metal of doubtful cleanliness, the orienting influence of the base becomes less important, and the observed orientation in electrodeposits is more likely to be determined by bath composition and plating conditions. Electrodeposits from comparatively simple salt solutions frequently have a preferred crystal orientation and commonly exhibit a fiber structure perpendicular to the base metal and extending in the direction of the current flow (15). Fischer (8c) has evolved an extended classification system of crystal structures in electrodeposits and has also dealt extensively with the effect of inhibitors on electrodeposition, Microscopic examination of coarser deposits such as from the acid copper bath reveals a predominance of long columnar grains, One might expect that the long direction of such crystals would be the same as the preferred direction for the continuation of single crystal structure and thus establish a correlation to the preferred orientation in the polycrystalline deposits. Some support for this point of view can be found in the results of Leidheiser and co-workers who found that the Watts nickel bath gives a preferred (100) orientation in polycrystalline deposits (16) and that it continues the single crystal structure on (100) faces of a single crystal (11e), although this conclusion is clouded by the fact that the single crystal base was of copper.

The more striking results of the experiments of this section are the profound effects of the thiourea on the electrodeposition of copper. The most important effect is the ability of the thiourea to interfere with the normal tendency of the acid copper bath to continue the propagation of a metal single crystal on the (111) faces. Similarly the interference operates on the growing crystals on the (100) faces of the single crystal sphere limiting their growth also, as evidenced by the fact that the matte coarsely crystalline deposits normally obtained in these regions from the plain bath becomes refined into a finely crystalline bright deposit from a bath containing thiourea. Thus the copper electrodeposits from a bright bath on single crystals show a uniform polycrystalline structure with no trace of influence from the base single crystal.

It would be expected that copper electrodeposits made on a polycrystalline base would also show the inhibition effect of brighteners. Microscopic examination was made of copper electrodeposits from a standard acid copper bath and from bright acid copper using thiourea as a brightener. The nonbright deposit exhibited the typical coarse, grainy structure with some tendency toward a columnar structure. In the bright deposit there was no evidence of graininess and columnar growth. While no grain structure can be resolved, bright deposits are crystalline as shown by our x-ray results and as shown for nickel by Denise and Leidheiser (16), and others. It is interesting to note that the bright copper deposit obtained from an acid bath containing thiourea exhibits the laminar structure which is frequently, if not invariably, found in bright electrodeposits.

It is not possible from these plating results to decide whether thiourea exercises its inhibiting action on only certain crystal faces. While grain refinement could occur in the case of the electrodeposition of a metal of such highly symmetrical crystal structure as copper if adsorption were to occur on only certain crystal faces, one cannot exclude the possibility that inhibition could occur on several types of faces and perhaps even on all faces indiscriminately. One possible method of deciding between these various possibilities is a direct meaurement of adsorption using tracer methods.

Radiotracer Studies of the Adsorption of Thiourea on Copper Single Crystals

In the preceding section it was shown that the presence of thiourea in the acid copper bath profoundly influenced the crystalline structure of the copper electrodeposit and that this influence, or at least the effect of this influence, appeared to be greater on (111) faces than on the (100) faces. It was suggested that the adsorption of thiourea on copper might be selective on the various crystal faces. In order to make a direct experimental test of this possibility, radiotracer studies were undertaken.

Metal single crystals in the form of spheres are well suited to studies of this type because the surface of a single crystal sphere presents all possible crystal planes and all possible interatomic distances to the reaction medium being studied. If the reaction of the medium with the metal is a function of crystal face and spacing, a definite macroscopic pattern will develop on the surface of the crystal sphere. Gwathmey, *et al.* (11) have shown numerous examples of this pattern development such as those resulting from the etching action of a solution of cupric chloride in hydrochloric acid on copper single crystal spheres, the deposition of carbon on nickel crystal spheres during the thermal decomposition of car-

bon monoxide, oxidation films, wetting by lubricants, electrodeposition, etc.

Accordingly, if thiourea is adsorbed selectively on particular crystal faces of copper because of a preference for a particular interatomic spacing, then it is reasonable to expect that the adsorbed material would be arranged in such a regular macroscopic pattern on the crystal sphere. If thiourea-S^{35} is employed in the adsorption study, by means of the appropriate radioactivity detection technique, it should be possible to determine whether or not a radioactivity pattern corresponding to an adsorption pattern occurs. Since the films of interest would be expected to be monomolecular, sensitive detection methods are required.

Experimental

Electrolytically polished single crystal spheres such as described in the preceding section were used to carry out the adsorption studies. Immediately after they were taken out of the polishing bath and washed in running water, the spheres were dipped in solutions containing carrier-free thiourea-S^{35} which had been synthesized according to the procedure of Bills and Ronzio (17). Two types of solutions were used; one being an aqueous solution containing 0.01 g/l thiourea-S^{35} and the other being a typical acid copper plating bath of the composition used in the preceding section to which 0.01 g/l thiourea-S^{35} had been added. The time of immersion in the solution was usually 30 min to insure the attainment of equilibrium. Exposures were also made of short flash electrodeposits as well as simple immersion without current.

Gas phase adsorption experiments were conducted in a glass tube similar to the outside jacket of a vacuum sublimator. The crystal was suspended from a glass hook at the bottom of the solid ground glass stopper used to close the tube. A small amount of radioactive thiourea was dropped into the tube which was then evacuated at room temperature. After evacuation, the temperature of the whole tube was raised by means of an infra-red lamp operated through a transformer. At 50°C, the adsorption was allowed to continue for about 12 hr, while for a temperature of 100°C it was heated for 30 min and 1 hr in two experiments.

Two methods were employed for the detection of radiation on the spheres which had been exposed to the thiourea-S^{35} in various media. One was an autoradiographic method and the other a method employing a two-circle goniometer and a Geiger counter with scaler. These two methods with their results will be treated separately below.

The autoradiographic detection method of the present work is based on the fact that a photographic emulsion is darkened by the β-particles from the S^{35} in the thiourea-S^{35}. The location of the blackening on development serves as a means of determining the location of the adsorbed thiourea. The procedure used, patterned after that described by Gomberg (18), is as follows. After the adsorption procedure, each sphere was coated with a thin, chemically inert coating of Saran by dipping the sphere into a 4% solution of Saran F-120[8] in methyl ethyl ketone. This coating prevents the subsequent photographic emulsion from reacting with the copper base, and at the same time it is transparent to all radiations coming out. The 4% solution leaves about 2.5 μ of protective plastic coating. After this coating was dried, the photographic emulsion was applied over it.

The emulsion used was du Pont's DH dehydrated emulsion which was prepared, applied, and developed according to the instructions of the manufacturer. All handling, dissolving, coating, and processing steps were carried out in a photographic darkroom equipped with a du Pont S-55x safelight. The emulsion was applied by simply dipping the crystal sphere into the emulsion and rotating the sphere to spread the emulsion evenly over the entire surface. After the application of the emulsion the spheres were placed in a rack in a well closed dark box for exposure. Exposure times were determined from the β-count per unit area per unit time of the individual sphere and the emulsion requirement of 5×10^6 emissions per cm^2 for suitable contrast. The emulsion dried during the first part of the exposure period, and after exposure the film was developed and fixed without peeling it from the sphere.

The experimental results using the autoradiographic technique all turned out to be quite similar. All of the emulsion coatings developed to be uniformly dark over the surface of each sphere. In no case could any gradation be detected in the darkening, and certainly no regular pattern of localization of any kind was evident. The only conclusion that could be drawn was that the adsorption was uniform and that no preferential adsorption of thiourea on the copper single crystal spheres occurred. Several factors existed which gave a basis for doubting the validity of the autoradiographic results, among them possible migration of sensitive material in the emulsion during drying and subsequent exposure time, saturation and reversal effects in the exposure, and imperfect insulation of the emulsion from the base copper by the Saran coating allowing catalytic non-exposure reduction of the silver. These were proved to be unnecessary worries by further tests on blanks and graded exposures, but it was felt desirable in any case to proceed with an independent method of radiation detection employing the two-circle goniometer and Geiger counter.

The apparatus shown in Fig. 2 was used to count directly the emissions from various locations on the sphere. It consisted of a two-circle goniometer for fixing the position of the sphere and a TGC-2 mica window (2.3 g/cm^2) Geiger counter tube (Tracerlab, Inc.) which was used with a Raychronix Model A-4 64-scaler.

The crystal sphere was held in the goniometer clamp in such a position that the axes of both vertical and horizontal rotation passed through the center of the sphere. The crystal holder could be rotated 360° about its own axis and simultaneously through 180° about the vertical axis. Thus, any point on a hemisphere of the crystal sphere could be located

[8] Dow Chemical Co. vinyldene chloride.

Fig. 2. Apparatus used for scanning the radioactivity on copper single crystal spheres having adsorbed thiourea-S^{35}.

with respect to a chosen reference point which, in this case, was the pole of the horizontal axis opposite the handle of the crystal.

The Geiger tube was held horizontally on a ring stand. In front of and parallel to the Geiger tube window, 8 mm away, was a ⅛-in. lead sheet, in the middle of which was a small hole of known size, so positioned that the hole was in the horizontal plane through the horizontal axis and along a radius through the vertical axis. When the Geiger tube and lead shield were fixed in position, the crystal sphere could be so rotated that all positions on the hemisphere could be located and its emissions counted. The surface of the sphere was about 1 mm from the load shield so that emissions from the surface would give a fairly true representation of the number of counts from an area of the order of that of the hole in the lead sheet.

A typical set of counting results is shown in the polar projection of Fig. 3. The size of the black dots is proportional to the number of counts. The number of counts is referred to a pin-hole area of 0.0914 cm^2. The background count is subtracted. The locations of the various crystallographic regions on the crystal are also projected on the chart.

The direct counting method in the main substantiated the results of the autoradiographic method. While a finer discrimination in the detection of the degree of adsorption was possible, in that the counts varied from 50 to 90 over different points, again no definite pattern of adsorption could be detected. As shown in Fig. 3, no correlation can be found between strong and weak adsorption and crystallographic position.

The important result of the experiments of this section is that thiourea is strongly adsorbed on the various faces of a copper single crystal sphere. Contrary to the predictions of the structure sensitive hypothesis, no localization of adsorption was found which might have resulted if a specific fit were required between the brightener structure and interatomic distances on the metal crystal surface.

The differences in the amount of adsorption on the various parts of the single crystal spheres were not large in that they covered only a twofold range of variation. Such small variations might have been due to differences in metal surface areas or to migration of the brightener during the drainage and drying periods. In any case the differences were too small to differentiate between the various crystal faces in terms of adsorption power so that the present results lead to the conclusion that the adsorption of the thiourea is uniform on the various crystal faces.

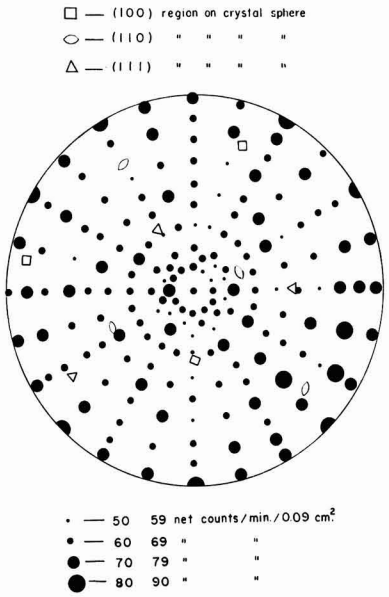

Fig. 3. Polar projection plot of radioactivity from adsorbed thiourea-S^{35} on a copper single crystal sphere. Smallest circles represent 50-59 counts/min/area of 0.09 cm^2; next, 60-69; then, 70-79; and largest, 80-90. Crystallographic regions are represented: (100) by squares, (110) by ellipses, and (111) by triangles.

However, while these results are valid for the conditions used, there remains a lingering suspicion that other methods of carrying out the experiments might reveal a preferential adsorption. Perhaps in the present experiments, the adsorption is sufficient to saturate all faces, indicating that the media studied here have plenty of thiourea available for even the presumably weakest adsorbing faces of the copper to take on substantially the saturation amount of thiourea. This possibility suggests further experiments such as a mapping of the entire concentration vs. adsorption curve for thiourea on copper, or adsorption studies similar to the ones done here but in a medium with insufficient material to give saturation, or selective desorption studies by washing with various solvents, by heating, etc., performed on a saturated single crystal.

Summary and Conclusions

It has been shown by direct tracer measurements that thiourea is strongly adsorbed on the surface of a copper metal crystal or electrode. This adsorption takes place even in the absence of applied potential or electrolysis conditions, but this does not exclude the possibility of modification and perhaps enhancement of the adsorption under conditions of electrolysis.

The effect of the thiourea on the metal electrode during electrodeposition of copper from the acid bath is to modify the crystal structure of the deposit severely. The action of the brightener is one of inhibition of the crystal growth process so that there is a relative enhancement of the nucleation process. This results in a finer grained deposit. The adsorption process appears to have no selectivity for the various crystal faces of the metal so that the inhibition must be a general one governed by conditions other than crystal character of the metal.

Manuscript received Sept. 3, 1957. Most of the work was performed under Contract DA-20-018-ORD-12079 between Wayne University and the Office of Ordnance Research, U. S. Army, during the period of February 1952 to January 1954. Some later confirmatory work is included. Further details are given in Ref. (25).

Any discussion of this paper will appear in a Discussion Section to be published in the December 1959 JOURNAL.

REFERENCES

1. M. Rubinstein, *Metal Finishing*, **48**, No. 5, 54; **78**, No. 8, 51, 58 (1950).
2. J. A. Henricks, *Trans. Electrochem. Soc.*, **82**, 113 (1942).
3. E. F. Kern, *ibid.*, **15**, 441 (1909).
4. W. D. Bancroft, *ibid.*, **23**, 266 (1913).
5. Wm. Blum, Trans. *ibid.*, **36**, 213 (1919).
6. F. C. Mathers, *ibid.*, **29**, 417 (1916); **38**, 133 (1920).
7. L. B. Hunt, *J. Phys. Chem.*, **36**, 1006 (1932); *Trans. Am. Electrochem. Soc.*, **65**, 413 (1934).
8. (a) Wm. Blum and G. B. Hogaboom, "Principles of Electroplating and Electroforming," McGraw-Hill Book Co., New York 1949).
   (b) Wm. Blum and W. R. Meyer, "Modern Electroplating," A. G. Gray, Editor, p. 43, John Wiley & Sons, New York (1953).
   (c) H. Fischer, "Elektrolytische Abscheidung und Elektrokristallisation von Metallen," Springer-Verlag, Berlin, (1954).
9. F. L. Clifton and W. M. Phillips, *Proc. Am. Electroplaters Soc.*, **1942**, 92.
10. J. F. Beaver, Jr. U. S. Pat. 2,391,289, Dec. 18, 1945.
11. (a) A. T. Gwathmey and A. F. Benton, *J. Phys. Chem.*, **44**, 35 (1940).
    (b) A. T. Gwathmey and A. F. Benton, *ibid.*, **46**, 969 (1942).
    (c) H. Leidheiser, Jr., and A. T. Gwathmey, *Trans Electrochem. Soc.*, **91**, 95 (1947).
    (d) A. T. Gwathmey, Proc. Pittsburgh International Conference on Surface Reactions, Corrosion Publishing Co., Pittsburgh (1948).
    (e) H. Leidheiser, Jr., and A. T. Gwathmey, *This Journal*, **98**, 225 (1951).
12. B. Ke, Ph.D. Thesis, Wayne University (1952).
13. B. Ke, J. J. Hoekstra, and D. Trivich, *Rev. Sci. Instr.*, **25**, 1033 (1954).
14. B. C. Sison, Jr., M. S. Thesis, Wayne University (1955).
15. C. S. Barrett, "Structure of Metals," p. 439, McGraw-Hill Book Co., New York (1943).
16. F. Denise and H. Leidheiser, Jr., *This Journal*, **100**, 490 (1953).
17. C. W. Bills and A. R. Ronzio, AECU-619 (1949).
18. H. J. Gomberg, *Nucleonics*, **9**, 28 (1951).
19. E. B. Leffler and H. Leidheiser, Jr., *Plating*, **44**, 388 (1957).
20. J. D. Thomas, *Proc. Am. Electroplaters' Soc.*, **43**, 60 (1956).
21. O. Kardos, *ibid.*, **43**, 181 (1956).
22. D. G. Foulke and O. Kardos, *ibid.*, **43**, 172 (1956).
23. A. W. Hothersall and G. E. Gardam, *J. Electrodepositors' Tech. Soc.*, **15**, 127 (1939).
24. H. Leidheiser, Jr., *Z. Elektrochem.*, **59**, 756 (1955).
25. D. Trivich, Technical Report No. 1 (Aug. 1953) and Final Report (Oct. 1954) on Contract DA-20-018-ORD-12079, Office of Ordnance Research.

The Source of the Nitrogen Impurity in Electrodeposited Chromium

N. Ryan and E. J. Lumley

Aeronautical Research Laboratories, Department of Supply, Commonwealth of Australia, Melbourne, Victoria, Australia

ABSTRACT

High-purity chromium deposited from chromic acid electrolytes containing either sulfate or fluoride catalysts invariably contains small amounts of nitrogen as an undesirable impurity. The amount of this nitrogen impurity is shown to be increased by increased nitrate ion concentration in the electrolyte but not affected by dissolved atmospheric nitrogen or ammonium compounds. It is demonstrated that the nitrate impurity is decomposed at the cathode by reduction with hydrogen to form ammonia as the major product. Some of the atomic nitrogen which is possibly formed at a stage during this reduction is probably adsorbed continuously into the electrodeposited metal.

The nitrogen content of high-purity chromium produced by the electrolysis of chromic acid electrolytes varies according to the bath conditions (1-3). In the chromium prepared at these laboratories it is usually present in the range 0.001-0.004%. Investigations into the ductile-brittle behavior of chromium and its alloys have revealed that small increases in the nitrogen impurity can influence the mechanical properties detrimentally to a remarkable degree (4,3). Hence there is a strong need to eliminate, as far as possible, this nitrogen impurity and for this reason to trace its source.

Possible sources of primary nitrogen contamination immediately apparent are: (*a*) atmospheric nitrogen dissolved in the electrolyte, and (*b*) nitrogen-containing compounds dissolved in the electrolyte.

If atmospheric nitrogen were the main source of

the nitrogen contamination it would be expected that chromium deposited by electrolysis in an atmosphere free from nitrogen would have a low nitrogen content, while that produced under high nitrogen concentrations would have a higher value.

Regarding the second source, the most commonly occurring nitrogen impurity in chromic acid is the nitrate ion, probably arising from the nitric acid wash during manufacture. The nitrate impurity is present in amounts usually of the order 0.004%. This appears a relatively small value, but represents 0.003 g of available nirogen in 1 liter of a 300 g/l chromic acid solution. If 5 g[1] of chromium containing 0.003 wt % nitrogen is deposited from this solution, only 0.00015 g of the 0.003 g of available nitrogen is used. Therefore, it is possible that the nitrogen contamination of electrodeposited chromium could originate from the nitrate impurity in the electrolyte. If this is the case, an increase in the electrolyte nitrate impurity should result in increased nitrogen contamination of the electrodeposited metal.

The experiments here described were carried out to test the above hypotheses.

In general, electrolysis in the sulfate- and fluoride-containing electrolytes was carried out for 5-hr and 1-hr periods, respectively. Because of the higher current efficiencies when using the fluoride electrolytes (2),[2] hourly runs produced sufficient chromium for analysis.

Apparatus

The apparatus, basically a completely enclosed glass vessel, was designed primarily to investigate the effect of dissolved atmospheric nitrogen and was subsequently employed for all experiments. It consisted of two sections: (i) the cell section for 300 ml of electrolyte, cathode, and anode, and (ii) the upper section connected to the cell via a ground glass socket joint. This section contained inlet and outlet arms for (*a*) introduction of the electrolyte, (*b*) anode and cathode connections, and (*c*) a reflux condenser (through which passed gases generated during electrolysis) to reduce evaporation losses.

The chromium was deposited on ½ in. diameter, 2 in. long copper tubes which were subsequently removed by digestion in nitric acid. Pure lead anodes were used in sulfate electrolytes, and 0.5% tin-lead anodes in the fluoride electrolytes. The nitric acid extraction does not influence the nitrogen content of the chromium as it has been found that chromium chipped from the electrode has the same value as that extracted in the nitric acid. Power to the cell was supplied by a 60-amp capacity selenium rectifier.

It has been found (2) that only slight contamination of the electrolyte with SiF_6^{--} occurs when using the fluoride electrolytes in glass vessels.

Chemical analysis.—The chromic acid used contained between 0.002-0.004% nitrate impurity together with the following nominal impurities 0.02% SO_4, 0.01% Fe, and 0.1% Na.

The oxygen content of the chromium deposits was determined using the "Adcock" method and the nitrogen content was determined by a semi-micro Kjeldahl procedure using a colorimetric finish for the low nitrogen values and an acid-alkali titration finish for the high nitrogen values.

Results

Effect of electrolyte atmosphere.—The conditions of electrolysis and the composition of the electrolytes used in these tests are recorded in Table I.

In the first test series, no precautions were taken to exclude air contamination, and these runs are recorded in Table I as having been deposited in an air atmosphere. This however is not entirely correct as the oxygen and hydrogen produced during electrolysis rapidly replaces the air above the electrolyte in the enclosed vessel. Results had been obtained previously for chromium deposited from open vats under otherwise similar conditions, and these showed the same gas content as the chromium produced "in air" in the experimental cell. In the second series of tests a rapid stream of nitrogen was bubbled through the electrolyte during plating.

To investigate deposition under nitrogen-free conditions the apparatus was completely evacuated and flushed with pure hydrogen. The electrolyte was introduced from an attached reservoir, into the evacuated vessel while the current was applied through the electrodes. The oxygen and hydrogen generated were free to escape through the reflux condenser via a water seal, once the internal pressure exceeded that of the external atmosphere.

Analyses of the chromium deposit obtained under the above conditions are recorded in Table I. It is apparent that dissolved nitrogen has an insignificant

[1] The approximate weight of chromium deposited from 1 l of electrolyte during a normal production run in the chromic acid-sulfate electrolyte.

[2] For brevity, the terms "fluoride electrolyte" and "sulfate electrolyte" are used to denote chromic acid solution containing fluoride and sulfate additions, respectively. "Fluoride chromium" and "sulfate chromium" similarly refer to the products of these electrolytes.

Table I. Effect of electrolyte atmosphere

Electrolyte composition CrO_3, g/l	SO_4, g/l	F, g/l	Atmosphere	Current density, amp/ft²	Temp, °C	Current efficiency, %	Oxygen, wt %	Nitrogen, wt %
300	4	—	Air	954	80	11	0.02	0.002
300	4	—	Nitrogen bubbled through	910	82	12	0.02	0.002
300	4	—	Evacuated prior to run	1000	80	10.5	0.015	0.002
295	—	5.4	Air	960	100	39	0.03	0.003
295	—	5.4	Nitrogen bubbled through	980	100	37.5	0.02	0.003

Probable analytical error of nitrogen figures is ±0.0004%. Results given to first significant figure.

Table II. Effect of nitrate impurity in electrolyte

CrO_3, g/l	Electrolyte composition SO_4, g/l	F, g/l	NO_3, g/l	Current density, amp/ft²	Temp, °C	Current efficiency, %	Oxygen, wt %	Nitrogen, wt %
300	4	—	0.012	1000	82	12	0.02	0.002
300	4	—	0.1	980	80	12.5	0.02	0.4*
300	4	—	0.5	980	84	10.6	0.02	0.8*
300	—	5.2	0.006	880	100	35	0.02	0.001
290	—	5.4	0.2	910	100	39	0.03	0.28
290	—	5.4	0.15	900	100	37	0.03	0.19

* These results are given only to the first decimal place, as the method used for the analysis was not fully suited to such high nitrogen contents.

influence on the amount of nitrogen codeposited with the chromium.

Effect of nitrate impurity in the electrolyte.—Chromium was deposited under the conditions detailed in Table II from 300 g/l as-received chromic acid solutions containing either 4 g/l sulfate or 5.4 g/l fluoride as the active catalyst, the nitrate impurity being 0.012 g/l and 0.006 g/l, respectively. The chromium obtained from these tests was found to contain 0.002 wt % and 0.001 wt % nitrogen, respectively. These deposits were used as comparison standards.

In order to vary the nitrate impurity, nitric acid was added to electrolytes of similar composition to the above, and electrolysis was carried out under the conditions described in Table II. These deposits were analyzed for both oxygen and nitrogen, and results showed that the nitrogen content of the chromium was increased markedly.

Effect of electrolyte temperature.—Investigations into the production of high purity chromium from various electrolytes have given some indication that reduction in nitrogen content of the chromium occurs with increasing electrolyte temperature (2). In these experiments chromic acid with only trace amounts of nitrate impurity was used. Chromium deposited from an electrolyte containing sulfate at 100°C was found to contain less than the chemically detectable amount of nitrogen, but, as shown in Table III, the current efficiency was only 2.5%.

For a further series of tests, an electrolyte containing 300 g/l CrO_3, 5.3 g/l F, and 1 g/l NO_3 was prepared. This was electrolyzed at 1000 amp/ft² for 1-hr periods at 70°, 85°, 92°, and 100°C. Analyses of the chromium deposits obtained from these experiments are recorded in Table III. They indicate that the nitrogen content was unaffected by electrolyte temperature.

Effect of ammonium compounds in the electrolyte.—It is well known that ammonia is produced during the electrolytic reduction of nitrates. In order to find the effect of this ammonia on the nitrogen content of the electrodeposited chromium, the following tests were performed. Normal chromic acid electrolytes in which the active catalyst radicals were introduced as the corresponding ammonium salts were electrolyzed under the conditions listed in Table IV. The results indicate that the ammonium ion does not influence the nitrogen content of the chromium to any significant extent since the nitrogen values obtained lie within the usual scatter found in successive chromium deposits during normal production.

Electrolytic reduction of nitrate impurity.—In the preceding sections of this paper it has been demonstrated that there is a definite relationship between nitrate additions to the chromic acid electrolyte and the increased nitrogen content of the electrodeposited metal, while molecular nitrogen and ammonium compounds are without effect. The manner in which this contamination takes place is a matter for speculation and has been discussed briefly in a previous report (5). Nitrogen is obviously introduced into the chromium at some stage during the electrolytic reduction of the nitrate electrolyte impurity.

In order to study this relationship more closely a solution containing 300 g/l CrO_3, 5.84 g/l F, and 2.7 g/l NO_3 was prepared. This solution was electrolyzed at 100°C and 1015 amp/ft² current density. Chromium deposits were plated from this electrolyte for consecutive time intervals of 1 hr, ½ hr, ¾ hr, and ½ hr. Fresh cathodes were used for each successive electrodeposition. These deposits were analyzed to determine the nitrogen content, and samples of the electrolyte, after each succeeding deposit,

Table III. Effect of electrolyte temperature

CrO_3, g/l	Electrolyte composition SO_4, g/l	F, g/l	NO_3, g/l	Current density, amp/ft²	Temp, °C	Current efficiency, %	Oxygen, wt %	Nitrogen, wt %
300	4	—	0.012	960	82	10	0.02	0.002
300	4	—	0.012	984	100	2.5	Not detected	
310	—	5.25	0.006	1100	100	40	0.03	0.003
300	—	5.3	1	1000	70	26	0.18	0.098
300	—	5.3	1	1000	84	32	0.12	0.10
300	—	5.3	1	1000	92	36	0.09	0.096
300	—	5.3	1	1000	100	39	0.03	0.098

Table IV. Influence of ammonium compounds

Electrolyte composition									
CrO_3, g/l	SO_4, g/l	SO_4 as $(NH_4)_2SO_4$, g/l	F, g/l	F as NH_4F, g/l	Current density, amp/ft²	Temp, °C	Current efficiency, %	Oxygen, wt %	Nitrogen, wt %
300	4	—	—	—	960	82	10	0.02	0.002
300	—	4.2	—	—	980	84	11	0.01	0.003
300	—	—	5.2	—	880	100	35	0.02	0.001
300	—	—	—	5	910	100	39.5	0.03	0.002

Table V. Electrolyte composition, 300 g/l CrO_3, 5.84 g/l F. Electrolyte temp. 100°C; current density 1015 amp/ft²; current efficiency 32%

	NO_3,* g/l	NH_3, g/l	NO_3 equivalent of NH_3 produced, g/l	Nitrogen in electrodeposit, wt %
Fresh solution	2.7	0.0023	—	—
1-hr deposition	0.052	0.55	2.0	0.24
1½-hr deposition	0.024	0.64	2.3	0.084
2¼-hr deposition	0.012	0.70	2.4	0.040
2¾-hr deposition	0.008	0.74	2.7	0.025

* The nitrate ion was added as potassium nitrate.

were analyzed to determine ammonia and residual nitrate, i.e., during the 1-hr deposition the nitrate was reduced from 2.7 to 0.052 g/l and so on. Results are recorded in Table V and Fig. 1.

It can be seen that the nitrate content decreased rapidly during the first hour of electrolysis and then more steadily with time, the ammonia content showing a corresponding increase. The nitrogen content of the chromium samples decreased with the nitrate content of the electrolyte.

Discussion

The main conclusions to be drawn from this investigation are that dissolved nitrogen and ammonium salts in the electrolyte do not influence the nitrogen contamination of electrodeposited chromium, but that nitrate impurities markedly raise the nitrogen pickup. Increasing the electrolyte temperature does not in any way effect a reduction in the nitrogen impurity, at least in electrolytes containing fluoride and considerable amounts of nitrate. However, the limited evidence from the sulfate electrolyte could suggest a decrease in nitrogen content with increasing electrolyte temperature. It has been shown in Table V and Fig. 1 that the progressive electrolytic reduction of nitrate results mainly in production of an equivalent amount of ammonium ion, and that the reaction follows a typical reaction rate time curve, asymptotic to the time axis. This implies long times for substantially complete conversion of nitrate to ammonia.

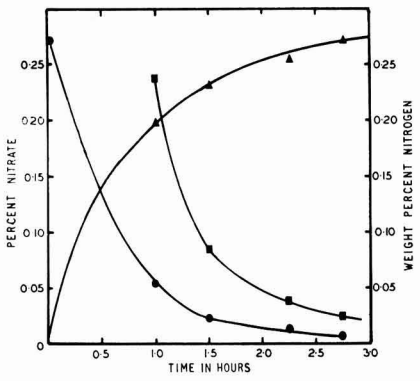

Fig. 1. ●—Reduction in nitrate during electrolysis; ▲—increase in ammonia in electrolyte expressed as equivalent nitrate; ■—nitrogen content in successive chromium deposits.

The manner by which nitrogen enters the chromium is not definitely known. The nitrogen impurity in the chromium is obviously introduced at some stage during electrolytic reduction of the electrolyte nitrate impurity. It is possible that atomic nitrogen is formed at some stage during this reduction, and that a portion of this nitrogen enters the electrodeposited chromium (5). The electrochemical reduction of nitrate is known to be complex (6), and many nitrogen-containing compounds can be formed depending on the various cathode conditions.

It is obvious that if some means could be found of eliminating the nitrate impurity in chromic acid electrolytes the nitrogen content of electrodeposited chromium could be reduced to a much lower level than is normally obtained at present. It is suggested that the impurity could at least be substantially reduced by electrolyzing solutions of chromic acid for long periods under conditions favoring the generation of large volumes of hydrogen at the cathode without any recoverable chromium deposition. Low concentrations of nitrate may however be very difficult to remove. Low-nitrate chromic acid could also be produced by replacing the nitric acid wash during manufacture by hydrofluoric acid, or by repeated recrystallization.

Acknowledgments

The authors wish to express their thanks to Mr. A. R. Edwards for his helpful criticism in the preparation of this paper which is published by permission of the Chief Scientist, Department of Supply, Australia.

Manuscript received Aug. 25, 1958.

Any discussion of this paper will appear in a Discussion Section to be published in the December 1959 JOURNAL.

REFERENCES

1. H. T. Greenaway, *J. Inst. Metals*, **83**, 121 (1954-5).
2. N. E. Ryan, Report A.R.L./Met 26, Oct. 1957.
3. "Ductile Chromium," American Society for Metals, Cleveland, Ohio (1957).
4. H. L. Wain, E. Henderson, S. T. M. Johnstone, and N. Louat, *J. Inst. Metals*, **86**, 281 (1957-58).
5. E. J. Lumley, A.R.L./Met. Note 7 Feb. 1957.
6. M. J. N. Pourbaix, "Thermodynamics of Dilute Aqueous Solutions," Edward Arnold and Co., London.

Electroplating on Thorium

John G. Beach and Glenn R. Schaer

Battelle Memorial Institute, Columbus, Ohio

ABSTRACT

A method was developed for treating thorium whereby adherent electroplates of most metals can be applied. The method involves anodic pickling in hydrochloric acid and chemical pickling in sulfuric acid prior to plating. Factors affecting the adherence and protective qualities of the coatings are discussed.

The use of thorium in nuclear reactors prompted an interest in coatings that could provide desirable surface properties. Thorium, like magnesium, uranium, and zinc, oxidizes easily and corrodes readily in boiling water.

Coatings on thorium that could prevent oxidation and corrosion, or that would aid joining to other metals, for example by soldering, were deemed desirable. A process for plating on thorium has been worked out (1), and electroplated and conversion coatings that protect thorium in boiling water were studied briefly (2).

A review of the known properties of thorium and its compounds plus its electrochemical activity suggested that the problems involved should be similar to those encountered in plating on aluminum, magnesium, and uranium. The principal problem was the preparation and activation of the thorium surface. When the thorium was properly prepared, most metals could be electrodeposited satisfactorily by established procedures. Known methods for preparing aluminum, magnesium, and uranium for electroplating did not provide satisfactory adherence of electrodeposits on thorium. However, the method developed in these studies for plating on thorium is also applicable to aluminum.

Method of Electroplating on Thorium

Pretreatment of thorium.—Anodic and chemical pickling were used to activate thorium for electroplating. The procedure is as follows: descale mechanically (abrasive blast, machine, etc.); degrease (trichlorethylene); cathodic alkaline clean, conventional multipurpose alkaline cleaner, 180°F, 25 amp/ft^2, 2 min; cold-water rinse; anodic pickle, hydrochloric acid, 1.2*N* HCl, HCl (1.19 g/cc)—10% by volume, 80 = 10°F, 50 amp/ft^2, 5 min; chemical pickle (without rinsing), sulfuric acid, 3.6*N* H_2SO_4, H_2SO_4 (1.84 g/cc)—10% by volume, 80 = 10°F, immersion 5 min; cold-water rinse; electroplate (immerse with the current on).

Electroplating on pretreated thorium.—The above pretreatment permitted adherent electroplating of aluminum, chromium, copper, gold, indium, iron, lead, nickel, silver, tin, and zinc directly on thorium. The listing below describes the types of solutions that were used.

Metal Plated	Type of Solution
Aluminum	Aluminum chloride—lithium chloride—ether (3)
Chromium	Chromium acid—sulfuric acid (4)
Copper	Copper sulfate—sulfuric acid (4)
Iron	Iron sulfate—chloride—formate (5)
Nickel	High *p*H bath (6) (used for direct plating on aluminum)
Gold	Cyanide (4)
Indium	Cyanide (4)
Silver	Cyanide (4)
Zinc	Acid sulfate (4)
Lead	Complex alkaline tartrate (7)
Tin	Alkaline stannate (4)

Although most types of plating baths are suitable for plating on thorium not all plating baths were satisfactory. For example, chloride-containing baths that had a *p*H lower than 4 were unsatisfactory. Also, the high-temperature chromic acid solution for depositing low-contraction chromium was unsuitable for direct deposition on thorium.

Stripping of electrodeposits.—Most electrodeposits could be stripped, with little or no attack on the thorium, by immersion of the plated thorium in 50% nitric acid or by anodic treatment in a caustic solution.

Electropolishing (Anodizing) of Thorium

Electropolishing was tried as a means of improving the thorium surface for plating. Thorium treated anodically under the following conditions was smoothened uniformly but retained a film that prevented uniform activation for plating. However, the film presumed to be thorium phosphate also provided protection against oxidation and corrosion.

Sulfuric acid	9*N* H_2SO_4
Phosphoric acid	11*N* H_3PO_4
130°F	150 amp/ft^2

1500 amp-min/ft^2/mil of surface metal removed

Heating the electropolished thorium in vacuum at 600°F for about 30 min increased the protective quality of the anodized film.

Evaluation of Coatings on Thorium

Qualitative adherence, solderability, thermal-cycling, and corrosion tests were made to provide data for engineering design of protective coatings on thorium.

For the research reported here, "adherence" is narrowly defined as the attachment at the basis metal-electroplate interface. The term "bond strength" (8) is used to indicate the force required to separate the electroplated metal from the basis metal regardless of the location of fracture. Bond strength is of ultimate importance and whether or not a given bond strength is satisfactory is, of course, governed by the end use.

Adherence.—The adherence of the above electroplates to pretreated thorium was excellent. In no case could the electroplated metal be peeled from the thorium at the electroplate-thorium interface by the tests described below.

Adherence tests for copper, nickel, and silver-plated thorium were made by: filing and/or grinding across the interface (in a direction to drag the plate away from the thorium); chiseling along the interface; and bending a flat 40-mil-thick specimen around a ¼-in. mandrel, reflattening, and bending back around the mandrel. A minimum thickness of 1 mil of electroplate was deposited for the above tests.

Solderability.—Soldering copper- or nickel-plated thorium pieces together with a lap joint and separating by flexing the joint fractured the sample in the soft solder. Thus the adherence of the plate exceeded the strength of the soft solder, about 6000 psi.

Cyclic heating and cooling.—Copper-, nickel-, and silver-plated thorium specimens were cyclicly heated (in argon) for 15 min at 100° intervals up to 700°C successively and quenched through air into cold water. Zinc-plated thorium was heated only to 400°C.

Bend tests were made to find the temperature at which diffusion alloying would degrade the bond strength. The bond of zinc-plated thorium was satisfactory after heating to 400°C (19°C below the melting point of zinc). The bond of copper-, nickel-, and silver-plated thorium was satisfactory up to 500° or 600°C. Since thorium metal or alloy remained firmly attached to the electroplates when the samples were bent after heating to 600° or 700°C, the bond failure was attributed to the interfacial alloy layers that were weaker than the electrodeposited metal or the thorium.

Thorium is known to alloy with most metals. Interdiffusion of the electroclad metal and the thorium, along with the melting point of the clad or eutectic alloys formed, appears to establish limiting conditions for the use of plated thorium at elevated temperatures.

Corrosion.—Thorium corrodes readily in hot water, oxidizing and/or hydrating to form a layer of loose powdery corrosion products that can be brushed off easily. Corrosion weight changes of +72 mdd to −14 mdd have been reported. No doubt the variance in data is due to retention or removal of loose corrosion products for obtaining the weight-change data.

Table I. Corrosion rate in distilled water at 203°F (95°C)
Duration of test: 6 weeks

Surface coating on thorium	Corrosion rate in mdd
None*	−7.4
Anodized*	−1.7
Anodized and heated*	−0.7
Copper electroclad†	+0.9

* Loose corrosion products removed before weighing.
† Copper was plated in several steps with intermediate burnishing (to close porosity) and periodic heat treating in vacuum at 400°C (to decompose hydrides and remove entrained hydrogen). Copper tarnished during corrosion.

Anodizing (electropolishing) and heat treating or copper electrocladding appreciably reduced the corrosion of thorium. The corrosion data are presented in Table I. The corrosion of thorium was reduced about 90% by anodizing and heating to form a protective thorium phosphate film. The slight weight gain for copper-electroclad thorium was attributed to tarnishing of the copper and possibly to entrapment of water in the copper cladding.

Conclusions

Thorium surfaces pretreated by anodic pickling in hydrochloric acid and chemical pickling in sulfuric acid can be electroplated with coatings of most metals. The adherence of the plated coatings is excellent and passes all the conventional adherence tests. Electroplated metals on thorium can protect thorium in boiling water and can aid soldering and/or joining to other metals. The use of electroclad metals on thorium for high-temperaure applications will depend on the proper selection of metals that form suitable alloys with thorium by interdiffusion.

Copper, iron, nickel, and silver directly on thorium offer promise for protecting thorium. However, further data on the diffusion of the electroplated metals and thorium along with the properties of the alloys formed are needed.

Electropolishing (anodizing) of thorium and heat treating imparts a protective coating that resists hot-water corrosion.

Manuscript received Sept. 25, 1958. This paper was prepared for delivery before the Ottawa Meeting, Sept. 28-Oct. 2, 1958. Work was performed under AEC Contract W-7405-Eng-92.

Any discussion of this paper will appear in a Discussion Section to be published in the December 1959 JOURNAL.

REFERENCES

1. J. G. Beach, G. R. Schaer, and C. L. Faust "Electroplating of Metals on Thorium," Report BMI T-7 (Feb. 1 1949).
2. J. G. Beach, W. C. Schickner, L. E. Vaaler, and C. L. Faust, "Electroplating on Thorium," Report BMI 802 (Jan. 9, 1953).
3. D. E. Couch and A. Brenner, *This Journal,* **99**, 234 (1952).
4. "Metal Finishing Guidebook," 27th Ed., published by Metals and Plastics Publications, Inc. (1959).
5. J. G. Beach, *Plating,* **43**, 616 (1956).
6. J. G. Beach and C. L. Faust, *This Journal,* **100**, 276 (1953).
7. A. W. Liger (Battelle Memorial Institute), U. S. Pat. 2,474.092, June 21, 1949.
8. C. L. Faust, *Monthly Rev. Am. Electroplaters' Soc.,* 223 March 1946, (see errata, May 1946, issue); *Plating,* 1221, December 1948.

The Effect of Magnesium Salts on Nickel Plating Baths

Ahmad Geneidy[1] **and W. A. Koehler**

Department of Chemical Engineering, West Virginia University, Morgantown, West Virginia

and Willi Machu

Department of Chemical Engineering, Cairo University, Cairo, Egypt

ABSTRACT

The effect of magnesium salts was measured in Watts-type and Wesley all-chloride type nickel plating baths. The deposition potential of nickel was lowered (metal became more noble), polarization was reduced, and results on decomposition potentials were inconclusive. Nickel deposited from all baths under test had a face-centered cubic lattice, and magnesium was present only in spectroscopic traces. It was found that addition of magnesium salts increased cathode current efficiency, improved throwing power, and reduced porosity of the nickel, as revealed by the ferroxyl test. At low concentrations of magnesium salts the mechanical properties of nickel deposits were not changed materially, but at high concentrations deposits were harder, more brittle, and had a higher tensile strength. The effect on residual stress in nickel deposits was not measured.

It has been shown that properties of electrodeposited nickel are dependent on a number of factors. One of these is the nature and concentration of the so-called "conducting salts"; the most common of these salts are those of sodium, ammonium, and magnesium.

Addition of magnesium salts to nickel baths has aroused a controversial issue in the plating industry, since many beneficial and some harmful effects have been observed and reported. Opinions expressed by scientific workers as well as by practical platers were, in many cases, conflicting. Data to support both sides of the argument have appeared in the literature. However, no systematic study confirmed with quantitative data has yet been conducted. Needless to say, the presence of such data will, undoubtedly, help the plater to control behavior of the bath as well as properties of the deposit. To this end the present investigation was directed. Carefully controlled tests were made to determine the net effect of magnesium salts on the operation of nickel baths and on the properties of nickel deposit, and whether or not these effects are due to codeposition of magnesium.

The chief advantage of adding conducting salts to nickel plating baths is to increase the conductivity of the baths. Apart from the economic advantage of increasing the conductivity, better conductivity usually leads to better deposits, prevents formation of trees and rough deposits (1), and improves the throwing power (2-4). The effect of magnesium salts on the conductivity of nickel plating baths was reported by Hammond (5) and by Nicol (6). Reactions, functions, and mechanisms of magnesium and other conducting salts were discussed at length (8-11).

As a conducting salt, magnesium sulfate was added to nickel baths since the very beginning of the nickel plating industry. Adams, who commercialized nickel plating in Boston in 1869 (12), introduced in the following year his well-known patent (13) of a nickel bath containing magnesium salts and in 1899 Kugel established another patent (14).

The first study on the effect of magnesium was conducted in 1902 by Coehn (15) followed by Siemens in 1904 (16). Since then, magnesium sulfate additions have been recommended for nickel baths used in various fields of applications; for commercial rapid (17-20) and barrel plating (21) and also for plating on iron and stainless steel (22), as well as on nonferrous metals and alloys, particularly zinc and zinc base die castings (23-32) aluminum and is alloys (33-41), and lead (42).

Magnesium sulfate additions have also been reported in nickel baths recommended for producing a rust-resisting nickel plate (43, 44), a detachable and elastic nickel film on a nickel base (45), and for plating phonograph records (46). Magnesium sulfate has also been added to improve throwing power (47), to produce mat silver-white deposits (48) that are free from pitting (49).

Nickel deposited from baths containing magnesium sulfate is soft, easy to buff (50), and can be bent, twisted, or rolled without stripping or peeling off the plate (51). However, Makar'eva (52) found that the addition increases hardness and produces a deposit that is more lustrous and more uniform in texture, and that changed very little with change in current density or temperature. The effect of magnesium on stress is not yet agreed upon (53, 54).

Robinson (55) considered magnesium sulfate as the most suitable conducting salt in nickel baths. Baths containing this salt kept up their metallic concentration, produced even anode corrosion, and showed no pitting. Nickel deposited from such baths were whiter, resisted action of acids and did not rust as quickly, retained their luster longer, and were

[1] Present address: Cairo University, Cairo, Egypt.

more readily cleaned and polished than deposits obtained in the absence of magnesium sulfate. Thirteen years later, Barrows (56) confirmed Robinson's findings relative to that "indifferently recognized aid to better plating."

In spite of reported beneficial effects of adding magnesium sulfate to nickel plating baths, some objections against its use had been raised (57-59).

Magnesium chloride additions are also common, although to a lesser extent. The function is either to increase conductivity (60) or to increase anode corrosion in sulfate baths (61-65) or as a halogen carrier in a bright bath (66).

In addition to being introduced intentionally as magnesium slats, magnesium can be also introduced in small amounts from nickel salts (67), nickel anodes (68-71), water (72-74), and from chemicals added to introduce ions or radicals other than magnesium (75-77).

Experimental

Purification and preparation of the test baths.— This was effected in a Pyrex glass cylindrical container. Heating was accomplished by immersing the container in a constant temperature water bath while agitating by bubbling purified compressed air through a perforated Pyrex glass coil which rested on the bottom of the container. Air was purified by passing it through columns packed with glass wool and charcoal to capture any entrained oil.

Concentrated solutions of plater's grade nickel sulfate and of nickel chloride were prepared and to each solution 2 ml of 30% hydrogen peroxide was added per liter of solution. The temperature was raised to 70°-75°C (158°-167°F), and the pH was then raised to 5.8 by slow addition of a freshly prepared slurry of nickel carbonate. Solutions were stirred vigorously at that temperature and pH for 2 hr, after which the precipitates were allowed to settle. After filtration, the solutions were electrolyzed at low current density. Due to the limited available quantity of electrolytic nickel, platinum anodes were used; cathodes consisted of thin nickel sheets to avoid the possibility of introduction of impurities at very low current density areas, as might be the case if steel or nickel plated steel were used. Electrolysis was continued at 0.2 amp/dm^2 (2 a.s.f.) until 120 amp-hr/gal were passed, and then at 0.5 amp/dm^2 (4.6 a.s.f.) until at least 30 amp-hr/gal had passed. Finally, the solutions were electrolyzed at 5 amp/dm^2 (46 a.s.f.) for 6 hr. The hot and well-agitated solutions were then treated with 7.5 g/l (1 oz/gal) of activated carbon. After allowing the solutions to stand for a few hours, they were filtered.

The effectiveness of this purification cycle was tested by spectroscopic analysis of a nickel sheet deposited nonadherently on a stainless steel cathode at the specified operating conditions. After thus purifying the separate concentrated solutions of nickel sulfate and nickel chloride, test baths shown in Table I were prepared by mixing and/or dilution of purified concentrated solutions.

Baths chosen for this investigation are the Watts sulfate and Wesley all-chloride types of nickel baths since they are the two most commonly used baths apart from the bright ones. Of the different types of Watts baths, the one selected was chosen because it is very widely used in actual practice; it has nearly the same nickel content as the Wesley bath, and it has been subjected to some investigations.

Since anions have a decided influence on the character of the deposit, it was decided to add magnesium sulfate to Watts bath and magnesium chloride to Wesley bath. Furthermore, in order to permit a fair comparison of the effects of magnesium ions in the two baths, magnesium salts were added in equinormal amounts rather than in equal percentages. Concentrations of the magnesium salts were selected to cover the range of usual additions. In order to facilitate reference to the different test baths, a bath symbol was assigned to each type; the letter S (sulfate) is a symbol of the Watts sulfate bath while C (chloride) indicates the Wesley chloride bath. The bath symbol is followed by a numeral which indicates the normality of the magnesium salt added.

Operating conditions. — Operating conditions chosen for this investigation were as follows: current density, 4.3 amp/dm^2 (40 a.s.f.); temperature, 60°C (140°F); pH (electrometric) 2.

Measurement of cathode and decomposition potentials.—Measurements of the deposition potentials were effected in a small rectangular glass trough measuring 15 x 6 x 6 cm. The two anodes and the cathode measuring 6 x 1.0 x 0.1 cm each were cut from electrolytic nickel sheet and placed 5 cm apart. Although dimensions of the electrodes did not allow ideal conditions of uniform density, results thus obtained were in agreement with those obtained by Wesley and Roehl (78) with measurements made in a box similar to Haring cell which provides better means for measuring electrode potentials. The close

Table I. Composition of the test nickel baths

Bath No.	Bath symbol	Bath type	Constituents in g/l					
			$NiSO_4 \cdot 7H_2O$	$NiCl_2 \cdot 6H_2O$	H_3BO_3	$MgSO_4 \cdot 7H_2O$	$MgCl_2 \cdot 6H_2O$	NaCl
1	S-0.0	Watts	325	45	30	—	—	—
2	S-0.1	Watts	325	45	30	12.3 (0.1*N*)	—	—
3	S-1.0	Watts	325	45	30	123 (1.0*N*)	—	—
4	S-2.0	Watts	325	45	30	246 (2.0*N*)	—	—
5	C-0.0	Wesley	—	300	30	—	—	—
6	C-0.1	Wesley	—	300	30	—	10.2 (0.1*N*)	—
7	C-1.0	Wesley	—	300	30	—	102 (1.0*N*)	—
8	C-2.0	Wesley	—	300	30	—	204 (2.0*N*)	—
9	C-2.0Na	Wesley	—	300	30	—	—	117 (2.0*N*)

agreement between the two data indicate the reliability of the measurements carried out in the previously mentioned manner. Moreover, we were chiefly concerned with reproducible relative values rather than exact absolute ones. The potential of the cathode was measured against a saturated calomel electrode. Connection with the cathode was effected through a glass U-tube, one stem of which was drawn to a capillary, which was bent through 90° and pressed against the cathode.

The electrolysis cell, containing 400-500 ml of solution under test, was immersed in a constant-temperature water bath at 50° ± 0.1°C, while the calomel electrode was at room temperature. The solution was not stirred. No difference was observed when the solutions were tested as prepared or after being boiled to expel dissolved oxygen. After recording the static potential, a very small current was applied for a sufficient length of time to attain equilibrium. Equilibrium was assumed to exist if two consecutive readings of the potential made 4 or 5 min apart differed only by a fraction of a millivolt. Usually equilibrium was attained within 20 min.

Decomposition potentials were made in the same cell and in the same manner except that the electrodes were all made of platinum sheet. No effort was made to measure decomposition potentials with great precision.

Cathode current efficiency and throwing power.—Cathode current efficiencies were determined by the increase in weight of a nickel cathode. Measurements were made in a rectangular glass trough 12 x 7 x 6.5 cm (4¾ x 2¾ x 2½ in.). The two anodes and the cathode were all cut from thin nickel sheet 1 mm (0.04 in.) thick. With the cathode placed midway between the two anodes and the area of all electrodes exactly filling the cross section of the trough, a uniform current density was secured on the cathode.

Measurements were made in triplicate with the efficiency cell at 60°C while a copper coulometer connected in series was at room temperature. For each bath, the current efficiency was determined at three current densities: 2.1, 4.3, and 6.4 amp/dm^2 (20, 40, and 60 a.s.f.). Results were reproducible to ±1%.

Throwing power determinations were made in the same troughs. The anodes were perforated with 3/32 in. holes. Determinations were made at two primary current distribution ratios: 5:1 and 2:1. In calculating the current density, only the areas of the two sides of the cathode facing the anode were considered. A run lasted usually 45 min.

Mechanical properties.—For testing mechanical properties, a sheet of nickel 0.25 mm (0.01 in.) thick was prepared from each bath by plating nonadherently on a stainless steel sheet, type 302, about 0.079 mm (0.031 in.) thick. The cathode measured 20 x 18.7 cm (8 x 7.5 in.)

The plating jar consisted of a rectangular glass trough measuring 20.6 cm long x 36.5 cm high x 16.2 cm wide (8¼ in. x 3 in. x 6.5 in.). The anode consisted of electrolytic nickel which was analyzed by spectroscopic methods and was enclosed in a high-quality cotton bag. One anode and one cathode were used, both filling the cross section of the plating jar. The pH of the solution, which always tended to rise, was kept constant at the required value by allowing acid to drip from a buret. Agitation of the solution was effected by two electrically driven propeller-type glass rods. Pitting was prevented by adding 0.4-0.5 ml of 30% hydrogen peroxide to every liter of the bath. Decomposition of the hydrogen peroxide was ascertained by testing with a dilute solution of potassium permanganate.

The electroformed nickel sheet obtained from each bath was cut into 2.5 cm (1 in.) strips with the long dimension corresponding to the horizontal dimension of the original sheet. Strips were then machined to the form recommended by A.S.T.M. specifications E8-46 for thin sheet material, except that the length of the strip was 18.7 cm (7.5 in.) instead of 20.3 cm (8 in.). Specimens were tested in a Baldwin hydraulic testing machine. After the tensile strength test was completed, the zone where fracture occurred was noted and the dimensions of that zone, previously measured, were used in the calculation of the cross-sectional area. The per cent elongation was calculated by the increase of a 5 cm (2 in.) gauge length. Usually two sets of gauge marks were made in the reduced section of the specimen so that the fracture would very likely take place with one, if not both pairs. However, in some specimens the fracture occurred just near or even outside the gauge marks; in such cases no elongation measurements were obtained. At least five specimens of each type of deposit were tested. Reproducibility of the tensile strength measurements was within 10% while that of the elongation measurements was very much poorer, although all specimens were free of pits and microscopic defects.

Hardness measurements were made by an Eberbach microhardness tester using a load of 323.2 g. Indentations were made on the cross section of the deposit (cross-sectional hardness) as well as on the inner surface of the deposit which was adjacent to the basis metal (surface hardness). Usually, at least seven hardness measurements were taken for each type of deposit. Reproducibility of the results was within 10%.

Structure.—To obtain samples for metallographic examination, two small pieces were cut from the electroformed nickel sheet; one of these pieces was mounted in Bakelite in such a way that the cross section perpendicular to its plated surface was exposed. The other piece was mounted so that the surface originally adjacent to the stainless steel cathode was exposed. Electrolytic etching using different electrolytes under varying conditions did not give satisfactory results. Good results were obtained through using the "flat solution," consisting of a mixture of equal volumes of concentrated nitric and glacial acetic acids. The structure was photographed in a Bausch and Lomb metallograph.

X-ray patterns were obtained by the powder method in a North American Philips Diffraction unit using a cobalt tube and an iron filter.

Porosity.—Samples for porosity were obtained by coating a thin layer of nickel 0.025 ± 0.0025 mm (0.001 ± 0.0001 in.) thick on low carbon (0.15% C)

steel pieces measuring 18.7 x 20 cm (7.5 in. x 8 in.). Steel cathodes were prepared according to the A.S.T.M Designation B 183-49 (79).

The corrosive solution used was that recommended by Thon, *et al.* (80) which consists of 50 g/l of potassium ferricyanide and 0.2 g/l sodium chloride. The test was carried out in the manner mentioned in the British Standard 1224-1945. At least five determinations were made from each bath.

Determination of magnesium. — Spectrograms were obtained by shaping two pieces of the electroformed nickel sheets from each bath to form the two electrodes for the spectrograph. These were then excited by a d-c arc at 5 amp for 60 sec. The nickel standard was excited for 5 sec only. Analysis was then conducted in the usual manner using the internal standard method.

Results

Cathode potentials and cathode polarization curves are shown in Fig. 1, 2, and 3. Figures 4 and 5 show the effect of magnesium on the cell voltages and on the decomposition potentials of the different baths.

Results of cathode current efficiencies are shown in Fig. 6 and 7.

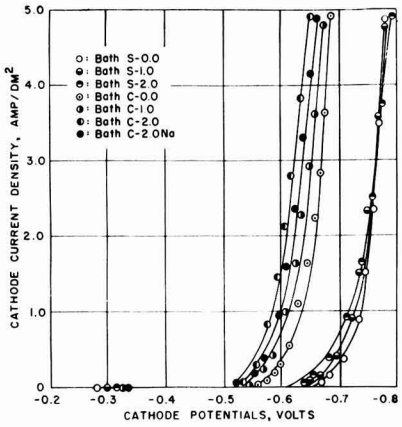

Fig. 1. Cathode potentials for nickel baths at 50°C against a saturated calomel electrode.

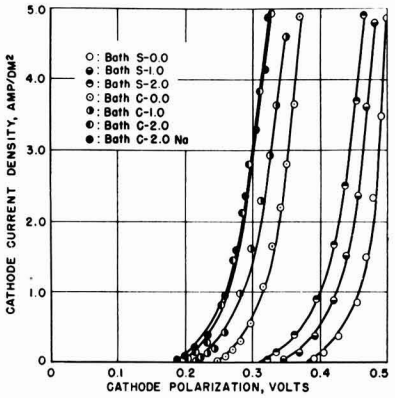

Fig. 2. Cathode polarization in nickel baths at 50°C

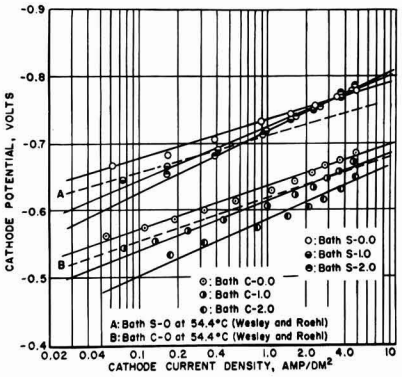

Fig. 3. Cathode potential vs. current density curves for nickel baths.

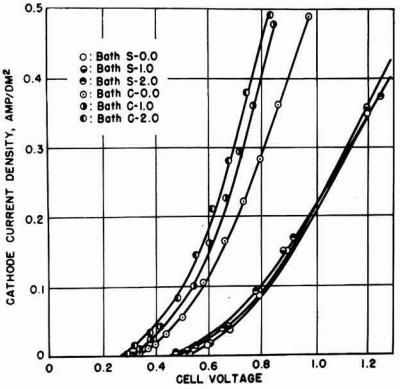

Fig. 4. Cell voltages in nickel baths

Throwing power data are plotted in Fig. 8. Data are submitted on the three scales: Haring and Blum scale (3), Heatley's modification (81), and the British Standard Institution (B.S.I.) scale. Each point on each curve is the average of three determinations.

Mechanical properties data are plotted in Fig. 9, 10, and 11. In Fig. 10, the elongation value corresponding to bath S-0.1 was not included since the fracture of the specimens occurred either outside the gauge marks or just adjacent to them.

Photomicrographs of the various deposits are shown in Fig. 12, 13, 14, and 15. X-ray patterns for the Wesley baths are shown in Fig. 16.

Corrosion resistance data are plotted in Fig. 17. Corrosion resistance is expressed as the reciprocal of the number of spots revealed by the ferroxyl test per square decimeter of the tested deposit.

Figure 18 shows spectrograms obtained from the standard nickel specimen and deposits from Wesley-type baths.

Table II summarizes some of the important data obtained in this investigation.

Discussion

Deposition potential, polarization, and decomposition potential.—Deposition potential and polarization data were investigated since they influence the

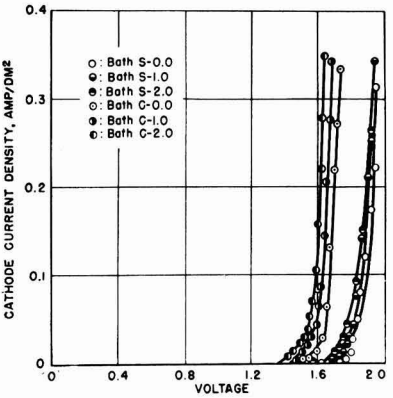

Fig. 5. Decomposition potentials for nickel baths at 50°C

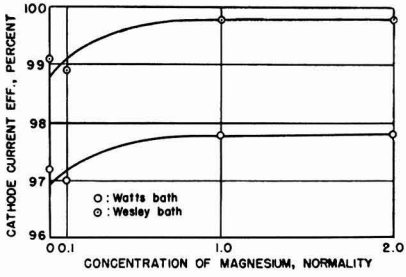

Fig. 6. Effect of magnesium content of nickel baths on the cathode current efficiency at 50°C and 40 a.s.f.

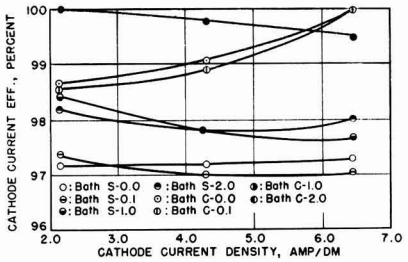

Fig. 7. Effect of the magnesium content of nickel baths on the rate of change of cathode efficiency with current density.

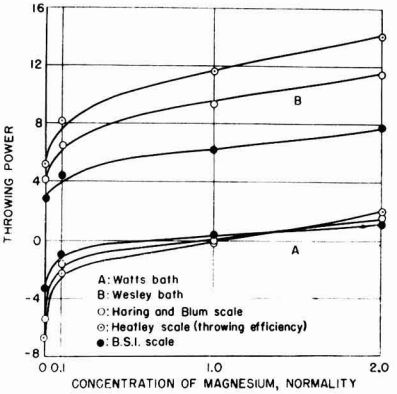

Fig. 8. Effect of the magnesium content of nickel baths on the throwing power. (Linear ratio, L = 5).

following four characteristics (82): (*a*) structure of the deposit; (*b*) cathode current efficiency; (*c*) throwing power; and (*d*) alloy deposition.

It has been shown by others that there exists a relation between cathodic polarization and the structure of the deposit (1, 83-85). In some cases, the relation was not verified (86-90). This led to the introduction of the "interference" concept (91). However it is believed by some investigators that there must be some connection between cathode potentials and formation of electrodeposited metal (92).

Concerning throwing power, high cathodic polarization improves that important property (93, 2, 94). In this respect, the significant criterion is the slope of the cathode potential vs. current density curve.

Cathodic polarization affects alloy deposition in the same manner as it affects hydrogen evolution.

In the present study it is evident from Fig. 1 and 2 that addition of magnesium slightly makes the potential of nickel more noble and lowers cathodic polarization. That this effect is not due to formation of insoluble magnesium hydroxide is shown by the fact that bath C-2.0Na showed the same trend as the other baths.

The previous result is not in agreement with that of Thompson (27) who reported that magnesium increased cathodic polarization and cathodic current

Table II. Effect of adding magnesium salts on the operation of Watts and Wesley baths and on the physical properties of the electrodeposited nickel

Bath	Cathode efficiency at 40 a.s.f., %	Throwing* power	Tensile strength, psi	Elongation,† %	Hardness‡ Vickers	Corrosion resistance	Magnesium content in deposit, %
S-0.0	97.2	—5.4	6700	17.6	143	12.0	—
S-0.1	97.0	—1.7	6400	—	142	20.8	0.011
S-1.0	97.8	—0.3	6300	19.3	144	37.0	0.014
S-2.0	97.8	1.6	7700	13.7	163	100.0	0.014
C-0.0	99.1	4.2	9200	16.1	204	12.3	—
C-0.1	98.9	6.5	9000	14.9	204	14.5	0.014
C-1.0	99.8	9.3	9400	16.7	202	58.8	0.018
C-2.0	99.8	11.5	9700	10.9	224	76.9	0.021

* As measured in a throwing power box with a linear ratio of 5:1 applying the Haring and Blum formula.
† In 2-in. gauge marks.
‡ Determined by an Eberbach microhardness tester applying a load of 323.2 grams.

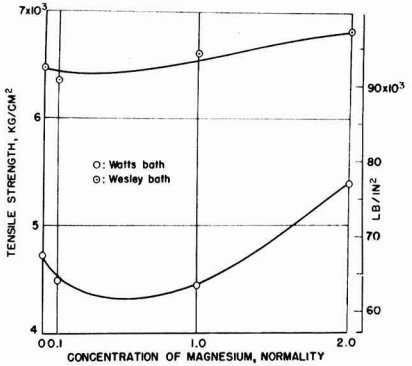

Fig. 9. Effect of the magnesium content of nickel baths on the tensile strength of the deposits.

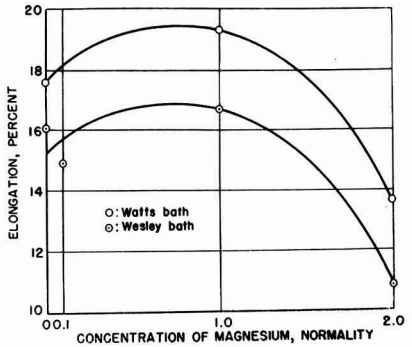

Fig. 10. Effect of the magnesium content of nickel baths on the elongation of the deposits.

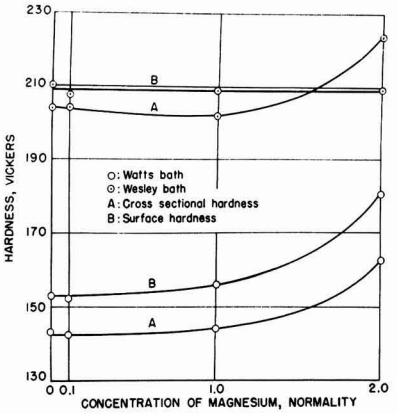

Fig. 11. Effect of the magnesium content of nickel baths on the hardness of the deposits.

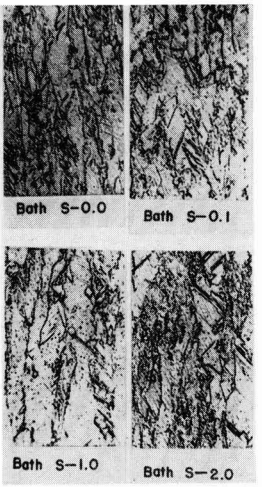

Fig. 12. Effect of the magnesium content of Watts-type bath on the structure of electrodeposited nickel. Section parallel to the direction of growth of deposit. Magnification 250X.

efficiency as well. Thompson attributed these two contradictory phenomena to the common ion effect and to increased density and viscosity of the solution due to addition of magnesium salt. If this is the case, addition of magnesium chloride to a nickel chloride bath should also increase cathodic polarization. However, this was not verified by Verdick, *et al.* (95) who found that, at high concentrations of magnesium chloride, nickel was deposited more easily. These workers tried to explain this and similar phenomena by a theory involving complex ion formation.

It seems that the problem is open to more fundamental study to establish the possibility of complex ion formation and to reveal the part played by the degree of dissociation and solvation of molecules and similar factors which govern the very nature of the delicate process of deposition.

Figure 3 shows that the addition of magnesium increases the slope of the cathode potential vs. current density curve. This should tend to improve the throwing power of the baths.

Curves of Fig. 5 indicate that addition of magnesium causes a slight decrease in the over-all potential. This decrease may be entirely due to decrease in resistance of the bath.

Cathode current efficiency.—Cathode current efficiency is significant as it determines the useful portion of electric power consumed, liberation of hydrogen, maintenance of a constant *p*H during plating, and throwing power of plating baths.

Figure 6 shows that the baths under test have high cathodic current efficiencies. There is, however, a slight increase in these efficiencies after addition of magnesium. This is in agreement with results obtained earlier (27).

Concerning the rate of change of cathodic current efficiency with current density which affects throwing power, Fig. 7 indicates that there is no consistent change in one direction or the other, and differences observed are within the reproducibility of results and experimental errors. It is concluded, therefore, that this factor will have very little, if any, effect at all on the throwing power of the nickel baths under test under the conditions of this investigation.

Throwing power.—Good throwing power is a desirable property in plating solutions since it is generally found that a bath with a good throwing power

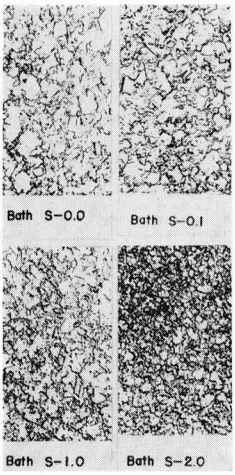

Fig. 13. Effect of the magnesium content of Watts-type bath on the structure of electrodeposited nickel. Section perpendicular to direction of growth of deposit. Magnification 250X.

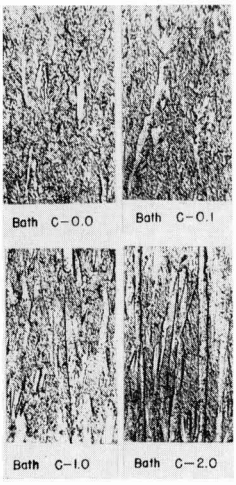

Fig. 14. Effect of magnesium content of Wesley-type bath on the structure of electrodeposited nickel. Section parallel to direction of growth of deposit. Magnification 250X.

usually yields a good smooth deposit. It helps to give uniform thickness of plate with subsequent economic advantage. It is also important in plating more electronegative metals and alloys.

Figure 8 shows that there is a small but consistent increase in throwing power with increasing concentrations of magnesium. There was contradiction in the results of earlier investigations (27, 59). However, magnesium sulfate was usually added to improve the throwing power in nickel baths (47, 50).

The effect of magnesium can be predicted by analyzing its effect on the three factors which determine throwing power, namely, conductivity, rate of change of cathode potential and of cathode current efficiency with current density. By referring to Fig. 4 and to the work of Hammond (5) and Thompson (27) it will be clear that addition of magnesium sulfate increases the conductivity of nickel baths. Also, it was previously shown that addition of magnesium increases the slope of the cathode potential vs. current density curves. The third factor is not affected as has already been stated. It may be concluded therefore that addition of magnesium improves the throwing power partly due to an increase in conductivity of the bath and partly due to an increase in the rate of change of cathode potential with current density.

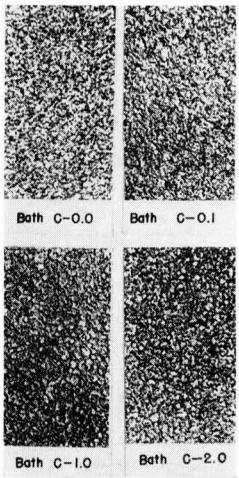

Fig. 15. Effect of magnesium content of Wesley bath on the structure of electrodeposited nickel. Section perpendicular to direction of growth of deposit. Magnification 250X.

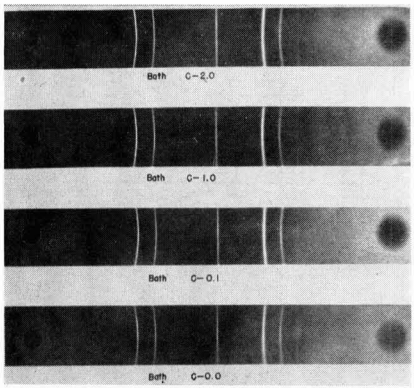

Fig. 16. Powder method diffraction patterns of nickel deposited from Wesley baths.

Mechanical properties.—Mechanical properties are of prime importance in determining the engineering qualities of electrodeposited metals. The tensile strength indicates the amount of distending force per unit area that the deposit can withstand before its fracture. Ductility is important if the plate is subjected to deformation or to machining operations. Elongation is associated with ductility and is usually taken as a measure of the latter. Hardness is also important in determining the ease of polishing and buffing. It is related to the resistance of abrasion.

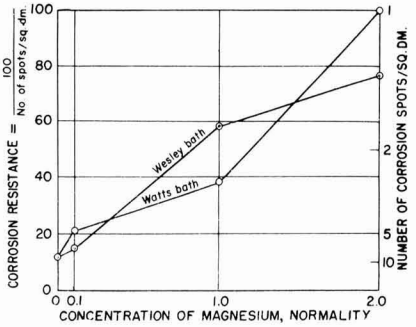

Fig. 17. Effect of magnesium content of nickel baths on the corrosion resistance of the deposits.

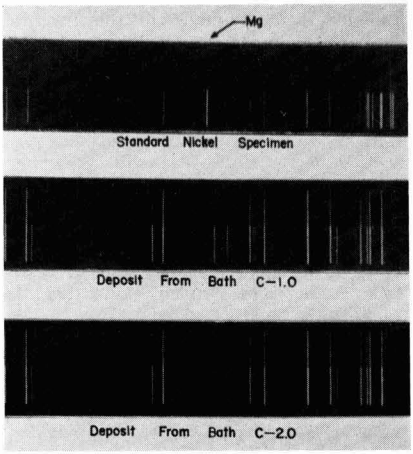

Fig. 18. Magnesium lines in the spectrum of nickel deposited from Wesley bath containing different concentrations of magnesium chloride.

Mechanical properties are affected by a large number of factors and many theories have been propounded to account for the net influence of these factors, the latest being that of Brenner and his associates (96).

Figures 9, 10, and 11 show that up to a concentration of one normal of magnesium salts, there is no appreciable change in the mechanical properties. When the concentration of the salts is twice normal, the resultant deposit has a higher tensile strength, is less ductile, and is harder. Opinions concerning the effect of magnesium are quite contradictory (97, 52, 73, 50). The recent investigation of Brenner and his associates (96) has proved that addition of 0.5*N* sodium sulfate or potassium sulfate to Watts-type bath did not result in any appreciable effect on mechanical properties. This has been shown, in the present investigation, to be true also in the case of magnesium salts up to a concentration of 1*N*. It is also found that the effect of magnesium is almost independent of the anion associated with it. The effect of high concentration of magnesium could not be attributed to codeposition of magnesium since this metal was found only in spectroscopic amounts as will be demonstrated later. The effect may be attributed to different factors such as increased density and viscosity of the solution, changing the rate of arrival of hydrogen and nickel ions to the cathode surface, or changing the nature and thickness of the cathode film. Unfortunately, our present knowledge based on available data is not quite sufficient to clear out this point.

Figure 11 shows that there is some difference between the cross-sectional and surface hardness with a general trend toward greater hardness on the surface. A similar phenomenon was observed by Cuthbertson (98) who attributed it to the anisotropic nature of electrodeposits, but it may also be due to the finer grain size of the deposit first laid down.

Structure.—The structure of electrodeposits is quite significant because of the relation which exists between it and mechanical properties. The structure was studied in the two directions parallel to the two different directions of linear crystallization, i.e., parallel to and normal to the cathode.

The effect of magnesium on structure has not been reported except in very few general statements (7, 99). In the present investigation, some modification in the structure was noticed usually at higher concentration of magnesium. In Fig. 13, for example, it is seen that the surface structure of the deposit obtained from bath S-2.0 is somewhat finer than that obtained from bath S-0.0. Also, in Fig. 14, the deposit from bath C-2.0 has a more pronounced needle-like structure. It has already been demonstrated that this modification in structure is accompanied by a change in hardness.

Structure by x-ray diffraction.—X-ray diffraction methods were conducted to examine the influence of magnesium on the crystal structure of electrodeposited nickel, and to detect the presence of magnesium or nickel-magnesium alloys if they were present in a fairly large percentage, as was reported earlier.

X-ray diffraction patterns, Fig. 16, show that the addition of magnesium has not changed the crystalline structure of nickel which is deposited from all baths under test with a face-centered cubic structure. It has been reported previously that, according to conditions, nickel can be deposited with a face-centered cubic structure or a hexagonal close-packed structure or a combination of both (100-102).

The patterns show also that magnesium lines do not appear. It is concluded, therefore, that nickel deposits do not contain magnesium or nickel-magnesium alloys, at least not in appreciable amounts. This necessitated further analysis of the deposits for trace amounts by spectroscopic methods.

Porosity.—Porosity determines to a large extent the protective value of nickel in ordinary atmospheres. Many methods have been used for determination of porosity. While atmospheric exposure tests are the most reliable, the ferroxyl tests are extensively applied and, in many cases, they give the best reproducible results which are parallel to those obtained by atmospheric exposure tests. In the present investigation, porosity was determined by hot water and ferroxyl tests. The former did not give consistent results.

Figure 17 shows that there is no essential difference in the porosity of deposits, expressed as corrosion resistance, between the Watts- and Wesley-type baths. However, the addition of magnesium to both baths has resulted in a marked increase in corrosion resistance of the resultant deposit. Increased corrosion resistance may be the result of the lower deposition potential mentioned before. This may have reduced the tendency for the nickel deposits to be pitted.

Magnesium in nickel deposits.—Early investigators had reported that magnesium was codeposited with nickel at fairly high percentages (15, 16, 103, 97), which may amount to as high as 10%. These results had led to the belief that magnesium is codeposited with nickel from aqueous solutions and that changes in the nature (104) and whiteness (29) of these deposits are attributed to such deposition. Later investigations could not verify these earlier claims (27, 59, 105) and neither does the present investigation. Table II shows that magnesium is found in deposits from baths containing magnesium but only in spectroscopic amounts. There is, however, a gradual increase in the magnesium content following concentration of magnesium in the bath. The source of the magnesium present may be either from occluded solution or from magnesium hydroxide inclusions which may have been precipitated at the high pH prevailing in the cathode film.

Conclusions

As a result of the present investigation, it is concluded that addition of high concentration of magnesium to nickel baths makes the deposition potential of nickel more noble, reduces cathode polarization, does not change the face-centered cubic lattice of nickel, codeposits only spectroscopic traces of magnesium, increases cathode current efficiency slightly, improves the throwing power, reduces porosity, and makes nickel deposits harder, stronger, and less ductile.

In the plating industry, use can be made of the effect of magnesium additions to nickel baths. It is shown that by addition of 2*N* magnesium sulfate to the Watts bath, properties of the new bath, bath S-2.0, lie nearly midway between those of Watts and Wesley baths. This can be realized easily by inspection of Table II. It is true that the same effect can be brought about by increasing the chloride content of the Watts bath, but addition of magnesium sulfate has certain advantages:

1. Magnesium sulfate is less expensive than nickel chloride.

2. The corrosive nature of the Watts bath will not be increased, whereas it will be much increased if the nickel chloride content is increased. In the latter case, additional precautions against corrosion of the equipment will be necessary.

3. In the presence of magnesium salts, nickel baths hold their metallic concentration better than they do without magnesium salts; addition of acid to correct the pH is less often needed.

4. Addition of magnesium sulfate will improve the corrosion resistance of the deposit, whereas increasing the nickel chloride content will not improve that property. An evidence of this is the fact that the Wesley bath, which is made solely of nickel chloride, gives deposits having corrosion resistance identical to that of deposits obtained from the Watts bath. This result was found by Wesley and Carey (106) and was confirmed in the present work.

It is worthy to note that the above point stimulates the necessity of further research to determine whether or not addition of still higher concentration of magnesium sulfate to Watts bath will result in deposits having mechanical properties closer to those of deposits obtained from Wesley bath without the disadvantage of higher tensile stresses characteristic of these deposits.

Acknowledgment

Acknowledgment is made to the International Nickel Company, Inc., for furnishing materials used in this investigation.

Manuscript received Feb. 21, 1957.

Any discussion of this paper will appear in a Discussion Section to be published in the December 1959 JOURNAL.

REFERENCES

1. W. D. Bancroft, *Trans. Am. Electrochem. Soc.*, **23**, 261 (1913).
2. W. G. Horsch and Tyler Fuwa, *ibid.*, **41**, 363 (1922).
3. H. E. Haring and William Blum, *ibid.*, **44**, 313 (1923).
4. E. Mantzell, *Z. Elektrochem.*, **43**, 174 (1937).
5. L. D. Hammond, *Trans. Am. Electrochem. Soc.*, **45**, 219 (1924).
6. A. E. Nicol, *Metal Ind.* (London), **30**, 90 (1927).
7. E. F. Kern, *Trans. Am. Electrochem. Soc.*, **15**, 441 (1909).
8. F. J. Liscomb, *Quart. Rev. Am. Electroplaters' Soc.*, **1**, No. 2, 10 (1913).
9. E. W. Heil, *Monthly Rev. Am. Electroplaters' Soc.*, **3**, No. 8, 4 (1916).
10. William Blum, *Trans. Am. Electrochem. Soc.* **36**, 213 (1919).
11. C. H. Proctor, *Metal Ind.* (N. Y.) **19**, March 1921.
12. Isaac Adams, *Trans. Am. Electrochem. Soc.*, **9**, 211 (1906).
13. Isaac Adams, U. S. Pat. 100,961, March 22, 1870.
14. M. Kugel, German Pat. 117,054 Nov. 5, 1899.
15. Alfred Coehn, *Z. Elektrochem.*, **8**, 593 (1902).
16. Siemens, *Z. Anorg. Chem.*, **41**, 249 (1904).
17. K. Altmannsberger, *Oberflachentech.*, **8**, 185 (1931); *Metals and Alloys, Cur. Met. Lit. Abs.*, **2**, 306 (1931).
18. Eugen Werner, *Oberflachentech.*, **12**, 219 (1935).
19. N. I. Larin, *Korroziya i Bor'ba s Nei*, **5**, No. 3-4, 112 (1939).
20. C. W. J. Morley, *Electroplating*, **3**, 400 (1950).
21. Henry Strow, *Proc. Am. Electroplaters' Soc.*, **1947**, 201.
22. H. Krause, *Korrosion u. Metallschutz*, **16**, 304 (1940).
23. C. H. Proctor, *Metal Ind.* (N. Y.), **11**, 11 (1913).
24. R. J. Hazucha, *Monthly Rev. Am. Electroplaters' Soc.*, **4**, No. 10, 11 (1917).
25. S. Herrich, *Metal Ind.*, (N. Y.), **20**, 354 (1922).
26. A. K. Graham, *Trans. Am. Electrochem. Soc.*, **44**, 347 (1923).
27. M. R. Thompson, *ibid.*, **47**, 163 (1925).
28. C. H. Proctor, *Metal Ind.*, (N. Y.), **23**, 415 (1925).
29. C. H. Proctor and O. J. Sizelove, *Monthly Rev. Am. Electroplaters' Soc.*, **12**, No. 7, 15 (1925).
30. Samuel Gordon, *Metal Cleaning Finishing*, **2**, 765 (1930).
31. Marcel Ballay, *Trans. Electrochem. Soc.*, **62**, 91 (1932).

32. J. L. Roberts, Jr., *Monthly Rev. Am. Electroplaters' Soc.*, **23**, No. 3, 24 (1936).
33. C. H. Proctor, *Metal Ind.*, (N.Y.), **17**, 25 (1919).
34. Benjamin Fess, *Monthly Rev. Am. Electroplaters' Soc.*, **16**, No. 11, 7 (1929).
35. Eugen Werner, *Metallborse*, **20**, 1434 (1930).
36. A. V. Re, *Trans. Electrochem. Soc.*, **61**, 337 (1932).
37. H. Krause, *Mitt. Forschungsinst. Probieramt Edelmetalle*, **7**, 87 (1933).
38. M. Ballay, *Rev. Aluminum*, **11**, 2365 (1934).
39. G. Blonda, *Chimica*, **2**, 237 (1935); *Chemie et Industrie*, **35**, 328 (1935).
40. Jean Frasch, French Pat. 810,010, March 13, 1937.
41. Eugen Werner, *Werkstatt u. Betrieb*, **72**, 103 (1939).
42. Joseph Underwood, *Monthly Rev. Am. Electroplaters' Soc.*, **5**, 16, 44 (1929).
43. T. C. Eichstadt, *Metal Ind.* (London), **26**, 603 (1925).
44. Anon, *Metallwaren-Ind. u. Galvano-Tech.*, **23**, 605 (1925).
45. S. M. Kochergin, *J. Appl. Chem.* (U.S.S.R.), **12**, 44 (in French, 45) (1939).
46. S. Herrich, *Metal Ind.* (N. Y.), **16** (1918).
47. J. Underwood, *Monthly Rev. Am. Electroplaters' Soc.*, **13**, No. 9, 14 (1926).
48. L. M. Evlannikov and D. S. Neiman, *Trans. Leningrad Ind. Inst.*, 1939 No. 1, Sec. Met. No. 1, 3.
49. H. J. Richards and F. P. Menninges, *Monthly Rev. Am. Electroplaters' Soc.*, **12**, No. 7, 23 (1925).
50. Myron B. Diggin, *ibid.*, **33**, 513, 524 (1946).
51. J. Walters, *ibid.*, **4**, No. 5, 10 (1917).
52. S. Makar'eva, *Bull. acad. sci. U.S.S.R., Classe sci. math. nat., Ser. chim.*, (1938), 1211 (in English), 1223.
53. V. Kohlschuetter and E. Vuilleumier, *Z. Elektrochem.*, **24**, 300 (1918).
54. Bernard Martin, *Proc. Am. Electroplaters' Soc.*, June 1944, 206.
55. D. W. Robinson, *Metal Ind.* (N. Y.), **14**, 133 (1916).
56. W. S. Barrows, *Can. Machinery*, **40**, No. 19, **71** (1929).
57. Joseph Haas, Jr., *Metal Ind.* (N. Y.), **19**, 364 (1921).
58. C. P. Madsen, *Trans. Am. Electrochem. Soc.*, **39**, 483 (1921).
59. R. E. Harr, *Trans. Electrochem. Soc.*, **68**, 425 (1935).
60. W. A. Wesley, *et al., Proc. Am. Electroplaters' Soc.*, **36**, 79 (1949).
61. F. C. Mathers, *et al., Trans. Am. Electrochem. Soc.*, **29**, 383 (1916).
62. E. P. Later, *Foundry*, **45**, 333 (1917).
63. R. L. Dorrance and W. C. Gardiner, *Trans. Am. Electrochem. Soc.*, **54**, 303 (1928).
64. V. M. Guskov and A. Z. Rivkind, *Metallurg*, **9**, No. 1, 69 (1934).
65. Myron Diggin, *Monthly Rev. Am. Electroplaters' Soc.*, **28**, 793 (1941).
66. Max Schlotter, Brit. Pat. 459,887, Jan. 18, 1937.
67. M. R. Thompson and C. T. Thomas, *Trans. Am. Electrochem. Soc.*, **42**, 79 (1922).
68. C. T. Thomas and William Blum, *ibid.*, **45**, 193 (1924).
69. E. Raub, *Mitt. Forschungsinst Probieramt Edelmetalle*, **10**, 37 (1936).
70. C. G. Beiber and M. P. Buck, (to the International Nickel Co., Inc.) U. S. Pat. 2,117,284, May 17, 1938.
71. H. Silman, "Chemical and Electroplated Finishes," p. 286, Chapman and Hall Ltd., London (1952).
72. G. B. Hogaboom, *Metal Ind.* (N. Y.), **37**, 165 (1939).
73. M. B. Diggin, *Metal Finishing*, **39**, 13 (1941).
74. J. B. Kushner, *Monthly Rev. Am. Electroplaters' Soc.*, **29**, 751 (1942).
75. Henry Brown, (to The Udylite Corp.) U. S. Pat. 2,523,190-1, Sept. 19, 1950.
76. Henry Brown, (to The Udylite Corp.) U. S. Pat. 2,523,190-1, Sept. 19, 1950.
77. H. Komusaari, *Metalloberflache*, **6**, No. 11, 162 (1952).
78. W. A. Wesley and E. J. Roehl, *Trans. Electrochem. Soc.*, **86**, 419 (1944).
79. "Specifications and Tests for Electrodeposited Metallic Coatings," American Society for Testing Materials, Philadelphia, Pa. (1949).
80. N. Thon and Denis Kelemen, *Proc. Am. Electroplaters' Soc.*, **1947**, 128.
81. A. Harold Heatley, *Trans. Am. Electrochem. Soc.*, **44**, 283 (1923).
82. H. Bandes, *Metal Finishing*, **44**, 516 (1946).
83. A. H. W. Aten and L. M. Boerlage, *Rec. Trav. Chim. Pay-Bas*, **39**, 720 (1920).
84. William Blum and H. S. Rawdon, *Trans. Am. Electrochem. Soc.*, **44**, 397 (1923).
85. V. Kohlschutter, *ibid.*, **45**, 229 (1924).
86. H. E. Haring, *ibid.*, **49**, 417 (1926).
87. A. K. Graham, *ibid.*, **52**, 157 (1929).
88. D. J. Macnaughtan and A. W. Hothersall, *Trans. Faraday Soc.*, **24**, 387 (1928).
89. S. Glasstone and E. B. Sanigar, *Trans. Faraday Soc.*, **25**, 590 (1929).
90. B. Clark and E. O. Jones, *ibid.*, **25**, 583 (1929); **26**, 96 (1930).
91. L. B. Hunt, *J. Phys. Chem.*, **36**, 1006 (1932).
92. S. Glasstone, *Trans. Faraday Soc.*, **31**, 1232 (1935).
93. Kurt Arndt and Oskar Clemens, *Chem. Ztg.*, **46**, 925 (1922).
94. H. E. Haring, *Trans. Am. Electrochem. Soc.*, **46**, 109 (1924).
95. Ralph Verdieck, *et al., Trans. Electrochem. Soc.*, **80**, 41 (1941).
96. A. Brenner, *et al., Plating*, **39**, 865 (1952).
97. K. Engermann, *Review d'Electrochemie et d'Electrometallurgie*, p. 199, July 1912.
98. J. W. Cuthbertson, *Trans. Electrochem. Soc.*, **77**, 157 (1940).
99. R. S. Dean and M. Y. Chang, *Chem. Met. Eng.*, **19**, 83 (1918).
100. A. Colombani and J. Wyart, *Compt. rend.*, **215**, 129 (1942).
101. Ling Yang, Ph.D. Thesis University of London (1948).
102. Ling Yang, *J. Electrochem. Soc.*, **97**, 241 (1950).
103. K. Engermann, *Z. Elektrochem.*, **17**, 910 (1911).
104. A. J. Allmand and H. J. T. Ellingham, "The Principles of Applied Electrochemistry," 2nd ed., p. 361, Edward Arnold and Company, London, (1924).
105. A. A. Bulakh, *Korroziya i Bor'ba s Nei*, **4**, No. 2, 164 (1938).
106. W. A. Wesley and J. W. Carey, *Trans. Electrochem. Soc.*, **75**, 209 (1939).

Color Centers in Cadmium Fluoride

Martin Rubenstein[1] **and Ephraim Banks**

Department of Chemistry, Polytechnic Institute of Brooklyn, Brooklyn, New York

ABSTRACT

Single crystals of CdF_2, purified and containing additions of NaF, CeF_3, and equimolar quantities of NaF and CeF_3, were grown from the melt in graphite crucibles in a helium atmosphere.

Physical constants of CdF_2 were measured. Optical transmission spectra were obtained before and after x-irradiation on slices of single crystals (about 1.5 mm thick), at 28°, −78°, −190°C. Crystals containing 0.05-4 mole % NaF, when irradiated at 28° or at −78°C, showed a radiation-induced absorption near the fundamental absorption edge; this induced absorption is stable at 28°C. These same crystals, when irradiated at −190°C, showed another absorption which is unstable at −78°C. CdF_2, pure, and containing low concentrations of CeF_3, NaF, or equimolar CeF_3 and NaF, all showed one x-ray induced absorption band, unstable above −10°C. CdF_2 x-irradiated at room temperature showed a very stable absorption band.

Color centers in alkali halides (1, 2), and to a lesser extent in alkaline earth halides (3-5), have been and are being investigated extensively. Only limited data have been published on the compound CdF_2 (6, 7), and there have been no investigations on color centers in this compound.

The density, melting point, optical transmission spectrum, and lattice constant of CdF_2 have been reported (6, 7). These characteristics were reinvestigated and are reported here. Since no color centers had been reported in CdF_2, we obtained transmission spectra (200-1200 mμ and 2000-15,000 mμ) of single crystals of CdF_2, pure, and with various additions before and after x-irradiation at 28°C (room temperature), −78°C (acetone and solid CO_2), and −190°C (liquid nitrogen).

Experimental Procedures

Chemical compounds and materials.—"Standard luminescent" grade $CdCO_3$ powder[2] was purified by dissolving the carbonate in concentrated aqueous ammonia solution, filtering repeatedly, precipitating with concentrated aqueous hydrofluoric acid, and leaching this precipitate repeatedly with boiling concentrated aqueous hydrofluoric acid. The purified CdF_2 was dried and used in the preparation of single crystals with and without additives.

Cerium (III) fluoride (CeF_3) was prepared by dissolving ammonium hexanitratocerate (IV)[3] in water and reducing with 3% aqueous H_2O_2 solution; a gelatinous precipitate was obtained on acidification with aqueous hydrofluoric acid, washed repeatedly with doubly distilled water, centrifuged, and heated to dryness.

Growth of single crystals.—Single crystals of about 8 g in weight were prepared by placing CdF_2 powder, with or without additions, in covered graphite[4] crucibles; the crucibles were placed in vitreous silica tubes (one end closed); a flow of helium (purified) was maintained in the silica tube; the silica tube was placed in a furnace. The furnace temperature was raised to 1120°C and the setting of the furnace controller was lowered in a step-wise manner (cut down 10° in 2 min, held for 8 min, and then this cycle was repeated) until room temperature was reached. The additions of CeF_3 were prepared by mixing CeF_3, prepared by using the method mentioned in the previous section; the additions of NaF were prepared by mixing reagent grade NaF with CdF_2. The smaller concentration additions were made by using portions of solid solutions of larger concentrations.

Density measurements.—The density of CdF_2 was obtained by using a 10 ml solid pycnometer, fragments of melted CdF_2 (each fragment about 5 mm in diameter), and doubly distilled water as the immersion liquid. The water level in the pycnometer was reached by using a water bath maintained at 36.5°C.

Melting point.—The melting point of pure CdF_2 was determined by recording heating curves. The CdF_2 powder was placed in a graphite crucible with the same apparatus as used for crystal growth. The temperature was measured by a Pt-Pt 10% Rh thermocouple whose junction was positioned in the wall of the graphite crucible—the distance between the thermocouple junction and the melt being less than 1/32 in. The thermocouple was calibrated using gold (mp 1063°C). The furnace temperature was raised and the arrest in the plot of thermocouple temperature vs. time was noted as the melting point.

Lattice constants.—The lattice constants of pure CdF_2 and CdF_2 with additions were obtained by means of the Debye-Scherrer technique, using a 57.32 mm radius Straumanis-type camera with nickel-filtered copper radiation. Eight back-reflection lines of the x-ray diffraction diagram were measured and the precision lattice constants were

[1] Present address: Materials Engineering Depts., Solid State Electronics Engineering Dept., Westinghouse Electric Corporation, Pittsburgh, Pa.

[2] Mallinckrodt.

[3] G. F. Smith Chemical Co., certified grade. NaF was reagent grade.

[4] AUC grade from National Carbon Corp.

calculated by the Straumanis calibration (8) and the Bradley-Jay (9) extrapolations.

Crystal slices.—The single crystals grown were cylinders about 12.5 mm in diameter and 12.5 mm in height. These crystals were sliced with a diamond-impregnated saw on a milling machine. These slices were mounted in polystyrene, polished with emery papers, and the final polishing was accomplished on a metallurgist's wheel using a silk cloth, Linde "B" Alumina, and water as a lubricant.

Optical measurements.—The transmission measurements were obtained at 28°C by a Process and Instruments Co. recording spectrophotometer, and at other temperatures by a Beckman DU Spectrophotometer, using a modified cell described by Casler, Pringsheim, and Yuster (10). The primary modifications were: standard tapered joints were replaced by ball and socket joints to provide maneuverability, and the beryllium window was replaced by an aluminum foil (0.2 mm) window. Transmissions were measured against an air path.

Irradiation.—The crystal slices were x-irradiated by a Machlett OEG-50-6 x-ray tube. The tungsten target permitted the generation of a white radiation x-ray spectrum. The tube was run as a self-rectified tube at 26 ma and 42 peak kv.

Ultraviolet irradiation was accomplished by a Conte-Glo lamp (3650Å). Infrared irradiation was obtained by a commercial infrared lamp.

Results

Physical constants.—The density of CdF_2 as previously reported (6) was 6.33 ± 0.06 g/cm^3. Our pycnometric value for purified CdF_2 was 6.40 ± 0.02 g/cm^3. The density calculated from the lattice constant (5.3883Å) was 6.386 g/cm^3. The pycnometric density of CdF_2 with 16 mole % CeF_3 in solid solution was 6.32 ± 0.02 g/cm^3.

The melting point of CdF_2 as previously reported was $1049° \pm 2°C$ (6). Our value from melting point curves of purified CdF_2 was $1072° \pm 2°C$.

The lattice constant of CdF_2 (fluorite structure) previously was reported as 5.3880 ± 0.0005Å (6). Our value for the lattice constant of purified CdF_2 was 5.3883 ± 0.0005Å. The difference between these two values probably is not significant.

The lattice constants of CdF_2 with additions of NaF indicate that the limit of solid solution is at 3 mole % NaF; the lattice constants form a straight line function from pure CdF_2 to the limit of solubility of NaF in CdF_2, with lattice constants increasing with NaF concentration. Concentrations greater than 3 mole % NaF produced no further increase in lattice constant, but did produce a two phase system. The lattice constant of a sample with 3 mole % NaF in CdF_2 is 5.3897 ± 0.0005Å, which is an expansion

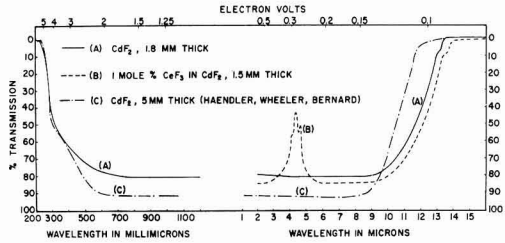

Fig. 1. Optical transmission spectra of single crystals

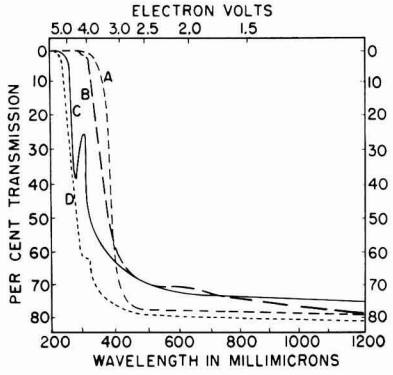

Fig. 2. Optical transmission spectra of CdF_2 with additions of CeF_3 measured at 28°C. A, CdF_2 with 10 mole % CeF_3; B, CdF_2 with 1 mole % CeF_3; C, CdF_2 with 0.01 mole % CeF_3; D, CdF_2 with 0.0005 mole % CeF_3.

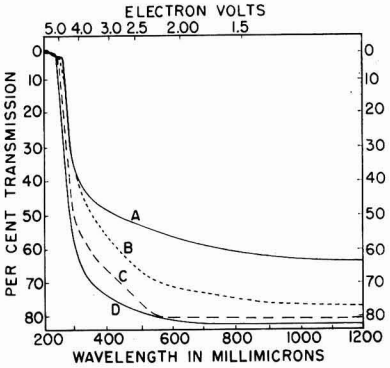

Fig. 3. Optical transmission spectra of CdF_2 with additions of NaF, measured at 28°C. A, CdF_2 with 5 mole % NaF; B, CdF_2 with 1 mole % NaF; C, CdF_2 with 0.05 mole % NaF; D, CdF_2 with 0.005 mole % NaF.

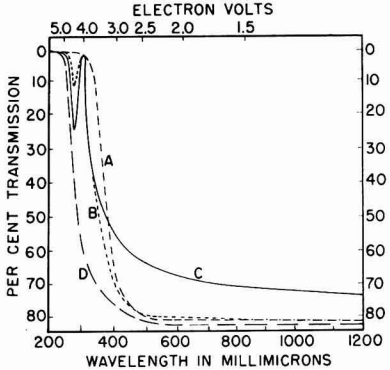

Fig. 4. Optical transmission spectra of CdF_2 with equimolar additions of NaF and CeF_3, measured at 28°C. A, CdF_2 with 5 mole % NaF and 5 mole % CeF_3; B, CdF_2 with 0.5 mole % NaF and 0.5 mole % CeF_3; C, CdF_2 with 0.05 mole % NaF and 0.05 mole % CeF_3; D, CdF_2 with 0.0005 mole % NaF and 0.0005 mole % CeF_3.

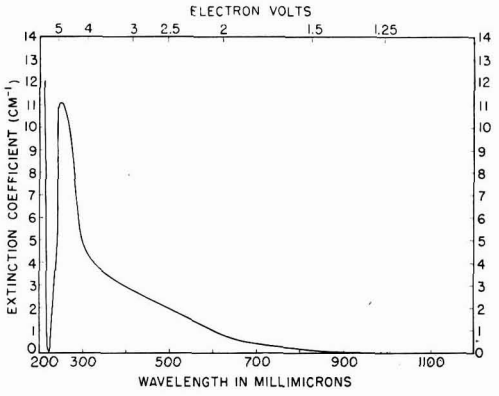

Fig. 5. Absorption spectrum of CdF_2 x-irradiated for 13 hr, x-irradiated and measured at 28°C.

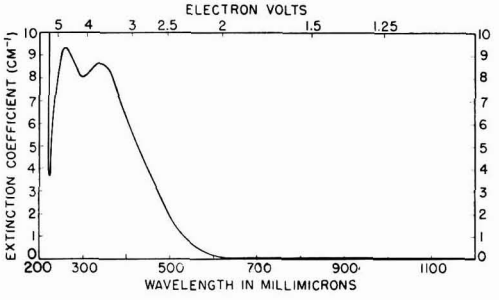

Fig. 6. Absorption spectrum of CdF_2 x-irradiated for 5 hr, x-irradiated and measured at —190°C.

of 0.0014 ± 0.0005Å. Similarly the lattice constants of CdF_2 with additions of CeF_3 indicate that the limit of solid solution is at 18 mole % CeF_3; this series also demonstrates a linear lattice expansion to 5.5032 ± 0.0005Å for the 18 mole % sample, which is an expansion of 0.0064 ± 0.0005Å per mole % CeF_3 in CdF_2. The lattice constant of a sample with 16 mole % CeF_3 in CdF_2 is 5.4890 ± 0.0005Å.

The maximum solubility of equimolar additions of NaF and CeF_3 in CdF_2 is 4.75 mole % NaF and CeF_3; this sample has a lattice constant of 5.4091 ± 0.0005Å. It should be noted that this lattice constant value would be attained in the solid solution containing no NaF at a composition of only 3.5 mole % CeF_3.

The optical transmission spectra from our data and from Haendler's (7) data are shown in Fig. 1. The fundamental absorption edge (the center of the portion of the transmission spectrum having the greatest slope before zero transmission) is at 265 mμ. Transmission spectra of polished crystal slices of CdF_2 with additions of CeF_3, NaF, and equimolar additions of CeF_3 and NaF are shown in Fig. 2, 3, and 4.

The transmission from 700 mμ to 10μ is almost constant with transmission of about 80%. At 10μ the transmission begins to fall and by 13.1μ there is no transmission; this edge is due to reststrahlen. In the range 2-15μ, crystals of CdF_2, purified, and with additions of NaF gave the same spectrum. However, CdF_2 crystals with CeF_3 and with equimolar additions of NaF and CeF_3, in addition to the reststrahlen edge, demonstrated another set of peaks around 4.40μ (2880 cm^{-1}). Two shoulders on both sides of the main peak at 4.17μ (2400 cm^{-1}), and at 4.64μ (2150 cm^{-1}) are observed in crystals of CdF_2 with CeF_3. In crystals with equimolar additions of CeF_3 and NaF, the main peak shifts to 4.45μ (2250 cm^{-1}) and the two shoulders appear at 4.18μ (2390 cm^{-1}) and 4.63μ (2160 cm^{-1}). The shoulder at the largest wave length is much more poorly defined with NaF plus CeF_3 in CdF_2 than with CeF_3 alone in CdF_2.

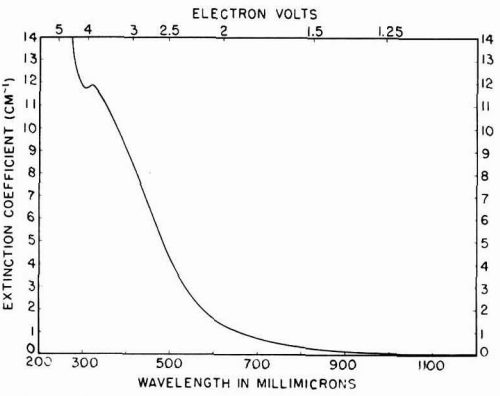

Fig. 7. Absorption spectrum of CdF_2 with 1 mole % NaF, x-irradiated 3.5 hr at 28°C, measured at —190°C.

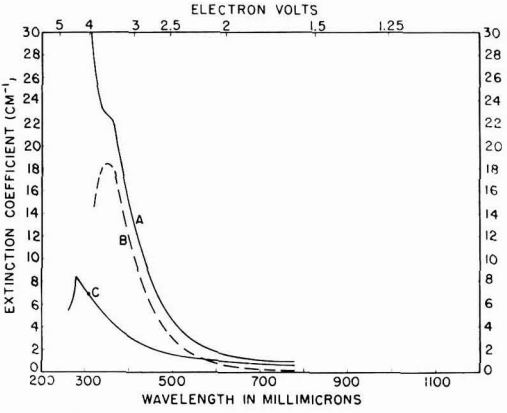

Fig. 8. Absorption spectra of CdF_2 with 1 mole % NaF. A, X-irradiated 2.6 hr at 28°C, measured at 28°C; B, Portion of Curve A bleached by heating 8 hr in 150°C oven; C, Portion of Curve A unbleached by heating 8 hr in 150°C oven.

X-radiation-induced absorption bands.—Four apparently independent x-ray-induced absorption bands were observed.

I. CdF_2 irradiated for several hours at room temperature causes an absorption band peaking at 255 mμ (see Fig. 5). This band does not bleach with heat (up to 150°C), ultraviolet radiation, or infrared radiation.

II. CdF_2, pure, and containing low concentrations of CeF_3 (less than 0.0005 mole % CeF_3), low equimolar concentrations of CeF_3 and NaF (less than 0.0005 mole % CeF_3 and NaF), and low concentra-

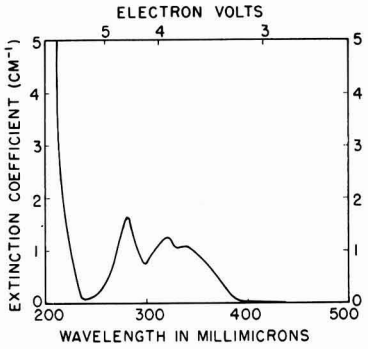

Fig. 9. Absorption spectrum of CdF_2 with 4 mole % NaF, x-irradiated 2.5 hr at −190°C, and measured at −190°C.

tions of NaF (less than 0.0005 mole % NaF) showed a double band (see Fig. 6). This band was produced by x-irradiation at −190°, or −78°C and was completely bleached by raising the temperature above −10°C. Irradiation with 3650Å at −190°, or −78°C, produced no bleaching.

III. CdF_2 with additions of NaF (in concentrations greater than 0.05 mole % NaF) when x-irradiated at −78° or 28°C produced an absorption band which could not be bleached completely. The band was relatively stable at 28°C. Partial bleaching could be accomplished by heating the crystal to 100° or 150°C in an oven, or by irradiating with 3650Å, or by irradiating with a commercial infrared lamp. The absorption band in Fig. 7 has a smaller extinction coefficient than that in Fig. 8A because the crystal in Fig. 7 was positioned further from the focal point and received a smaller dose of x-rays. Figure 8B shows that portion of A bleached by heating in an oven. Figure 8C shows the portion of A unbleached by this heating.

IV. CdF_2 with additions of NaF (also in concentrations greater than 0.05 mole % NaF) when x-irradiated and measured at −190°C produced the absorption bands in Fig. 9. This absorption was bleached by raising the temperature to −78°C or by irradiation with 3650Å at −190°C. This is a triple band.

To calculate the number of color centers per cubic centimeter, we assume that the expression derived by Smakula (11) applies. Smakula applied the theory of dispersion to F-center bands of alkali halide crystals to determine the density of F-centers. Among his assumptions were the following: the absorption transition is analogous to the 1s-2p transition in atomic hydrogen; the extinction coefficient of the bulk material is zero in the vicinity of the F-center bands. Since the bands are close to the absorption edge, this equation cannot apply exactly.

Table I summarizes some data on the above mentioned four primary x-ray induced absorptions.

Discussion and Conclusions

If one compares the transmission spectrum of 0.005 mole % NaF in CdF_2 (Fig. 3, curve D) and the spectrum of the CdF_2 without any additions (Fig. 1), one notices that the transmission of the CdF_2 with NaF is greater than that of the CdF_2 without any additions in the visible and in part of the ultraviolet. This difference of transmission is real and not instrumental. This apparent anomaly is probably caused by $S^=$ ions. If CdS is added to CdF_2 in a concentration of 1 ppm, the resulting crystal is quite yellow. The optical absorption at wave lengths less than 5000Å is total. The CdF_2 crystals prepared in this investigation undoubtedly had some $S^=$ ions but much less than 1 ppm. The addition of NaF to CdF_2, even at low concentrations of NaF, seemed to reduce the $S^=$ ion concentration.

CdF_2 with 16 mole % CeF_3 has a pycnometric density of 6.32 ± 0.02 g/cm³ and a lattice constant of 5.4921 ± 0.0005Å. A density of 6.335 g/cm³ may be calculated using this lattice constant, by assuming that a Ce (III) ion substitutes for a Cd (II) ion and an interstitial fluoride ion is present for charge compensation. If one uses a molecular weight assuming that two Ce (III) ions substitute for three Cd (II) ions, the calculated density would be 5.851 g/cm³. Therefore, it is concluded that a Ce (III) ion substitutes for a Cd (II) ion and the charge compensatory ion is an interstitial fluoride ion. This conclusion is consistent with the findings of Zintl and Udgard (12) on the CaF_2-YF_3 system and the findings of Ketelaar and Williams (13) on the SrF_2-LaF_3 system. Although the substitutional Ce (III) ion would tend to cause a small electrostatic contraction

Table I. Description of absorption bands

Crystal	Band	Position of peak, mμ	Position of peak, e.v.	Absorption coefficient in cm⁻¹ at peak	Half band-width, e.v.	No. of color centers (Smakula equation*)
Pure CdF_2, x-irradiated 15 hr at 28°C, and measured at −190°C	I, Fig. 5	255	4.85	0.97	11.1	1.125×10^{17}
Pure CdF_2, x-irradiated and measured at −190°C	II, Fig. 6	340	3.64	8.6	1.62	1.45×10^{17}
CdF_2 with 1 mole % NaF, irradiated at 28°C and measured at −190°C	III, Fig. 7	315	3.92	11.9	2.38	2.95×10^{17}
CdF_2 with 1 mole % NaF, irradiated and measured at 28°C	III, Fig. 8A	350	3.53	21.6	1.56	3.50×10^{17}
Bleachable portion of Fig. 8A	III, Fig. 8B	350	3.53	18.2	1.18	2.24×10^{17}
Unbleachable portion of Fig. 8A	III, Fig. 8C	280	4.42	8.0	1.32	1.10×10^{17}
CdF_2 with 4 mole % NaF, irradiated and measured at −190°C	IV, Fig. 9	340	3.64	1.1	0.60	6.87×10^{16}
		320	3.86	1.25	0.55	7.16×10^{16}

* The oscillator strength is assumed to be unity in these calculated values.

of the lattice, the larger size of the Ce (III) ion (ionic radius of Cd (II) = 0.97Å; ionic radius of Ce (III) = 1.07Å) would tend to cause an appreciable expansion of the lattice, and the interstitial fluoride ion (ionic radius = 1.33Å) would also cause an appreciable expansion of the lattice.

CdF_2 crystals with additions of NaF show a small lattice expansion: 0.0005Å/mole % of NaF. The expansion of CeF_3 in CdF_2 shows a much larger expansion of 0.0064Å/mole % of CeF_3. If the Na (I) ion were to enter the CdF_2 lattice interstitially in any way (either a fluoride ion could also enter interstitially or a Cd (II) ion vacancy could allow two interstitial Na (I) ions to enter the lattice) one would expect a larger lattice expansion than observed. Therefore, it has been assumed that on this basis and on the x-ray induced absorption band data (discussed in the next paragraphs), each Na (I) ion entering the CdF_2 lattice does so substitutionally for a Cd (II), and an anionic vacancy is present to achieve electrical neutrality.

In the case of solid solutions of NaF in CdF_2, both the substitution of Na (I) ion for Cd (II) ion and the formation of anionic vacancies would lead to an expansion of the lattice by virtue of the local decrease in charge density. The expansion is probably diminished by the decrease in overlap repulsion when a Cd (II) ion is replaced by a Na (I) ion and when fluoride ions are removed. This may account for the relatively small expansion actually observed. Since the ionic radius of Cd (II) ion is 0.97Å and the ionic radius of Na (I) ion is also 0.97Å, no expansion or contraction of the lattice would be expected because of a difference in ionic radii.

It seems quite apparent that the number of anionic vacancies has been reduced by a similar reduction of the number of interstitial fluoride ions in crystals of CdF_2 with equimolar additions of CeF_3 and NaF (the number of anionic vacancies here is compared to solid solutions of CdF_2 and NaF and the number of interstitial fluoride ions here is compared to solid solutions of CdF_2 and CeF_3), for the following reasons:

1. The crystals of CdF_2 with equimolar additions of CeF_3 and NaF (in concentrations greater than 0.05 mole % CeF_3 and NaF) did not show x-ray induced absorption stable at room temperature, while crystals of CdF_2 with NaF additions greater than 0.05 mole % demonstrate this absorption band (Fig. 7).

2. We have proved that CdF_2 with additions of CeF_3 has an interstitial fluoride ion for each substitutional Ce (III) ion. The lattice constant of such crystals of CdF_2 with equimolar additions of CeF_3 and NaF is less than if the same percentage of CeF_3 alone were incorporated (the expansion of CdF_2/mole % NaF is 0.0005Å, the expansion of CdF_2/mole % CeF_3 is 0.0064Å, and the expansion of CdF_2 with equimolar additions of CeF_3 and NaF is 0.0044Å/mole % of CeF_3 or NaF). Since we have indicated that CdF_2 with additions of NaF has an anionic vacancy for each substituted Na (I) ion, and since CdF_2 with additions of CeF_3 produces interstitial fluoride ions, the combination of NaF and CeF_3 incorporated together allows most of the interstitial fluoride ions to enter the anionic vacancies.

It has been proved (14) that the shoulder at about 4.18 μ (2400 cm^{-1}) is an artifact caused by CO_2 absorption in the beam path of the spectrophotometer. In using a double-beam spectrophotometer in this region of the spectrum, the response of the recording pen falls to zero since the CO_2 in the air is high enough to cause almost total absorption in both beams. In this region the electrical circuit becomes insensitive so that if the transmission is the same below and above this region, there is usually a small pip, which has been subtracted in Fig. 1A (the spectrophotometer is insensitive immediately about 4.18 μ, but is quite sensitive at wave lengths above and below this immediate region). In the case of solutions of CeF_3 in CdF_2, the absorption spectra of the crystal are rising to a peak in the region of 4.18 μ (Fig. 1B), and it could not be decided whether this was a separate peak or an artifact caused by the CO_2 absorption. Using a single-beam spectrophotometer and a nitrogen gas path for the beam instead of air, it was proved that this was not a separate peak but merely an artifact due to the CO_2 absorption (14). Mandel also obtained a value of 2×10^{-6} oscillators per atom from the calculated intensity of the absorption of the Ce (III) ion involving only a 4f shell transition. He has suggested, by analogy with other work on rare earth spectra, that this infrared absorption may be the $2F_{5/2}$-$2F_{7/2}$ transition.

The x-ray induced absorption band which is stable at 28°C could involve electrons trapped at anionic vacancies, since the crystals demonstrating this absorption do have a high concentration of anionic vacancies before x-irradiation. This band was resolvable into a bleachable and a difficultly bleachable(unbleached portion) band (see Fig. 8). Since bleaching by means of 3650Å irradiation was observed at temperatures as low as −78°C (but no bleaching was observed at −190°C), we must assume a thermal step is involved in the bleaching [Gurney and Mott indicate that a thermal step is necessary for the bleaching of F-centers in alkali halides (15)].The more difficultly bleached band may involve the absence of levels sufficiently shallow for the thermal step to be accomplished at the temperature at which the measurements were made.

Since the x-ray induced absorption band (Fig. 7) which is stable at room temperature is not observed when crystals of NaF in CdF_2 are x-irradiated at −190°C, one must conclude that a thermal step is involved in the production of the centers causing this band. The triple absorption band (Fig. 9) produced when NaF in CdF_2 is x-irradiated at −190°C is bleached by 3650Å irradiation or by warming to −78°C.

The absorption band (Fig. 6) common to pure CdF_2 and CdF_2 with low concentrations of cerium (III) fluoride, NaF, and equimolar additions of NaF and CeF_3 is not bleached by 3650Å at −78°C, or −190°C, but is bleached by warming to temperatures greater than −10°C. This band is independent of the impurities added to CdF_2. Apparently bleaching requires only a thermal step.

The increase in extinction coefficients at the high energy end of the spectra in Fig. 5, 6, and 9 is due to the logarithmic differences between the reciprocals

of small transmissions of questionable accuracy. Since the Beckman spectrophotometer is not as accurate at very low transmissions as it is at higher transmissions, the values of the transmissions at small transmissions are not very accurate, the differences between such small transmissions are less accurate, and the logarithms of such differences exaggerate the inaccuracy. Therefore, it is doubtful whether the increase in extinction coefficients at the high energy end of the spectra involved is real.

Acknowledgment

The authors wish to thank Henry F. Ivey for reading this manuscript.

Manuscript received Nov. 10, 1958. This paper is part of a thesis submitted by one of the authors (M.R.) in partial fulfillment of requirements for the Ph.D. degree to the Polytechnic Institute of Brooklyn. This paper was prepared for delivery before the Washington, D. C., Meeting, May 13-16, 1957.

Any discussion of this paper will appear in a Discussion Section to be published in the December 1959 JOURNAL.

REFERENCES

1. F. Seitz, *Revs. Modern Phys.*, **18**, 384 (1946).
2. F. Seitz, *ibid.*, **26**, 6 (1954).
3. A. Smakula, *Phys. Rev.*, **77**, 408 (1950).
4. S. Barile, *J. Chem. Phys.*, **20**, 297 (1952).
5. J. H. Schulman, R. J. Ginther, and R. D. Kirk, *ibid.*, **20**, 1966 (1952).
6. H. M. Haendler and W. J. Bernard, *J. Am. Chem. Soc.*, **73**, 5218 (1951).
7. H. M. Haendler, G. M. Wheeler, Jr., and W. J. Bernard, *J. Optical Soc. Am.*, **43**, 215 (1953).
8. M. E. Straumanis, *J. Appl. Phys.*, **20**, 726 (1949).
9. A. J. Bradley and A. H. Jay, *Proc. Phys. Soc.*, **44**, 563 (1932).
10. R. Casler, P. Pringsheim, and P. Yuster, *J. Chem. Phys.*, **18**, 887 (1950).
11. A. Smakula, *Z. Physik*, **59**, 603 (1930).
12. E. Zintl and A. Udgard, *Z. anorg. u. allgem. Chem.*, **240**, 150 (1939).
13. J. A. A. Ketelaar and P. J. H. Williams, *Rec. trav. chim.*, **56**, 29 (1937).
14. G. Mandel, Bachelor's Dissertation, Polytechnic Institute of Brooklyn, 1957.
15. (a) R. W. Gurney and N. F. Mott, *Trans. Faraday Soc.*, **34**, 506 (1938).
    (b) N. F. Mott, *Proc. Phys. Soc.*, **50**, 196 (1938).

The Luminescent Center in Self-Activated ZnS Phosphors

J. S. Prener and D. J. Weil

Research Laboratory, General Electric Company, Schenectady, New York

ABSTRACT

A model for the ground state of the self-activated luminescent center in ZnS phosphors proposed by Prener and Williams in 1956 has been confirmed experimentally. It is shown that a Zn vacancy is involved in the blue luminescence and that the spectrum depends on whether the required coactivator can occupy a Zn or S site near the vacancy. The calculated energy levels of the center using a simple model are in qualitative agreement with the observed spectra.

If pure ZnS is heated to a high temperature in the presence of a halogen (e.g., NaCl or H_2S, HCl gas mixture) or with small amounts of Al or Ga (1), a blue emitting phosphor is obtained. The atomic nature of the defect responsible for this "self-activated" emission has been the subject of much discussion in the literature (2, 3). Recognizing that a neutral Zn vacancy may act as a double acceptor, Kröger and Vink (2) proposed that this defect was such a vacancy with one of the bound holes ionized. However, a concentration of such centers of about 2×10^{16} cm^{-3} or greater should have led to a measurable paramagnetic contribution to the magnetic susceptibility of this phosphor in the experiments of Bowers and Melamed (3); yet they failed to find such a contribution. More recently, Prener and Williams suggested that the defect in question consists of a Zn vacancy in which both the holes are ionized, leaving the vacancy doubly negatively charged, and an ionized donor impurity (Cl, Br, I, Al, or Ga) associated at nearest possible sites in the ZnS lattice (4). Such a center, in its ground electronic state, is not paramagnetic.

It is the purpose of this paper to present experimental evidence for such an associated center. The role of Zn vacancies in the formation of the center is shown by the expected variation in the intensity of the blue fluorescence with changes in the pressure of S vapor over the phosphor during preparation. That the coactivator is also part of the center is shown by the differences in spectral distribution of the fluorescence when halogens or group IIIB elements are used as coactivator impurities. Deductions based on a model for such a center are shown to be consistent with these observed differences.

In a series of papers Bube (5) and Addamiano (6) discussed the preparation of self-activated ZnS with blue fluorescence, by high-temperature firing in air or nitrogen without the use of any added coactivators. Their interpretation was that the center responsible for the fluorescence was a Zn vacancy which was formed thermally at high temperatures. Careful and numerous experiments performed in our laboratories have convinced us that previous observations were the result of faulty experimental techniques. If a "luminescent grade" of ZnS is carefully protected from dust and is fired in a stream of purified, dry H_2S in clean apparatus, first at low temperatures (400°C for several hours) and then slowly at increasingly higher temperatures until 1150°-1200°C is reached, no visible luminescence is found even at liquid nitrogen temperature! If, on the

other hand, the firing temperature is raised rapidly to 1150°C, very frequently bright blue luminescence is indeed observed. We presume that even the best ZnS available probably has some coprecipitated halide which can be volatilized or converted to sulfide by low temperature H_2S firing. At higher temperatures the halogen may diffuse into the ZnS lattice producing the characteristic blue luminescence. Our general conclusion is therefore that under conditions most likely to produce Zn vacancies (H_2S firing rather than nitrogen) no self-activated luminescence can be induced in ZnS without the use of coactivators.

Experimental and Results

Emission Spectra of ZnS:xCu:yAl *as a Function of Atmosphere during Preparation*

Many phosphors containing various amounts of Cu and Al were prepared by adding appropriate quantities of copper sulfate and aluminum sulfate solutions to pure ZnS and firing at 950°-975°C for 2 hr in a stream of purified and dry H_2S. Parts of these phosphors, all of which showed bright blue and green fluorescence under 3650Å excitation, were refired in oxygen-free, dry H_2 for an additional 2 hr at the same temperature. Emission spectra were taken at liquid nitrogen temperatures with 3650Å excitation (General Electric BH-4 high-pressure mercury lamp with a Corning 5840 filter) using a recording spectroradiometer. The powdered samples were contained in a holder which permitted us to position each sample accurately with respect to the exciting light and the entrance slit of the spectroradiometer and also to obtain spectra at low temperatures.

In Fig. 1 are shown emission spectra, typical of many obtained, for phosphors in which $x = 0$, $x < y$, $x = y$, and $x > y$. The results show the sensitivity of the "self-activated blue" emission to H_2 refiring and the absence of any such marked effect on the "copper green" emission and the "copper blue" emission always obtained when $x > y$. The different spectral distribution of the copper blue band at liquid nitrogen temperatures compared to the self-activated blue emission has been cited as evidence that two different types of centers are responsible for these two blue bands (7). The different behavior of the fluorescent intensity after H_2 refiring is further evidence for this.

To test the reversibility of this effect on the intensity of the blue self-activated emission after H_2 refiring, as well as its reproducibility, four phosphor samples were prepared, all of the composition ZnS:5 x 10^{-6} Cu:10^{-4} Al. These were then subjected to the following firing schedules at 975°C: (*a*) 2 hr in H_2S; (*b*) 2 hr in H_2S followed by 2 hr in H_2; (*c*) 2 hr in H_2S, 2 hr in H_2, 2 hr in H_2S; (*d*) 2 hr in H_2S, 2 hr in H_2, 2 hr in H_2S, and finally 2 hr in H_2. The emission spectra shown in Fig. 2 show again that there is a marked decrease in the intensity of the blue self-activated band on H_2 refiring. Furthermore, the effect is clearly reversible and reproducible. There appears also to be a small decrease in the green copper band intensity after H_2 refiring of those phosphors in which $y > x$. For $y = x$ and $y < x$, no such effect is observed within the limits of experimental reproducibility. The effect of H_2 refiring on the green band is very much smaller than on the self-activated blue band. The reason for this effect is not known at present but may very well be due to the increased association at nearest neighbor sites of the negatively charged copper acceptors with the larger concentration of available positively charged Al donors available at the high temperature when the phosphor is fired in H_2 and ionized Zn vacancies are destroyed. The effect of H_2 refining on the intensity of the self-activated blue emission described above for ZnS:Al has also been observed in ZnS:Ga phosphors. (See the third section of Discussion).

Spectral Distribution of the Self-Activated Emission in Cubic ZnS

ZnS:Al and ZnS:Ga phosphors were prepared as described in the previous section, except that the firing was carried out at 850°C. ZnS:Cl and ZnS:Br phosphors were prepared by firing ZnS in a stream of H_2S containing several per cent of anhydrous HCl or HBr at 850°C for 2 hr. Bright blue fluorescing materials were obtained in all cases. The low firing

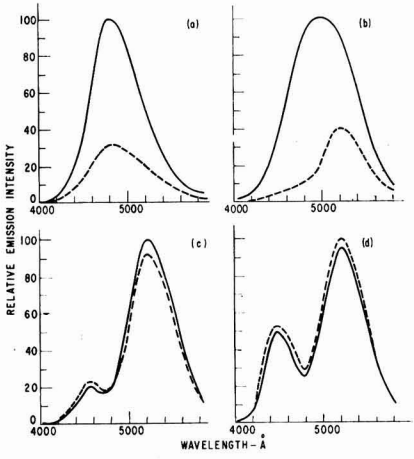

Fig. 1. Typical emission spectra at —196°C with 3650Å excitation of ZnS:xCu:yAl phosphors fired at 950°C in H_2S ————; and refired at 950°C in H_2 - - - - - . (a) x = 0; y = 10^{-4}; (b) x = 2 x 10^{-6}; y = 10^{-4}; (c) x = 10^{-4}; y = 10^{-4}; (d) x = 10^{-4}; y = 10^{-5}.

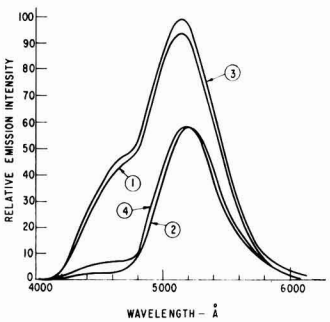

Fig. 2. Emission spectra at —196°C with 3650Å excitation of ZnS:5 x 10^{-6} Cu:10^{-4} Al subjected to the firing schedules described in the text.

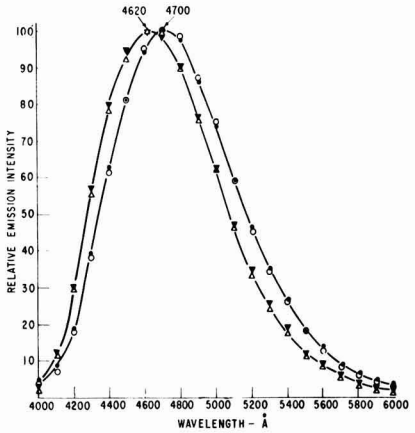

Fig. 3. Emission spectra at room temperature with 3650Å excitation of ZnS:10^{-5} Al, solid circle; ZnS:10^{-3} Ga, open circle; ZnS:Cl, open triangle; ZnS:B, solid inverted triangle; all fired at 850°C.

temperatures were used to assure the absence of any hexagonal phase in the ZnS phosphors, since it is known that the emission spectra are different for the cubic and hexagonal phases. The absence of any hexagonal phase was confirmed by obtaining long exposure x-ray diffraction patterns of the fired phosphors.

The emission spectra of four phosphors taken at room temperature are shown in Fig. 3. It is seen that the spectra of ZnS:Al and ZnS:Ga are identical as are the spectra of ZnS:Cl and ZnS:Br. However, the peak of the emission band of the latter two phosphors occurs at about 80Å toward shorter wave lengths than the peak of the first two phosphors. This effect of the coactivator impurity on the spectral distribution of the self-activated blue emission was also observed by Kröger and Dikhoff (1), although they placed no significance on this difference and indicated that the blue emission was independent of the coactivator. We believe this 80Å difference to be significant and this is discussed later in this paper.

The emission spectra of those phosphors containing halogen were also found to be independent of how the halogen was introduced. In Fig. 4, the emission spectra of halogen-containing phosphors prepared from HCl and H_2S, HBr and H_2S, NaCl, and NaI are compared to the phosphor ZnS:Al (10^{-3}) by plotting the ratios of the emission intensities (normalized to unity at 4700Å) at various wave lengths. The emission spectrum of the self-activated emission was found not to depend on the concentration of the coactivator. In Fig. 5, emission spectra of ZnS:Al (10^{-4}, 5×10^{-5}) and ZnS:Ga (10^{-3}, 10^{-4}) are compared to ZnS:Al (10^{-3}) by again plotting the ratios of emission intensities. Similar measurements of the emission intensity of various phosphors as a function of wave length compared to ZnS:Al (10^{-3}) also showed that the emission spectra were dependent neither on firing temperature so long as no hexagonal ZnS were formed, nor on the intensity of the exciting ultraviolet. The general conclusion is that

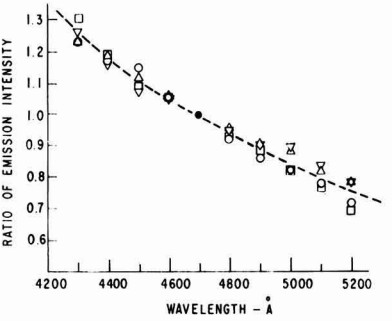

Fig. 4. Ratio of the emission intensity at room temperature and 3650Å excitation of the various phosphors given below to the emission intensity of ZnS:10^{-3} Al, as a function of wave length. (Intensities normalized to unity at 4700Å). Open circle, ZnS fired in H_2S containing HCl at 850°C; open square, ZnS fired in H_2S containing HBr at 850°C; open triangle, ZnS:5% NaCl fired in N_2 at 850°C; open inverted triangle, ZnS:2% NaI fired in N_2 at 925°C.

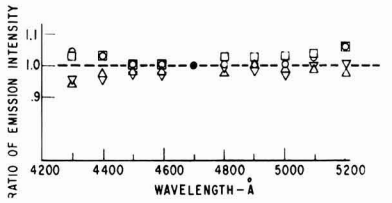

Fig. 5. Ratio of the emission intensity at room temperature and 3650Å excitation of the various phosphors given below to the emission intensity of ZnS:10^{-3} Al as a function of wave length. (Intensities normalized to unity at 4700Å). All phosphors were fired in H_2S at 850°C. Open circle, ZnS:10^{-4} Al; open square, ZnS:5×10^{-5} Al; open triangle, ZnS:10^{-3} Ga; open inverted triangle, ZnS:10^{-4} Ga.

the spectral distribution of the blue emission depended only on whether the coactivator used was one of the Group III or Group VII elements.

Discussion

Formation and Ionization of Zn *Vacancies*

ZnS phosphors prepared by firing at high temperatures will contain neutral Zn vacancies and S vacancies (V_{Zn}^0 and V_S^0) whose equilibrium concentration will depend on the temperature and pressure of S in the gas phase with which the solid is in equilibrium. The assumption will be made that lattice defects in ZnS are primarily vacancies, not interstitials. Work on CdS (8), CdSe (9), and other binary compounds has indicated that metal atom vacancies can behave as acceptors. Since the removal of a neutral Zn atom from ZnS removes two of the eight electrons in the four bonds to the neighboring sulfurs, a neutral Zn vacancy has two holes bound in its vicinity. These may be thermally ionized into the valence band as shown in Eqs. [1] and [2].

$$V_{Zn}^0 \rightleftharpoons V_{Zn}^{-1} + p - \epsilon_1 \qquad [1]$$

$$V_{Zn}^{-1} \rightleftharpoons V_{Zn}^{-2} + p - \epsilon_2 \qquad [2]$$

In these equations, p represents a hole in the valence band, and ϵ_1 and ϵ_2 are the thermal ionization energies. The energy released by the optical capture of a hole into V_{Zn}^{-1} can be computed approximately us-

ing a Bethe model (10). This energy would be equal to the ionization energy of a hydrogen atom in a polarizable medium whose static dielectric constant is that of ZnS. Similarly the energy released on capturing a hole optically into V_{Zn}^{-2} should be approximately the ionization energy of He^{+1} in a polarizable medium (11). For ZnS, with a static dielectric constant of 8, these energies are 0.21 e.v. and 0.84 e.v. These values can only be approximate for ZnS due to the fact that the holes move in small orbits around the charged Zn vacancies so that the details of the potential in the vicinity of the vacancy are important. Once the hole is captured in the center, the atoms surrounding the vacancy will move to new equilibrium positions, and the energy required for the optical ionization of the hole will be greater than 0.21 or 0.84 e.v. depending on the lattice polarization energy. The thermal ionization energies ϵ_1 and ϵ_2 will lie somewhere between these two limits (12).

Association of Charged Zinc Vacancies and Ionized Donor Impurities

Coactivator impurities such as Al or Cl in ZnS are donors and therefore constitute a single positively charged species when ionized (13). For the thermal ionization of Al we have

$$Al^0 \rightleftharpoons Al^{+1} + n - \epsilon_3 \qquad [3]$$

Here n is a conduction electron. These ionized centers interact coulombically with negatively charged Zn vacancies, and the equilibrium distribution of these two defects will therefore be a nonrandom one. Of particular interest is the strong interaction between V_{Zn}^{-2} and Al^{+1} or Cl^{+1}. For a concentration of each of 10^{-4}M at 1000°K, the fraction of V_{Zn}^{-2} and Al^{+1} associated into $V_{Zn}^{-2} - Al^{+1}$ pairs at neighboring Zn sites is about 0.9 (14). For $V_{Zn}^{-2} - Cl^{+1}$ the fraction will be even higher. At a large distance the associated pair appears as a single negative charge in ZnS and should therefore be capable of binding a hole in a localized orbital. This hole can be thermally ionized as follows

$$(V_{Zn} - Al)^0 \rightleftharpoons (V_{Zn} - Al)^{-1} + p - \epsilon_4 \qquad [4]$$

The energy released by the optical capture of a hole into the ionized acceptor can be estimated using a Bethe-type model in which the hole moves in the potential of a $-2e$ and a $+1e$ charge separated by a distance R in a polarizable medium. For cubic ZnS the distance R is 2.35Å when Cl, Br, or I are the donors and 3.84Å when Al or Ga are the donors. The particular group IIIB or VIIB impurity used would be expected to affect the position of the localized level only to a slight extent because the trapped hole moves in an orbit close to the doubly negatively charged Zn vacancy and therefore does not feel the inner potential peculiar to the donor impurity. Our primary interest is the difference in the binding energy of a hole to the two types of associated pairs characterized by the different distances R and particularly the sign of this difference. Therefore, the binding energy of a hole to such an associated pair embedded in a medium of dielectric constant 8 was calculated as a function of R. At very small or very large values of R the binding energy

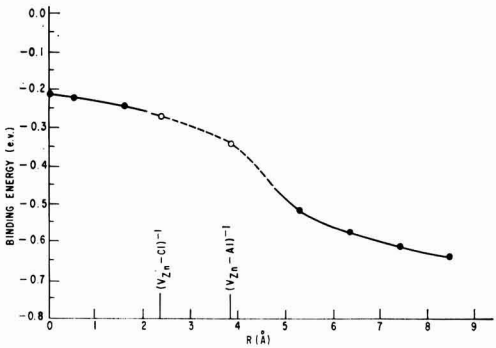

Fig. 6. Binding energy of a positive hole to fixed charges of $-2e$ and $+1e$ separated by a distance R (Å) in a polarizable medium of dielectric constant 8.

of a hole can be obtained by a perturbation treatment using hydrogen 1*s* wave functions. The binding energy in electron volts is:

$$E(\text{small } R) = -\frac{27.2}{2k^2} + \frac{27.2}{k^2R}\left[(0.529\,k - R) - (0.529\,k + R)\,e^{-2R/0.529\,k}\right] \qquad [5]$$

$$E(\text{large } R) = -\frac{54.4}{k^2} + \frac{27.2}{k^2R}\left[0.529\,k - (0.529\,k + 2R)\,e^{-4R/0.529\,k}\right] \qquad [6]$$

E is shown as a function of R in Fig. 6 for the dielectric constant $k = 8$. The two values of R of particular interest do not lie within the range where the simple perturbation treatment would be expected to be valid. Accordingly, for these two distances the energies were calculated using the continued fraction solutions given by Baber and Hassé for the ground state of the unsymmetrical hydrogen molecule ion (15). These two values are also given in Fig. 6 and are seen to differ by 0.07 e.v., the level due to $(V_{Zn} - Al; Ga)^{-1}$ lying higher above the valence band than the level due to $(V_{Zn} - Cl; Br; I)^{-1}$. This energy difference amounts to a 100Å difference at 4700Å and is therefore in accord with the observed difference of the emission spectra as shown in Fig. 3, both as to the direction and magnitude of the difference, provided that we assume that the lattice polarization energy following excitation of the phosphor is largely independent of the donor impurity making up the center. As was pointed out, the hole moves in an orbit close to the Zn vacancy so that it is not unreasonable to imagine that it is the vacancy which primarily governs the lattice polarization.

Concentration of Luminescent Centers $(V_{Zn} - Al)^{-1}$ as a Function of Sulfur Pressure

ZnS, heated for a sufficiently long time in a very slow stream of a gas, will attain a stoichiometry dependent on the composition of the gas (16). When H_2 is used as the gas atmosphere during firing we can show that the final effective sulfur pressure with which the solid phase is in equilibrium and which therefore determines the stoichiometry of the solid

is obtained by a solution of the equation (taking sulfur to be S_2 molecules in gas phase):

$$2p_{S_2}^{3/2} + K_d P_{H_2} p_{S_2} - K_p = 0 \qquad [7]$$

P_{H_2} is the pressure of H_2, usually 1 atm, and K_d is the equilibrium constant for the dissociation of H_2S.

$$H_2 + \frac{1}{2} S_2 \rightleftharpoons H_2S \qquad [8]$$

$$K_d = (p_{H_2S}/p_{S_2}^{1/2} \cdot p_{H_2}) \qquad [9]$$

K_p is the equilibrium constant for the dissociation of ZnS molecules in the gas phase multiplied by the equilibrium pressure of ZnS molecules at the firing temperature:

$$ZnS \text{ (solid)} \rightleftharpoons ZnS \text{ (gas)}; \; p_{ZnS} = \text{constant} \qquad [10]$$

$$ZnS \text{ (g)} \rightleftharpoons Zn \text{ (g)} + \frac{1}{2} S_2 \text{ (g)} \qquad [11]$$

$$K_p = K_{ZnS} \cdot p_{ZnS} = p_{Zn} \cdot p_{S_2}^{1/2} \qquad [12]$$

At 1000°K, Kelley (17) gives K_d as 144 $atm^{-1/2}$ and, according to Pogorelyi (18), $K_p = 1.63 \times 10^{-10}$ $atm^{3/2}$. With $P_{H_2} = 1$ atm, we get from Eq. [7] that $p_{S_2}^{1/2} = 1.06 \times 10^{-6}$ $atm^{1/2}$. On the other hand, if H_2S is used as the firing gas, we can show that p_{S_2} is obtained from:

$$2K_d p_{S_2}^2 + 2p_{S_2}^{3/2} - p_{S_2}^{1/2} (P_{H_2S} + K_p K_d) - K_p = 0 \qquad [13]$$

With P_{H_2S}, the initial pressure of H_2S, equal to 1 atm, we get from Eq. [13] that $p_{S_2}^{1/2} = 0.15$ $atm^{1/2}$. These results show that firing ZnS phosphors for a sufficiently long time in a slow stream of H_2S at 1000°K followed by H_2 is equivalent to lowering the square root of the sulfur pressure by about five orders of magnitude.

We did not determine whether or not the gas flow rates we used were sufficiently slow to maintain equilibrium between the solid and gas phases. Thus in our experiments the ratio of effective values of $p_{S_2}^{1/2}$ might very well not have been as low as 10^{-5}. For this and, more important, for other reasons to be pointed out in the following paragraphs, only a qualitative comparison of experiment with calculations can be made at this time.

The method developed by Kröger and Vink (19) for calculating the concentrations of various defects as a function of sulfur pressure, can be applied to the system ZnS:Al (2.54×10^{18} cm^{-3}) by using the values of the equilibrium constants given in Table I.

If the concentrations of defects, impurities and charge carriers are expressed as number per cubic centimeter, then K_1 to K_4, which are the equilibrium constants for the reactions given in Eqs. [1] to [4], are taken to have the form $K = 2(2\pi mkT/h^2)^{3/2} \exp(-\epsilon/kT)$, the free electron mass being used. K_g is the equilibrium constant for the thermal production of electron-hole pairs.

$$ZnS \text{ (ground state)} \rightarrow n + p - \epsilon_g \qquad [14]$$

$$K_g = [n]\,[p] \qquad [15]$$

K_g is taken to be of the form $4\,(2\pi mkT/h^2)^3 \exp(-\epsilon_g/kT)$. Finally, the reciprocal of K_a is the equilibrium constant for the dissociation of the associated pair

$$(V_{Zn} - Al)^{-1} \rightleftharpoons V_{Zn}^{-2} + Al^{+1} \qquad [16]$$

$$K_a = [(V_{Zn} - Al)^{-1}]/[V_{Zn}^{-2}]\,[Al^{+1}] \qquad [17]$$

Neutral Zn vacancies are formed by the reaction

$$(1 - \delta)\; ZnS + \delta/2\; S_2 \rightleftharpoons Zn_{1-\delta}\; (V_{Zn}^{0})_\delta S \qquad [18]$$

The application of the law of mass action for $\delta << 1$ gives

$$K_v = [V_{Zn}^{0}]\; p_{S_2}^{-1/2}\; cm^{-3}\; atm^{-1/2} \qquad [19]$$

Since K_v is unknown for ZnS, the concentrations of all other defects and charge carriers were calculated as functions of $K_v\, p_{S_2}^{1/2}$ for ZnS:Al (2.54×10^{18} cm^{-3}) at 1000°K using the method of reference (19). The Schottky constant for ZnS, giving the equilibrium product of the concentrations of neutral Zn and S vacancies, is also unknown, so that we assumed that, in the range of sulfur pressures used, the concentration of ionized sulfur vacancies which can act as donors was much less than the concentration of Al^{+1}. After the high-temperature concentrations were determined, the concentrations at liquid nitrogen temperature were found by assuming that the total concentration of lattice defects and associated pairs is frozen in at 1000°K as the phosphor is cooled, whereas electrons and holes distribute themselves among the various available states in accordance with the equilibrium Eqs. [1] to [4] and [14] using the values of the equilibrium constants at 77°K also given in Table I. The results, shown graphically in Fig. 7, are to be taken only as an indication of the behavior of ZnS:Al because of the approximations used, some of which have been cited. Somewhat different approximations would still lead to the same general qualitative behavior with varying sulfur pressure. Nevertheless, it is of interest to note that the model used leads to the concentration of

$$(V_{Zn} - Al)^{-1}$$

Table I. Equilibrium constants for the system ZnS:Al

	Temp, 77°K		Temp, 1000°K		
	K_i	ϵ_i (e.v.)*	K_i	ϵ_i (e.v)*	Remarks
K_a	—	—	2.3×10^{-17}	—	From calc. deg. of assoc. (14)
K_1	2.1×10^{-20}	0.58	4.1×10^{17}	0.51	Assumed same as K_4
K_2	3.3×10^{-136}	2.32	7.6×10^{9}	2.0	ϵ_2 taken as four times ϵ_1
K_3	1.2×10^{2}	0.25	1.2×10^{19}	0.22	From thermal glow curve data (20)
K_4	2.1×10^{-20}	0.58	4.1×10^{17}	0.51	From temperature quenching data (21)
K_g	1.6×10^{-204}	3.66	1.6×10^{24}	3.20	From optical band gap data applying a correction of -5×10^{-4} ev/deg (22).

* All levels assumed to decrease with temperature at the same rate as the optical band gap.

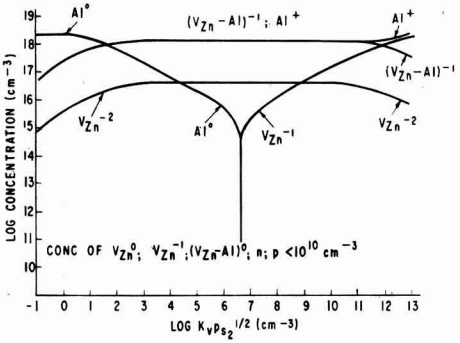

Fig. 7. Concentration of defects in ZnS:Al (2.54×10^{18} cm^{-3}) at —196°C after equilibration at 1000°K and various pressures of sulfur in the gas phase.

being practically constant at one-half the total Al concentration over a range of values of $p_{S_2}^{1/2}$ of about eight orders of magnitude. The indicated decrease in the concentration of this associated pair at low sulfur pressures is in accord with the experimental results given in this paper and the interpretation that a Zn vacancy is part of the luminescent center. The indicated decrease in the concentration of self-activated luminescent centers at high sulfur pressures was observed in CdS:Ga by Kröger, *et al.* (8), although the authors interpreted their results differently. Also, over a wide range of sulfur pressures the concentrations of Al°, V_{Zn}°, V_{Zn}^{-1}, and $(V_{Zn} - Al)^{\circ}$ are less than 2×10^{16} cm^{-3}. Since these would be paramagnetic defects, it can be seen that only under special conditions of preparation would this phosphor be expected to have a measurable paramagnetic susceptibility.

Summary

Associated $(V_{Zn} - Al; Ga)^{-1}$ or $(V_{Zn} - Cl; Br; I)^{-1}$ pairs can form in ZnS containing Al, Ga, or a halogen as an impurity due to the strong coulombic interaction between ionized donor impurities and Zn vacancies. Calculations show their concentration can remain fairly constant at one-half the concentration of the donor impurity over a considerable range of sulfur pressures. At decreasing sulfur pressures the concentration of these pairs decreases. This is in accord with the observed decrease in the intensity of the blue luminescence after H_2 refiring of the self-activated phosphor.

The peak of emission spectrum of the blue luminescence depends on whether a group IIIB or group VIIB element is used as a coactivator indicating that the coactivator is a part of the luminescent center. Simple considerations suggest that the observed shift in peak position is in the right direction and of the correct order of magnitude.

On the basis of these results we conclude that the luminescent center in self-activated ZnS is a V_{Zn}^{-2} associated with the coactivator at a nearest possible site in ZnS. The associated pair gives rise to a localized acceptor level above the valence band just as do the usual activators such as Cu or Ag.

Acknowledgments

The authors acknowledge the help given them by Dr. F. J. Studer and Miss G. Lloyd in obtaining the emission spectra of the many phosphors prepared in the course of this study. Dr. B. Segall aided greatly in obtaining the solutions to the two-center problem used in this paper. Dr. D. T. F. Marple carried out the careful measurements of intensity ratio as a function of wave length of many phosphors containing Al, Ga, Cl, and Br. Finally the many discussions with Dr. F. E. Williams were instrumental in clarifying our ideas on the interpretation of the data and the model presented here for the self-activated luminescent center.

Manuscript received Oct. 27, 1958. This paper was prepared for delivery before the New York Meeting, April 27-May 1, 1958.

Any discussion of this paper will appear in a Discussion Section to be published in the December 1959 JOURNAL.

REFERENCES

1. F. A. Kröger and J. Dikhoff, *Physica*, **26**, 297 (1950).
2. F. A. Kröger and H. J. Vink, *J. Chem. Phys.*, **22**, 250 (1954).
3. R. Bowers and N. T. Melamed, *Phys. Rev.*, **99**, 1781 (1955).
4. J. S. Prener and F. E. Wiliams, *J. Chem. Phys.*, **25**, 361 (1956).
5. R. H. Bube, *Phys. Rev.*, **80**, 655 (1950); *J. Chem. Phys.*, **20**, 708 (1952); *J. Phys. Chem.*, **57**, 785 (1953).
6. A. Addamiano, *J. Chem. Phys.*, **23**, 1541 (1955).
7. R. E. Schrader and S. Larach, *Phys. Rev.*, **103**, 1899 (1956).
8. F. A. Kröger, H. J. Vink, and J. Van den Boomgaard, *Z. physik. Chem.*, **203**, 1 (1954).
9. D. de Nobel, Thesis, University of Leiden, May, 1958.
10. H. Bethe, M.I.T. Radiation Laboratory Report No. 43-12 (1942).
11. H. M. James and K. Lark-Horowitz, *Z. physik. Chem.*, **198**, 107 (1951).
12. M. Schön, *Z. Naturforschg.*, **6a**, 287 (1951).
13. J. S. Prener and F. E. Williams, *This Journal*, **103**, 342 (1956).
14. J. S. Prener, *J. Chem. Phys.*, **25**, 1294 (1956).
15. W. G. Baber and H. R. Hassé, *Proc. Cambridge Phil. Soc.*, **31**, 564 (1935).
16. J. Bloem and F. A. Kröger, *Z. physik. Chem. (Frankfurt)*, **7**, 15 (1956).
17. K. K. Kelley, *U. S. Bur. Mines Bull. 406* p. 20 (1937).
18. A. D. Pogorelyi, *J. Phys. Chem. U.S.S.R.*, **22**, 731 (1948).
19. F A. Kröger and H. J. Vink, Relations between the Concentrations of Imperfections in Crystalline Solids, in "Solid State Physics," Vol. 3, pp. 307-435, Academic Press, Inc. (1956).
20. W. Hoogenstraaten, *This Journal*, **100**, 356 (1953); F. A. Kröger, *Physica*, **21**, 637 (1956).
21. M. Schön, *Z. Naturforschg.*, **6a**, 287 (1951).
22. W. W. Piper, *Phys. Rev.*, **92**, 23 (1953).

A Double Diffused Silicon High-Frequency Switching Transistor Produced by Oxide Masking Techniques

J. F. Aschner, C. A. Bittmann, W. F. J. Hare, and J. J. Kleimack

Bell Telephone Laboratories, Incorporated, Murray Hill, New Jersey

ABSTRACT

The relative merits of two double diffused transistor structures are discussed, one of which employs a localized emitter. A process for producing the localized emitter structure is described employing the masking property of SiO_2 against the subsequent phosphorus diffusion. The dimensions of each emitter are controlled closely by etching away this oxide mask from only those regions not protected by a specially prepared photo resist coating. Transistors have been produced which switch 30 ma with a gain of 12, in times in which the sum of the turn-on, storage, and turn-off time is less than 0.1 μsec. Small signal alphas of 0.97, and alpha cut-off frequencies in the common base connection in excess of 300 mc have been achieved.

The need for high-frequency transistors, requiring extremely narrow base layers, has led to the development of new fabrication techniques. The adaptation of solid-state diffusion (1) has been found to permit a high degree of control of both the depth and concentration of an impurity necessary to produce such layers. In this paper an n-p-n silicon switching transistor is discussed, in which both the emitter and base layers are formed by diffusion. By making use of the masking properties of a specially prepared oxide layer, precise regulation of the geometry of the emitter region is attained. The electrical characteristics of transistors prepared by these techniques are presented.

Double Diffused Structure

In Fig. 1(a) the essential features of a transistor produced by a double diffusion process (2) are illustrated. A p-type impurity is diffused first into the n-type wafer to form a collector junction about 0.2 mils from the surface. An n-type emitter dopant having a much higher impurity concentration is then diffused into this layer. This overcompensates the original diffused impurity until such a depth is reached that their concentrations are equal. The emitter junction, so formed, is located at this depth. The separation of the two junctions, defining the base layer, can be reproduced to within 0.005 mils.

In this type of transistor, since the emitter layer entirely covers the base layer, a metallic base contact is alloyed through the emitter. Furthermore, the regrowth region around this contact must form a rectifying junction with the emitter layer, in order for the device to operate as a transistor; otherwise, the base would be shorted to the emitter. With a suitable choice of materials, this technique is quite feasible, and transistors have been built this way. However, certain limitations are imposed. In order to have a rectifying junction between the base contact and the emitter layer through which it passes, an upper limit is placed on the surface concentration of the emitter diffusant, thus limiting emitter efficiency. Alternatively, the highly doped portion of the emitter immediately surrounding the base contact may be removed by an etching process. The latter, in fact, is the preferred choice but suffers from control difficulties as the electrical characteristics of the transistor are quite sensitive to the depth reached by this etch.

The present paper is concerned with a process in which the masking properties of a silicon dioxide layer against certain diffusants have been exploited to circumvent these difficulties (3, 4). By removing the oxide from selected regions on the surface, the emitter diffusant can penetrate into the base layer only at each of these designated areas, leaving the base layer exposed to the surface everywhere else [Fig. 1(b)]. Contact to the base region thus may be made without difficulty after the remaining oxide has been removed. The elimination of any emitter etch and the freedom to make use of high emitter

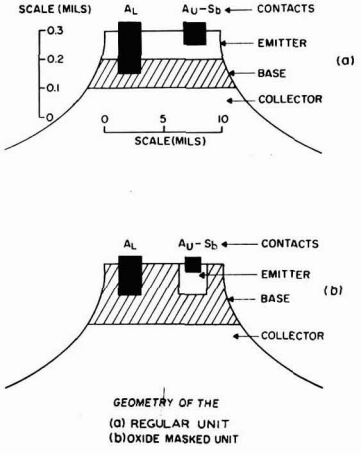

Fig. 1. Cross section of two double diffused transistor structures. Geometry of (a) regular unit, (b) oxide masked unit.

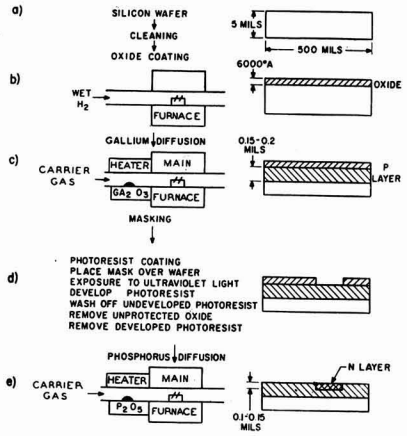

Fig. 2. Detailed diffusion and masking process.

concentrations are considerable advantages. In addition, limiting the emitter area results in a lower emitter capacity.

Oxide-Masking Technique

The masking process is illustrated in detail in Fig. 2. N-type silicon wafers of about 0.3 ohm-cm resistivity are cut into squares and lapped to obtain the highly polished surface essential to the production of uniform diffused junctions. A silicon dioxide layer is now grown over the surface; a simple method is illustrated, in which wet hydrogen is passed over the heated wafers to produce the 8000Å oxide layer required. Using the technique developed by Frosch (3, 4), the base layer dopant, gallium, is diffused into the wafer to a depth of about 0.2 mils. The oxide coating only slightly inhibits the rate of gallium diffusion.

The oxide now must be removed, selectively, from the 100 3 mil x 6 mil designated areas on the surface into which emitters are to be diffused. For clarity, only one emitter area, much enlarged, is shown in Fig. 2. To achieve this, the wafer is dipped into a photo resist solution,[1] dried in air, and exposed to ultraviolet light through a film mask which covers only those areas which are to be the emitters. The photo resist over these areas is not exposed to the light and, after the exposed portion is developed, is easily washed off in water. The oxide unprotected by the photo resist is removed in a slow etch. Finally, all of the photo resist is dissolved to give the structure in Fig. 2(d).

The second diffusion, with phosphorus as the impurity, is now carried out. In the time necessary to diffuse through the exposed regions to the required depth of about 0.1 mil, there is no diffusion through the oxide. To produce much deeper emitter junctions, thicker oxide layers would have to be prepared to insure complete masking. The final diffused structure of a single transistor is shown in Fig. 2(e).

To illustrate the control attained over the geometry of the emitters, an actual photomicrograph of a unit is presented in Fig. 3. The transistor has been lapped at an angle of five degrees to the surface and the base layer stained with a hydrofluoric-nitric acid etch (5) to delineate the junctions clearly. Both collector and emitter junctions are seen to be quite straight, any imperfections being much less than the layer thicknesses.

[1] Such as one made by the Eastman Kodak Co. A description of the general properties of this material is given in the pamphlet "Industrial Uses of Kodak Photo Resist," a manual prepared by Eastman Kodak Co., Rochester 4, N. Y.

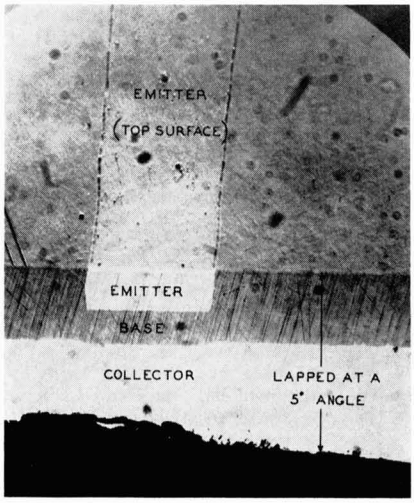

Fig. 3. Photomicrograph of an oxide masked double diffused unit. The junction has been exposed by beveling at a slight angle and staining the p-layer.

In the next step, Au-Sb emitter contacts and Al base contacts are evaporated through masks. To insure that the former fall entirely within the emitter areas and that the latter are positioned accurately close to the emitter edges but within the base layer, the masks are indexed carefully with respect to the original film mask used to prepare the emitters. Again, considerable control is needed in the definition of the emitter areas on the surface to prevent emitter-to-base shorts. The unlapped part of the wafer in the photomicrograph of Fig. 3, showing one such emitter area prior to the evaporation of contacts, clearly illustrates the close control of the emitter geometry that can be achieved by this masking technique.

The subsequent fabrication process follows standard procedures of collector bonding, lead attachment, and encapsulation.

Results and Discussion

The electrical characteristics of n-p-n, silicon, switching transistors prepared using the above techniques are presented in Table I. The base layers are normally from 0.05 to 0.10 mils in width. As some of the electrical parameters are quite sensitive to this width, results from some experimental units with a much thinner base layer (0.029 mils) are also shown.

The static characteristics of the normal units show a high collector to emitter breakdown voltage, a low emitter junction breakdown due to the high impurity gradient at this junction, and the low reverse saturation currents expected with silicon devices.

Table I.

	Normal median values	Thin base median values	Units
Number of units	9	20	
Emitter thickness	0.09	0.04	mils
Base thickness	0.08	0.029	mils
BV_{CBO} at $I_{co} = 1\ \mu a$	65	27	volts
BV_{EBO} at $I_{eo} = 1\ \mu a$	3	8	volts
I_{co} at $V_{CB} = 4.5$ V	2×10^{-10}	9×10^{-9}	amps
C_c at $V_{CB} = 4.5$ V	5	6	$\mu\mu f$
hie at $V_{CE} = 5V$, $I_c = 10$ ma	400	450	ohms
Switching times			
at $I_c = 30$ ma, $I_{B_1} = 2.5$ ma			
$V_{B_2} = O$ V			
t_0	0.03	0.03	μsec
t_1	0.03	0.03	μsec
t_2	0.04	0.03	μsec
V_{CE} at $I_C = 30$ ma, $I_B = 2.5$ ma	0.5	0.9	volts
V_{BE} at $I_C = 30$ ma, $I_B = 2.5$ ma	0.9	1.1	volts
Small signal alpha			
at $V_{CB} = 4.5$ V			
$I_E = 0.1$ ma	0.927	0.939	
1 ma	0.960	0.976	
10 ma	0.973	0.987	
30 ma	0.972	0.985	
hfe at $f = 30$ mc, $V_{CE} = 5V$	14	21	db
$I_E = 5$ ma			

The small size of the unit is reflected in the low collector capacitance of 5 $\mu\mu$f. Base resistances of 200-300 ohms are encountered normally.

The electrical parameters of interest for switching applications also are summarized in Table I. In the circuit used for measuring the switching time, the units are usually in the ON or saturation condition, with 2.5 ma base drive and 30 ma collector current. They are turned off by a negative pulse to the base which thus is driven to ground potential. The total switching time is the sum of storage time t_1, turn-off time t_2, and turn-on time t_0. For switching 30 ma with a gain of 12, total switching times of the order of 0.1 μsec have been measured.

Finally, the gain characteristics are given. The low-frequency short-circuit current gain, alpha, is fairly high for this transistor and varies only slightly over the operating range. The variation both with emitter current and collector voltage is presented in Fig. 4. The fact that alpha is independent of the reverse collector voltage is of considerable advantage in the design of circuits using the unit. The advantage gained from the use of such a narrow base device is apparent from the current gain at high frequency (hfe). For the normal units, the measured gain of 14 db at 30 mc corresponds to an alpha cut-off frequency of approximately 150 mc.

An analysis of the data for the extremely thin base experimental units emphasizes the favorable high-frequency behavior. The gain has been measured as a function of frequency both for the common emitter and common base connection (Fig. 5) for a thin base unit. The alpha cut-off frequency of 350 mc is comparable to the best germanium transistors if the difference in mobility is taken into account. These units also show a small but significant

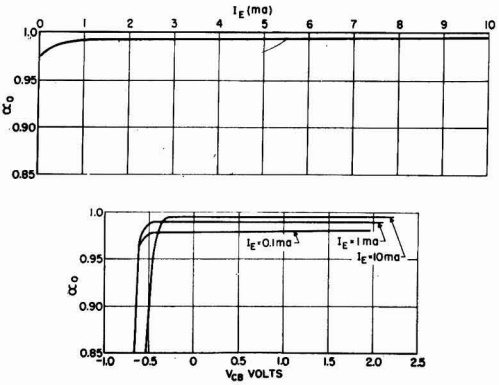

Fig. 4. The variation of alpha with emitter current and collector voltage for an oxide masked unit.

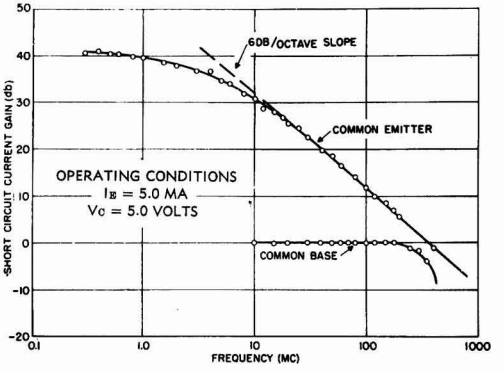

Fig. 5. The current gain vs. frequency for a thin base unit, both in the common emitter and common base connection.

improvement in the low frequency alpha. The collector to base reverse breakdown voltage is substantially lower than in the regular units due to reach-through effects; however, it is still high enough for many switching circuit applications.

Acknowledgments

The authors wish to acknowledge the contributions of W. C. Hittinger, who suggested this approach to the problem, M. Mandel (now at Stanford University), and D. L. Kushler. Thanks are also due to D. E. Thomas for making the frequency measurements.

Manuscript received July 18, 1958. This paper was prepared for delivery before the New York Meeting, April 27-May 1, 1958.

Any discussion of this paper will appear in a Discussion Section to be published in the December 1959 JOURNAL.

REFERENCES

1. C. A. Lee, *Bell System Tech. J.*, **35**, 23 (1956).
2. M. Tanenbaum and D. E. Thomas, *ibid.*, **35**, 1 (1956).
3. C. J. Frosch and L. Derick, U. S. Pat. 2,802,760.
4. C. J. Frosch and L. Derick, *This Journal*, **104**, 547 (1957).
5. C. S. Fuller and J. A. Ditzenberger, *J. Applied Phys.*, **27**, 544 (1956).

Equilibrium Reduction of Tungsten Oxides by Hydrogen

Robert C. Griffis

Refractory Metals Laboratory, General Electric Company, Cleveland, Ohio

ABSTRACT

A complete study has been made of the heterogeneous equilibrium involving the four tungsten oxides, water, and hydrogen, using a modified static equilibrium apparatus. These data show that the initial results, previously reported, are in error due to thermal diffusion. The new data were used to compute the standard heats of formation and entropies of the solid oxide species as follows:

WO_2, $\Delta H_f° = -134.0 \pm 0.7$ kcal/g-atom W, $S°_{298} = 19.7 \pm 1.0$ e.u./g-atom W
$WO_{2.72}$ ($W_{18}O_{49}$), $\Delta H_f° = -180.3 \pm 1.4$ kcal/g-atom W, $S°_{298} = 25.0 \pm 1.4$ e.u./g-atom W
$WO_{2.90}$ ($W_{20}O_{58}$), $\Delta H_f° = -193.1 \pm 1.4$ kcal/g-atom W, $S°_{298} = 23.6 \pm 1.4$ e.u./g-atom W
WO_3, $\Delta H_f° = -202.8 \pm 1.4$ kcal/g-atom W, $S°_{298} = 19.1 \pm 1.4$ e.u./g-atom W

Since the previous paper (1) there have been several significant developments in the literature which warrant notice. The high-temperature form (above 740°C) of WO_3 has been the subject of two more investigations (2, 3). Vasil'eva, *et al.* (3) have made a thermodynamic study of the series of suboxides formed from the high-temperature species of WO_3. They reported that the structure of the oxide formed by the reduction of WO_3 is determined by the structure of the WO_3. This gives rise to a series of heretofore unreported tungsten suboxides. In addition to this, some very interesting evidence as to metallic nature of beta tungsten has been presented (4, 5).

The purpose of this paper is to discuss the etiology of the thermal diffusion error in the initial results for the heterogeneous equilibrium involving H_2-W-WO_2-H_2, and to present new data for the heterogeneous equilibrium involving the complete reduction of WO_3 to W.

Experimental Procedure

All reagents were prepared as previously described (1). X-ray analyses of the products of the equilibrium reactions are discussed in the next section.

The extension of the reported experimental techniques to the higher oxide systems was found to be impracticable (1). The limiting H_2O vapor pressure resulted in large relative errors when the value of K_p was greater than one. It was experimentally difficult to thermostat the condensing bulb at higher than room temperature since provision had to be made for cooling the cold finger. There was also an indication of increased mass transfer of the oxides in the vapor phases, especially at high H_2O vapor pressures and temperatures. This increase in volatility in the presence of H_2O has been reported in the literature (6, 7). Effects encountered here were cumulative in nature only, and the amount of oxide lost in any one run was negligible, but the effects of 10-20 runs resulted in a visible oxide film at the exit of the reaction chamber. The original reaction chamber, due to its circular nature, could not be cleaned out in a reasonable time. The situation was aggravated also by accidental spillage inside the chamber.

Apparatus.—The design and construction of the new experimental apparatus closely followed the original work of Emmett and Schultz (8). The entire apparatus is present in Fig. 1. It should be noted that the hot reaction gases over the sample are pumped into the restricted section of the reaction chamber and thence to the H_2O vapor saturator. This design also facilitates removal of the chamber for periodic cleaning. The temperature of the water bath is regulated to within ±0.02°C by means of a mercury thermoregulator and zero current relay. The container is a Pyrex glass jar 12 in. in diameter and 18 in. high, holding approximately 7 gal of double distilled water. It is fitted with a plastic cover to minimize evaporation losses and to keep out dust. The supports for the water saturator and man-

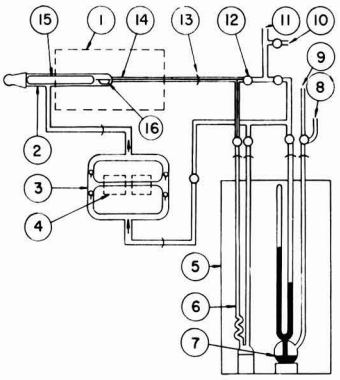

Fig. 1. Equilibrium apparatus: 1, furnace; 2, quartz reaction chamber; 3, gas pump; 4, solenoids; 5, thermostated, constant temperature water bath; 6, water vapor saturator; 7, mercury manometer; 8, to atmosphere; 9, to high vacuum; 10, to hydrogen or argon; 11, to high vacuum manifold; 12, 4 mm high vacuum stopcocks; 13, 18/7 spherical high vacuum glass joints; 14, restricted section and exit capillary; 15, sealed quartz tube used as plug; 16, sample boat.

ometer are fashioned from brass, copper, and Teflon.

The basic design for the gas solenoid pump was furnished by Seybolt (9) and is similar to that recently described by Bennett (10). A Teflon encased drill rod is used as a piston. This piston was machined to give a tight fit in ½ in. OD Pyrex glass tubing. This size of glass tubing was chosen so as to fit the readily available commercial solenoids. The piston was then hand lapped to give a smooth sliding action. A port is also provided for easy removal of the piston, if necessary. Small blocks of iron transformer core were placed on the upper part of the glass tube on the outside of the solenoids next to the vertical sections of the pump. When the solenoid is energized the iron blocks attract the iron core of the piston and tend to lengthen the stroke. This action results in a floating effect which enables the pump to run continuously for 8-10 hr at a temperature of 60°C without variation in pumping speed. The pumping frequency is 60 cycles/min and is obtained by a cam, synchronous motor, and breaker point assembly. The pumping capacity was measured as 250 cc/min by a water displacement method at atmospheric pressure. There was no evidence of decomposition of the Teflon piston at 60°C when it was operated in a vacuum.

All the glass tubing, including stopcocks, is heated with asbestos-covered resistance wire and wrapped with Al foil strips. The high vacuum stopcocks operate efficiently at 60°C if the proper greasing technique is used. Enough heat is conducted from the quartz reaction chamber to prevent condensation of H_2O in this section. The H_2O vapor pressure therefore is determined only by the temperature of the water bath which is carefully regulated. The same reaction furnace was used. The constant temperature zone (± 1°C) was increased to 4 cm due to increased end insulation and radiation shielding. The control thermocouple and recorder were rechecked against a Bureau of Standards Certificate Pt-Pt-10%Rh to ± 1°C for the entire temperature range. The mercury manometer readings were made with a precision cathetometer to ±0.03 mm.

This new experimental apparatus was used to determine once again the $Fe\text{-}H_2O\text{-}H_2\text{-}Fe_3O_4$ equilibrium over the temperature range 400°-550°C. Data were some 20% higher than those obtained with the initial apparatus, while data for the system $H_2\text{-}W\text{-}WO_2\text{-}H_2O$ were slightly lower than the previous data. Vasil'eva and Gerasimov (11) suggested some changes in the experimental apparatus. They were of the opinion that the flow of the hot reaction gases was not great enough to eliminate thermal diffusion. At their suggestion the exit capillary of the reaction chamber was made 1 mm ID and most of the space in the reaction chamber was occupied by inserting a sealed quartz tube after the sample boat was inserted. This resulted in a much higher flow of gases through the hot reaction zone.

These improvements enabled data to be obtained for the system $Fe\text{-}H_2O\text{-}H_2\text{-}Fe_3O_4$ which agreed essentially with that obtained using the original apparatus (1); however, the K_p's now obtained for the system $H_2\text{-}W\text{-}WO_2\text{-}H_2O$ were considerably lower than those obtained previously. The apparent paradox can be explained by examining the conditions under which the original apparatus was used. In the original apparatus the entire reaction chamber was insulated by Al foil guards. The auxiliary furnace was operated at about 300°C while the reaction furnace varied from 400° to 550°C for the reference $Fe\text{-}H_2O\text{-}H_2\text{-}Fe_3O_4$ system. Under these conditions the temperature gradient was not large enough over the closed tube chamber to bring thermal diffusion effects into play and/or convection circulation was sufficient to overcome this effect. In working with the tungsten oxide system, however, the temperature ranged from 500° to 1000°C. Under these conditions the effects of thermal diffusion evidently had a considerable influence on the data obtained.

Therefore, it is believed that thermal diffusion effects were eliminated in the system described above because; (*A*) the positive pressure action of the pump maintained a forced circulation of the reaction gases; (*B*) the velocity of the gases in the reaction chamber was increased by eliminating as much as possible of the dead space by means of the sealed quartz tube; and (*C*) the exit gases were conducted by means of a 1 mm capillary directly to the water vapor saturator.

X-ray studies.—The x-ray investigation was concerned with two areas of interest. The first area involved routine x-ray examinations of the solid phases in the equilibrium samples, using powder camera techniques. This study showed only the tungsten oxide phases as reported by Magneli, *et al.* (12).

The second area of interest concerned the new structures of the suboxides described by Vasil'eva, *et al.* (3). Samples in this study consisted of the pure tungsten oxides in contrast to the solid two-phase samples encountered in the equilibrium samples. A General Electric XRD-5 x-ray diffractometer was used to examine the quenched samples so as to obtain the data as soon as possible. Copper K radiation was used since the resolution achieved was sufficient for this study. It has been pointed out that reliable determination of angular position and intensities of the diffraction peaks requires considerable attention to the preparation and mounting of the sample powders (13). The samples were mounted according to the procedure as outlined by McCreery (14). Several samples were examined for each oxide in order to detect gross variations. The pure oxide samples were sealed in quartz tubes after careful evacuation at less than 0.1 μ pressure for a period of 8 hr. These capsules were held at 1000°C for approximately 18 hr. The samples were quenched to room temperature by dropping the hot capsule into a reservoir of water. The quenched powder which was still under vacuum was removed by breaking the capsule. Total time required for quenching and preparing the sample was 3 min. In one instance a sample of WO_3 was heated in air, quenched directly into water, filtered, washed with acetone for drying purposes, and then prepared for x-ray.

Table I. Equilibrium data for the system WO_3-H_2-$WO_{2.90}$-H_2O

Temp, °C	$K_p = \frac{P_{H_2O}}{P_{H_2}}$	Temp, °C	$K_p = \frac{P_{H_2O}}{P_{H_2}}$	Temp, °C	$K_p = \frac{P_{H_2O}}{P_{H_2}}$
600	2.30	700	5.10	800	8.40
600	2.21	700	4.91	800	9.20
600	2.39	700	5.30	800	9.61
600	2.28	700	5.24	800	9.12
600	2.25	700	5.05	800	9.71
600	2.32	700	5.12	800	9.54

Table II. Equilibrium data for the system $WO_{2.90}$-H_2-$WO_{2.72}$-H_2O

Temp, °C	$K_p = \frac{P_{H_2O}}{P_{H_2}}$	Temp, °C	$K_p = \frac{P_{H_2O}}{P_{H_2}}$	Temp, °C	$K_p = \frac{P_{H_2O}}{P_{H_2}}$
600	1.20	700	3.20	800	7.20
600	1.25	700	3.10	800	7.37
600	1.17	700	3.27	800	7.02
600	1.19	700	3.30	800	7.15
600	1.21	700	3.17	800	7.23
600	1.23	700	3.22	800	7.10

Table III. Equilibrium data for the system $WO_{2.72}$-H_2-WO_2-H_2O

Temp, °C	$K_p = \frac{P_{H_2O}}{P_{H_2}}$	Temp, °C	$K_p = \frac{P_{H_2O}}{P_{H_2}}$	Temp, °C	$K_p = \frac{P_{H_2O}}{P_{H_2}}$
600	0.880	700	1.10	800	1.31
600	0.892	700	1.05	800	1.29
600	0.894	700	1.13	800	1.35
600	0.873	700	1.08	800	1.33
600	0.850	700	1.10	800	1.27
600	0.861	700	1.05	800	1.33
900	1.50				
900	1.45				
900	1.54				
900	1.48				
900	1.51				
900	1.47				

Table IV. Equilibrium data for the system WO_2-H_2-W-H_2O

Temp, °C	$K_p = \frac{P_{H_2O}}{P_{H_2}}$	Temp, °C	$K_p = \frac{P_{H_2O}}{P_{H_2}}$	Temp, °C	$K_p = \frac{P_{H_2O}}{P_{H_2}}$
600	0.175	700	0.269	800	0.390
600	0.168	700	0.272	800	0.385
600	0.178	700	0.260	800	0.394
600	0.164	700	0.267	800	0.401
600	0.173	700	0.265	800	0.388
600	0.171	700	0.263	800	0.386
900	0.535	1000	0.687		
900	0.521	1000	0.667		
900	0.540	1000	0.690		
900	0.550	1000	0.665		
900	0.525	1000	0.670		
900	0.531	1000	0.683		

Results and Discussion

All of the data was obtained by alternate reduction and oxidation of the samples. The sample consisted of a mixture of the two solid phases concerned for the particular heterogeneous equilibrium being investigated. This is in contradistinction to the method of Vasil'eva, *et al.* (3) who prepared the phases *in situ* by the reduction of WO_3. The two phases were introduced in order to achieve equilibrium conditions as soon as was practicable and to avoid excessive sintering effects which sometimes invalidate the data obtained for experimental runs involving long times and/or high equilibrium gas ratios. The 2-g sample was evacuated to less than 0.1 μ and held there for at least 3 hr. Each sample was subjected to conditioning runs under oxidizing and reducing conditions before the final run was made. The system was evacuated after the final equilibrium measurements were made and the sample cooled to room temperature. All equilibrium samples then were examined by x-ray, using powder camera techniques, to identify the solid phases present. The temperature regions investigated were limited by the significant volatility of the higher tungsten oxides in the presence of water vapor, as was pointed out in the first paragraph.

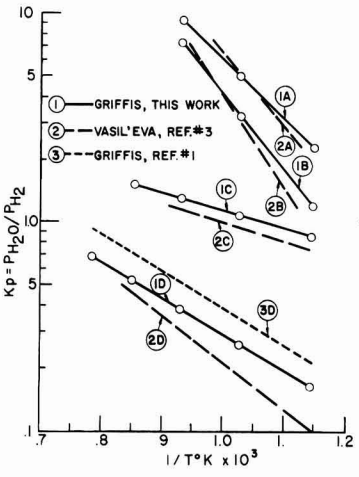

Fig. 2. Plot of log $K_p = \frac{P_{H_2O}}{P_{H_2}}$ vs. $\frac{1}{T°K}$ for the systems:

(1A)(2A)—WO_3-H_2-$WO_{2.90}$-H_2O
(1B)(2B)—$WO_{2.90}$-H_2-$WO_{2.72}$-H_2O
(1C)(2C)—$WO_{2.72}$-H_2-WO_2-H_2O
(1D)(2D)(3D)—WO_2-H_2-W-H_2O

The data are summarized in Tables I-IV, and Fig. 2.

C_p's for the equilibrium reactions were calculated on the basis of literature values for H_2, H_2O, WO_3 (15), W (16), and Kopp's rule for the tungsten oxides since no literature values are available. The equilibrium values in Tables I-IV were treated by means of sigma functions and the method of least squares. Literature values (17) of $\Delta F°_{298}$ (−109, 200 cal) and $\Delta H°_{298}$ (−115, 600 cal) for the reaction $2H_2+O_2 \rightarrow 2H_2O$ were used to calculate $\Delta H°_T$ for each oxide. The standard entropy values of W and O_2 (18) were used to calculate the standard entropies of the oxides. The results of these calculations are tabulated in Table V.

The lack of reliable heat capacity data accounts for the large estimated error assigned to these values. The heats of formation reported here (Table VI) are compared with those obtained by direct combustion techniques (1).

Table V. Results of thermodynamic calculations

(A) $10\ WO_3 + H_2 \rightarrow 10\ WO_{2.90} + H_2O$

$\Delta H^\circ = 42{,}300 + 1.90T - 33.1 \times 10^{-3} T^2 + 0.04 \times 10^5\ T^{-1}$

$\Delta F^\circ = 42{,}300 - 1.90T\ln T + 33.1 \times 10^{-3} T^2 + 0.02 \times 10^{-5}\ T^{-1} - 66.0T$

$\Delta H^\circ_{298} = +39.9 \pm 1.0$ kcal

$\Delta F^\circ_{298} = +22.4 \pm 1.0$ kcal

$W + 3/2\ O_2 \rightarrow WO_3$

$\Delta H^\circ_{298} = -202.8 \pm 1.4$ kcal/g-atom W

$S^\circ_{298}\ WO_3 = 19.1 \pm 1.4$ e.u./g-atom W

(B) $100/18\ WO_{2.90} + H_2 \rightarrow 100/18\ WO_{2.72} + H_2O$

$\Delta H^\circ = 19{,}100 - 3.35T + 0.89 \times 10^{-3} T^2 + 0.04 \times 10^5\ T^{-1}$

$\Delta F^\circ = 19{,}100 + 3.35T\ln T - 0.89 \times 10^{-3} T^2 + 0.02 \times 10^5\ T^{-1} - 44.1T$

$\Delta H^\circ_{298} = +18.2 \pm 1.0$ kcal

$\Delta F^\circ_{298} = +11.6 \pm 1.0$ kcal

$W + \frac{2.90}{2} O_2 \rightarrow WO_{2.90}$

$\Delta H^\circ_{298} = -193.1 \pm 1.4$ kcal/g-atom W

$S^\circ_{298}\ WO_{2.90} = 23.6 \pm 1.4$ e.u./g-atom W

(C) $100/72\ WO_{2.72} + H_2 \rightarrow 100/72\ WO_2 + H_2O$

$\Delta H^\circ = 6110 - 3.35T + 0.89 \times 10^{-3} T^2 + 0.04 \times 10^5\ T^{-1}$

$\Delta F^\circ = 6110 + 3.35T\ln T - 0.89 \times 10^{-3} T^2 + 0.02 \times 10^5\ T^{-1} - 28.6T$

$\Delta H^\circ_{298} = 5.2 \pm 1.0$ kcal

$\Delta F^\circ_{298} = 3.2 \pm 1.0$ kcal

$W + \frac{2.72}{2} O_2 \rightarrow WO_{2.72}$

$\Delta H^\circ_{298} = -180.3 \pm 1.4$ kcal/g-atom W

$S^\circ_{298}\ WO_{2.72} = 25.0 \pm 1.4$ e.u./g-atom W

(D) $\frac{1}{2}\ WO_2 + H_2 \rightarrow \frac{1}{2}\ W + H_2O$

$\Delta H^\circ = 10{,}125 - 3.48T + 1.08 \times 10^{-3} T^2 + 0.04 \times 10^5\ T^{-1}$

$\Delta F^\circ = 10{,}125 + 3.48T\ln T - 1.08 \times 10^{-3} T^2 + 0.02 \times 10^5\ T^{-1} - 30.7T$

$\Delta H^\circ_{298} = +9.2 \pm 0.5$ kcal

$\Delta F^\circ_{298} = +6.8 \pm 0.5$ kcal

$W + O_2 \rightarrow WO_2$

$\Delta H^\circ_{298} = 134.0 \pm 0.7$ kcal/g-atom W

$S^\circ_{298}\ WO_2 = 19.7 \pm 1.0$ e.u./g-atom W

Table VI. Heats of formation of tungsten oxides

Oxide	ΔH_f° kcal/g-atom W, Combustion	ΔH_f° kcal/g-atom W, Equilibrium
WO_3	-199 ± 1	-202.8 ± 1.4
$WO_{2.90}$	-193 ± 1	-193.1 ± 1.4
$WO_{2.72}$	-183 ± 1	-180.3 ± 1.4
WO_2	-137 ± 1	-134.0 ± 0.7

The x-ray examination of the equilibrium samples, as was previously pointed out, showed no evidence of the structure reported by Vasil'eva, *et al.* (3). The structure of the equilibrium oxide phases corresponded only to those reported by Magneli, *et al.* (12).

The x-ray examination of the pure oxides phases, as outlined under the second area of interest, was also unsuccessful in revealing any new structures for the tungsten oxides. All of the samples heated at 1000°C and quenched gave only the tungsten oxide patterns as previously reported (12). The tetragonal structure of WO_3 above 740°C had been confirmed by dilatometric (19), x-ray, and differential thermal analysis data (20-22). Perri, *et al.* (2) showed that there is a smooth transition from the monoclinic form of WO_3 to the orthorhombic form at about 300°C, and a sharp transition to the tetragonal form at 720°C. The high-temperature form (above 740°C) of WO_3 was described as orthorhombic by Vasil'eva on the basis of examination of rapidly cooled samples of WO_3. As stated above, this study failed to detect any "quenched-in" high-temperature form. The one sample of WO_3, which was cooled by pouring the hot powder into H_2O, did show some evidence of increase in the *d* values obtained from 001, 020, 200 reflections. This comportment indicates a shift to the orthorhombic structure. The peaks were recorded in their normal positions, however, after 15 min. The data obtained from the diffractometer, especially at slow scanning speeds, were sufficiently precise so as to show the possible shift in structure for all the tungsten oxides. The question as to whether the tungsten oxides prepared *in situ* by Vasil'eva and subsequently cooled rapidly have a different structure from those prepared by direct synthesis, using WO_3 and W, is difficult since the high-temperature structure for WO_3 was not reported by Vasil'eva. The equilibrium data certainly suggest that there is a distinct and measurable difference. Further work is planned in examining the phase transitions of each of the oxides by means of a high-temperature x-ray camera. The characteristics of those oxides prepared by reduction of WO_3 *in situ* and those prepared by direct synthesis of WO_3 and W (12) will be compared.

Acknowledgments

The author wishes to thank many members of the Refractory Metals Laboratory, and other divisions of the General Electric Company for their helpful assistance. He wishes to thank Dr. A. U. Seybolt for the gas pump design. He is especially grateful for the helpful discussion with Professor Gerasinov and Candidate Chem. Science Vasil'eva.

Manuscript received Nov. 5, 1958. This paper was prepared for delivery before the Buffalo Meeting, Oct. 6-10, 1957.

Any discussion of this paper will appear in a Discussion Section to be published in the December 1959 JOURNAL.

REFERENCES

1. R. C. Griffis, *This Journal*, **105**, 398 (1958).
2. J. A. Perri, E. Banks, and B. Post, *J. Appl. Phys.*, **28**, 1272 (1957).
3. I. A. Vasil'eva, Ya. I. Gerasimov, and Yu. P. Siamanov, *J. Phys. Chem.* (U.S.S.R.), **331**, 682 (1957).
4. T. Millner, A. J. Hegedus, K. Sasvari, and J. Neugebauer, *Z. anorg. u. allgem. Chem.*, **289**, 288 (1957).
5. J. Neugebauer, A. Hegedus, and T. Millner, *ibid.*, **293**, 241 (1957).
6. T. Millner and J. Neugebauer, *Nature*, **163**, 601 (1949).
7. O. Glemser and H. Volz, *Naturwissenschaften*, **43**, 33 (1956).
8. P. Emmett and J. Schultz, *J. Am. Chem. Soc.*, **55**, 1376 (1933).
9. A. U. Seybolt, Private communications.
10. W. Bennett, *Rev. Sci. Inst.*, **28**, 1092 (1957).
11. I. A. Vasil'eva and Ya. I. Gerasimov, Private communications.
12. A. Magneli, G. Anderson, B. Bloomberg, and L. Kihlborg, *Anal. Chem.*, **24**, 1998 (1952).

13. H. Klug and L. Alexander, "X-ray Diffraction Procedures," pp. 290-305, John Wiley & Sons, Inc., New York (1954).
14. G. L. McCreery, *J. Am. Ceram. Soc.*, **32**, 141 (1949).
15. O. Kubaschewski and E. Evans, "Metallurgical Thermochemistry," pp. 312, 320, John Wiley & Sons, Inc., New York (1956).
16. K. K. Kelley, *U. S. Bur. Mines Bull. 476* (1949).
17. O. Kubaschewski and E. Evans, *op. cit.*, p. 248, 334.
18. K. K. Kelley, *U. S. Bur. Mines Bull. 434* (1948).
19. M. Foex, *Compt. rend.*, **200**, 917 (1945).
20. R. Ueda and T. Ichinokawa, *Phys. Rev.*, **82**, 563 (1951).
21. S. Sawada, *ibid.*, **91**, 1010 (1953).
22. W. Kehl, R. Hay, and D. Wahl, *J. Appl. Phys.*, **23**, 212 (1952).

Polarographic Behavior of Nitro and Nitrosoguanidine

Gerald C. Whitnack and E. St. Clair Gantz[1]

General Research Branch, U. S. Naval Ordnance Test Station, China Lake, California

ABSTRACT

The general behavior of nitro and nitrosoguanidine at the dropping mercury electrode has been studied under various alkaline, neutral, and acidic conditions. Different mechanisms of reduction are postulated and discussed. Optimum conditions are specified, with other details, both for the determination of the nitroso compound in the presence of the nitro compound, and for the reduction of the nitro compound to either the amino or nitroso compound. Half-wave potentials, diffusion current constants, and n-values are reported for each compound in several media. The multiple waves obtained with these compounds at some pH values are discussed in terms of different ionic and molecular forms in solution.

The reduction of nitroguanidine has been a subject of considerable study for many years (1-5). Nitrosoguanidine has been established as the first product in the chemical reduction of nitroguanidine (1, 3). Thiele described the preparation of nitrosoguanidine by the careful reduction of nitroguanidine with tin and dilute hydrochloric acid. Steinbach (5) studied the chemical reduction of nitroguanidine in neutral, acidic, and alkaline solutions and the electrochemical reduction in acidic and alkaline solutions. He showed that the product of the chemical reduction depended mainly on the type of reducing agent and the amount of reductant present. Aminoguanidine and nitrosoguanidine were the end products. Smith and Sabetta, and Davis and Rosenquist (4, 23) proposed a method for the preparation of nitrosoguanidine by the reduction of nitroguanidine with zinc dust in an ammonium chloride solution. The oxidation potential for the half-cell, nitro-nitrosoguanidine, has been measured (4,6); however, very little fundamental information has been reported on the polarographic behavior of this very involved system.

Nitro and nitrosoguanidine exhibit amphoteric characteristics (7) and their different possible molecular and ionic forms have been the subject of considerable controversy (8-13). The dissociation constants of several derivatives of nitroguanidine (14) and the effect of substituents on the absorption spectrum of nitroguanidine have been determined spectrophotometrically (15). A hydroxylaminoguanidine intermediate has been proposed in the reduction of nitroguanidine by titanium (III) chloride (16).

In the fall of 1955, a paper on the polarographic behavior of nitro and nitrosoguanidine was published by Lanza, *et al.* (17). In addition, Namba and Suzuki (18) in 1955 published some work on nitrourea and nitroguanidine. In general, where their work overlapped with the work presented in this report, good agreement was obtained.

The present study was initiated so that additional fundamental knowledge about the mechanism and products of reduction and the general polarographic behavior of nitro and nitrosoguanidine might be obtained. It is the purpose of this report to present and discuss such data.

Experimental

Apparatus and materials.—A Sargent Model XXI recording polarograph and a Fisher "Elecdropode" were used in these studies. Mercury pool potentials and half-wave potentials ($E_{1/2}$) vs. the saturated calomel electrode (SCE) were determined with the "Elecdropode" (19). The $E_{1/2}$ values (vs. Hg pool) were calculated by the method of intersecting lines from polarograms obtained with the Sargent Model XXI polarograph. It is recognized that $E_{1/2}$ (vs. Hg pool) values do not have exact significance and are reported for relative comparison only. The potential of the mercury pool was fairly constant in a Britton and Robinson buffer system through the pH 3-7 range.

Solutions used in these studies had cell resistances of less than 500 ohms (as determined with a Wheatstone bridge) and the iR correction was negligible in computing the $E_{1/2}$ values (20). All pH measurements were made with a Beckman Model G pH meter.

Several dropping mercury electrodes were used in this work. The $m^{2/3}t^{1/6}$ values are reported in the tables.

Small borosilicate glass beakers (30 ml) were used as polarographic cells. A rubber stopper to which were attached the dropping mercury elec-

[1] Present address: Aircraft Gas Turbine Division, General Electric Co., Cincinnati, Ohio.

trode, contact electrode, and a glass tube with a fritted disk, was placed over the top of the small beakers. The current-voltage curves were obtained in a constant temperature bath at 30° ± 0.1°C.

Dissolved oxygen was removed from all solutions with pure nitrogen just prior to the polarographic examination. The nitrogen was passed through a portion of the solution being examined polarographically and finally through the solution in the polarographic cell.

Clark and Lubs' and Britton and Robinson buffer solutions (21, 22) were prepared double strength (2x), and then the buffer was added to varying amounts of aqueous stock solutions of nitro and nitrosoguanidine so that the final polarographic solutions were about 0.1M in buffer. Methyl red (0.001%) was used as a maxima suppressor in these studies, and redistilled mercury, C.P. grade, was used as the anode. The ionic strength of the polarographic solutions was controlled carefully by the addition of ionic strength agents whenever needed.

Nitrosoguanidine was prepared by the method of Davis and Rosenquist (23). The material was recrystallized once from water and analyzed 98.6% by a permanganate titration.

The nitroguanidine used in this work was a commercial grade known as "picrite." This material was recrystallized three time from distilled water and had a melting point of 234°-236°C.

Diffusion Coefficient and n-Value Measurements

The diffusion coefficient (D) for nitroguanidine was determined by a procedure adapted from that employed by Stokes (24). In this method, porous diaphragm cells were used, which embodied a magnetic stirring mechanism. The cells were calibrated by the usual method of allowing 0.1M potassium chloride to diffuse into water at 25°C until 25% had passed through the diaphragm. The diffusion constant of potassium chloride for these conditions is known to be 1.867×10^{-5} cm²/sec.

Since nitrosoguanidine decomposes in aqueous solutions (25), a more rapid method of determining its diffusion coefficient and n-value was needed. A millicoulometric method reported by Reynolds (26), and recently modified in this laboratory (27), was employed. In this method the polarograph served as a coulometer and a source of constant applied potential. The integration method was used in calculation. An n-value for nitroguanidine was also determined by this technique.

Results and Discussion

Effect of pH, mercury height, and concentration.— Nitro and nitrosoguanidine were investigated in ammonium chloride and ammonium sulfate solutions (pH 4.5). Only one wave was observed for nitroguanidine in these salt solutions, and the $E_{1/2}$ was more negative in the ammonium sulfate solution than in the ammonium chloride solution. However, in 1N HCl and H_2SO_4 solutions, two waves were observed. The $E_{1/2}$ values were more negative in the H_2SO_4 solution than in the HCl solution. Nitrosoguanidine gave two waves in the salt solutions but only one in the 1N acid solutions. Thus it appeared

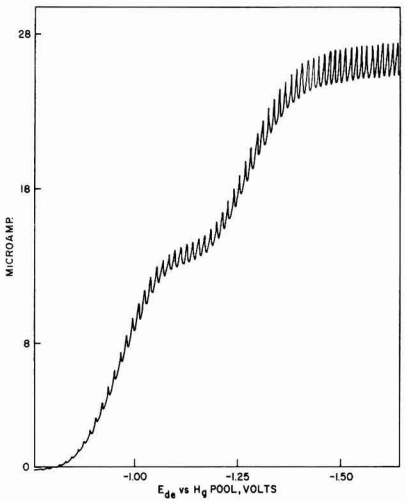

Fig. 1. Polarographic waves of 1.70 mM nitrosoguanidine solution. Britton and Robinson buffer (2X), pH 5.5, 0.001 % methyl red, $m^{2/3}t^{1/6} = 1.45$ mg$^{2/3}$ sec$^{-1/2}$.

that these waves were greatly dependent on the pH and the medium, Therefore, nitro and nitrosoguanidine solutions were studied in Clark and Lubs' and in Britton and Robinson's buffer solutions. The ionic strength of the polarographic solutions was maintained below 0.2M to minimize effects on half-wave potentials. In general, two well-defined waves were obtained over the acid and neutral pH range and one well-defined wave was obtained in alkaline solutions with a pH > 10. The definition of the waves appeared to be better in the Britton and Robinson buffer solutions and a typical polarogram is shown in Fig. 1 for nitrosoguanidine in this system. The first wave is referred to as the more positive in voltage. The effect of pH on the i_d values and the $E_{1/2}$ values of the two individual waves and the total waves, respectively, is shown in Tables I and II. The $E_{1/2}$ values of the first waves increased linearly with an increase in pH to about a pH of 4. The slope of

Table I. Effect of pH on i_d and $E_{1/2}$ of nitroguanidine 1.007 mM nitroguanidine solution containing 0.001% methyl red $m^{2/3}t^{1/6} = 1.45$ mg$^{2/3}$ sec$^{-1/2}$

pH*	$E_{1/2}$ (vs. SCE), v		$i_d/Cm^{2/3}t^{1/6}$	
	1st	2nd	1st	2nd
2.4	—0.73	—1.13	5.28	4.67
3.1	—0.85	—1.45	4.32	3.43
3.7	—0.94	—1.43	3.43	4.53
4.4	—1.16	—1.36	3.43	5.22
4.9	—1.26	—	10.09	—
5.5	—1.26	—	10.09	—
6.3	—1.24	—	10.02	—
6.9	—1.24	—	9.95	—
7.8	—1.22	—	9.95	—
9.1	—1.22	—	9.75	—
10.9	—1.16	—	9.06	—
11.6	—1.15	—	9.06	—
11.8	—1.15	—	8.92	—

* 18 ml Britton and Robinson buffer solutions with 2 ml of stock nitroguanidine solution. pH 2.4 well-defined waves, pH 3.1-4.4 ill-defined waves, pH 4.9-11.8 one well-defined wave.

Table II. Effect of pH on i_d and $E_{1/2}$ of nitrosoguanidine 1.043 mM nitrosoguanidine solution containing 0.001% methyl red $m^{2/3}t^{1/6} = 1.45$ mg$^{2/3}$ sec$^{-1/2}$

pH*	$E_{1/2}$ (vs. SCE), v			$i_d/Cm^{2/3}t^{1/6}$		
	1st	2nd	Total†	1st	2nd	Total†
2.4	−0.73	−1.15	−0.94	7.82	0.66	8.48
2.8	−0.78	−1.19	−0.98	7.02	1.19	8.35
3.2	−0.79	−1.22	−0.98	5.83	2.52	8.35
3.6	−0.84	−1.24	−1.02	5.43	2.98	8.41
4.0	−0.86	−1.26	−1.05	5.17	3.24	8.48
4.6	−0.89	−1.27	−1.06	4.57	3.24	8.15
5.0	−0.89	−1.28	−1.06	3.98	3.38	7.82
5.7	−0.90	−1.20	−1.06	3.64	3.71	7.62
6.1	−0.91	−1.18	−1.06	3.64	3.71	7.62
6.7	−0.89	−1.15	−1.06	3.25	3.84	7.09
7.1	−0.91	−1.15	−1.06	3.05	3.84	6.76
8.0	−0.98	−1.20	−1.04	2.85	3.58	6.43
8.7	−1.00	−1.21	−1.07	1.99	4.24	6.23
9.5	−1.01	−1.19	−1.08	1.39	4.57	5.96
10.8	—	−1.14	−1.14	—	5.56	5.56
11.7	—	−1.12	−1.12	—	5.17	5.17

* 18 ml Britton and Robinson buffer solution with 2 ml of stock nitrosoguanidine solution.
† Total, refers to total diffusion current. pH 2.4-5.0 waves well defined, pH 5.7-8.7 waves ill-defined, pH 9.0-11.7 one well-defined wave.

the $E_{1/2}$ vs. pH plots for nitrosoguanidine (1st wave) is about ½ that for nitroguanidine in this pH range. The diffusion current constants become smaller for the first wave and larger for the second wave with an increase in the pH of the solution. It should be noted (Table II) that in the narrow pH range of 5.7-6.1 the diffusion current constants for each wave of nitrosoguanidine are nearly the same. It appears that nitro and nitrosoguanidine have nearly the same reduction potentials in acid solution with a pH < 2.5. Nitrosoguanidine appears to be slightly the better depolarizer ($E_{1/2}$ more positive) in solutions with a pH > 2.5, although the differences in the $E_{1/2}$ values are very small. Thus, it would seem that if one tried to reduce nitroguanidine electrochemically, any nitrosoguanidine that might form would be immediately reduced further. It should be noted also from the data in Tables I and II that a pH range of 5 to 6 appears to be best for a good separation between the first wave of nitrosoguanidine and the wave of nitroguanidine. Thus, a quantitative analysis of nitrosoguanidine in the presence of nitroguanidine should be possible in this pH range.

Data on the effect of the mercury column height on the diffusion current for each wave of nitro and nitrosoguanidine indicates diffusion controlled processes throughout the entire pH range studied; i.e., the limiting current varies with the square root of the corrected mercury height (Tables VII and VIII).

The effect of concentration on the $E_{1/2}$ and i_d values of nitro and nitrosoguanidine is shown in Table III and was obtained in a Clark and Lubs' buffer solution of pH 6. At this pH a double wave was observed with 1.0 mM solutions of the guanidines but only the total wave was defined well enough for accurate measurement. Over the concentration range of 0.5-6.0 mM the total wave appeared to be proportional to concentration ($i_d = KC$) for nitroguanidine. However, for the total wave of nitrosoguanidine,

Table III. Effect of concentration on $E_{1/2}$ and i_d of nitro and nitrosoguanidine, Clark and Lubs' buffer (2x), pH 6.0, 0.001% methyl red $m^{2/3}t^{1/6} = 1.92$ mg$^{2/3}$ sec$^{-1/2}$

Compound	Concentration, mM	i_d, μa	$E_{1/2}$ (vs. Ha pool), v
Nitroguanidine	0.5	8.15	−1.29
Nitroguanidine	1.4	24.20	−1.33
Nitroguanidine	4.0	66.60	−1.38
Nitroguanidine	6.0	94.20	−1.42
Nitrosoguanidine	0.5	7.29	−1.12
Nitrosoguanidine	1.7	20.20	−1.15
Nitrosoguanidine	4.0	39.90	−1.17
Nitrosoguanidine	6.0	50.70	−1.25

$i_d = KC$ over the shorter range of 0.5-2 mM solutions. Since the $E_{1/2}$ values depend on concentration and become more negative with increasing concentration for both nitroguanidine and nitrosoguanidine solutions, and since plots of log $i/(i_d - i)$ do not give a linear relationship, the over-all reduction process at the cathode appears to be irreversible for each compound.

With solutions containing two or more organic compounds, the possibility exists that one compound may affect the diffusion process of the other compound at a dropping mercury electrode. Table IV gives data on the effect of nitroguanidine on the first wave of nitrosoguanidine. Small amounts of nitrosoguanidine can be determined in the presence of nitroguanidine. However, when the ratio of these compounds exceeds 1:1 there is difficulty in precise measurement of the first nitrosoguanidine wave.

Effect of temperature, solvent, and acid concentration.—In a Clark and Lubs' buffer solution (pH 5.5), the total wave for each compound is lower at 5°C than at 30°C. This is what one would expect, as the diffusion coefficients depend on temperature and are larger at the higher temperatures. However, at the lower temperature the i_d of the first nitroguanidine wave decreased and the i_d of the second wave increased. This may indicate a change in state and concentration of the reducible species in solution with a change in temperature. With nitrosoguanidine solutions, the height of the first wave and the $E_{1/2}$ values, respectively, are nearly the same at 5°C as they are at 30°C. Only the second wave appears to be greatly affected by the change in temperature. This unusual behavior of the polarographic waves with a change in the temperature of the solution is difficult to explain. It may be due to the de-

Table IV. Effect of nitroguanidine on first wave of nitrosoguanidine, Clark and Lubs' buffer (2x), pH 5.5, 0.001% methyl red $m^{2/3}t^{1/6} = 1.92$ mg$^{2/3}$ sec$^{-1/2}$

Nitroguanidine concentration, mM	Nitrosoguanidine concentration, mM	i_d, μa
0.0	1.0	7.2
0.5	1.0	7.0
1.0	1.0	7.1
2.0	1.0	7.5*
3.0	1.0	8.0*

* First wave of nitrosoguanidine not as well-defined.

Table V. Effect of ethyl alcohol on $E_{1/2}$ and i_d of nitroguanidine, 1.40 mM solution of nitroguanidine
$m^{2/3}t^{1/6} = 1.92$ mg$^{2/3}$ sec$^{-1/2}$, 0.001% methyl red

Ethyl alcohol %*	$E_{1/2}$ (vs. Hg pool), v		i_d, μa	
	1st	2nd	1st	2nd
0	−0.93	−1.33	11.7	12.5
10	−1.34	−1.55	13.9	6.0
25	−1.39	−1.61	12.4	5.5
50	−1.49	−1.71	15.2	7.5
75	−1.50	−1.71	17.0	8.2

* Remaining per cent is Clark and Lubs' buffer (2x), pH 6.0.

Table VI. Effect of HCl concentration on $E_{1/2}$ and i_d of nitroguanidine
$m^{2/3}t^{1/6} = 1.45$ mg$^{2/3}$ sec$^{-1/2}$, 0.001% methyl red

Nitroguanidine concentration, mM	HCl normality	$E_{1/2}$ (vs. Hg pool), v		i_d, μa	
		1st	2nd	1st	2nd
1.007	0.1	−0.62	−1.01	9.0	3.9
1.038	0.2	−0.54	−0.95	9.5	3.5
1.038	1.0	−0.39	−0.85	14.7	1.7
1.081	2.0	−0.36	−0.85	14.6	1.1
1.077	6.0	−0.25	—	15.6	—

gree of solvation of different reducible species in solution.

Ethyl alcohol was used to study the effect of a nonaqueous solvent on the waves of nitroguanidine (Table V). Although the separation of the waves is not as sharply defined in the presence of ethyl alcohol, there are two distinct waves for nitroguanidine in these solutions. The $E_{1/2}$ values and i_d values are dependent on the concentration of ethyl alcohol in the medium. It should be noted that the $E_{1/2}$ values are shifted to more negative potentials in the presence of ethyl alcohol, and the i_d value of the total wave appears to go through a minimum around 25% ethyl alcohol. With reducible metal ions an increase in the product $i_d\eta^{1/2}$, where η is the viscosity of the solution, is observed up to about 25% ethyl alcohol (28). However, it can be seen that a decrease in the product $i_d\eta^{1/2}$ is observed with solutions of nitroguanidine up to about 25% ethyl alcohol. Thus, it would appear that with up to 25% ethyl alcohol an increase in the size of the solvated reducible nitroguanidine ion occurred as the activity of water decreased; or that the decreasing dielectric constant favored and caused ion-pair formation and thus an increase in the size of the diffusing species. The increase of "apparent" pH of the final solution with increasing ethyl alcohol concentrations could account also for some difference in wave heights. As the percentage of ethyl alcohol is increased beyond 25% the wave heights of both the total and individual waves increase. The total wave is about the same height in a 70% ethyl alcohol solution as it is in a purely aqueous solution; however, the individual wave heights are just the opposite (first wave height larger and second wave height smaller) in alcohol. These data would seem to rule out ion-pair formation and suggest that the degree of solvation of nitroguanidine was about the same in 75% ethyl alcohol and purely aqueous pH 6.0 buffer solution. Since the first wave height is greater in the 75% ethyl alcohol solution than in the purely aqueous solution, it might also be suggested that nitroguanidine is more highly protonated in the 75% ethyl alcohol solution, and that the first wave is due to the reduction of a protonated species and the second wave is due to the reduction of the unprotonated molecule.

The effect of hydrochloric acid concentration on the $E_{1/2}$ and i_d values of nitroguanidine is shown in Table VI. Again two waves were observed. With a decrease in acid concentration the $E_{1/2}$ value of the first wave became more negative and the i_d value decreased. Only one well-defined wave was observed in 6*N* acid, although a very small second wave was found in 2*N* acid. In strong acid solution a highly protonated specie should predominate, and very little of the unprotonated molecule would be present. In acidic solution a shift of half-wave potentials to more negative values with an increase in pH sometimes can be thought of as a direct reaction of the compound with a proton to form an intermediate ion which is reduced more easily. At the higher pH values the molecule itself is reduced, followed by a reaction of the anion with water as hydrogen ions (29).

Nitro and nitrosoguanidine are weak ampholytes. For nitroguanidine $pK_a = 12.20$ and $pK_b = 14.5$, while for nitrosoguanidine $pK_a = 11.70$ and $pK_b = 11.90$ (30). As a consequence, different ionic and molecular species may exist in solution depending upon the pH. This fact suggests a possible explanation for the existence of two waves at some pH values and only one wave at other values. For simplicity in explanation of the observed polarographic waves, only the following ionic and molecular forms[2] need to be considered.

[2] Since nitro and nitrosoguanidine molecules may be considered as resonating among various hybrids (8), numerous other forms with various charge separations may also be written, but these are not important in the present discussion.

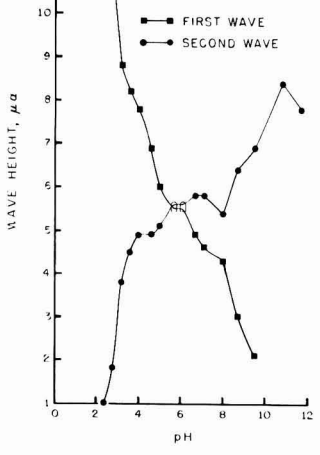

Fig. 2. Effect of pH on i_d of 1.043 mM solution of nitrosoguanidine. Britton and Robinson buffer system (2X).

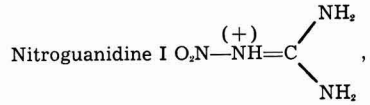

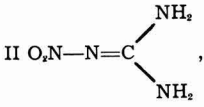

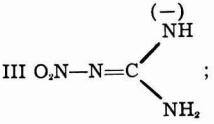

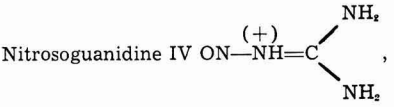

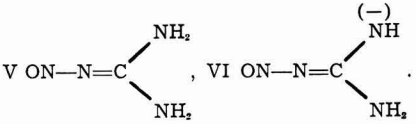

Thus, in 6*N* HCl, forms I and IV would be the predominant species; in *p*H from 1 to 4, I and II or IV and V; about *p*H 7, II and III or V and VI; and at *p*H 8-9 and above, III and VI should be the major forms present. Only one wave was observed in solutions more alkaline than *p*H 9 and more acid than 2*N* acid. In the Britton and Robinson buffer system, the two wave heights obtained with millimolar solutions of nitrosoguanidine vary greatly with *p*H and appear to be of equivalent height around a *p*H of 6 (Fig. 2). Both these waves appear to be diffusion-controlled (i_d varies as $h^{-1/2}$) (Tables VII and VIII) and the $E_{1/2}$ values vary with a change in *p*H. These data would suggest that if the existence of two waves for nitrosoguanidine in this medium is due to two reducible species in solution, then, at a *p*H of 6 forms IV and V probably give rise to the equivalent wave heights shown in Fig. 2 as first wave and second wave, respectively. The two waves obtained with

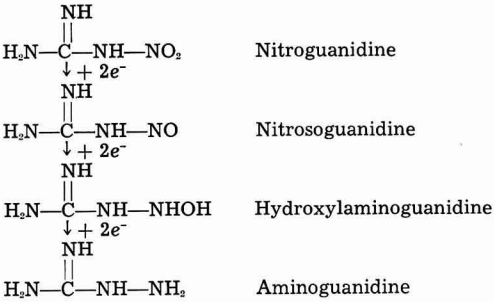

Fig. 3. Possible reduction mechanism for the nitro-nitrosoguanidine system.

Table VII. Effect of mercury column height on i_d of nitroguanidine, Clark and Lubs' buffer (2x), *p*H 6.11, 1.44 mM solution of nitroguanidine containing 0.001% methyl red
$m^{2/3}t^{1/6} = 1.92$ mg$^{2/3}$ sec$^{-1/2}$

Mercury column h, cm	i_d, μa			$i_d h^{-1/2}$		
	1st	2nd	Total	1st	2nd	Total
95.2	12.8	10.2	25.4	1.31	1.05	2.61
71.1	11.3	8.9	22.0	1.34	1.06	2.61
59.7	10.7	8.4	20.4	1.38	1.08	2.63
47.0	9.4	7.6	18.0	1.37	1.11	2.63

Table VIII. Effect of mercury column height on i_d of nitrosoguanidine, Clark and Lubs' buffer (2x), *p*H 5.5, 1.70 mM solution of nitroguanidine containing 0.001% methyl red
$m^{2/3}t^{1/6} = 1.92$ mg$^{2/3}$ sec$^{-1/2}$

Mercury column h, cm	i_d, μa			$i_d h^{-1/2}$		
	1st	2nd	Total	1st	2nd	Total
95.2	13.2	11.9	26.5	1.35	1.22	2.72
87.6	12.5	11.1	25.0	1.34	1.19	2.68
71.1	11.6	10.2	22.8	1.37	1.21	2.70
59.7	11.2	9.5	20.9	1.44	1.23	2.70

solutions of nitroguanidine were not as sharply defined and accurate measurements were not possible in the intermediate *p*H ranges of the buffered systems.

Determination of the n*-value and reduction mechanism.*—The porous diaphragm cell method with magnetic stirring has been used successfully in these laboratories for the determination of the diffusion coefficients (D) of some organic compounds (31). A D value of 2.37 x 10^{-5} cm^2 sec^{-1} was obtained for nitroguanidine by this method in a 2M ammonium sulfate solution. This value for D, when used in the Ilkovic equation ($n = i_d/607D^{1/2}Cm^{2/3}t^{1/6}$), gave an n-value of 3.48 electrons. From the Stokes-Einstein equation, $D(\text{cm}^2/\text{sec}) = 2.96 \times 10^{-7}/\eta(V_m)^{1/3}$ at 25°C, where η is the solution viscosity in dyne seconds per cm^2 and V_m is the molar volume, an n-value of 4.88 electrons was obtained. Since these values were not in agreement and since nitrosoguanidine decomposes rather rapidly in aqueous solutions, a direct and rapid method for the determination of n was thought desirable. With the direct and rapid method for n-values (millicoulometric) that was recently investigated and modified in these laboratories (26, 27), an n-value of 5 was obtained for nitroguanidine in a Clark and Lubs' buffer solution of *p*H 10 where one well-defined wave occurred. Nitroguanidine in a Clark and Lubs' buffer solution of n-value of 3. These values of 5 and 3 are repeatable, and, although the n-values are not 4 and 2 as expected, the 2 electron difference in values indicates that the reduction process of nitroguanidine passes through the nitrosoguanidine state in *p*H 10 buffered solutions (Fig. 3).

It is known that in strong acid solutions nitroguanidine is reduced directly to aminoguanidine (3, 32). In 6*N* hydrochloric acid solutions an n-value of 6 was obtained for nitroguanidine by the millicoulometric technique (26). However, in neutral and alkaline solutions the reduction mechanism appears to be complicated and n-values are of little help in elucidating the over-all process.

The n-value of 5 for nitroguanidine, obtained by millicoulometry in a pH 10 Clark and Lubs' buffer solution, may be explained by a coupling of the products of a 2 and 6 electron reduction respectively (Fig. 3). It has been shown that nitrosoguanidine and aminoguanidine can react to form a tetrazene (33), which should be further reducible. The n-value of 3.5, obtained in the 2M ammonium sulfate solution (pH 4.5) from an experimental D value, would seem to indicate the reduction of nitroguanidine to hydroxylaminoguanidine (Fig. 3) in weakly acidic or neutral solutions. This latter compound was suggested as the end product in the reduction of nitroguanidine in alkaline medium ($pH > 12$) by Lanza and co-workers (17). Hydroxylaminoguanidine has never been isolated. It would be expected to decompose rapidly to guanidine and hyponitrous acid. It appears that in neutral and alkaline solutions there is more than one process occurring at the dropping mercury electrode. These processes are probably occurring at different rates and the products may undergo "dearrangement." Thus, it is difficult to establish the over-all reduction mechanism of either nitroguanidine or nitrosoguanidine at a dropping mercury electrode in these solutions.

The authors prepared nitrosoguanidine at a mercury cathode in 20% yields by the large-scale electrolysis of nitroguanidine in a 2M-ammonium sulfate solution. Polarographic techniques were used to determine the optimum conditions for the preparation. The addition of nickel II ions to the solutions produced excellent yields of a red nickel-nitrosoguanidine complex salt. The complex salt is extremely stable and attempts to quantitatively recover the nitrosoguanidine from the complex were unsuccessful. The formation of this salt established nitrosoguanidine as the first step in the reduction of nitroguanidine in neutral or weakly acidic solution at a mercury cathode (Fig. 3). As fast as nitrosoguanidine is formed, it complexes with the nickel ions and a bright red precipitate appears in the electrolysis solution.

Acknowledgment

The authors wish to express their sincere appreciation and gratitude to G. B. L. Smith (deceased), Ronald A. Henry, and William G. Finnegan, for their invaluable help and encouragement during this work. The authors also wish to thank Robert D. Weaver for obtaining the n-value data.

Manuscript received March 10, 1958. This paper was prepared for delivery before the Pittsburgh Meeting, Oct. 9-13, 1955.

Any discussion of this paper will appear in a Discussion Section to be published in the December 1959 JOURNAL.

REFERENCES

1. G. Pellizzari, *Gazz. chim. ital.*, **21**, II, 405 (1891).
2. T. L. Davis, *J. Am. Chem. Soc.*, **43**, 669, 2234 (1921); **44**, 2598 (1922).
3. F. K. J. Thiele, *Liebigs Ann. Chem.*, **270**, 1, 383 (1892); **273**, 133 (1893).
4. G. B. L. Smith and V. J. Sabetta, *J. Am. Chem. Soc.*, **54**, 1034 (1932).
5. O. P. Steinbach, Jr., "Reduction of Nitroguanidine," Thesis, Polytechnic Institute of Brooklyn, 1927.
6. C. Hahn, E. Pribyl, E. Lieber, B. P. Caldwell, and G. B. L. Smith, *J. Am. Chem. Soc.*, **66**, 1223 (1944).
7. V. J. Sabetta, D. Himmelfarb, and G. B. L. Smith, *J. Am. Chem. Soc.*, **57**, 1478 (1935)
8. J. H. Bryden, L. A. Burkardt, E. W. Hughes, and J. Donohue, *Acta Cryst.*, **9**, (July 1956).
9. W. D. Kumler, *J. Org. Chem.*, **18**, 676 (1953).
10. W. D. Kumler and P. P. T. Sah, *ibid.*, **18**, 669 (1953).
11. A. F. McKay, M. A. Weinberger, J. P. Picard, W. B. Hatton, M. Bedard, and H. E. Rooney, *J. Am. Chem. Soc.*, **76**, 6371 (1954).
12. S. S. Barton, R. H. Hall, and G. F. Wright, *ibid.*, **73**, 2201 (1951).
13. M. W. Kirkwood and G. F. Wright, *J. Org. Chem.*, **18**, 629 (1953).
14. J. E. DeVries and E. St. Clair Gantz, *J. Am. Chem. Soc.*, **76**, 1008 (1954).
15. A. F. McKay, J. P. Picard, and P. E. Brunet, *Can. J. Chem.*, **29**, 746 (1951).
16 W. W. Brandt, J. E. DeVries, and E. St. Clair Gantz, *Anal. Chem.*, **27**, 392 (1955).
17. P. Lanza, A. Delmarco, A. F. McKay, and G. Semerano, *Sperimentali di Polargrafia*, **2**, 1 (1955).
18. K. Namba and K. Suzuki, *Bull. Chem. Soc.* Japan, **28**, 623 (1955).
19. I. M. Kolthoff and J. J. Lingane, "Polarography," 2nd ed., pp. 373-375, Interscience Publishers, New York (1952).
20. I. M. Kolthoff and J. J. Lingane, *ibid.*, p. 374.
21. N. A. Lange, "Handbook of Chemistry," 8th ed., p. 938, Handbook Publishers, Inc., Sandusky, Ohio (1952).
22. H. T. S. Britton and R. A. Robinson, *J. Chem. Soc.*, **1931**, 1456.
23. T. L. Davis and E. N. Rosenquist, *J. Am. Chem. Soc.*, **59**, 2114 (1937).
24. R. H. Stokes, *ibid.*, **72**, 763 (1950).
25. T. L. Davis, "Chemistry of Powder and Explosives," Vol. I, p. 392, New York (1941).
26. G. F. Reynolds and H. I. Shalgosky, *Anal. Chim. Acta*, **10**, 386 (1954).
27. R. D. Weaver and G. C. Whitnack, *ibid.*, **18**, 51 (1958).
28. L. Meites, "Polarographic Techniques," p. 57, Interscience Publishers, Inc., New York (1955).
29. I. M. Kolthoff and J. J. Lingane, *op. sit.*, p. 627.
30. J. E. DeVries and E. St. Clair Gantz, *J. Am. Chem. Soc.*, **76**, 1008 (1954).
31. G. C. Whitnack, J. Reinhart and E. St. Clair Gantz, *Anal. Chem.*, **27**, 359 (1955).
32. E. Lieber, and G. B. L. Smith, *J. Am. Chem. Soc.*, **59**, 2283 (1937).
33. E. Lieber and G. B. L. Smith, *Chem. Rev.*, **25**, No. 2, 220 (1939).

Electrodeposition of Adherent Titanium Coatings on Induction Heated Cathodes in Fused Salts

B. J. Fortin, J. G. Wurm, L. Gravel, and R. J. A. Potvin

Laval University, Quebec, Quebec, Canada

ABSTRACT

A new electrolytic method for the deposition of adherent coatings of titanium on steel cathodes is described. The procedure involves the use of fused alkali-halide baths composed of eutectic mixtures of lithium, potassium or sodium iodides, bromides, chlorides, and fluorides, with a high-frequency heated cathode and a soluble titanium anode. The bath composed of KI-KF performed best and deposited a very smooth and uniform titanium coating. Conversely, the bath composed of KI-NaI and TiI_4 (2 to 5%) yielded dendritic Ti and is therefore considered more suitable for an electrorefining process. Equipment and operating conditions are described and the microstructure of the coating produced is reported. A series of decomposition voltage curves is included and discussed, and the mechanism of the electrolytic reactions is studied in detail.

A complete literature survey of the electrodeposition of titanium from molten salts has been published recently by Steinberg (1). Ti diffusion coatings were obtained by Straumanis, *et al.* (2, 3) from fused baths containing dispersed Ti crystals or Ti salts. Much remains to be investigated, however, on the deposition of uniform and strongly adherent coatings of Ti.

The present work deals with an electroplating method involving the use of an induction-heated cathode and a soluble Ti anode in fused salt baths. The induction-heated cathode acts at the same time as a heating element to maintain the bath in a molten state. In this manner, the cathode is at a temperature appreciably higher than the surroundings. In fact, the anodic zone, far removed from the cathode area, may be kept much colder. This provides, therefore, means to control the rate of solution of the anode as well as volatilization losses and secondary reactions. The skin effect due to induction current creates a maximum temperature zone on the very surface of the cathode, speeding up degassing and facilitating diffusion of the deposited Ti. Furthermore, the electrolysis may be carried out in a Pyrex or transparent quartz cell which makes it convenient to see directly the phenomena taking place.

Description of Cells

Two types of cells are used. These cells are made up of a Pyrex or quartz tube closed at the bottom and covered at the top by a gas-tight asbestos lid which holds also the electrodes and inert gas ducts.

In the first type, as shown in Fig. 1, the anode is composed of Ti sponge which covers the bottom of the cell: a shielded W wire passing through the molten electrolyte is provided to carry current to the anode. The cathode, in this particular case, is made of steel wire 2-mm diameter and has the form of a ring which is located in the center of the high-frequency coil.

The second type of cell differs from the first one in that the relative positions of the anode and cathode are reversed: the anode is located in the upper portion of the bath and consists of either Ti wire or a cylindrical W grid filled with Ti sponge. The ring-shaped cathode reaches near the bottom of the cell and is held by means of a connecting wire shielded with a Pyrex glass tube. The design of the cell shown in Fig. 1 was found in practice to be preferable. In fact, in this cell, there exists a marked difference in temperature between the anode and the cathode zones, which cannot be obtained in the other type of cell where the cathode, close to the bottom, favors stronger convection resulting in a more uniform heat distribution.

A variety of cathode shapes made of iron or steel were used. These included massive pieces such as threaded rods, flat washers, or lighter pieces made of wire wound in different shapes.

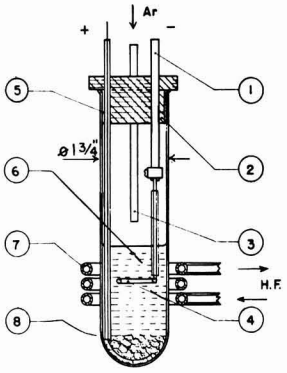

Fig. 1. Electrolytic cell with a heating cathode (Type 1). 1, Cathode holder; 2, asbestos stopper; 3, argon inlet; 4, heating cathode ring; 5, W wire in Pyrex tube; 6, electrolytic bath; 7, high-frequency coil; 8, Ti sponge anode.

Experimental Procedure

Electrolytic baths composed of low-fusing halides of lithium, sodium and potassium were selected. Each bath contained about 150 g of an eutectic mixture of these salts which were placed in the cell tube and melted in a separate furnace for dehydration while flushing with dry argon. Finally, the assembled cell was rapidly transferred to the high-frequency coil. An optical pyrometer was used to observe the cathode temperature, and a thermocouple introduced through the argon outlet tube served to determine the temperature of the bath at different depths. The temperature of the cathode during electrolysis was kept constant within 25°C and was approximately 200°C above the average temperature in the bath.

At the very first stage of electrolysis, the cathode became surrounded with a bluish-violet cloud which within a few minutes extended to the whole bath. At the end of the electrolysis, the cell was cooled rapidly in an air blast while maintaining a difference of potential of about 1 v between the electrodes in order to prevent any interaction between the bath and the deposited Ti. The cathode products and the remainder of the bath after solidification were submitted to a combined chemical and x-ray analysis. It was considered that rapid cooling of the bath after electrolysis minimized postelectrolytic reactions, and therefore it was assumed that analytical results obtained on the solidified melts could serve as a basis for proposing a probable explanation of the mechanism involved.

In some experiments, TiI_4 and K_2TiF_6 were injected into the molten eutectic during electrolysis.

Results

The first series of experiments reported in Table I dealt with electrolytic baths composed of mixtures of halides of eutectic composition, using a soluble anode and a ring-shaped cathode made of a 2-mm steel wire. Cathode current densities were kept fairly constant during the whole of the electrolysis: values from 0.42 to 1.0 amp/cm^2 were used. It was observed that the Ti deposit was mainly dendritic, nonuniform and poorly adherent when the temperature at the cathode was below 850°C, while it was more adherent for higher temperatures; in fact, it was found, in this first series of experiments, that at the start of the electrolysis a compact, adherent and shiny deposit of Ti appeared on the cathode. This deposit grew up regularly for about 10 min, after which some dendritic deposit showed up at various spots and continued to develop, forming an irregular surface or even bridging up to give rise to a spongy layer. This latter effect was more marked for the iodide and bromide baths. At the end of the electrolysis, the zone next to the cathode gave a definitely alkaline aqueous solution while that from the anode was acid. Furthermore, as the electrolysis proceeded the zone near the anode turned from a faint bluish-violet to a reddish-brown in the case of the bromide and iodide baths and to a pale green in the case of the chloride baths. The latter is ascribed to the formation of $NaTiCl_4$ described by Steinberg (1). The current efficiency was high, slightly above 90% in most of the experiments mentioned in Table I. On the other hand, the amount of Ti dissolved at the anode exceeded considerably the theoretical value; this may result in part from the formation of lower valence Ti compounds which have been detected in the bath.

In the second series of experiments, Nos. 9-12 in Table I, small proportions of TiI_4 were injected under argon in baths containing the eutectic mixture NaI-KI. One experiment also is reported on a bath containing KI-KF in which K_2TiF_6 was injected in the same manner. At the end of the electrolysis the baths containing only iodides had a reddish-brown color; as in the previous series, the salts surrounding the cathode gave a very strongly alkaline reaction while those surrounding the anode had a low *p*H when dissolved in water. The coatings in this series of experiments were in general of a heavier adherent type than in the previous; however, they had a rough and nonuniform surface as may be seen in Fig. 2a. When the temperature of the cathode was increased to 975°C, as in experiment No. 11, the surface became smoother and more uniform but it was found that the amount of anode dissolved during electrolysis was still greater than in the previous series, reaching 215% of the theoretical value based on Faraday's law. This is not surprising in view of the strong reaction between the injected TiI_4 and the anode at a high temperature.

The third series of experiments, Nos. 13-17 of Table I, concerned only baths composed of a KI-KF eutectic mixture using Ti anodes or Zr anodes in the

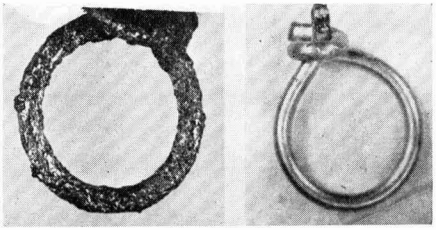

Fig. 2. (a) (left) Rough and nonuniform surface obtained in a KI-NaI bath with TiI_4 addition (Expt. 10, Table I). (b) (right) smooth and uniform coating obtained in KI-KF bath (Expt. 15, Table I). Approx. 2/3 size.

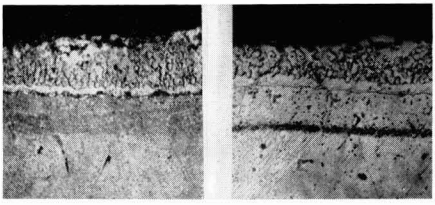

Fig. 3. (a) (left) Micrograph showing the Ti deposit obtained in a KI-NaI bath (Expt. 5, Table I). The HF etch has revealed the more or less granular deposit of Ti crystals separated by a clear white, compact and very hard intermediary zone from a darker etching zone. The Ti at the surface contained below 0.001% metallic elements as determined spectrographically, save for Fe, which reached a value of 11% near the interface. The darker zone is much harder than the low carbon steel of the base as shown by the microindentations in (b) (right), suggesting that Ti has diffused in that zone to the darker line limiting the soft steel and appearing in (b) after a Nital etch. Magnification 300X.

Table I. Electrolytic operating conditions*

Expt. No.	Type of cell	Bath composition, g		Soluble anode**	Volts	Amps	Cat. C.D., amp/cm²	Time, min	Cathode temp, °C	Bath temp, °C	Results
1	Fig. 1	NaCl	85	Ti	6.0	3.0	0.50	18	900-925	725	Very thin, nonuniform, poor coating.
		KCl	65								
2	Fig. 1	NaCl	85	Ti	4.5	2.0	0.50	20	900-925	725	Thin, poor coating, irregular.
		KCl	65								
3	Fig. 1	LiCl	80	Ti	3.5	3.0	0.52	15	875-900	700	Thin, more or less uniform coating.
		KCl	70								
4	Fig. 1	NaBr	79	Ti	2.6	3.0	1.00	18	900-925	725	Uniform coating, with dendritic crystals.
		KBr	71								
5	Fig. 1	NaI	63	Ti	5.0	5.0	0.77	30	925-950	750	Shiny coating with dendritic crystals.
		KI	87								
6	No. 2	NaI	63	Ti	2.5	5.0	0.42	45	900-925	725	Heavy dendritic sponge formation.
		KI	87								
7	Fig. 1	NaI	63	Ti	4.5	3.0	0.53	35	925-950	750	Abundant coating with dendritic shiny crystals.
		KI	87								
8	Fig. 1	NaI	63	Zr	3.5	2.0	0.70	20	900-925	725	Uniform coating with sponge formation.
		KI	87								
9	No. 2	NaI	63	Ti	4.5	3.5	1.0	20	900-925	725	Heavy adherent coating, shiny but nonuniform.
		KI	87								
		TiI_4	7.5								
10	Fig. 1	NaI	63	Ti	2.5	2.0	0.90	30	925-950	750	Heavy adherent coating, shiny but nonuniform.
		Ti	87								
		TiI_4	7.5								
11	Fig. 1	NaI	63	Ti	3.5	2.0	0.40	15	950-975	775	More uniform but thin coating.
		KI	87								
		TiI_4	3								
12	Fig. 1	KF	29	Ti	3.7	3.0	0.40	10	900-925	725	Poor coating.
		KI	121								
		K_2TiF_6	3								
13	Fig. 1	KF	29	Ti	2.5	2.0	0.66	15	900-925	725	Excellent coating, very uniform, no sponge.
		KI	121								
14	Fig. 1	KF	29	Ti	2.5	3.0	0.40	18	925-950	750	Excellent coating, very uniform.
		KI	121								
15	Fig. 1	KF	29	Ti	2.2	2.0	0.70	20	925-950	750	Excellent coating, very uniform.
		KI	121								
16	Fig. 1	KF	29	Zr	2.3	2.0	0.70	20	925-950	750	Uniform coating, some dark spots.
		KI	121								
17	Fig. 1	KF	29	Zr	2.2	2.0	0.70	15	900-925	725	Very uniform coating.
		KI	121								

* Induction heating cathode process.
** Anode: Ti or Zr sponge except for Expts. 6 and 9 where a 2 mm Ti wire was used.

type of cell depicted in Fig. 1. The Ti coatings obtained with this type of bath were adherent, compact, smooth and shiny either on ring-shaped or flat pieces; in all cases, as may be seen in Fig. 2b, they showed no pitting or dark spotted or spongy areas. Contrary to the other two series, the salts surrounding the cathode and the anode both showed an alkaline reaction at the completion of the electrolysis and the bath had a pinkish color. In this latter series also, the inside wall of the Pyrex or quartz cell was free from any Ti mirror which always tends to form in the two other series of experiments; such mirrors have already been observed by Straumanis, *et al.*, on ceramic materials during titanizing experiments (4).

Metallographic examination.—Figures 2-5 illustrate some of the types of Ti coatings obtained with the main baths described above.

Decomposition Voltages and Mechanism of the Electrolytic Reactions

The decomposition voltages were determined for the main eutectic mixtures selected for the above experiments using first an insoluble anode, and then a soluble Ti anode. These decomposition voltages were obtained in the usual way by extrapolating the experimental current-voltage curves to zero current. All measurements were carried out under an argon atmosphere in a graphite crucible containing the molten salts held uniformly at 725°C. The use of a crucible heated in a resistance furnace eliminated the excessive variations brought about by the stirring action obtained in induction heating and, in particular, facilitated the determination of the needed data on the anodic phenomena under the same average bath temperature as in the electroplating experiments described in Table I. The steel cathode was spaced ¾ in. from the anode. Both electrodes were immersed 1 in. into the fused salts. The salts were always submitted to a preliminary electrolysis at 1.8 v for 30 min using graphite electrodes in order to remove the last traces of water. The curves in question are shown in Fig. 6-8. In these figures are also given the current-voltage curves when TiI_4 or, in one case, K_2TiF_6, were injected into the bath prior to measurements.

The extrapolation of curve A in Fig. 6 corresponds to the decomposition of NaCl (3.2 v), indicating that the electrolysis of a NaCl-KCl mixture yields Na as a primary product. On the other hand, when a Ti

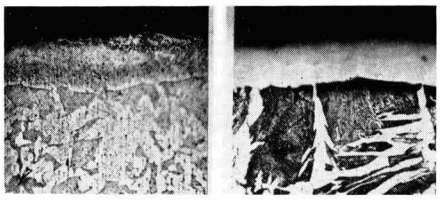

Fig. 4. (a) (left) Micrograph showing the 0.03 mm thick Ti coating built up on the steel cathode (sample appearing in Fig. 2b); the HF etch reveals that interdiffusion of Ti and Fe has taken place in the coating. (b) (right) Micrograph of a section similar to (a), but with a Nital etch to reveal with better contrast the Ti deposit which is left practically unetched and also the coarse Widmanstatten structure of the steel underneath. Magnification 300X.

Fig. 5. Micrograph of a section from a sample plated with Ti in a KI-KF bath (Expt. 15, Table I). The microindentations in the Ti deposit correspond to a hardness of about 180 Vickers which is of high order and possibly results from some diffusion of the steel constituents into the Ti coating at the temperature at which the cathode was held during the electrolysis (950°C).
1% HF + Nital etch Magnification: 500X

anode is used, there is a considerable drop in the decomposition voltage corresponding to 1.7 v as shown by comparison with the extrapolated voltage of curve B. Of the known Ti chlorides, $TiCl_2$ is the one the free energy of which corresponds the closest to the voltage drop mentioned above. It suggests, therefore, the possible following reaction as predominant:

$$Ti + Cl_2 \rightarrow TiCl_2 (E_{725°C} = 1.7 \text{ v}) \qquad [1]$$

It appears also from Fig. 6 that the addition of TiI_4 shifts the decomposition voltage to a slightly lower value for both W and Ti anodes.

Somewhat similar conclusions may be inferred from examination of the decomposition voltage curves of Fig. 7 dealing with KI-NaI baths. In this case, however, the extrapolation of curve A to zero current gives a decomposition voltage of 2.65 which falls between those of NaI and KI. It is therefore likely that K is formed to some extent along with Na as a primary reaction product. On the other hand, since the drop in the decomposition voltage, when using Ti as anode (see curve B), is 0.90 v, it seems that the Ti at the anode, as in the case of the NaCl-KCl bath, also forms a divalent salt; in fact, the voltage drop observed corresponds to the formation of $TiI_2 (E_{725°C} = 0.86 \text{ v})$ which is the Ti iodide having the highest decomposition voltage.

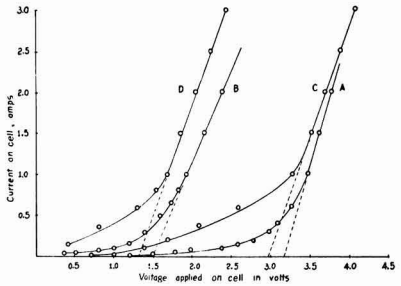

Fig. 6. Decomposition voltage curves of fused KCl-NaCl baths at 725°C with and without addition of TiI_4 using a Fe cathode. A, KCl-NaCl bath, W anode; B, KCl-NaCl bath, Ti anode; C, KCl-NaCl bath + TiI_4 (1.5%), W anode; D, KCl-NaCl bath + TiI_4 (1.5%), Ti anode.

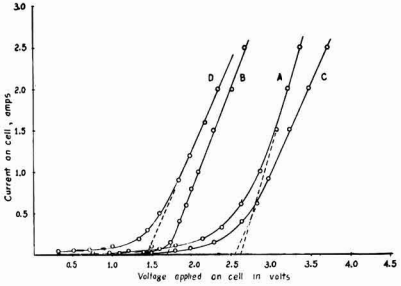

Fig. 7. Decomposition voltage curves of fused KI-NaI baths at 725°C with and without addition of TiI_4 using a Fe cathode. A, KI-NaI bath, Pt anode; B, KI-NaI bath, Ti anode; C, KI-NaI bath + TiI_4 (1.5%), Pt anode; D, KI-NaI bath + TiI_4 (1.5%), Ti anode.

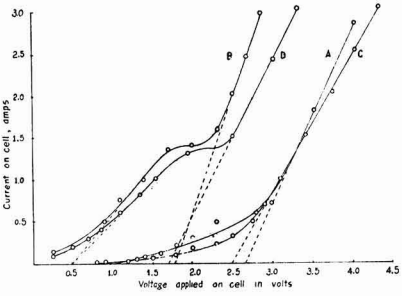

Fig. 8. Decomposition voltage curves of fused KI-KF baths at 725°C with and without addition of K_2TiF_6 using a Fe cathode. A, KI-KF bath, Pt anode; B, KI-KF bath, Ti anode; C, KI-KF bath + K_2TiF_6 (1.5%), Pt anode; D, KI-KF bath + K_2TiF_6 (1.5%), Ti anode.

The extrapolation to zero current of curve A in Fig. 8 indicates that, in the case of a mixed halide bath such as KI-KF, only KI is decomposed because the value of 2.7 v found for the decomposition voltage corresponds closely to the calculated value for KI. Otherwise, a much higher decomposition voltage would be observed (E for KF at 725°C = 4.7 v). When a Ti anode is used, the curve obtained exhibits two distinct branches which may be extrapolated to give two different decomposition voltages; this points to a double type of reaction at the anode. It appears in fact that at low voltage Ti forms only fluorides; formation of such fluorides is highly exo-

Table II. General mechanism of reactions

A—Primary steps

(a) At the Cathode: reduction of an alkali halide.
$M^+ + e^- \rightarrow M$ [7] (Primary cathode reaction according to decomposition voltage curves), where M^+ is an alkali ion in the form of a halide MX contained in the electrolyte and X is the most active halogen.

(b) At the Anode: Formation of Ti ions.
$Ti - ne^- \rightarrow Ti^{n+}$ [8]

B—Secondary steps

(a) At the Anode $Ti^{n+} + nX^- \rightarrow TiX_n$ [9]

(b) At the Cathode $TiX_n + nM \rightarrow Ti + nMX$ [10]

C—Over-all Electrolytic reaction

$$Ti + nMX \underset{b}{\overset{a}{\rightleftharpoons}} TiX_n + nM \quad [11]$$

1. Process: $\overset{a}{\rightharpoonup}$ The anodic dissolution (endothermic): the Ti anode is attacked and converted into halide.
2. Process: $\overset{b}{\leftharpoondown}$ The cathodic reaction (exothermic): the Ti halide is decomposed by the free alkali metal formed at the cathode as a primary product

thermic and, consequently, leads to the low decomposition voltage obtained by the extrapolation of the first branch of curve B shown in Fig. 8. The formation of TiF_3 is the most likely to be favored since this salt has a higher decomposition voltage than TiF_2 and TiF_4 and one which is closer to the experimental value inferred from the curves shown in Fig. 8. Furthermore, TiF_2 is not stable even at room temperature because of disproportionation to metal and TiF_3(5) according to the reaction

$$3TiF_2 \rightarrow 2TiF_3 + Ti \quad [2]$$

On the other hand, TiF_4, if formed in the molten bath, would be converted into trivalent fluoride as was shown in a previous paper (6).

When the voltage is increased to a point corresponding about to the extrapolation of the second branch of curve B to zero current, another anodic reaction starts and becomes predominant with increasing voltage, as may be inferred by the shape of the last portion of curve B. The difference between the decomposition voltages corresponding to curve A and the upper branch of curve B is 0.9 v, which is in agreement with the value mentioned in the above paragraph for the formation of TiI_2. It seems, therefore, that the formation of TiI_2 would take place predominantly at the surface of the anode at higher current densities. This TiI_2 would tend, however, to be transformed rapidly in presence of KF according to the reaction

$$TiI_2 + 2KF \rightarrow \underset{\downarrow}{TiF_2} + 2KI \quad [3]$$
$$TiF_3 \text{ (due to reaction [2])}$$

In fact, reaction [3] is very exothermic, and furthermore it was found that the reddish-brown color of TiI_2 did not show up at the end of the electrolysis of the KI-KF bath. To prove reaction [3] by way of similitude, TiI_4 was added to a molten KF bath, and it was observed that the brown color of TiI_4 vanished to form KI as was established by x-ray diffraction analysis; the violet complex of TiF_3 and KF identified as K_3TiF_6 was also found. The following reactions occur

$$TiI_4 + 4KF \rightarrow TiF_4 + 4KI \quad [4]$$

$$TiF_4 + 2KF \rightarrow K_2TiF_6 \quad [5]$$

$$K_2TiF_6 + KF \rightarrow K_3TiF_6 + \tfrac{1}{2}F_2 \quad [6]$$

During the plating operations in the fused salt baths using Ti as anode, there is a transfer of the Ti from the anode to the cathode. As may be seen from the decomposition voltages, this transfer would involve, as a primary step, the reduction of an alkali halide at the cathode and the simultaneous formation of Ti halide at the anode; in turn, the alkali metal would reduce the Ti halide at the cathode where it is deposited (see Table II). As may be inferred from the decomposition voltage curves, the process of cathodic deposition of Ti cannot proceed before some alkali metal has been deposited at the cathode or before some Ti halide has been injected in the bath. This latter condition applies in the case of the experiments in Table I where the addition of Ti salts started earlier the cathode reaction [11](b), Table II.

It may be seen by comparing the curves in Fig. 6-8 that the decomposition voltages for KCl-NaCl or KI-NaI baths using a Ti anode are much higher and the slope indicating the anode polarization much steeper than for KI-KF baths at lower current densities. It results therefore that in the latter bath Ti may be deposited at very low voltages with relatively high current density; energy efficiency is therefore better as also the Ti deposited.

After the electrolysis was completed in the KI-KF baths using a Ti anode, the salt mixture left was submitted to x-ray diffraction analysis (7) and was found to contain besides KI and KF some unidentified compound not described in the available literature which was definitely not K_2TiF_6 nor K_3TiF_6 (6). This compound is most likely the result of the following reaction

$$TiF_3 + n\,KF \rightarrow n\,KF,\ TiF_3 \quad [7]$$

On the other hand, the absence of K_2TiF_6 in the electrolytic bath confirms the view that TiF_4 is not formed at the anode. It follows, therefore, that the reaction at the cathode would be in this particular case

$$TiF_3 + 3K \rightarrow Ti + 3KF \quad [8]$$

The reduced Ti obtained by reaction [8] under the conditions mentioned in Table I produces a smooth and uniform deposit. This is ascribed to the fluidity of the KI-KF bath and to the high temperature of

the cathode which therefore remains clean and free from any excess of K metal on account of its low boiling point (774°C). Conversely, this explains in part the dendritic formation observed in baths containing Li or even Na, the boiling points of which are higher.

Acknowledgment

The authors wish to express their indebtedness to the Defence Research Board of Canada for financial assistance. They also wish to thank Dr. J. Convey, Director, Dr. J. F. Rowland, and Dr. N. F. H. Bright of the Bureau of Mines and Technical Surveys, Ottawa, for their continued interest and collaboration.

Manuscript received Nov. 24, 1958. This paper was prepared for delivery before the New York Meeting, April 27-May 1, 1958.

Any discussion of this paper will appear in a Discussion Section to be published in the December 1959 JOURNAL.

REFERENCES

1. M. E. Sibert and M. A. Steinberg, *This Journal*, **102**, 641 (1955).
2. M. E. Straumanis and P. C. Chen, *ibid.*, **98**, 234 (1951).
3. A. W. Schlechten, M. E. Straumanis, and C. B. Gill, *ibid.*, **102**, 81 (1955).
4. M. E. Straumanis, S. T. Shih, and A. W. Schlechten, *ibid.*, **104**, 17 (1957).
5. L. L. Quill, "Chemistry and Metallurgy of Miscellaneous Materials (Thermodynamics)," p. 126, McGraw-Hill Book Co., New York (1950).
6. J. G. Wurm, L. Gravel, and R. J. A. Potvin, *This Journal*, **104**, 301 (1957).
7. J. F. Rowland and N. F. H. Bright, Internal Report MDT-58-5, Department of Mines and Technical Surveys, Mines Branch, Ottawa.

Electrodeposition Behavior of Trace Amounts of Copper

Richard C. DeGeiso[1] and L. B. Rogers

Department of Chemistry and Laboratory for Nuclear Science, Massachusetts Institute of Technology, Cambridge, Massachusetts

ABSTRACT

Deposition, onto inert electrodes, of copper in amounts insufficient to form a monolayer takes place more readily than predicted using the Nernst equation. The undervoltage is a function of the acidity, the anion present, and the amount of copper deposited. Examination of the literature for silver and for zinc indicated that, as the lattice dimension of the deposited element approached that of the electrode material, the undervoltage increased. Copper undervoltage appears to follow the same trend, but the observed differences are small and open to question.

The electrodeposition of less than a monolayer of an element onto an "inert" electrode sometimes takes place much more readily than one would predict using the Nernst equation (1). For example, deposition of silver from a 10^{-6}M solution onto a platinum electrode takes place at potentials about 0.5 v less cathodic than onto a silver electrode (2). Because silver and copper are quite similar in many chemical and metallurgical properties, a systematic study involving copper was made in the hope of obtaining more information about variables which affect the undervoltage. The fact that copper could be present in more than one valence state was a complication not encountered in the earlier work with silver.

Experimental

Apparatus and Solutions

Deionized water, with conductivity three times less than that of distilled water, was used for all dilutions. In order to insure a minimum of contamination from copper and other elements (as well as organic impurities), all solutions, except concentrated acids, were pre-electrolyzed overnight at −0.8 v vs. S.C.E. using a large platinum gauze cathode.

The concentration of copper in an electrolytic solution was between 10^{-7} and 10^{-9}M. The lower limit was set by the copper impurity in the zinc-oxide cyclotron target (Johnson, Mathey and Co. Ltd.). Copper −61, −63, and −64 produced in the bombardment were much smaller, each being about 10^{-12}M. An upper limit of 10^{-7}M was established by finding no copper in typical tracer solutions when a coulometric procedure, sensitive to somewhat less than 10^{-7}M, was used.

The radio-copper was a mixture of 3.0 hr copper −61 and 12.8 hr copper −64 as shown by half-life measurement, gamma-ray spectrometry, and aluminum absorption analysis. Usually, only 6-10 deposition runs could be completed in the three-day period following isolation of a tracer preparation before its activity became too low to permit precise measurements to be made. As a result, a large number of tracer preparations were used, each of which was undoubtedly somewhat different in concentration of total copper from the others.

Procedures involving electrolysis, anion exchange (3), and solvent extraction were compared briefly as methods for separating the radio-copper from the accompanying zinc and gallium activities. The dithizone extraction procedure, based on that of Haymond, *et al.* (4), was found to be the fastest. The procedure involved dissolution of the target material in concentrated hydrochloric acid, adjustment of the pH to 1.0-1.2 by dilution with deionized water, and extraction of the radio-copper using

[1] Present address: Experimental Station, E. I. du Pont de Nemours & Co., Inc., Wilmington, Del.

0.001% dithizone in carbon tetrachloride. The organic extract was washed with 0.1M sulfuric acid and then wet-ashed with a mixture of 1-2 drops of 18M sulfuric acid and 2 ml of 15M nitric acid. After evaporation to dryness, the radio-copper was taken up in 1M perchloric acid. Usually 2 ml of this solution were added to 200 ml of background electrolyte in preparing a solution designated as a "trace" concentration of copper. A pH of 2.0 was used in all depositions unless otherwise stated. Additional amounts of natural copper (II) salt were added if higher concentrations were to be studied.

The electrodes used in this study were of two types. Platinum gauze of approximately 80 cm^2 geometrical area, sealed into 6 mm lead-glass tubing, was used for most of the experiments. In addition, foil electrodes of platinum, palladium, gold, iridium, and rhodium were prepared and had, as nearly as possible, the same geometrical area, estimated to be 29.8 cm^2.

Several procedures for pretreatment of the electrodes were compared and found to give virtually the same results. The procedure finally chosen consisted of rinsing them in ethanol and allowing them to dry in air. They then were immersed in boiling 6*N* nitric acid, rinsed thoroughly with deionized water, and placed directly in the electrolytic cells.

Electrolyses were performed in lipless tall-form beakers, 20 cm tall and 6 cm in diameter. The beakers were covered with Plexiglass to protect the solutions from contamination by atmospheric dust. Salt bridges containing 2M sodium perchlorate connected the reference cell and the working anode with the main electrolytic cell. The ends of the bridges were plugged with unfused Vycor glass which had been previously soaked overnight in sodium perchlorate. The volume of solution in the electrolytic cells was 200 ml in all cases. Nitrogen was bubbled vigorously through the solutions prior to and during the electrolyses in order to keep the oxygen concentration to a minimum. Solutions were stirred by Teflon-covered bars driven by magnetic stirrers.

Immediately after the electrodes had been immersed, a 1-ml sample was removed from the cell. This sample was used as a standard against which all later samples were compared in order to correct for decay of the mixture of radio-copper nuclides. A potential was applied and regulated by potentiostats (5) for the time necessary for the amount deposited to reach a virtually constant value. (For the 80-cm^2 platinum gauze electrodes this time was 1 hr; for the 29.8 cm^2 foils, 3 hr.) At the end of that time, another 1-ml sample was taken and compared with the standard. From the relative difference in activity, the percentage of copper deposited at that potential was calculated. Then the potential usually was changed 0.05 v in the cathodic direction and the procedure repeated. In this manner, the percentage of copper deposited was obtained as a function of cathode potential. Stripping curves were obtained by changing the potential in the opposite direction.

A single-channel differential discriminator coupled through a linear amplifier to a 2-in. well-type, thallium-activated, sodium iodide crystal scintillator was used for measuring the gamma-ray spectrum to characterize the radio-copper. Coupled to an ordinary binary scaler, it was used to count the radio-copper samples in the deposition studies. Usually 3000-3500 counts above background (about 250 cpm) were obtained for each sample. Using the square root of the total counts as an estimate, the standard deviation was about 2%.

The reproducibility of the deposition data was primarily a function of the amount of copper present and the slope of the curve at the potential in question. At the millimolar level, the run-to-run reproducibility was ± 5 mv. Curves at the trace level were reproducible within ± 20 mv (corresponding to an estimated 3-7% variation in observed percentage of copper deposited), although for a given electrode and a particular batch of tracer, the reproducibility was ± 10 mv. Some variability was caused undoubtedly by variation in the copper contamination from one preparation to another.

Potentials for 50% deposition, $E_{50\%}$, in various media, were compared with half-wave potentials, calculated from formal potentials obtained from millimolar copper, using platinum microelectrodes and a Sargent polarograph, Model XXI. Half-wave values could usually be reproduced within ± 10 mv or less.

Results

Perchlorate media

Because a study of the deposition of silver (2) from dilute solutions indicated that the largest undervoltage was obtained in perchlorate medium, 0.1M sodium perchlorate was the first medium studied in the present investigation. Figure 1 shows the deposition behavior of copper in sodium per-

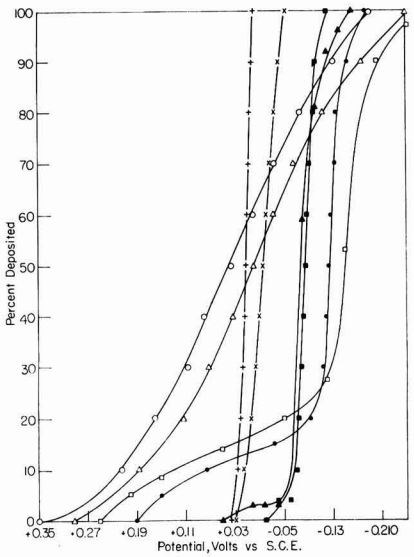

Fig. 1. Effect of initial concentration of copper on its deposition behavior onto 80 cm^2 platinum gauze electrodes from 0.1M sodium perchlorate. ○, trace; △, 1×10^{-6}M; □, 5×10^{-6}M; ●, 1×10^{-5}M; ▲, 5×10^{-5}M; ■, 1×10^{-4}M; ×, 1×10^{-3}M; +, 1×10^{-2}M.

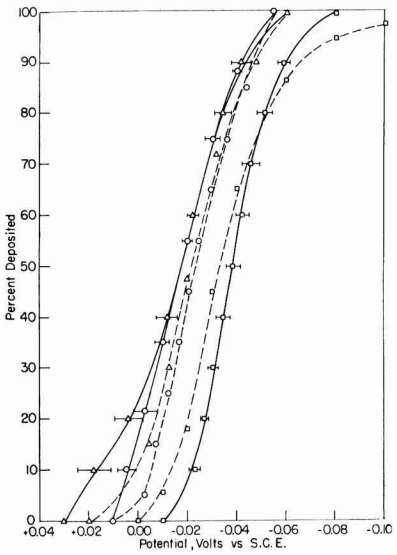

Fig. 2. Effect of pH on the deposition of 10^{-3}M copper from 0.1M sodium perchlorate onto 80 cm² platinum gauze electrodes. pH 0.0: open square with a dot joined by a solid line, deposition, open square with a dot joined by a broken line, stripping; pH 2.0: open triangle with a dot joined by a solid line, deposition, open triangle with a dot joined by a broken line, stripping; pH 5.0: open circle with a dot joined by a solid line, deposition, open circle with a dot joined by a broken line, stripping.

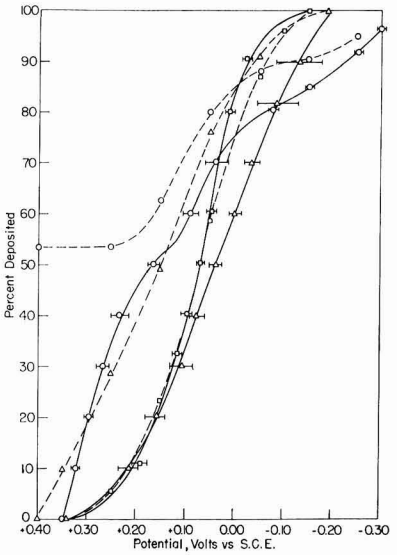

Fig. 3. Effect of pH on the deposition of trace copper from 0.1M sodium perchlorate onto 80 cm² platinum gauze electrodes. pH 0.0: square with a dot joined by a solid line, deposition; square with a dot joined by a broken line, stripping; pH 2.0: triangle with a dot joined by a solid line, deposition, triangle with a dot joined by a broken line, stripping; pH 5.0: circle with a dot joined by a solid line, deposition, circle with a dot joined by a broken line, stripping.

chlorate as a function of copper concentration. Undervoltage effects and changes in curve shape with increasing initial concentration of copper were reminiscent of those obtained for silver. Depositions of copper from 10^{-3}M and 10^{-2}M solutions agreed quite well with predictions based upon the Nernst equation.

The pH always was measured before and after a deposition study. Only in the deposition of millimolar copper from a solution initially at pH 5.0 was a change greater than 0.1 pH unit found, and then it was between 1 and 2 units higher.

Although a change from pH 2.0 to 0.0 had little effect on depositions at the millimolar level (Fig. 2), increased acidity facilitated deposition at the trace level just as it had for silver (2, 6), probably due to its effect on the platinum oxide surface film (Fig. 3). At pH 5.0, deposition appeared to be easiest but, unfortunately, sorption contributed substantially to the observed removal of copper as indicated by the stripping curve and by studies conducted at open circuit. At pH 2.0, however, sorption losses never exceeded 4%. Other effects of pH, particularly those encountered in halide media, are discussed below.

Other Media

A change from perchlorate to complexing media had resulted in lower undervoltages for the deposition of silver. However, Fig. 4 and Table I show the opposite effect for copper in that the ease of deposition increased in the order perchlorate, sulfate, bromide, chloride, and nitrate. The data for nitrate do not fit the trend although it is widely known from macro experiments that depositions from nitrate are difficult to reproduce in the absence of a substance to remove nitrous acid.

The undervoltage for silver had been studied as a function of acidity only in perchlorate medium (2, 6), so a brief study using copper in different media

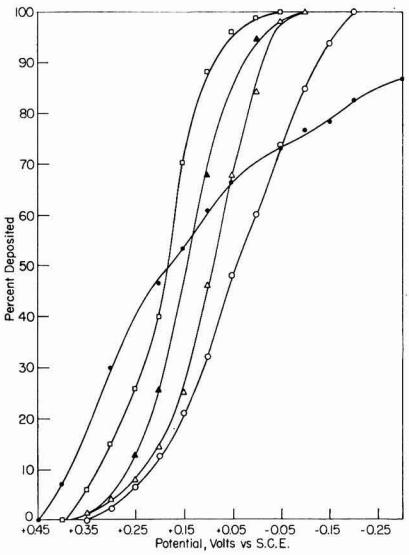

Fig. 4. Deposition behavior of trace copper onto 80 cm² platinum gauze electrodes from 0.1M solutions of sodium perchlorate, sodium sulfate, sodium bromide, sodium chloride, and sodium nitrate. ▲, sodium bromide; □, sodium chloride; •, sodium nitrate; ○, sodium perchlorate; △, sodium sulfate.

Table I. Comparison of experimental $E_{50\%}$ values for trace copper with those predicted for 10^{-7}M solutions from polarographic data on 10^{-3}M solutions

Medium	$E_{1/2}$ for 10^{-3}M, v vs. S.C.E.	Predicted $E_{1/2}$ for 10^{-7}M, v	$E_{50\%}$ of trace, v	Undervoltage
$NaClO_4$	−0.03	−0.15	+0.04	0.19
$NaNO_3$	−0.04	−0.16	(+0.18) *	(0.33) *
Na_2SO_4	−0.06	−0.18	+0.09	0.27
NaCl (Cu^+)	+0.14	+0.14	+0.18	0.04
(Cu^{++})	−0.25	−0.49	+0.18	0.67
NaBr (Cu^+)	+0.15	+0.15	+0.14	−0.01†
(Cu^{++})	−0.26	−0.50	+0.14	0.64

* Unreliable, see text.
† Within experimental error of zero undervoltage.

seemed advisable. For 0.1M sodium perchlorate a change in acidity from pH 2 to 1M (in perchloric acid) produced only a 20 mv anodic shift, a change not much larger than the limits of reproducibility. Halide media, however, showed interesting differences. A 0.1M solution of sodium chloride, after being made 1M with hydrochloric acid, gave a cathodic shift of 0.1 v; a similar run in 1M sodium chloride (at pH 2) agreed with the 0.1M solution at pH 2 (i.e., no shift due to chloride alone). When a pH 2 solution of 0.1M sodium bromide was made 1M in hydrobromic acid, a cathodic shift of 0.2 v relative to 0.1M bromide at pH 2 was produced. These changes appear to be much too large to be accounted for by changes in activity coefficients or junction potentials. The important factor appears to be not the anion but the hydronium ion. Partial confirmation was obtained by making a 0.1M solution of sodium chloride 1M in perchloric acid and finding a 50 mv cathodic shift. The fact that this same acid produced a slightly anodic shift when added to sodium perchlorate would appear to rule out contamination with copper as the cause for the cathodic shift.

Because the largest undervoltage was observed for deposition from chloride medium, deposition behavior was examined as a function of concentration. Figure 5 shows that a distinct plateau, which extended for 0.2 v, appeared at copper concentrations of 5 x 10^{-6}M and 10^{-5}M. Depositions from 10^{-4}M and 10^{-3}M copper agreed within 0.02 v with the predictions based upon the Nernst equation.

Chloride is known to complex with platinum as well as with copper. It aids in removing oxide films and might also act as a bridging ion. However, preelectrolysis in chloride did not seem to affect the deposition of "trace" copper from 0.1M sodium perchlorate although it is possible that the oxide was first removed in chloride medium and then restored in perchlorate. The following experiment then was performed to study the effect of various amounts of chloride on the deposition of trace amounts of copper from 0.1M sodium perchlorate. The cathode potential was held at +0.15 v vs. S.C.E. in a solution of trace copper in 0.1M sodium perchlorate. At this potential only 21% copper deposited under ordinary conditions. After making this solution 10^{-5}M in chloride, the percentage of copper deposited increased to 24%, a small but possibly significant change. At 10^{-3}M, the per cent increased only to 26%. However, after an increase in chloride concentration to 0.1M, the per cent deposited increased to 38%. This increase, which corresponded to a 0.05 v shift of the entire deposition curve toward less cathodic potentials, seems greater than could be accounted for on the basis of a change in either activity coefficient or junction potential. The fact

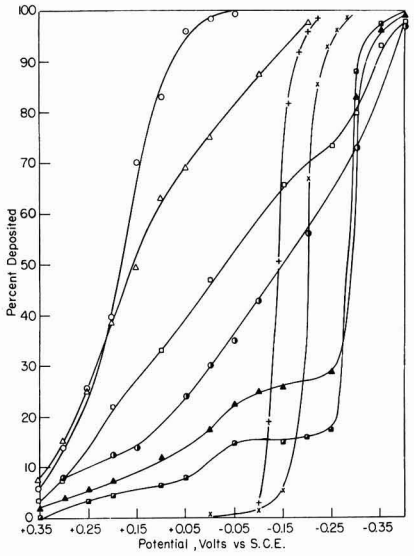

Fig. 5. Effect of initial concentration of copper on its deposition behavior onto 80 cm^2 platinum gauze electrodes from 0.1M sodium chloride. ○, trace; △, 1x10^{-6}M; □, 2x10^{-6}M; ●, 3x10^{-6}M; ▲, 5x10^{-6}M; ■, 1x10^{-5}M; ×, 1x10^{-4}M; +, 1x10^{-3}M.

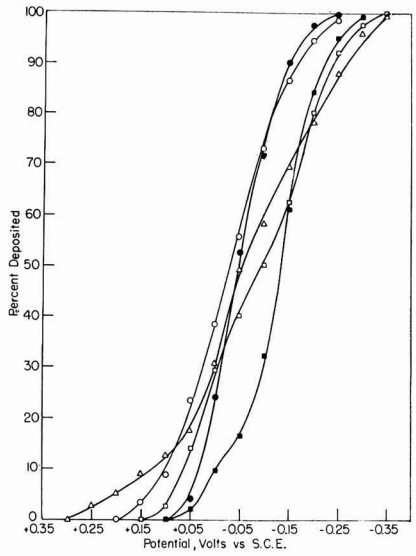

Fig. 6. Deposition behavior of trace copper on 29.8 cm^2 foil electrodes of gold, platinum, palladium, iridium, and rhodium from 0.1M sodium perchlorate. □, gold; ○, iridium; ●, palladium; △, platinum; ■, rhodium.

that the chloride curve in the presence of perchlorate was displaced cathodically from the curve for chloride electrolyte alone may indicate competition for the platinum surface, interference with the discharge reaction, or possibly contamination.

Effects of Electrode Size and Material

Electrodes comparable in size and shape to the standard platinum gauze electrodes were not available for other elements so, in order to be able to make comparisons more easily, foils of platinum as well as gold, palladium, iridium, and rhodium were cut so as to have uniform geometric areas of 29.8 cm^2. As expected (2, 17), a comparison of the deposition curves for the gauze and foil of platinum showed a cathodic displacement for the smaller electrode. A brief comparison of a shiny and a dull platinum foil did not show a difference in behavior greater than the usual experimental error, although it might have on a more extended series of runs (2).

Figure 6 compares the behavior of trace copper using different metal foils. It is interesting that differences could still be observed at the millimolar level (Fig. 7) although, at 10^{-2}M, all experimentally significant differences had disappeared. Calculations show that complete deposition of 10^{-8}M copper would correspond to 1000 layers, assuming a roughness factor of unity. The fact that differences could be observed through many layers is consistent with observations (7) that the early layers of deposit assume the crystal structure of the substrate.

Electrolysis as an Isolation Procedure

Because carrier-free copper deposits so readily, electrolysis should be a suitable method for separating radio-copper from radio-zinc and radio-gallium. It was found that copper could indeed be deposited essentially completely on platinum without depositing zinc or gallium. The following procedure gave radiochemically pure copper activities. It is somewhat more time consuming than solvent extraction but should be adapted more easily to remote operation.

A platinum-gauze electrode was placed in a solution of the target material in 0.5M sulfuric acid. A potential of −0.5 v vs. S.C.E. was applied for 1 hr, following which the electrode was removed, without disconnecting the leads to the potentiostat, and carefully washed by submersion in a beaker containing deionized water. The electrode then was placed in fresh 0.5M sulfuric acid and electrolysis was continued for another hour. A total of three electrolyses were made and, after each one, estimates were made of the activity remaining in solution, the activity in the washings, and the activity on the electrode. The final activity on the electrode was pure radio-copper. Small amounts of zinc and gallium activities present in the washings were presumably carried over by entrainment.

Discussion

Qualitatively, undervoltage appeared to be greater when the lattice dimensions of the electrode material more nearly matched those of the deposited trace element. This was first noted in a re-examination of the data for silver (2) (see Table II and Fig. 8). It was found then that, although quantitative deposition data are not available, qualitative statements for zinc behavior indicate that it follows the same trend. The fact that zinc is normally hexagonal close-packed, while the other metals are face-centered cubes, is probably not as important as the lattice dimensions themselves (8). On that basis, predictions of the order in which the electrode undervoltages would fall were made for copper. Except for rhodium, which also gave anomalous results with silver, the electrode materials fell in the expected order (Fig. 8). Admittedly the differences are small, but they were observed consistently on many batches of copper, the uncertainty being less than ± 10 mv when repeated runs were made using a single preparation of tracer.

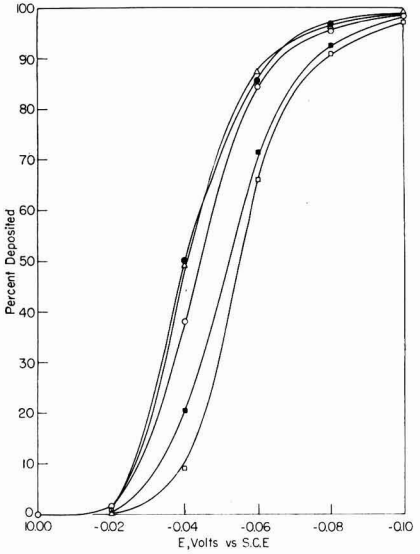

Fig. 7. Deposition behavior of 10^{-3}M copper on 29.8 cm^2 foil electrodes of gold, platinum, palladium, iridium, and rhodium from 0.1M sodium perchlorate. □, gold; ○, iridium; •, palladium; △, platinum; ■, rhodium.

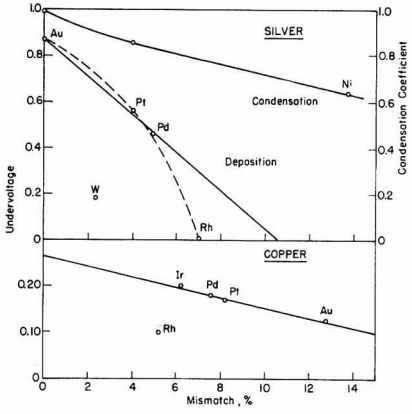

Fig. 8. Undervoltages of silver (2) and copper, and condensation coefficient for silver (10) as a function of lattice mismatch.

Table II. Lattice parameters and deposition data for silver, copper, and zinc

Trace element	Electrode	Nearest neighbor, Å (19)	% Mismatch[a]	Undervoltage[b]
Ag	Rh	2.684	7.0	0.00
	Pd	2.745	4.9	0.46
	Pt	2.769	4.0	0.56
	W	2.816	2.3	0.18
	Au	2.878	0.2	0.87
	Ag	2.882	—	—
Cu	Cu	2.551	—	—
	Rh	2.684	—5.2	0.10
	Ir	2.709	—6.2	0.20
	Pd	2.745	—7.6	0.18
	Pt	2.769	—8.2	0.17
	Au	2.878	—12.8	0.13
Zn	Ni	2.486	6.4	"Slight"[c]
	Cu	2.551	4.0	"Moderate"[d]
	Zn	2.660[g]	—	—
	Pt	2.769	—4.1	"Large"[e]
	Pb	3.493	—31.2	"None"[f]

[a] (Trace metal—Electrode metal)/Trace metal.
[b] Calculated on the basis of 10^{-2}M silver and 10^{-7}M copper in weakly acidic nitrate and perchlorate media, respectively.
[c] Small shift toward nobility at very low initial concentrations.
[d] $E_{50\%}$ remains constant with decreasing initial concentration.
[e] Shift of $E_{50\%}$ toward nobility is inversely proportional to decrease of initial concentration.
[f] Follows Nernst even at very low initial concentrations.
[g] If the value for zinc were 2.75Å (20), the difference in behavior between copper and platinum would be resolved.

On the silver diagram, the discrepancies for tungsten and rhodium are quite probably due to the presence of oxide films which led to anomalous dissolution behavior (2) as well. (Note: the points for rhodium and tungsten have been mislabeled in Fig. 4 of reference 2.) Such films would tend to minimize, or even eliminate (10), the effect of the substrate. While it might be attractive to believe that rhodium fell on a smooth curve, the large percentage of mismatch and the obviously discrepant behavior of rhodium in both the copper and silver series leads one to favor a linear decrease in undervoltage with an increase in mismatch (8).

Extrapolating to zero undervoltage, the silver data give a figure for critical mismatch of about 11%; copper, 23%. [Assuming the data of Yang, *et al.* (10) to be linear rather than curved, one can determine a minimum value of mismatch of about 30%.] Because other determinations of critical mismatch give values in the range from 10 to 20% (11-13) before a continuous film of deposit will fail to form, the limits extrapolated from trace deposition appear reasonable.

That a correlation should exist between mismatch and undervoltage seems plausible on the basis of electron-diffraction and microscopic studies of deposits which have shown that the first few layers tend to follow the structure of the substrate and that smoother deposits are obtained as the lattice parameters of the deposit and electrode approach one another. We are indebted to Taylor and Datz (9) for pointing out the existence of comparable data for the condensation coefficients of silver on different metals (10) and for alkali halides on one another (11, 12).

It is important to note that the undervoltage scale for copper in Fig. 8 is double that for silver. This was done to convert the observed values into slopes equivalent in terms of the decrease in activity of the deposit relative to the standard state. That is, a decrease of 0.060 v for silver corresponds to 0.030 v for copper due to the difference in number of electrons transferred. Even so, the slope for copper was only about half that for silver. Part, if not all, of the difference may be due to differences in surface coverage. The concentration of silver may well have been one hundred times more dilute than the copper, although the sixfold larger geometric area of the electrodes used in the present study would tend to counteract this factor. In any event, it is obvious that a study using the same set of electrodes and as nearly as possible the same concentrations of trace elements would be desirable. At the same time, a reinvestigation of the zinc system to obtain more nearly quantitative data would be valuable, particularly in view of an apparent difference in behavior between copper and platinum electrodes, both of which mismatch about 4%. Zinc falls halfway between the larger platinum lattice and the smaller copper lattice.

There seems to be little question that copper deposited as the element from solutions of perchlorate and sulfate. However, in chloride and bromide media, the respective copper (I) salts probably deposited initially even though their solubility products (particularly for the chloride) were not exceeded. First, the $E_{50\%}$ value for trace deposition corresponded almost exactly with the $E_{1/2}$ for copper (II) to (I) reduction. Second, if one assumes that the nearest neighbors in the copper (I) chloride and bromide are the sums of the radii, values of 2.77Å (0.96 + 1.81) and 2.91Å are obtained. (Platinum is 2.77Å.) Depositions on two batches of copper tracer using both platinum and gold electrodes in both chloride and bromide media indicated somewhat easier reductions in chloride at both electrodes and easier reduction using platinum than gold. The important feature is the qualitative correspondence between ease of deposition and the small mismatch. (Cu-Cl: Pt mismatch 0%; Au, 4.0%, Cu-Br:Pt, 5.1%; Au, 1.4%). If mismatch had been the only factor involved, deposition onto gold from bromide should have been easier than onto platinum, but it was not. Unfortunately, another major program would have been required to explore fully the effects of different electrode materials.

A consideration that has been ignored in the above discussion is the fact that complexing anions, particularly halides in acidic solution, would tend to dissolve oxide coatings, thereby increasing the effective surface area of the electrode. From studies in perchlorate media, an increase in geometric surface area is known to result in easier deposition of copper just as it did in experiments involving silver (14). Comparable studies in fused halide melts would therefore be desirable because oxide films should be virtually absent.

In order to refine the correlations, studies employing the same amount of tracer as well as the same

Table III. Relative volatilities of thin films of metals as a function of lattice mismatch

Substrate	Distance, A		Lead[a]			Bismuth[b]			Polonium[e]		
				% Mismatch			% Mismatch			% Mismatch	
	Nearest	Next	$T_{50\%}$[c]	Nearest	Next	$T_{50\%}$[c]	Nearest	Next	$T_{50\%}$[c]	Nearest	Next
Au	2.88	4.15	770	17.7	18.6	815	20.9	14.0	380	13.6	—24.6
Pt	2.77	3.92	780	20.8	12.0	990	23.9	7.7	—	—	—
Pd	2.74	3.88	1050	21.7	10.9	~1030	24.7	6.6	780[f]	17.8	—16.6
Ni	2.49	3.53	620[d]	28.9	0.9	700[d]	31.6	—3.0	—	—	—

[a] Nearest neighbors 3.50Å; boiling point, 1525°C (21).
[b] Nearest neighbors 3.64Å; boiling point, 1420°C (21).
[c] Temperature in °C for evaporation of 50% of film in 10 min in air.
[d] Nitrogen atmosphere; hydrogen atmosphere gave temperatures lower by 70°C.
[e] Nearest neighbors (22): α-form 3.29Å, β-form 3.35Å; 3.33Å used in calculations of mismatch. Boiling point (23), 962°C.
[f] Palladium-gold alloy.

electrode area would be needed. These conditions might be approached much more closely by comparing several tracer elements using a given electrode at one potential. Such a study was beyond the scope of the present one which was designed to survey the suitability of copper for a comparison of that type.

Another precaution to observe would be the conservative use of lattice parameters, determined for carefully prepared crystals, in interpreting data obtained on foils whose surfaces will reflect, to a greater or lesser extent, the physical treatment encountered in their preparation. An outstanding example of the effect of electrode history has been cited already in an electrodeposition experiment with silver for which a gold crucible was used as an electrode (14). However, the differences incorporated by working a surface generally seem to be much smaller than those between any two elements used in the present comparison. Hence, the use of single-crystal parameters appears valid.

The concept of mismatch appears capable of extension by the use of lattice neighbors more distant than the nearest. For example, a collection of data (15) on the relative rates of volatility of thin metallic films from different substrates is given in Table III along with data on nearest and next-nearest neighbors, the latter calculated on the basis of a face-centered cubic structure. It is important to note, particularly for lead and bismuth, that the direction of change in mismatch using nearest neighbors is directly opposite to that using next-nearest. The latter trend, however, conforms to the concept of stronger sorption for smaller mismatch. The striking exception is nickel, for which the rationalization based on an oxide film seems unlikely because of the great care exercised to exclude air (16). The data for polonium are meager and, unfortunately, fall in a region of large mismatch on both bases. On any given surface, the interatomic distances undoubtedly vary widely and almost continuously so some sorption of any given substance will occur on any surface (8). However, lattice parameters will probably represent modes in a plot of the relative number of sites vs. interatomic distance.

Two other points are worth noting in the lead and bismuth data involving the noble metals. In the first place, although $T_{50\%}$ values for bismuth fall on a straight line when plotted against mismatch, values for lead show a sharp change in slope in going from platinum to palladium. The abrupt change occurs in going from 11 to 12% mismatch, values close to the critical 10% limit above which continuous films did not form in some studies (12, 13). Second, in spite of the fact that bulk bismuth boils 100°C lower than bulk lead, the smaller mismatch of bismuth raised its "50% volatilization" temperature as a thin film to values nearly identical with those for lead films.

The present study emphasizes the similarity between adsorption and trace deposition that has been pointed out earlier (13, 17). However, the presence of inert solute and solvent complicates the picture as they do in adsorptions from the liquid phase. As yet, the effect of changing the solvent remains to be explored, as does the effect of adding small amounts of adsorbable substances. The latter studies should provide a fruitful way of exploring the suggested leveling of activity of sites on an electrode (18), as well as supplementing data from polarographic and electrolytic studies in general.

Acknowledgment

The authors are grateful to the Atomic Energy Commission for partial support of this work.

Manuscript received Jan. 15, 1958. This paper is a part of a thesis submitted by R. C. DeGeiso in partial fulfillment of the requirements for the Ph.D. degree to the Massachusetts Institute of Technology, June 1957.

Any discussion of this paper will appear in a Discussion Section to be published in the December 1959 JOURNAL.

REFERENCES

1. L. B. Rogers, *Record Chem. Progress (Kresge-Hooker Sci. Lib.)* **16**, (3), 197 (1955).
2. L. B. Rogers, D. P. Krause, J. C. Griess, Jr., and D. B. Ehrlinger, *This Journal*, **95**, 33 (1949).
3. K. A. Kraus and G. E. Moore, *J. Am. Chem. Soc.*, **75**, 1460 (1953).
4. H. R. Haymond, R. D. Maxwell, W. M. Garrison, and J. G. Hamilton, *J. Chem. Phys.*, **18**, 258 (1951).
5. R. W. Lamphere, *Anal. Chem.*, **23**, 258 (1951).
6. J. C. Griess, Jr., J. T. Byrne, and L. B. Rogers, *This Journal*, **98**, 447 (1951).
7. G. I. Finch, H. Wilman, and L. Yang, *Discussions Faraday Soc.*, **1**, 144 (1947).
8. D. Turnbull and B. Vonnegut, *Ind. Eng. Chem.*, **44**, 1292 (1952); see also F. C. Frank and J. H. van

der Merve, *Proc. Royal Soc.* (London) **A198**, 216 (1949).
9. E. H. Taylor and S. Datz, Private communication, November 1957.
10. L. Yang, M. T. Simnad, and G. M. Pound, *Acta Met.*, **2**, 470 (1954).
11. L. G. Schulz, *Acta Cryst.*, **5**, 130 (1952).
12. *Ibid.*, **4**, 483 (1951).
13. G. E. Gardham, *Discussions Faraday Soc.*, **1**, 182 (1947).
14. J. T. Byrne, L. B. Rogers, and J. C. Griess, Jr., *This Journal*, **98**, 452 (1951).
15. N. A. Bonner and M. Kahn, "Radioactivity Applied to Chemistry," pp. 154-155, edited by A. C. Wahl and N. A. Bonner, John Wiley and Sons, Inc., New York (1951).
16. E. Holesch, *Sitzber, Akad. Wiss. Wien, Math-Naturw. Klasse, Abt. IIA*, **140**, 663 (1931).
17. J. T. Byrne and L. B. Rogers, *This Journal*, **98**, 457 (1951).
18. E. G. Neal and L. L. Shreir, *Trans. Faraday Soc.*, **53**, 1371 (1957).
19. L. Pauling, "The Nature of the Chemical Bond," p. 409, second edition, Cornell Univ. Press, Ithaca, New York (1944).
20. P. C. L. Thorne and A. M. Ward, "Inorganic Chemistry," pp. 36-37, Gurney and Jackson, London, (1939).
21. *Ibid.*, p. 42.
22. W. H. Beamer and C. R. Maxwell, *J. Chem. Phys.*, **17**, 1293 (1949).
23. L. S. Brooks, *J. Am. Chem Soc.*, **77**, 3211 (1955).

Mechanisms of Hydrogen Producing Reactions on Palladium

VI. Atomic Hydrogen Overvoltage on an α Pd-H Bielectrode

Sigmund Schuldiner

U. S. Naval Research Laboratory, Washington, D. C.

ABSTRACT

An electrochemical system was evolved in which the only reactions occurring on the cathode and anode surfaces of an α Pd-H bielectrode were the formation and ionization of atomic hydrogen, respectively. The atomic hydrogen overvoltage on this bielectrode was determined. A kinetic analysis of the system was supported by the experimental results.

In this paper a bielectrode system is described in which the net reaction, on the cathode side, is the reduction of hydronium ions to hydrogen atoms and, on the anode side, the oxidation of hydrogen atoms to hydronium ions. The electrochemical system consists of two cells in series in which the first cell is connected to the second by means of an α Pd-H bielectrode. In the first cell, the anode reaction is the oxidation of hydrogen atoms, which have diffused through a palladium tube, to hydronium ions. The cathode reaction on the α Pd-H bielectrode is the reduction of hydronium ions to hydrogen atoms. The hydrogen atoms formed on this cathode surface are transported through the α Pd-H bielectrode to the anode surface where they are oxidized to hydronium ions in the second cell. The cathode reaction in the second cell is the reduction of hydronium ions to hydrogen atoms which diffuse through a Pd tube cathode to react with oxygen on the inner surface of the tube.

In such an electrochemical system, for every equivalent of atomic hydrogen oxidized to hydronium ions at the anode in the first cell, an equivalent of hydrogen ions is transported through the bielectrode, and an equivalent of hydronium ions is oxidized to hydrogen atoms which are removed from the system through the cathode in the second cell. Hence, the concentration of hydronium ions in both cells remains constant, atomic hydrogen is consumed as fast as it is produced, and the system can be kept free of molecular hydrogen.

On the cathode side of the bielectrode, the adsorbed atomic hydrogen concentration will increase with increasing current densities, whereas on the anode side of the bielectrode, the adsorbed atomic hydrogen concentration will decrease with increasing current densities. At a limiting current density, the transport of hydrogen through the bielectrode will not be fast enough to furnish enough hydrogen atoms to support the current density on the anode side of the bielectrode. At this point the potential will rise sharply and an oxygen producing reaction also will occur on this surface. No longer will there be a complete transfer of the hydrogen atoms formed on the cathode side to the anode side.

Experimental

The electrochemical system used in this investigation is shown in Fig. 1. It is a modification of a previously described double cell (1). In this system the anode in the right hand cell is a Pd tube with a sealed bottom, 5 cm long, 3 mm in diameter, and with a wall thickness of 0.2 mm. During a run hydrogen gas is circulated through the inside of this tube. Some of the hydrogen diffuses through the wall of the tube and exists as hydrogen atoms on the outer surface in contact with the 2*N* sulfuric acid solution. Virtually all of these hydrogen atoms are oxidized to hydronium ions under an applied current flow. If the flow of atoms to the surface is too slow to support the applied current, an oxygen forming reaction at a sharply elevated positive potential occurs. Hence a determination of the polarization of this electrode indicates whether the reaction is completely the ionization of hydrogen atoms or not. During the runs reported here the maximum

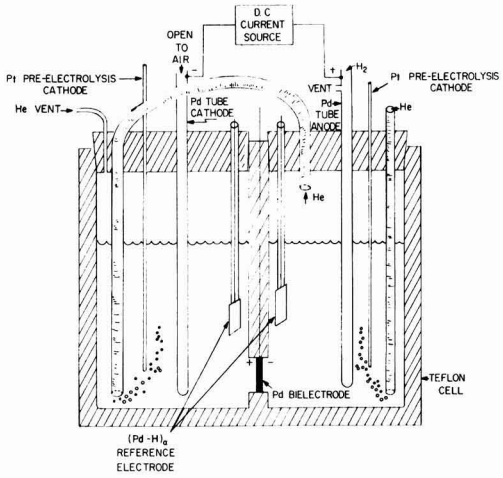

Fig. 1. Electrochemical system

polarization of the Pd tube anode was less than 0.1 v. This indicated that the diffusion of atomic hydrogen through the wall of the anode tube was fast enough to prevent an oxidation reaction other than ionization of atomic hydrogen. There is a possibility that at low current densities some molecular hydrogen could form on this surface of the Pd tube anode. However, even if this did occur the molecular hydrogen would be formed at a slow rate and, since the cells were swept continuously with a rapid stream of helium, the partial pressure of molecular hydrogen in the solutions would always be negligible.

The bielectrode consisted of a Pd diaphragm (0.004 in. thick with an apparent exposed area of 0.14 cm^2) charged to the maximum α phase (H/Pd atom ratio $\sim$ 0.03). During polarization the reaction on the cathode side consisted of the reduction of hydronium ions in the double layer to hydrogen atoms chemisorbed on the cathode surface. The hydrogen atoms formed on this surface are transported to the anode side of the bielectrode where they are oxidized to hydronium ions. A description of the transport mechanism already has been given (2).

The cathode in the left hand cell consisted of a Pd tube of the same dimensions as the anode in the right hand cell. This tube was open to the atmosphere. The reaction on the surface in contact with the solution was the reduction of hydronium ions to atoms which then migrated through the wall of the tube to react with oxygen on the inner surface. Polarization of this electrode for the maximum current applied was less than -0.05 v which indicated that virtually all of the atomic hydrogen formed on the outer surface did diffuse through the wall and react with oxygen on the inner surface of the tube.

The reference electrodes used in this investigation were $(Pd\text{-}H)_\alpha/H_3O^+$ electrodes of the maximum α composition (3).

A run was conducted in the following way. Using previously described techniques (4, 5) the double cell was cleaned thoroughly and about 5 ml of purified 2*N* sulfuric acid solution was added to each compartment. The solution was then "pre-electrolyzed" using the Pt wire electrodes shown in Fig. 1 as the pre-electrolysis cathodes. Purified hydrogen gas was circulated through the cells during the pre-electrolysis. During this treatment all of the Pd electrodes in the cells were anodically cleaned. After a minimum 16-hr pre-electrolysis, the Pt cathodes were removed from the cells (during current flow) by pulling them through the holes indicated in the Teflon stoppers in the cells. These wires then were cleaned by repeatedly dipping them in concentrated nitric acid and heating them white hot in a flame. The Pt wires then were reintroduced into the cells. Hydrogen gas was circulated through the cells until the potentials on the Pd bielectrode and reference electrodes were 0.05 v positive to the Pt/H_2 electrodes in each cell. This usually took from 4 to 6 hr. At this point the hydrogen flow was transferred to the anode tube electrode in the right hand cell and a purified stream of helium was passed rapidly through both cells. The open-circuit potential between the $(Pd\text{-}H)_\alpha/H_3O^+$ reference electrodes and each side of the α Pd-H bielectrode was equal to zero. Steady-state currents then were applied to the double cell in the circuit shown in Fig. 1. Overvoltages were determined under steady-state conditions at increasing current densities only, since at the highest current densities some oxygen formation reaction occurred on the anode side of the bielectrode. Current interrupter (6) measurements were made in order to verify surface cleanliness and to correct for the *IR* drop between the surfaces of the bielectrode and the reference electrodes. The temperature was 27° ± 1°C.

Results and Discussion

Four typical anodic and cathodic overvoltage curves are shown in Fig. 2. Actually about 15 runs

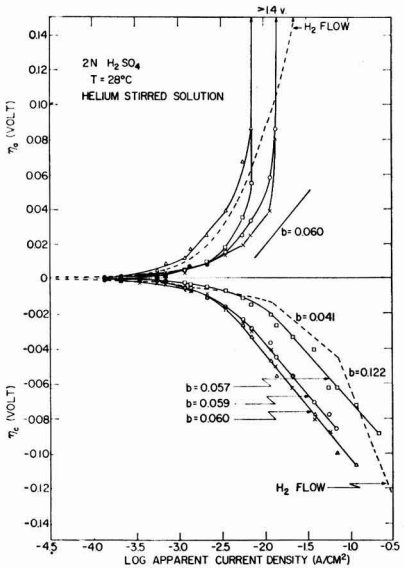

Fig. 2. Anodic and cathodic hydrogen overvoltage on an α Pd-H bielectrode. X, O, △, □ represent experimental points for four separate runs, and • represents the overlapping of three or more points of different runs. Broken line represents overvoltages in the presence of molecular hydrogen (2). The reference electrodes are $(Pd\text{-}H)_\alpha/H_3O^+$ (3).

were made, but the curves shown are representative. The curve with a broken line was taken from a previous investigation (2) and represents the overvoltage curves obtained for the same bielectrode system when molecular hydrogen is present in the system. As can be seen from Fig. 2 the presence of molecular hydrogen does markedly change the polarization behavior on both the anode and cathode sides of the bielectrode. Under open-circuit conditions the potential determining reaction on the α Pd-H electrodes was shown to be an equilibrium between hydronium ions in the solution and protons dissolved in the Pd (3). Upon polarization in a solution containing molecular hydrogen two simultaneous reactions occur on the bielectrode surfaces. The first reaction involves the reduction of hydronium ions to hydrogen atoms on the cathode side of the bielectrode, the transfer of part of the atoms through the bielectrode and the oxidation of the atoms to hydronium ions on the anode side of the bielectrode. The second simultaneous reaction involves the combination of those atoms, which do not migrate from the cathode to the anode sides of the bielectrode, to molecules on the cathode side and an equivalent amount of ionization of molecular hydrogen on the anode side to hydronium ions. Upon polarization in a solution which is free of molecular hydrogen, only the first reaction occurs. Hence all of the hydrogen atoms formed on the cathode side of the bielectrode are transferred to the anode side and there is no second reaction involving the formation or ionization of molecular hydrogen. Therefore, it is obvious that, in the case of the system free of molecular hydrogen, the overvoltage being observed is solely that of atomic hydrogen on the α Pd-H electrode of maximum hydrogen content.

The shapes of the curves shown in Fig. 2 were reproducible. However the effective exchange current density, i_o, values were only reproducible to the extent indicated. This most likely means that the atomic polarization was extremely sensitive to surface conditions. Since previous investigations (5) have shown that for the molecular hydrogen system the effective area remained fairly constant after the initial electrode treatment, this would indicate that the atomic hydrogen electrode in the absence of molecular hydrogen was more sensitive to active centers on the surface. It may be that molecular hydrogen exerts a buffering effect since there is an exchange between molecular hydrogen and hydrogen atoms adsorbed on the surface. When molecular hydrogen is eliminated from the system this source of atomic hydrogen is removed and the effect would be most marked in the low current density region. This would account for the poor reproducibility of i_o.

The rate constants $(-di/d\eta)$ for the over-all reactions found in the low current density overvoltage range in which the overvoltage is linearly dependent on current density varied from 0.14 to 0.33 mhos/cm^2. Since in the presence of molecular hydrogen, $-di/d\eta$ is 0.13 mhos/cm^2 (2), this indicates that the hydrogen transport through the bielectrode is somewhat faster than the surface H_2 evolution or ionization reaction. In the presence of molecular hydrogen 70% of the current was used in transporting hydrogen through the bielectrode and 30% was used forming and ionizing H_2 on the cathode and anode surfaces, respectively (2).

The rate of helium stirring made virtually no change in the overvoltage measurements. Stirring rates were reduced even to zero with no significant change in polarization potentials.

Overvoltage on the cathode side of the bielectrode. —During current flow the reactions occurring on the cathode side of the bielectrode are:

$$H_3O^+ + e^- = H_a + H_2O \qquad [1a]$$

$$H_a \xrightarrow{\text{slow}} H_i \qquad [1b]$$

$$H_i = H_i^+ + e^- \qquad [1c]$$

where H_a denotes hydrogen atoms chemisorbed on sites on the cathode side of the α Pd-H bielectrode; H_i, hydrogen atoms absorbed in the interior of the bielectrode; and H_i^+, protons in the interior of the bielectrode. Equation [1a] represents the formation of chemisorbed hydrogen atoms on the cathode surface. Equation [1b] represents the absorption of the adsorbed hydrogen atoms from the surface through the skin of the metal to some position in the interior of the metal. Equation [1c] represents the donation of hydrogen 1-s electrons to the d band of the metal. The atomic absorption step, Eq. [1b], is considered to be rate determining. Previous work (2) has indicated that the transfer of the hydrogen atoms through the skin of the metal is the rate-determining step in the migration of hydrogen atoms through a Pd bielectrode. The kinetic analysis which follows supports this conclusion since the experimental results are in accordance with the mechanism indicated in Eqs. [1a], [1b], and [1c].

Let us write the kinetic equations for the primary discharge step [1a].

$$\vec{i}_d = \vec{k}_d\,(H_3O^+)\,\exp\,(-\alpha\eta_c\,F/RT)$$

$$\overleftarrow{i}_d = \overleftarrow{k}_d(H_a)\,\exp\,[(1-\alpha)\eta_c\,F/RT]$$

where k_d is the rate constant; (H_3O^+), the concentration of hydronium ions; (H_a), the concentration of adsorbed hydrogen atoms on the cathode surface; α, the transfer coefficient; η_c, the cathodic overvoltage; F, the faraday; R, the gas constant; and T, the absolute temperature. Since step [1a] is considered to be virtually equilibrium, $\vec{i}_d = -\overleftarrow{i}_d$ and

$$(H_a) = (\vec{k}_d/\overleftarrow{k}_d)\,(H_3O^+)\,\exp\,(-\eta_c F/RT) \qquad [2]$$

For the rate-determining step [1b]

$$i_c = \vec{k}_a(H_a) + \overleftarrow{k}_a(H_i) \qquad [3]$$

Under conditions where the back reaction in the rate-determining step [1b] is negligible, the net cathodic current density is

$$i_c = \vec{k}_a(H_a), \qquad [4]$$

where $\vec{k}_a$ is the rate constant for the forward reac-

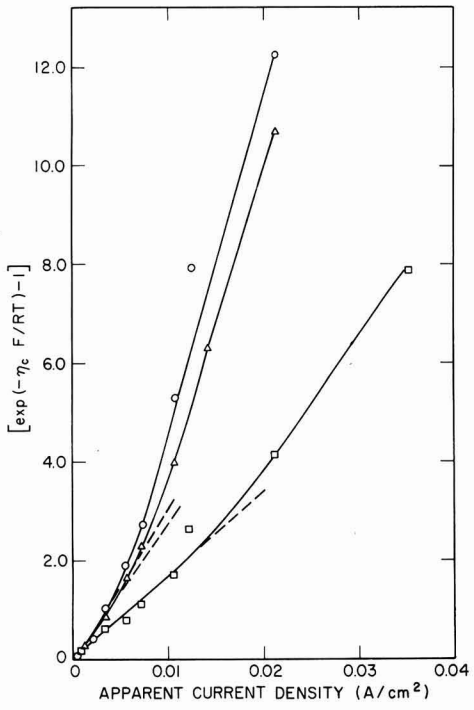

Fig. 3. Relationship between i_c and exp $(-\eta_c F/RT)-1$

tion of the atomic absorption step [1b]. Hence, substitution of Eq. [2] into Eq. [4] yields, after conversion to logarithms,

$$\eta_c = (RT/F)\ [-\ln i_c + \ln \text{const} + \ln\ (H_3O^+)\ ] \qquad [5]$$

Since (H_3O^+) represents the bulk concentration of hydronium ion, which is constant, the Tafel equation can be written $\eta_c = a - b \log i_c$, where the Tafel constant $b = 2.3\ RT/F$; at 27°C, b = 0.059 v.

Since the Tafel lines found in the cathode overvoltage curves in Fig. 2 are near a 0.059 slope this confirms that the slow step in the hydrogen atom production reaction is the absorption (solution) of hydrogen atoms.

The data in Fig. 2 show that the Tafel lines commence at overvoltages of about −0.02 v. This means that the back reaction in Eq. [3] must vanish at a much lower overvoltage than one would expect. Similar low values for the start of the Tafel slope were found for platinum and palladium (4-6).

From Eq. [3] and [4] one obtains $i_c = K \exp(-\eta_c F/RT) - \overleftarrow{k}_a(H_1)$. From Eq. [1c], $\vec{i}_{1c} = \vec{k}_{1c}(H_1)$, and $\overleftarrow{i}_{1c} = \overleftarrow{k}_{1c}(H_1^+)$. Since step [1c] can be considered to be virtually at equilibrium and (H_1^+) is constant at low overvoltages, $(H_1) = K'$. Therefore the net cathodic current is

$$i_c = K \exp\ (-\eta_c F/RT) - K' \qquad [6]$$

At equilibrium, $i_c = 0$, $\eta_c = 0$, and $K' = K$, hence,

$$i_c = K\ [\exp\ (-\eta_c F/RT) - 1] \qquad [7]$$

Figure 3 shows a plot of exp $(-\eta_c F/RT) - 1$ vs. i_c for three separate runs which had about the maximum deviation from one another. These curves clearly show that Eq. [7] holds only up to overvoltages of about −0.02 v. This means that $K' = K$ near equilibrium only. The experimental shift to a Tafel slope at about −0.02 v could be accounted for by an increase in K and a decrease in K′ with increasing current density. This implies a larger increase in the forward reaction in the rate-determining step [1b] and a larger decrease in the back reaction. This is owing to the increase in concentration of H_a on the cathode surface.

Overvoltage on the anode side of the bielectrode. —Using a derivation analogous to that for Eq. [6], one finds for the anode side of the bielectrode

$$i_a = K'' - K \exp\ (-\eta_a F/RT) \qquad [8]$$

where $K'' = K$ at low overvoltages. Hence at low current densities $\eta_a = -\eta_c$. This is experimentally observed in Fig. 2.

The anodic polarization slopes shown in Fig. 2 do not show a clear region in which an 0.059 slope exists, although for a short current density range such a slope can be drawn. This is because in the higher current density range the depletion of adsorbed hydrogen atoms becomes such that it cannot support the current density flowing from the anode. Hence, as the concentration of adsorbed atomic hydrogen approaches zero, there is a sharp rise in potential. At higher potentials (>0.1 v) a secondary reaction involving an oxygen formation reaction occurs in the region shown in Fig. 2 where the anodic potential rises vertically. Equation [8] shows that as a limiting condition, $i_a = K''$. The atomic hydrogen supply on the anode surface is limited by the rate of the deabsorption of atomic hydrogen from the interior of the bielectrode, whereas the limiting step on the cathode surface of the bielectrode is the solution of atomic hydrogen through the skin of the metal. Hence on the cathode side the chemisorbed atomic hydrogen concentration can build up to a large value, whereas on the anode side the depletion of the atomic hydrogen will occur at a relatively low current density, since the atomic hydrogen concentration cannot be larger than that on an α Pd-H reversible electrode of maximum hydrogen concentration.

It should be noted that in the electrochemical system reported here, the interior of the Pd bielectrode is the maximum α Pd-H alloy. This is because this is the alloy at zero current density and this composition is maintained, except at the highest current densities, because hydrogen is dissolved into the interior of the bielectrode from the cathode side at the same rate it is removed from the interior of the bielectrode on the anode side.

In the high current density range a reaction involving oxygen occurs on the anode side of the bielectrode and only part of the current flowing in the interior of the Pd is protonic, the remainder is an electronic current. This would mean that not all of the hydrogen atoms formed on the cathode surface would be transferred through the bielectrode to the

anode side. Most of these excess atoms probably dissolve in the interior of the palladium to form β Pd-H which coexists with the α phase. During the time interval in which measurements were taken in this high current density range (usually less than 1 hr, although in several cases currents were maintained for several hours with no potential change) only a relatively small amount of the β phase would be formed. The atomic hydrogen overvoltage on the cathode side of this two phase alloy does not deviate significantly from the pure α alloy since the cathodic Tafel lines in Fig. 2 show no change in the high current density region.

The anodic curves shown in Fig. 2 indicate that beyond a potential of 0.06 v, the concentration of atomic hydrogen on the surface must be very small. Since the concentration of hydrogen atoms on the surface at zero overvoltage would not be more than ten times higher, it can be concluded that the atomic hydrogen coverage on the maximum α Pd-H alloy under open-circuit conditions is quite small. Also, inasmuch as the potentials on both sides of the bielectrode are dependent on (H_a), one can approximate the change in (H_a) on the cathode side at the maximum overvoltage by use of the Nernst potential equation. Thus, at the maximum measured η_c of about -0.10 v, (H_a) on the cathode side will increase $\sim$50 times. This means that the initial atomic hydrogen coverage must be less than 2%.

Acknowledgment

The author is indebted to Drs. J. C. White and G. W. Castellan of the U. S. Naval Research Laboratory and to Dr. R. A. Marcus of the Polytechnic Institute of Brooklyn for valuable discussions concerning this work.

Manuscript received July 7, 1958.

Any discussion of this paper will appear in a Discussion Section to be published in the December 1959 JOURNAL.

REFERENCES

1. S. Schuldiner and J. P. Hoare, *This Journal*, **103**, 178 (1956).
2. J. P. Hoare and S. Schuldiner, *ibid.*, **104**, 564 (1957).
3. S. Schuldiner, G. W. Castellan, and J. P. Hoare, *J. Chem. Phys.*, **28**, 16 (1958).
4. S. Schuldiner, *This Journal*, **101**, 426 (1954).
5. J. P. Hoare and S. Schuldiner, *ibid.*, **102**, 485 (1955).
6. S. Schuldiner, *ibid.*, **99**, 488 (1952).

Technical Notes

Molybdenum Plating Inside of Large Bore Tubes

Paul L. Raymond

Metallurgical Department, National Research Corporation, Cambridge, Massachusetts

In early 1953 a program was initiated to develop equipment and procedures for coating the inside of alloy steel tubes with a uniform coating of molybdenum. The inside diameter of the tubes was about 1⅝ in. and the coated section was to be about 2 ft long. These tubes when coated were to be subjected to various tests for adhesion, wear resistance, corrosion resistance, etc.

Previous investigations (1, 2) had determined that: (*A*) high-purity molybdenum metal could be deposited at a high rate by the reduction of molybdenum pentachloride with hydrogen; (*B*) the temperature for this reaction ranged between 650° and 1100°C; and (*C*) excess hydrogen was necessary to yield complete reduction and to utilize efficiently the available pentachloride.

Work at this laboratory had shown further that: (*A*) the pressure at which reduction occurred most efficiently was approximately 20 mm Hg; (*B*) the plate followed surface contours without building up at discontinuities; and (*C*) high-purity molybdenum pentachloride required could be obtained by heating commercially pure $MoCl_5$ for an hour at a pressure of 1 mm Hg or less at 100°C.

With this general background it was proposed to coat the interior of tubes with molybdenum by hydrogen reduction of the pentachloride. The size of the tubes precluded the convenient use of an enclosed system for vacuum operation, and it seemed generally desirable to establish a system employing common engineering materials in order that tubes could be inserted rapidly for processing.

Equipment

Schematically, the equipment design for vapor plating is shown in the flow diagram, Fig. 1. Argon from high-pressure cylinders was heated and passed through molten molybdenum pentachloride.

It was then mixed as it passed through the lines with heated hydrogen. The mixture of hydrogen, argon, and molybdenum pentachloride vapor entered the reaction tube where it passed upward through a heated zone. Metallic molybdenum was deposited on the walls in this heated zone by the reduction of the pentachloride by the hydrogen. The reaction gases passed through a filter to remove solid by-products and the gases exhausted to atmosphere through a vacuum pump. The heated zone was

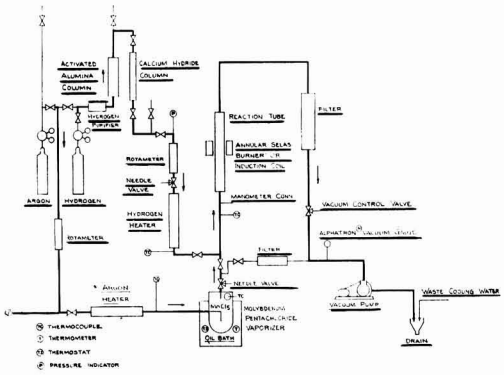

Fig. 1. Flow diagram

slowly moved downward throughout the length of the tube as the plating progressed.

Except for a series of stainless steel valves, the components containing molybdenum pentachloride and the products of the reaction were all mild steel, synthetic, or natural rubber. Operating temperatures of the vaporizer in use at the conclusion of the investigation did not exceed 250°C, so that only a slight amount of iron contamination was observed. A vacuum-tight vacuum system was developed with this equipment and an initial pump-down to 20 μ with the original mechanical vacuum pump was possible throughout the program. Rubber tubing was employed in some cases to facilitate connections to flowmeters and manometers. Experience indicated that the most suitable gasket material for hot connections at the reaction tube was compressed asbestos sheet packing. This material does not flow as do plastic materials and it will withstand high temperatures.

The flow diagram shows the sequence of equipment and operations, starting with the gas system.

Commercially pure water pumped hydrogen in high-pressure tanks was purified by a catalytic purifier followed by a column filled with activated alumina and one filled with calcium hydride lumps. Hydrogen from this system had a dewpoint below −70°C. Argon and helium used for purging and as carriers for molybdenum pentachloride vapor have extremely low dewpoints as-received and were used without further purification. Pressure regulators reduced gas pressures to approximately 1 atm. A manifold permitted the flow of either hydrogen or argon through rotameters to determine the flow rate. A pressure slightly above atmospheric was maintained in this system to preclude air leaking into the system. Needle valves reduced the gas pressure to 5-20 mm Hg and also controlled the flow. As this was generally a steady-state system, only slight adjustments during a plating run were required.

The gases were heated at atmospheric pressure by passing through a spiral finned resistance heater within an asbestos jacketed section of 1¼ in. iron pipe. Exit gas temperature was determined by thermocouples. Variable transformers were used to control power to the heating elements.

The molybdenum pentachloride vaporizer consisted of a 4 in. diameter cylinder about 8 in. long with a hemispherical base and flanged top. The vaporizing gas bubbled through the bath of molten molybdenum pentachloride and out through a pipe in the cover of the assembly. The entire assembly was immersed in a constant temperature oil bath to provide heat of vaporization and to control the vapor concentration.

Throughout the course of the investigation there probably were more changes in the vaporizer than in all other components concerned. In early experiments, heated hydrogen flowed past the molybdenum pentachloride suspended in a glass cloth bag while the outside of the vaporizer, which then consisted of a flanged section of pipe, was heated by gas burners. Poor control of vapor concentration and premature partial reduction of pentachloride resulted from this system.

Next, a mechanical screw-type feeder was employed to regulate the flow of pentachloride crystals to a heated plate where it was hoped that flash evaporation would occur, giving a controlled molybdenum pentachloride-hydrogen ratio. However, premature reduction and disproportionation were observed. Also, the feed screw became jammed frequently, resulting in no vapor flow at all.

The tank-type vaporizer was modified several times before the final model was developed. In the first model, heated hydrogen was passed over molybdenum pentachloride placed on trays in a vaporizer, which picked up the hydrogen vapor. It was hoped that a constant evaporation rate could be maintained throughout the duration of the run, but due to the changing surface conditions of the pentachloride crystals, the vapor concentration in the gas mixture decreased as the run progressed. After several attempts involving minor modifications of the system, it was decided to melt the molybdenum pentachloride before vaporizing. The $MoCl_5$ vapor was picked up in one hydrogen stream and diluted with a second hydrogen stream. Various amounts of partially reduced chlorides were observed in the reaction tube, and the system contained partially reduced chlorides in the form of dust, which at times caused either nonadherent coatings or nodules to be formed in the reaction zone. Through the use of heated argon as a vapor pick-up and carrier, the premature reduction of the pentachloride vapor was eliminated and much closer control of vapor ratio was obtained. In this case, hydrogen for the reaction was added after the argon had passed through the vaporizer and just prior to entrance into the reaction tube. In this way, it was not necessary to control closely the temperature of the diluent hydrogen gas but only to maintain the temperature of the resultant mixture above the dewpoint of the molybdenum pentachloride vapor present.

The use of argon as a means of picking up pentachloride vapor was extremely successful, as it was possible to control the hydrogen:pentachloride ratio sufficiently closely to permit uniform coating conditions throughout extended runs. In an effort to determine whether helium would work as well, two runs were conducted utilizing helium as a carrier

gas. In both of these runs, the coatings deposited were as good as those deposited when argon was utilized.

Measurements and Controls

With the vaporizer operating at approximately atmospheric pressure, near saturation conditions of $MoCl_5$ in argon existed. By varying the temperature of the oil bath or the temperature of the argon entering the vaporizer or both, it was possible to control closely the ratio of molybdenum pentachloride to argon. The diluting hydrogen stream was measured by a rotameter. Thus, the desired molybdenum pentachloride to hydrogen ratio could be maintained through an extended run.

During the project several schemes for actual measurement of the vapor concentration were attempted, but with poor success. Color comparison methods were of little value due to clouding of sight glasses and to variation of color with pressure. Considerable effort was expended in an attempt to develop a dewpoint type of measuring device, but here again, clouded sight glasses prevented precise measurements.

A tap at the reaction tube inlet was connected to a mercury manometer by means of copper tubing to determine the static pressure in the reaction tube. This arrangement functioned very satisfactorily throughout the project. The pressure in the system was maintained by a vacuum pump evacuating the system. The pumping rate was regulated by a globe-type vacuum valve to provide a controllable orifice. Solid products of the reaction frequently caused excessive friction to gas flow until a large area vacuum filter was installed ahead of the control valve.

Reaction Tubes

Most of the plating runs utilized tubes made from commercially drawn steel tubing with an approximate composition comparable to AISI 4620. The internal surface of the tubes was finished to a high polish. Initially, metallic "O" rings were used as gaskets at the tube ends, but experience proved that the asbestos sheet material provided a tighter seal.

The tubes were bored out to 1⅝ in. and were finished to a surface of better than 16 microinches rms. The tubes were approximately 36 in. long over-all permitting a coating length of about 30 in.

Various substrates were used as a basis for the molybdenum plate, in addition to cleaned but otherwise untreated steel. All tubes were carefully degreased with acetone. Electroplates of copper and of nickel and chemical plates of nickel and of cobalt were tested. Chemical plate was produced by the manner outlined by Brenner and Riddell (3) at the National Bureau of Standards. Since cobalt chemical coatings gave the best results in the early stages of development, all tubes used in the later stages were given this treatment.

Heating of the Reaction Tube

An induction heating coil was originally proposed for this study, but it was not possible to secure an adequate power supply in a reasonable time at the outset of the project. For the most part heating of the tube was accomplished by an annular high-temperature gas burner mounted on a moving platform. The burner was of the positive pressure, mixed air and gas type. It was capable of producing a narrow band of intense heat at the exterior of the tube and could be regulated within very close limits.

The burner was moved downward counter to the feed flow in order to allow the molybdenum to be deposited on a clean surface. With a plating run starting at the upper end of the tube, any partially reduced products of the reaction were deposited on the plated surface and could easily be removed.

During the final phase of the project, a 25 kw, 9600 cycle induction generator became available and it was decided to investigate the effect of an extended reaction zone on the process. A heated zone of from 8-10 in. was desired in place of the narrow 2-in. zone available from the gas burner. It was determined that about 2½-3 kw were required to maintain the tube at reaction temperature. This method of heating proved to be extremely successful, clean, easy to control, and produced less scaling on the outside of the tube than the gas burner. The temperature of the external tube surface was measured by a thermocouple and by a radiation pyrometer. Unfortunately, there was time for only four runs utilizing this equipment. Results are discussed later.

For all runs secondary heating by infrared lamps was utilized to maintain the temperature of the reaction tube above the condensation temperatures of molybdenum pentachloride in order to prevent a subsequent vaporization and enrichment of the vapor mixture as the burner traveled down the tube.

Effect of Variables on Plating Quality

Throughout the investigation, the effects of the following variables on plate quality and thickness were studied: total pressure, temperature of reaction zone, vapor concentration, hydrogen flow rate, surface preparation, and direction and rate of travel of the burner. The following were found to be the optimum conditions using the equipment described: (*a*) total reaction pressure 15-20 mm Hg; (*b*) tube temperature of 900°-950°C measured externally; (*c*) rate of travel of burner in the downward direction of 2 in./hr. (*d*) hydrogen flow of 7-9 liters/min measured at standard conditions.

When the pressure in the reaction tube rose above 20 mm, a vapor phase reduction occurred and the deposit became porous and nonadherent due to deposition of molybdenum particles which did not form a continuous coating. Below 10 mm total pressure it was impossible to obtain an adequate concentration of molybdenum pentachloride vapor to provide a sufficiently high rate of deposition. Most of the work was carried out at a pressure of 17 mm Hg.

The external temperature of the reaction zone as determined optically was usually between 875° and 975°C. These temperatures were correlated with measurements made by thermocouples to the internal tube temperature early in the project. Temperatures below 875°C were not high enough to produce a complete reduction at the existing gas velocities. Above 975°C there was an increased tendency to-

ward formation of large amounts of scale and toward decarburization of the exterior tube surface. No improvement in internal plate quality was gained by operating at temperatures in excess of 975°C.

While it was not possible to determine quantitatively the actual molybdenum pentachloride to hydrogen ratio, it was quite evident from the examination of the data that this was one of the fundamental variables of the process. When the vapor concentration was too low, an excessively long period was required to build up an adequate plate thickness. However, when very lean mixtures were used, the plate appeared to be dense and well bonded. With a high ratio of molybdenum pentachloride to hydrogen in the vapor a porous nonadherent coating was deposited. In the latter case there was a tendency for the coating to be much thicker, but because of side reactions, voids were apparent between the molybdenum and the base metal. The maximum plating rate for dense adherent coatings was 0.004 in./hr. When the plating rate was increased by increasing reactant rate or by increasing the vapor concentration, the deposit became less adherent, brittle, and less dense. When a low vapor concentration was used, the deposition rate was low but the quality of the deposit was excellent. Considerable effort was expended in an attempt to establish a means of determining quantitatively the molybdenum pentachloride-hydrogen ratio, but without success.

From the examination of a large number of plating runs, the conclusion was reached that downward travel of the burner consistently produced the best results; as the vapor mixture flowed through the heated zone, the reduction to metallic molybdenum was only partially complete. Some low molybdenum chlorides were also produced, which deposited on the internal tube surface in the cool zone. If the burner were moved concurrent with the flow, these lower chlorides might not be revaporized before they reached reduction temperature. This would result in a porous or powdery deposit with little or no adherence of the subsequent metallic plate. If on the other hand the heater were moved downward, incompletely reduced chlorides would be deposited on plate which had already been laid down and would be subjected to no additional heating. As the heater moved down, the plate would be deposited on fresh clean surface. When necessary, unreduced chlorides were removed with no difficulty by wire brushing.

Because of the reaction of the molybdenum and the carbon of the steel, it was determined early in the research that a barrier must be established to prevent this from taking place. Copper, nickel, and cobalt plates in various thicknesses were tried. The best results were obtained using a cobalt underplate of about 0.00025 in. This plate was easily applied nonelectrolytically and, once in place, provided excellent protection for the internal surface of the tube prior to molybdenum plating.

Time did not permit a more detailed study of the effect of increasing the width of the reaction zone. The results of the last four runs of the project were so much superior to all others that it appears that plating quality and rates could be improved greatly.

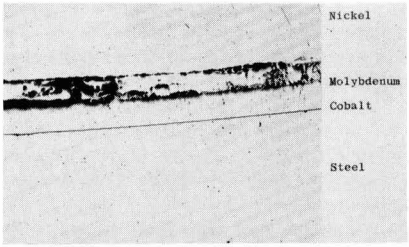

Fig. 2. Photomicrograph of molybdenum on cobalt on steel, unetched. Magnification 100X before reduction for publication. Photograph courtesy of Watertown Arsenal Laboratories.

Examination and Testing

Photomicrographs of coatings and base materials were made regularly to determine quality of the plate. Figure 2 shows the polished, but unetched, tube at 100X magnification (before reduction for printing). On the bottom is the base material of the tube. The line above is the cobalt substrate; next is the molybdenum deposit of about 0.004 in. The specimen was coated with electrodeposited nickel prior to metallographic examination, and the dark area between the molybdenum and the nickel is apparently due to the sample preparation.

Figure 3 shows the etched deposit at 500X. The base material, AISI 4620, is in the lower section, the cobalt interface and the molybdenum. The columnar structure of the deposited metal is readily observed. The protecting nickel coat is shown here as above.

The plated tubes have undergone utilization tests to determine resistance to abrasion and erosion. In addition to the metallographic examination of the coatings, several other tests were made to determine the efficiency of the plating process and the quality of the deposited molybdenum.

Samples of the coatings were subjected to various bend tests to determine the angle to which the plate and base material could be deformed before separation of the plate occurred. The specimen was bent with the plated surface out so that the plate was under tension. It was observed that the heavier the plate, the more readily it fractured. In all cases, the plate fractured when the bending angle exceeded 135° at a bending radius of ½ in. In several instances good plate showed failure at much lower bend angles because of the extreme columnar struc-

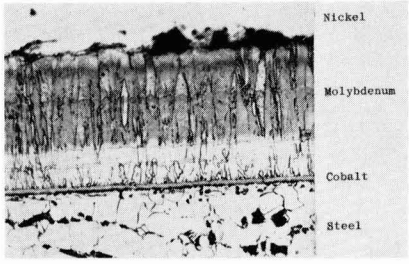

Fig. 3. Photomicrograph of typical molybdenum deposit, etched with alkaline $K_3Fe(CN)_6$. Magnification 500X before reduction for publication. Photograph courtesy of Watertown Arsenal Laboratories.

ture of the deposited material. When this type plate was examined under a low-power microscope, it was evident that the molybdenum failed by separation of the columnar grains as indicated by the many cracks extending from the base material to the outside surface of the plate. In spite of the failure of the molybdenum, it was evident that the cobalt plate below the molybdenum had remained intact during the bend test. Additional indications of quality of the molybdenum plate were obtained by observing the tube when it was sawed for sampling.

To further determine plate quality, various machining operations were performed on coated tubes. Sawing of a tube which had been plated with what was considered to be a high-quality plate produced a rolled-over edge of the coating at the edge of the cut. A poor coating would either flake off or chip away from the base material at the saw cut.

When a piece of coated tube was placed in a shaper and a strip of material removed lengthwise from the tube, good coatings would, as in the case of the sawed sample, remain attached to the section of base material removed from the tube. Poor quality coatings would flake and chip as the tool passed across the coating, and the coating would separate from the base material even though the base material were removed in a clean, even cut from the tube section.

Conclusions

A technique has been developed for the production of relatively heavy molybdenum plates inside of tubes. The best deposits were produced when the vapor concentration was held constant throughout the run. The wide hot zone produced by the induction coil proved superior to the narrow hot zone produced by the external gas burner. It was essential to maintain a large excess of hydrogen in the vapor stream to insure complete reduction, in order to produce dense deposits. Chemically clean surfaces for deposition were necessary to permit good bonding of the plate and substrate.

There should be uses for such plates in the chemical engineering field to take advantage of the mechanical strength and resistance to abrasion and erosion of molybdenum, as well as its high chemical and corrosion resistance. In the presence of air, at elevated temperatures, molybdenum undergoes catastrophic oxidation. However, for many uses in high-temperature, high-pressure reactors, this material could well be the answer to erosion problems where nonoxidizing conditions exist.

Acknowledgment

The author wishes to express his appreciation to the Ordnance Corps, Department of the Army, for permission to publish this information. Dr. Peter R. Kosting, Mr. Murray M. Jacobson, and Mr. Herbert F. Campbell of the Watertown Arsenal Laboratories were very helpful with assistance and suggestions. The author is also indebted to Mr. Morse Hill, the initial project manager, and to Mr. Philip J. Clough, Director, Metallurgical Department, National Research Corporation.

The technical assistance of Messrs. Donald Wilde and Henry Beanland is also acknowledged.

Manuscript received April 22, 1958. This paper was prepared for delivery before the Washington Meeting, May 12-16, 1957.

Any discussion of this paper will appear in a Discussion Section to be published in the December 1959 JOURNAL.

REFERENCES

1. C. F. Powell, I. E. Campbell, and B. W. Gonser, *J. (and Trans.)* Electrochem. Soc., **93**, 258 (1948).
2. W. J. Childs, J. E. Cline, W. M. Kisner, and J. Wulff, *Trans. Am. Soc. Metals*, Preprint 8, 17 pp. (1950).
3. Abner Brenner and G. E. Riddell, "Deposits of Nickel and Cobalt by Chemical Reduction," R. P. 1835, J. Research 39 November (1947) NBS.

Effects of Impurities on the Crystallographic Modifications of Calcium Metal

J. F. Smith and B. T. Bernstein

Institute for Atomic Research and Department of Chemistry, Iowa State College of Agriculture and Mechanic Arts, Ames, Iowa

Previous work at this laboratory (1) has shown that above room temperature very pure calcium exists in only two allotropic forms: f.c.c. between room temperature and 464°C and b.c.c. between 464°C and the melting point. It is the authors' belief that these results represent the behavior of the purest Ca which has been examined to date. This point of view is substantiated by the rapidity and reversibility of the observed transformation since such behavior is representative of high-purity metal. Subtraction of the analyzed impurity content indicated this metal to be 99.96 wt % Ca. No analytical data were available, however, for hydrogen, oxygen, or carbon content.

Indication that these nonanalyzed impurities play an important role in the allotropic behavior of Ca was found in a subsequent examination of a later preparation of Ca. The analytical data for this latter Ca [herein referred to as calcium D (Ca D)] was comparable to that for the original Ca. The values for Ca D were: Mg, <0.01 wt %; N, <0.009 wt %; C, ~0.02 wt %; Si, <0.005 wt %; Mn, Fe, Al, Ba, Be, <0.001 wt %; and Cd, Cu, K, Li, <0.0001 wt %. The observed crystal structures in Ca D showed the low-temperature f.c.c. form and the high-temperature b.c.c. form but showed in addition a h.c.p. modification at intermediate temperatures. This sequence of structures has also been observed by Melsert, Tie-

Table I. Analytical data for those elements showing possible differences in concentration in the two Ca preparations

Element	Analysis of Ca used by Smith, Carlson, and Vest (wt %)	Analysis of Ca D used in the present investigation (wt %)
C	No analysis	0.02
Fe	0.01	<0.001
Mn	0.005	<0.001
Si	Trace	<0.005
Ba	Not detected	<0.001

dema, and Burgers (2). The behavior of Ca D was such, however, that the Ca D must be concluded to be a less pure Ca preparation than the dimorphic Ca used in the original investigation. This conclusion is based on the observation of two-phase regions showing f.c.c. plus h.c.p. and h.c.p. plus b.c.c. The temperature ranges for the occurrence of these two-phase regions was a function of the thermal history of the sample, and indeed the appearance of a single-phase region of h.c.p. could be entirely eliminated after prolonged heating at elevated temperature. On the basis of the phase rule the occurrence of two-phase regions over a temperature range at constant pressure is precluded in a one-component system if the system is at equilibrium. It may be argued that the f.c.c. to h.c.p. transition is mechanistically difficult and that sluggish kinetics may defeat equilibrium; however, a similar argument is not valid for the h.c.p. to b.c.c. transition. In the latter case the transition is conceptually simple and may be visualized as occurring through a region of continuous strain. Such a transition should be rapid and reversible.

It seems evident, therefore, that the behavior of Ca D must be due to some contaminant present to a greater degree in Ca D than in the original Ca. In Table I are shown the analytical data for those elements exhibiting concentration differences in the two Ca preparations. These data were interpreted to mean that carbon or one of the nonanalyzed impurities was most probably responsible for the observed difference in behavior of the two Ca preparations. Substantiation of this point of view was made by re-examination of the only remaining sample of the original Ca preparation. This Ca had been stored for approximately 1½ years in a glass bottle with a plastic stopper. The bottle had been flushed with He and the glass-plastic juncture had been sealed with wax. Visual examination of the Ca taken from the bottle showed that the surface was discolored and obviously contaminated. Instead of the original dimorphic behavior, four structural modifications were observed: f.c.c., a low symmetry form originally reported by Graf (3), h.c.p., and b.c.c. The structural behavior was comparable to the least pure Ca (99.66%) examined in the previous investigation (1). By inference the change in behavior of the

Table II. Summary of diffraction results

Temp, °C	Uncontaminated Ca D	Ca D + oxygen	Ca D + ethane	Ca D + carbon	Ca D + nitrogen	Ca D + boron	Ca D + hydrogen	Uncontaminated Ca E	Ca E + hydrogen
100		Patterns essentially the same as uncontaminated Ca D plus the most intense reflections of CaO at all temperatures	f.c.c. + h.c.p.	f.c.c. + low sym. phase	f.c.c.	Patterns essentially the same as uncontaminated Ca D with some slight shifting of peak positions indicating solid solubility	f.c.c. + h.c.p.	f.c.c.	f.c.c. + h.c.p. + low sym. phase
200	f.c.c.		200°C f.c.c. + h.c.p. + low sym.						
300				300°C low sym.	300°C f.c.c. + low sym.			300°C	
400	350°C f.c.c. + h.c.p. 455°C		360°C h.c.p.	350°C h.c.p.	360°C h.c.p.		450°C h.c.p.	f.c.c + low sym. phase 450°C	435°C
500	h.c.p.* 520°C h.c.p. + b.c.c.		>490°C	>490°C h.c.p. + b.c.c. (the temperature limits of these two phase regions were not closely bracketed)	>490°C		525°C h.c.p. + b.c.c.		h.c.p. + b.c.c.
600	560°C b.c.c.		<575°C b.c.c.	<575°C b.c.c.	<575°C b.c.c.		570°C b.c.c.	b.c.c.	550°C b.c.c.
700									

* Behavior of Ca D in the temperature region 455°-560°C was a function of the thermal history of the sample since the single phase h.c.p. region could be eliminated by prolonged heating at elevated temperature.

high-purity Ca must have resulted from interaction with atmospheric components (O_2, N_2, CO_2, water vapor) which had diffused through the plastic stopper.

The present investigation was undertaken to determine which contaminants were associated with the appearance of the h.c.p. modification and which with the low symmetry structure. The low symmetry structure had already been shown to be a result of contamination (1) which result is corroborated by the recent work of Schottmiller (4).

Experimental Results

Any attempt to determine which contaminants were associated with the impurity phases by further purification studies seemed impractical because of the limitations of the analytical techniques. Therefore, it was decided to contaminate samples of Ca deliberately to see which impurities caused the appearance of the low symmetry and h.c.p. phases. Calcium D was considered to be satisfactory as a test material for the determination of the impurities associated with the low symmetry phase but, because the h.c.p. phase was already present, Ca D was not suitable for delineating the cause of the h.c.p. phase. Examination of other Ca preparations which were on hand showed one [herein referred to as calcium E (Ca E)] which exhibited the f.c.c., low symmetry, and b.c.c. phases but not the h.c.p. phase. Calcium E was, therefore, satisfactory for the determination of the impurity associated with the h.c.p. phase. Chemical analysis showed Ca E to be high in Mg content but otherwise of good purity: Mg, 0.027 wt %; C, 0.02 wt %; N, <0.009 wt %; Si, <0.005 wt %; Al, B, Ba, Be, Cu, Fe, <0.001 wt %; and Cd, K, <0.0001 wt %.

Oxygen, ethane, carbon, nitrogen, boron, and hydrogen were chosen as contaminants. Boron was included in the list in order to determine whether or not the structural effects were due simply to interstitial atoms. A summary of the diffraction results before and after contamination is shown in Table II. Diffraction patterns were taken with a modified Geiger-counter diffractometer (5) with the samples in the form of small bars. A slowly circulating atmosphere of purified He was maintained in the camera under a slight positive pressure. Temperatures were measured with a Pt-Pt 13% Rh thermocouple spot welded to the sample. It should be emphasized that the transition temperatures shown in Table II are approximate since diffraction patterns were taken at finite temperature increments, and no particular effort was made to precisely bracket a transition.

Gaseous contaminants were introduced into the experimental system by attaching to the system a 200-ml glass bulb filled with the gas. After first checking the sample to see that the structural behavior was typical and that inadvertent contamination had not occurred, the gas was vented into the system through a stopcock. Carbon and boron were added as powders, and contamination was accomplished in the following manner. The powder was sprinkled on a file, and the sample was inverted and lightly abraded across the file until a thin adherent film of the powder had collected on the calcium. The sample was then mounted in the camera and heated to ~500°C to allow reaction to occur.

In all cases the diffraction patterns were checked to determine that the sequence of phases was reversible in temperature. It was observed that in two-phase regions there was a general tendency for the intensity of the diffraction peaks of the low-temperature phase to decrease with increasing temperature with an accompanying inverse effect for the high-temperature phase.

It is evident from Table II that neither oxygen nor boron is responsible for the low symmetry or h.c.p. phases. However, both carbon and nitrogen were found to induce the appearance of the low symmetry phase. Since there might be some question with regard to adsorbed nitrogen on the graphite powder, carbon was also introduced in the form of ethane. Ethane contamination also caused the appearance of the low symmetry phase and, since contamination with hydrogen alone did not produce this result, the evidence indicates that carbon as well as nitrogen can cause the appearance of the low symmetry phase.

It is also evident from Table II that hydrogen is the impurity associated with the h.c.p. phase. Only hydrogen and ethane caused a significant change in the temperature range of stability of the h.c.p. phase in Ca D, and indeed hydrogen induced the appearance of the h.c.p. phase in Ca E. Although hydrogen does not cause the appearance of the low symmetry phase, the stabilization of this phase at lower temperatures in Ca E after hydrogen addition must indicate some degree of hydrogen solubility in the phase.

The effect of the thermal history of the samples on stability of the h.c.p. structure has been noted in the description of the behavior of Ca D. This effect is consistent with the conclusion that hydrogen is responsible for the occurrence of the h.c.p. phase since reduced stability of the phase after high-temperature annealing would be explicable on the basis of volatilization of hydrogen. Hydrogen would be expected to have an appreciable vapor pressure at elevated temperature, and volatilized hydrogen would be carried away by the slowly circulating helium atmosphere.

Discussion

On the basis of the results, there is little doubt that the free energy balance among the various structures is rather precarious and that small variations in the number and type of impurity atoms have significant effects. This sensitivity to nonmetallic impurities, readily available from the atmosphere, must be largely responsible for the disparity in results obtained by different investigators while measuring the physical properties of Ca metal and, in particular, for the diversity in reports concerning the allotropic behavior.

Calcium is known to be a highly reactive metal, especially so in the powdered form which has been used in other structural investigations. In the author's opinion the recent work of Schottmiller (4) on the Ca-Sr phase diagram illustrates this point.

Schottmiller found a marked difference between results obtained by x-ray diffraction using powder samples and results obtained by thermal analysis on massive samples of the same Ca metal. This occurred even though Schottmiller was particularly careful in the handling of his powder samples. The diffraction results showed a f.c.c. to h.c.p. transition at 342°-347°C and a h.c.p. to b.c.c. transition at 607°-612°C. In addition the low symmetry phase was found to exist in the temperature region 300°-345°C; it is not specified whether this was a single-phase or two-phase region. In comparison, the thermal data showed a transition at 281°-314°C which was attributed to the appearance of the low symmetry phase. But only one additional transition was found at 482°-516°C instead of the two transitions to be expected on the basis of the diffraction results.

It seems highly probable that the difference in results observed by Schottmiller was due to reaction of the Ca powder with some contaminant. Water vapor is the contaminant most difficult to exclude from an experimental environment since it adsorbs readily on most surfaces and in addition it will diffuse appreciably through many media.

Svec and co-workers (6, 7) have studied the reaction of Ca with water vapor and have found that the reaction occurs at the surface with the liberation of hydrogen. Hydrogen was found to have a high solubility in Ca and to diffuse rapidly into the metal, while the oxygen remained behind in a thin surface layer. The results provide a ready explanation for a source of hydrogen contamination and hence an explanation for the appearance of the h.c.p. phase in many Ca preparations. The degree of water vapor contamination which may occur before an oxide phase can be detected by x-ray diffraction is a function of the surface to volume ratio and is quite high in the case of powder samples.

In summary, the results of the present investigation show that nitrogen or carbon will induce the appearance of the low symmetry phase in Ca, and hydrogen will induce the appearance of the h.c.p. phase. In fairness, it should be emphasized that in neither case was the initial Ca completely pure and the observed results may have occurred because of a combined effect due to the added impurity plus impurities already present. Nonetheless, by inference the h.c.p. and low symmetry phases are both impurity-stabilized. This leaves f.c.c. and b.c.c. as the allotropic modifications of pure Ca with a transition temperature of ~450°C. The present investigation thus corroborates the results of the previous investigation and, in addition, provides an explanation for the occurrence of the low symmetry and h.c.p. phases. The transition temperature is also in reasonably good agreement with a thermal transition at 440°C listed by Kubaschewski (8) and for which he reports an averaged value for the enthalpy of transition of 0.24 ± 0.04 kcal/mol. Kubaschewski's value is based on a critical survey of available data, and he notes that only one transition is found consistently although an additional transition at lower temperature is also found by some investigators.

Acknowledgments

The authors wish to express their appreciation to Dr. O. N. Carlson for providing the calcium used in this investigation and to Mr. E. D. Gibson for his assistance in the initial stages of the investigation.

Manuscript received Oct. 20, 1958. Contribution No. 675. Work was performed in the Ames Laboratory of the U. S. Atomic Energy Commission.

Any discussion of this paper will appear in a Discussion Section to be published in the December 1959 JOURNAL.

REFERENCES

1. J. F. Smith, O. N. Carlson, and R. W. Vest, *This Journal*, **103**, 409 (1956).
2. H. Melsert, T. J. Tiedema, and W. G. Burgers, *Acta Cryst.*, **9**, 525 (1956).
3. L. Graf, *Physik. Z. vereinigt mit dem Jahrbuch der Radioaktivität und Elektronik*, **35**, 551 (1934).
4. J. C. Schottmiller, Ph.D. Thesis, Syracuse University (1958).
5. P. Chiotti, *Rev. Sci. Instr.*, **25**, 683 (1954).
6. D. S. Gibbs and H. J. Svec, *J. Am. Chem Soc.*, **75**, 6052 (1953).
7. H. J. Svec and C. Apel, *This Journal*, **104**, 346 (1957).
8. O. Kubaschewski, *Z. Elektrochem.*, **54**, 275 (1950).

The Synthesis of Some Pyridyl Glycols by Electrolytic Reduction

M. J. Allen and H. Cohen

Research Department, CIBA Pharmaceutical Products Inc., Summit, New Jersey

The synthesis of the pinacone, 3,3-di(p-aminophenyl)butanone - 2 - dihydrochloride (Amphenone B) (1) with subsequent elucidation of its interesting biological activities (2) led us to continue our investigations in an attempt to find pinacones analogous to Amphenone B which would retain the adrenal inhibitory effect of this compound but not its undesirable side effects.

It was decided to investigate the biological properties of the pinacones (3) prepared from the pinacols of 2-, 3-, and 4-acetylpyridine, but first it was necessary to prepare the respective pinacols. The electrolytic method was chosen for this purpose as it had proved itself quite satisfactory for the preparation of 2,3-bis(p-aminophenyl)-2,3-butanediol, the Amphenone B intermediate (4), as well as for other pinacols (5).

The pinacol of 3-acetylpyridine has been previously described (6). However, the experimental conditions which involved the use of an acidic medium resulted at times in difficulty in isolation of the pinacol with desired purity. Therefore as there is always the possibility of side reactions when using an acidic medium for a cathodic reduction of a ketone to its pinacol, it was decided to utilize basic conditions in our investigation. Although a potassium hy-

droxide medium was found to be quite satisfactory for the 2- and 4-acetylpyridines, the 3-acetylpyridine when electrolyzed in this medium gave extremely poor yields with an excessive amount of tarry material. In this instance a less basic medium, i.e., one containing potassium acetate, proved more satisfactory.

Experimental

The apparatus used for controlled potential electrolysis has been described (7) as has the 1500-ml cell used for the reductions of 2- and 4-acetylpyridine, except a regular paddle stirrer was used instead of a magnetic stirrer (6). The mercury cathode area in this cell was 111.3 cm^2. The reflux-type cell (8) used in the preparation of the 3-acetylpyridine pinacol had a mercury cathode area of 17.2 cm^2. In all the experiments reported the anode chamber contained a nickel anode and an aqueous 40% potassium carbonate solution.

2,3-Bis-(2-pyridyl)-2,3-butanediol. — The catholyte consisted of 100 g 2-acetylpyridine dissolved in 460 ml 1*N* KOH in 50% aqueous ethanol. At a reference potential of —1.6 v vs. S.C.E. the initial current was 5.6 amp and the applied voltage 16 v. The temperature was maintained at 23°-25° throughout the course of the reaction. After 256 min the current plateaued at 1.2 amp at which time the applied voltage was 4.5 v. The heavy precipitate which began to appear 40 min after onset of electrolysis, was filtered, washed with 25% ethanol, and dried. Yield 69 g (68.4%), mp 134°-137°, current efficiency 74.2%. Recrystallization from 50% aqueous methanol mp 138°-139°; anal. found: C, 69.06; H, 6.65; N, 11.77%. $C_{14}H_{16}N_2O_2$ requires, C, 68.82; H, 6.60; N, 11.46%.

2,3-Bis-(3-pyridyl)-2,3-butanediol. — A solution of 6 g 3-acetylpyridine in 35 ml ethanol, 15 g potassium acetate, and 17 ml distilled water was placed in the cathode compartment and the whole maintained at reflux throughout the course of the electrolysis. At a reference potential of —1.5 v the initial current was 8.9 amp and applied voltage, 11.4 v. After 25 min the current plateaued at 0.5 amp with an applied voltage of 2.1 v. The catholyte was distilled to a small volume under reduced pressure and, after chilling, the aqueous phase separated from the solid residue. This solid upon trituration with 20% acetone yielded 4.13 g (68.4%), mp 220°-224°, current efficiency 80.3%. Recrystallization from ethylene glycol gave mp 244°-245° (5).

2,3-Bis-(4-pyridyl)-2,3-butanediol. — The catholyte in this instance contained 100 g of the 4-acetylpyridine in 460 ml aqueous 1*N* KOH. At a reference potential of —2.2 v the initial current was 7.8 amp and applied voltage 12.5 v. After 176 min the current plateaued at 4.2 amp and the applied voltage was 7.0 v. The temperature throughout the course of this reaction was maintained at 23°-25°. The precipitate which had formed during the electrolysis was filtered, washed with water, and dried. Yield 99 g (98.2%), mp 209°-212°, current efficiency 97%. Recrystallization from methanol-ethyl acetate gave mp 219-220; anal. found: C, 68.51; H, 6.63; N, 11.33%. $C_{14}H_{16}N_2O_2$ requires C, 68.82; H, 6.60; N, 11.46%.

Manuscript received Nov. 25, 1958.

Any discussion of this paper will appear in a Discussion Section to be published in the December 1959 JOURNAL.

REFERENCES

1. M. J. Allen and A. H. Corwin, *J. Am. Chem. Soc.*, **72**, 117 (1950); W. Bencze and M. J. Allen, *J. Org. Chem.*, **22**, 352 (1957); J. Korman and E. C. Olson, *ibid.*, **22**, 870 (1957).
2. M. J. Allen, R. Hertz, and W. W. Tullner, *Proc. Soc. Exptl. Biol. Med.*, **74**, 632 (1950); R. Hertz, M. J. Allen, and W. W. Tullner, *ibid.*, **75**, 627 (1950); R. Hertz, *et al.*, *Recent Progr. in Hormone Research*, **11**, 119 (1955); A. E. Renold, *et al.*, *N. Engl. J. Med.*, **256**, 16 (1957).
3. W. Bencze and M. J. Allen, To be published.
4. M. J. Allen and A. H. Corwin, *J. Am. Chem Soc.*, **72**, 114 (1950).
5. M. J. Allen, "Organic Electrode Processes," Reinhold Publishing Corp. New York (1958).
6. M. J. Allen, *J. Org. Chem.*, **15**, 435 (1950).
7. M. J. Allen, *Anal. Chem.*, **22**, 804 (1950).
8. H. A. Levine and M. J. Allen, *J. Chem. Soc.*, **1952**, 254.

Technical Review

The Silver Oxide Electrode

T. P. Dirkse

Calvin College, Grand Rapids, Michigan

ABSTRACT

A review has been prepared of the electrochemistry of the silver oxide electrode. The discussion covers the structure and electrochemistry of the oxides of silver and their behavior in batteries.

With respect to the battery family, silver and its oxides are relatively new arrivals. There was some interest in these oxides for battery use around the turn of the century. In 1910 Morrison was issued several patents (1) covering various phases of the construction of a storage battery using silver oxides as positive plate materials. However, so far as is known, no commercial application was made of these patents.

Around the beginning of World War II interest was again aroused. Andre (2) once again suggested the use of silver oxides in a storage battery. To overcome the problem of a short shelf life he advised the use of a membrane as a sheath around the silver oxide plates. Some work at the National Bureau of Standards showed that silver oxides could serve well in a primary battery. The silver-zinc-alkali system was found to have a relatively high watt hour per pound value. At present this system is available both as a primary and as a secondary battery.

Because of this relatively short history of interest in the silver oxides as active materials for alkaline batteries, there is in the literature of silver and its oxides very little material dealing with the chemical problems peculiar to or associated with the battery industry.

There are several oxides of silver and, although their use as active materials in batteries has been limited to alkaline electrolytes, there is a good deal of literature dealing with the problem of silver oxides in acid solutions. Figure 1 is a modification of the diagram of Delahay, Pourbaix, and Van Rysselberghe (3). It gives a good survey of the relationship of silver to its oxides in a rather wide pH range. This diagram, of course, represents equilibrium conditions, and such conditions may not prevail at all areas of electrode-electrolyte interface during the operation of a battery. The areas of Ag, Ag^+, Ag_2O, and AgO seem fairly well defined, but there is uncertainty about the existence of oxides in which silver apparently has an oxidation number greater than two. Line a represents the reduction of H^+ to H_2 and line b the reduction of O_2 to water. For alkaline batteries the region of high pH is most significant. Here we find Ag, Ag_2O, and AgO as the thermodynamically stable phases.

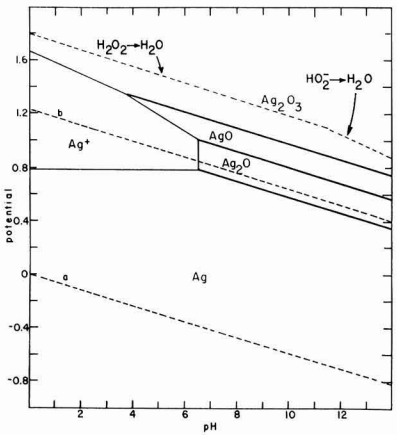

Fig. 1. Potential-pH diagram for silver and its oxides

Silver

Generally, the oxides used in these batteries are formed by the electrolytic oxidation of silver. Metallic silver is a good electrical conductor, having a specific resistance of 1.59×10^{-6} ohm-cm (4). During discharge, these oxides are reduced to silver, which then makes the plates better electrical conductors.

An interesting characteristic of silver is its ability to allow oxygen to diffuse through it (5). It has been suggested that this is done by the formation of Ag_2O (6).

The crystal structure of silver has been the subject of much investigation. It appears that there is only one crystal form, a face-centered cubic arrangement. The edge of a unit cube has a length of 4.078Å, and the distance between the centers of the nearest silver atoms is 2.884Å (7).

Although the crystal lattice seems fairly well established, there is some question about the electronic

configuration of the silver atoms. The K, L, and M orbits of the silver atom are complete, as are the 4s and 4p orbitals. This leaves 11 electrons to be allocated. One possibility is to assign 10 of these electrons to the 4d orbitals, completing them and leaving one electron for the 5s orbital. This is in agreement with the fact that silver is ordinarily univalent. However, Kaplan (8) contends that the 4d shell does not have the stability of the rare gas shells, and suggests the presence of 3 free electrons per atom in the lattice. This would account for the various oxides and valence states.

When the potential on a silver electrode in alkaline solution is raised, the first product formed is Ag_2O. This reaction proceeds efficiently and can be carried out with a polarization of less than 50 mv. However, only a thin film of Ag_2O is formed. It has been estimated to be of the order of 3 molecules in thickness (9).

Silver(I) Oxide

Silver(I) oxide, Ag_2O, is a rather well-defined substance. It has a deep brown color and gives a definite x-ray pattern. At one time it was suggested that there are two crystal modifications of this substance (10) with different electrode potentials. However, other investigators found no warrant for this (11).

The crystal structure of this oxide is basically the cubic type, the length of an edge being 4.72Å (12). It has a face-centered cubic arrangement of silver atoms or ions interpenetrated by a body-centered cubic arrangement of oxygen ions (13). Consequently, each oxygen ion is in the center of a tetrahedron of silver ions. Apparently then, the formation of Ag_2O does not alter the basic structure of silver but spreads it out a bit, increasing the length of the cube edge. If the basic lattice be divided into octants, the oxygen ions then occupy two octants of the unit cube. The distance between centers of nearest silver ions is 3.336Å and that between silver and oxygen is 2.043Å.

The electrochemical formation of Ag_2O can be represented by Eq. [1]. The variation of $E_{Ag\text{-}Ag_2O}$ with hydroxyl ion

$$2Ag + 2\,OH^- \rightarrow Ag_2O + H_2O + 2\,e \qquad [1]$$

concentration is in agreement with this equation. The exact value of E° for this reaction appears to be in some doubt. Hamer and Craig (14) have reviewed the situation, and point out that the lack of reproducibility of the potential of the Ag-Ag_2O couple in alkaline solution is not due to changes in the Ag_2O. They suggest that it is due to a chemisorbed film of oxygen on the silver, which film could be passive. They point out further that no value of E° has been determined for this change by measurement against a hydrogen electrode.

Two properties of Ag_2O limit its effectiveness as the positive active material in an alkaline cell. The first of these is its high electrical resistance. Le Blanc and Sachse (15) give the specific resistance as about 10^8 ohm-cm. This high resistance, or low conductivity, indicates the absence of mobile or unpaired electrons in the Ag_2O lattice. It naturally affects the conductivity of the electrodes in which it is found, and may be the reason why only a thin film of Ag_2O is formed on the Ag. The resistance of this film results in a rise of the applied voltage when such an electrode is charged by a constant current process.

The other property is the solubility of Ag_2O in alkaline solutions. This solubility, at least in the more dilute solutions, is a function of the hydroxyl ion and not of the cation. The solubility product at 25°C is of the order of 2×10^{-5} (16), and it increases with increasing temperature (17). The solubility is due to reaction [2]. A part of the dissolved

$$Ag_2O + 2\,OH^- \rightarrow 2AgO^- \text{ [or } Ag(OH)_2^-] + H_2O \qquad [2]$$

Ag_2O in alkaline solutions may also be in the form of $Ag_2(OH)^+$. This solubility of Ag_2O is at least partly responsible for the poor shelf life characteristics of the silver cell (18).

Silver(II) Oxide

Silver(II) oxide, AgO, has been investigated in numerous ways and has been studied both in alkaline and acid solutions. It is a grayish black substance and is now available commercially. It can be prepared in many ways, e.g., by the oxidation of silver or silver salts with ozone, persulfate, or permanganate. It is also prepared electrochemically by anodic treatment of silver or Ag_2O in alkaline solutions.

The latter reaction is an efficient one and the polarization is of the order of 100 to 150 mv. Luther and Pokorny (19) state that it proceeds reversibly as well. Jones, Thirsk, and Wynne-Jones (20), however, state that this process is irreversible. They used as their criterion the assumption that the discharge is an efficient process. This, however, is not necessarily the case. On discharge, particularly at appreciable current densities, only a part of the capacity of the AgO is delivered at the higher potential. There is still AgO present at the beginning of the lower voltage level during discharge (Fig. 2). The kinetics or mechanism of this reaction have not been established, but the equilibrium condition is likely represented by Eq. [3].

$$Ag_2O + 2\,OH^- \rightarrow 2AgO + H_2O + 2e \qquad [3]$$

This reaction is similar to [1]. Accordingly, the relation of the potential of [3] to hydroxyl ion con-

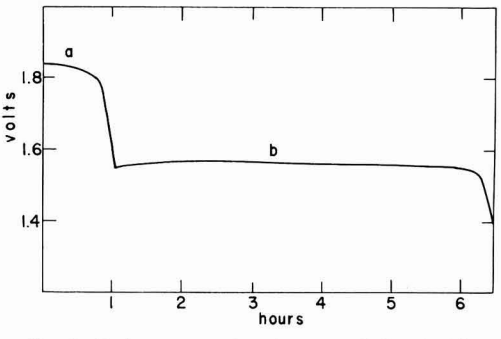

Fig. 2. Discharge curve for silver-zinc alkali cell; (a) reduction of AgO, (b) reduction of Ag_2O.

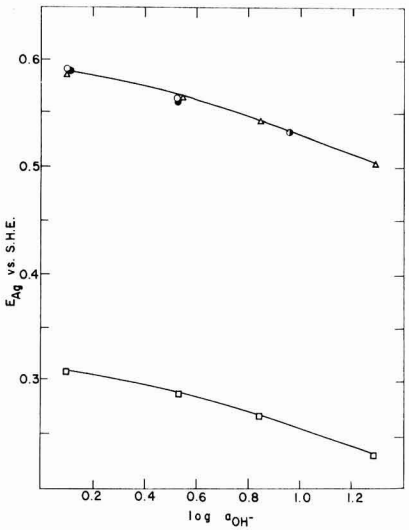

Fig. 3. Electrode potential of silver oxides. O—electrolytically prepared AgO; •—chemically prepared AgO; △—Ag_2O_3; □—Ag_2O.

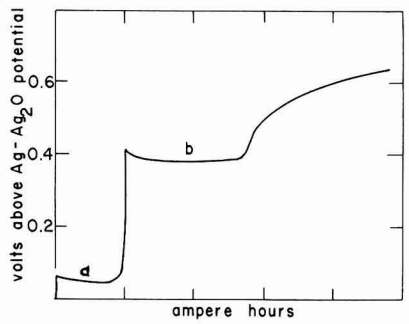

Fig. 4. Charge curve of silver electrode in alkaline solutions; (a) formation of Ag_2O, (b) formation of AgO.

centration is the same as that for reaction [1] (Fig. 3).

The layer of AgO formed in these electrochemical processes is thicker than that of Ag_2O. On Fig. 4, for example, the plateau for the formation of AgO is longer than that for the formation of Ag_2O. At moderate current densities both processes are about 100% efficient (21). Therefore the length of the plateaus is a relative measure of the depth of formation of the oxides. A constant potential charging process can give a product that is completely converted to AgO. In fact, we have produced in this manner products that on analysis appear to be Ag_2O_3. Yet these products have the same electrode potential (Fig. 3) and x-ray pattern that AgO has. It is possible that these products are the AgO plus adsorbed oxygen.

There has been some disagreement as to the mechanism of the transformation of the lower oxide to a higher one. The second plateau of the charge curve is preceded by a small peak (Fig. 4). This peak has been interpreted differently. Hickling and Taylor (9) consider it to represent the formation of Ag_2O_3 which then decomposes to AgO. Jones, *et al.* (20) suggest that this peak is due to the difficulty of forming nuclei of AgO. This could be somewhat similar to a resistive effect of Ag_2O which is decreased as soon as the better conducting higher oxide is formed (22).

Within the past year or so the structure of AgO has been clarified. The work of Scatturin, *et al.* (23) shows AgO to have a monoclinic structure, and the cell parameters have been evaluated. More recently Graff and Stadelmaier (24) have reached the same conclusions. Thus, when Ag_2O is oxidized to AgO the cubic arrangement of the silver atoms or ions is distorted or destroyed.

However, there still are questions concerning the structure of this substance. The material produced from the product obtained by anodizing a silver nitrate solution between platinum electrodes and that produced by extensive ozonization of silver gives a different x-ray diffraction pattern than the monoclinic form of AgO (24, 25). The monoclinic form is the one produced on a battery plate. Jones and Thirsk (26) have interpreted the nonmonoclinic x-ray pattern as revealing a face-centered cubic form of AgO. Graff and Stadelmaier (24) suggest that this may possibly be a higher oxide such as Ag_2O_3. This matter is as yet unresolved.

Various properties of AgO have been studied and the results of the several investigations have differed significantly. Some of this may be due to the fact that many data reported for AgO have been obtained by measurement and study of the nonmonoclinic variety (27, 28). The condition of the silver in the AgO has not been clarified. It has been suggested that there may be two Ag — O distances, and the bonding may be partly ionic and partly covalent (23). The specific resistance of AgO has been reported as 0.012 ohm-cm (26), 15 ohm-cm (29), and 10 ohm-cm (15). In any event, the conductivity is considerably better than that of Ag_2O and this indicates that there are unpaired or mobile electrons present in the solid material. The magnetic susceptibility per mole has been given as $+40 \times 10^{-6}$ (paramagnetic) (30) and -19×10^{-6} (diamagnetic) (29). The latter value was used as evidence for the conclusion that the bonding in the AgO lattice is covalent or metallic and the silver is trivalent. Two of these valences are used for bonding the oxygen atom and the other one for bonding with other silver atoms.

It is generally agreed that the silver in AgO has an oxidation number of +2. Klemm (30) used several criteria to establish this. He considered analytical evidence, oxidative ability, and isomorphism with CuO. To this may be added the fact that electrochemical reduction of this oxide yields two Faradays per mole (31). Addition of acids to this oxide yields oxygen but no hydrogen peroxide. This indicates that AgO is not a peroxide (26).

AgO dissolves in nitric acid to give a dark brown solution which is fairly stable in the cold. This solution has strong oxidizing powers. The color disappears on warming or on dilution. Barbieri (32) suggested that this dark colored solution contained tri-

valent and monovalent silver. However, later work showed that the dissolved silver is primarily bipositive (33). This was determined by a solubility method and by a determination of magnetic susceptibility. The magnetic moment corresponded closely to that calculated on the assumption of one unpaired electron. This then is a 4d electron.

For use in a battery it is necessary that a substance be fairly stable in the electrolyte, in this case an aqueous solution of NaOH or KOH. Denison (31) reported that the oxide is stable in 20-40% KOH solutions. However, pure AgO does decompose very slightly in alkaline solutions at room temperature. At higher temperatures this decomposition is more rapid (34). Practically, in a battery, pure AgO is never produced on charging, and the presence of unoxidized silver in such a plate further hastens the decomposition of the AgO (34).

Because of the higher oxidation state of silver, one would expect the AgO to be more soluble than Ag_2O in alkaline solutions. Some solubility data have been reported (34,35), and it appears that the solubilities of Ag_2O and AgO are not far different from each other in alkaline solutions. The solubility passes through a maximum with time but equilibrium is reached within a few hours (34).

Higher Oxides

Of the various higher oxides of silver mentioned, Ag_2O_3 is the most popular formula. The evidence for the existence of this oxide is, in the main, indirect. It is doubtful whether a pure sample has been isolated. Jirsa (36) claims that Ag_2O_3 can be prepared but cannot exist alone. Furthermore, it is readily decomposed by heating. Braekken (37) attempted to determine the structure by means of x-ray diffraction measurements but reached no conclusion other than that it had a cubic structure. However, the cube edge length seemed to vary with the method of preparation.

Three methods have been used to prepare this material. (*A*) Luther and Pokorny (19) were able to oxidize silver nitrate or sulfate anodically and obtain a product which appeared to be a mixture of AgO and Ag_2O_3. This couple had a potential about 200 mv higher than that of the Ag_2O-AgO couple. They were not able to produce this substance by anodic treatment of AgO in alkaline solutions. Somewhat similar work was done later (38) and it was concluded that Ag_3O_4 or Ag_4O_5 was formed. However, these oxides were not pure but contained $AgNO_3$ or Ag_2SO_4. Later Weber (39) prepared this same material and determined transference numbers of it in a nitric acid solution. On the basis of his results he concluded that at least some of the dissolved silver was trivalent.

(*B*) Yost (40) oxidized silver salts with peroxysulfuric acid and obtained a product which appeared to be $Ag_2O_3 \cdot x\,Ag_2(SO_4)_3$. De Boer and van Ormondt (41) also used acid solutions of persulfates as oxidizing agents and obtained a black precipitate which they considered to be a mixture of Ag_3O_4 and $Ag_2(SO_4)_2$ or $Ag_2S_2O_8$. However, the use of persulfates in alkaline solutions gave only the AgO.

(*C*) The third method for preparing this oxide involves the treatment of silver or Ag_2O with ozone (42), or the treatment of silver salts in acid solution with ozone (43). However, here the trivalent silver, AgO^+, had but a transient existence in solution.

In summary, there seems to be some evidence for the existence of a trivalent state of silver, e.g., Ag_2O_3. However, much of the evidence may also be interpreted in other ways (44). The potential value given for the AgO-Ag_2O_3 couple is very close to that for the formation or reduction of the HO_2^- ion in alkaline solutions or H_2O_2 in acid solutions (Fig. 1). Whatever the interpretation, this higher valence state is of little significance for use in alkaline batteries. This conclusion is substantiated by recent work at the Battelle Memorial Institute (45). Samples of Ag_2O_3 were prepared and used as the positive active material in an alkaline cell. The voltage curves and the ampere-hour capacity obtained from such plates were essentially those of AgO.

Conclusions

Although silver oxides are being used in commercial batteries, the performance of these batteries could stand improvement. Some of the troubles encountered are inherent in the system, e.g., the solubility of the oxides in the alkaline electrolyte. Others are due to or are aggravated by the method of assembly of the components. In order to understand this system better there are at least two areas that need to be more thoroughly investigated.

1. The higher voltage level on discharge, (AgO, Fig. 2), is rather unpredictable, particularly in a secondary battery. The capacity delivered at this voltage is sensitive to a variety of conditions, and it disappears on stand without a loss in total capacity. The latter phenomenon can be accounted for by reaction [4] which can take place readily (34). More work

$$Ag + AgO \rightarrow Ag_2O \qquad [4]$$

is necessary to determine precisely what conditions do affect this part of the discharge curve. It is necessary also that work be carried out to determine the polarization of these various processes, particularly the reduction of AgO to Ag_2O.

2. In a secondary battery the charge acceptance is erratic (44). While the current efficiency is high and the discharge capacity is equal to the charge capacity, the amount of charge capacity varies from cycle to cycle and tends to decrease during the life of the battery. Some of this may be due to design, but it is also possible that there are physical changes in the silver during cycling. This is an area in need of more investigation. Allied with this may be the problem of aging of the oxides during long periods of stand.

REFERENCES

1. W. Morrison, U. S. Pat. 975,980, 975,981, 976,092, Nov. 15, 1910.
2. H. Andre, *Bull. soc. Franc. elec.*, (6) **1**, 132 (1941).
3. P. Delahay, M. Pourbaix, P. Van Rysselberghe, *This Journal*, **98**, 65 (1951).
4. W. M. Latimer and J. H. Hildebrand, "Reference Book of Inorganic Chemistry," 3rd ed., p. 103, Macmillan Co., New York (1951).

5. L. Spencer, *J. Chem. Soc.*, **123**, 2124 (1923).
6. J. H. Simons, *J. Phys. Chem.*, **36**, 652 (1932).
7. R. B. Wilsey, *Phil. Mag.*, **46**, 487 (1923).
8. J. Kaplan, *Z. Physik.*, **52**, 883 (1928).
9. A. Hickling and D. Taylor, *Discussions Faraday Soc.*, No. 1, 277 (1947).
10. H. N. K. Rördam, *Kgl. Danske Videnskab. Selskab., Math-fys. Medd.*, **3**, No. 7 (1920).
11. (a) H. T. S. Britton, *J. Chem. Soc.*, **127**, 2956 (1925); (b) R. F. Newton, *J. Am. Chem. Soc.*, **50**, 3258 (1928).
12. P. Niggli, *Z. Krist.*, **57**, 253 (1922).
13. W. P. Davey, *Phys. Rev.*, **19**, 248 (1922).
14. W. J. Hamer and D. N. Craig, *This Journal*, **104**, 206 (1957).
15. M. Le Blanc and H. Sachse, *Physik. Z.*, **32**, 887 (1931).
16. H. C. Johnston, F. Cuta, and A. B. Garrett, *J. Am. Chem. Soc.*, **55**, 2311 (1933).
17. K. Jellinek and H. Gordon, *Z. physik. Chem.*, **112**, 207 (1924).
18. T. P. Dirkse and F. De Haan, *This Journal*, **105**, 311 (1958).
19. R. Luther and F. Pokorny, *Z. anorg. u. allgem., Chem.*, **57**, 290 (1908).
20. P. Jones, H. Thirsk, and W. F. K. Wynne-Jones, *Trans. Faraday Soc.*, **52**, 1003 (1956).
21. T. P. Dirkse and L. A. Vander Lugt, "A Study of the Oxides of Silver," Techn. Report No. 4 on Contract No. N onr-1682(01), June 30, 1957, Calvin College, Grand Rapids, Mich.
22. T. P. Dirkse, Tech. Report No. 6, Contract No. N onr-1682(01), June 20, 1958, Calvin College, Grand Rapids, Mich.
23. V. Scatturin, P. Bellon, and R. Zannetti, *Ricerca sci.*, **27**, 2163 (1957).
24. W. S. Graff and H. H. Stadelmaier, *This Journal*, **105**, 446 (1958).
25. G. M. Schwab and G. Hartmann, *Z. anorg. u. allgem. Chem.*, **281**, 183 (1955).
26. P. Jones and H. R. Thirsk, *Trans. Faraday Soc.*, **50**, 732 (1954).
27. F. Jirsa and J. Jelinek, *Z. anorg. u. allgem. Chem.*, **148**, 130 (1925).
28. F. Jirsa, J. Jelinek, and J. Srbek, *ibid.*, **158**, 33 (1926).
29. A. B. Neiding and I. A. Kazarnovski, *Doklady Akad. Nauk, USSR*, **78**, No. 4, 713 (1951).
30. W. Klemm, *Z. anorg. u. allgem. Chem.*, **201**, 32 (1931).
31. I. A. Denison, *Trans. Electrochem. Soc.*, **90**, 387 (1946).
32. G. A. Barbieri, *Atti accad. Lincei*, **13**, 882 (1931).
33. A. A. Noyes, K. S. Pitzer, and C. L. Dunn, *J. Am. Chem. Soc.*, **57**, 1229 (1935).
34. T. P. Dirkse and B. Wiers, *This Journal*, **106**, 284 (1959).
35. H. P. Gregor, N. Nakajima, D. H. Gold, E. M. Loebl, G. K. Hoeschele, and R. Gogan, Final Report, Aug. 31, 1954, Contract No. NObs-62383, Polytechnic Institute of Brooklyn, Brooklyn, N. Y.
36. F. Jirsa, *Chem. Listy*, **19**, 3 (1925).
37. H. Braekken, *Kgl. Norske Videnskab. Selskab. Forh.*, **7**, 143 (1935).
38. G. Baborovsky and G. Kuzma, *Z. physik. Chem.*, **67**, 48, (1909).
39. H. C. P. Weber, *Trans. Am. Electrochem. Soc.*, **32**, 391 (1917).
40. D. M. Yost, *J. Am. Chem. Soc.*, **48**, 152 (1926).
41. J. H. De Boer and J. Van Ormondt, Proc. Intern. Symposium Reactivity of Solids, Gothenberg, **1952**, 557.
42. F. Jirsa and J. Jelinek, *Z. anorg. u. allgem. Chem.*, **158**, 61 (1926).
43. A. A. Noyes, J. L. Hoard, and K. S. Pitzer, *J. Am. Chem. Soc.*, **57**, 1221 (1935).
44. C. P. Wales, NRL Report 5167, Aug. 11, 1958, Naval Research Laboratory, Washington, D. C.
45. A. B. Tripler, W. T. Buckingham, L. D. Mc Graw, and C. L. Faust, Final Report, Contract No. DA-36-039-SC-42682, Sept. 1, 1955, Battelle Memorial Institute, Columbus, Ohio.

The Performance of Zinc, Magnesium and Aluminum Primary Cell Anodes. A Review

R. Glicksman

RCA Laboratories, Radio Corporation of America, Princeton, New Jersey

ABSTRACT

In this paper some of the factors involved in the operation of a primary cell anode are presented. The effects of such variables as alloy composition, inhibitors, pH, electrolyte composition, current density, and type of service, on the performance characteristics of zinc, magnesium, and aluminum anodes are discussed.

The number of metals which can be used in a galvanic cell is large in theory, yet in practice only a few have proved satisfactory. The anode materials which are in common use today are those which have standard potentials of an intermediate value and high hydrogen overvoltages such as zinc, cadmium, and lead. Of these, Zn is used most widely in primary cell systems, finding use in both acidic and alkaline cells (1-5). Attempts have been made to use Mg (6, 7) and Al (8) in dry cells, and considerable success has been achieved with Mg anodes.

The requirements for secondary cell anodes are somewhat more stringent than for primary cell anodes in that the electrode reactions have to be reversible. Thus, Mg and Al are unsuitable for use in rechargeable cells. Lead and cadmium, which form insoluble compounds at the anode surface during discharge, find extensive use for this application (9-11). The use of Zn has also proved quite feasible in alkaline cells (12) despite the solubility of $Zn(OH)_2$.

In this paper some of the factors involved in the

Table I. Theoretical data for Mg, Al, and Zn anodes

Metal	Density, g/cc	Reversible electrode potential, v E° acid	E° base	Electrochemical equivalent, amp-hr/g
Magnesium	1.74	2.37	2.69	2.20
Aluminum	2.70	1.66	2.35	2.98
Zinc	7.14	0.76	1.245	0.82

operation of a dry cell anode are discussed, and in particular the performance of Zn, Mg, and Al anodes is considered.

Theoretical

Theoretically, the suitability of a metal for use as a galvanic anode can be ascertained simply from its position in the electrochemical series (13) and its electrochemical equivalent, as shown in Table I. The electrochemical equivalent provides a measure of the quantity of electricity (ampere-hours) contained in a unit weight of the metal and is defined by Faraday's law. On this basis, Mg and Al are more attractive anodes than Zn.

However, because of their protective oxide film, the high reversible potentials of Mg and Al are never achieved. In practice, Mg has anode potentials only 0.3 to 0.6 v higher than those of Zn, while Al is cathodic to Zn in neutral or acidic electrolytes, as evidenced by the data in Table II (14).

Effect of Current Density

The current density affects the anode in two ways: through its effect on the potential and on the current efficiency of the electrode.

Most electrodes used in battery applications are characterized by low polarization as a whole at reasonable current densities. Active metal anodes generally have large activation polarization with respect to hydrogen discharge and, hence, a low self-corrosion, but very little polarization with respect to the oxidation of the metal. Notable exceptions to the latter are Mg and Al in many electrolytes (15). For example, Robinson (16) showed that current density had relatively little effect on the potential of Mg anodes in aqueous chloride and sulfate electrolytes; however, when the electrolyte contains a high concentration of an anion capable of precipitating Mg^{++} ion, e.g., OH^-, $SO_3^=$, anodic polarization occurs. Thus the polarization characteristics of Mg in these electrolytes nullifies an otherwise acceptable electrode potential.

As one might expect from the results of dissolution studies of metal anodes and viscosity studies of cell electrolytes, at low temperatures there is a large increase in polarization with increasing current density and decreasing temperature (17). In order to minimize polarization at the low temperatures, the trend is toward increased electrode area for low-temperature batteries.

Another important index of anode performance which must be considered is the anode efficiency. This indicates how much of the stored electricity is recoverable as useful energy under service conditions. Although theoretically the consumption of Mg per ampere-hour should be only 0.37 times that of Zn, it actually is about 0.6 times. This has been explained by the fact that 40% of the consumed Mg is dissolved by wasteful corrosion during the discharge of the cell as compared to 5-10% for the Zn cell (18).

The effect of a polarizing current on the dissolution rate of a magnesium AZ10A[1] alloy in 2*N* $MgBr_2$ is shown in Fig. 1 (19). When the specimen is made anodic, the observed dissolution rate is the sum of the rate due to the external current and the rate due to local action. It is seen that the local corrosion rate increases with increasing anodic current density. This is known in the theory of corrosion as the negative difference effect. For Mg the magnitude of this effect has been found by Robinson (16) to be dependent on both the electrolyte and anode composition including alloy ingredients and level of impuritites.

[1] This alloy consists principally of magnesium but contains in addition 1% aluminum and 0.5% zinc.

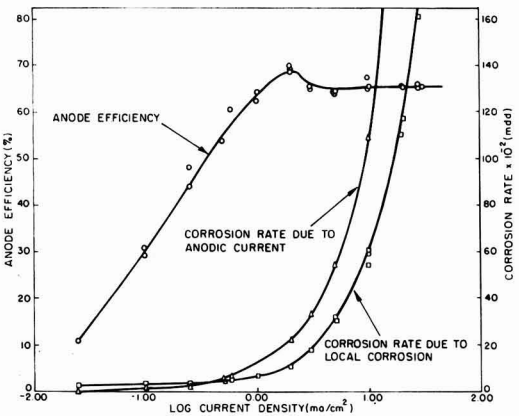

Fig. 1. Effect of current density on the local corrosion rate and anode efficiency of a MgAZ10A alloy dissolving in 2N $MgBr_2$ electrolyte [saturated with $Mg(OH_2)$]. [Glicksman 19)].

Table II. Electrode potentials* of Mg, Al, and Zn in various electrolytes (potentials referred to a standard hydrogen electrode) [Mears and Brown (14)]

Metal	1.0M NaCl	1.0M Na_2SO_4	1.0M Na_2CrO_4	1.0M HCl	1.0M HNO_3	1.0M NaOH	1.0M NH_4OH	St'd $Ca(OH)_2$	St'd $Ba(OH)_2$
Mg	1.38	1.41	0.62	1.34	1.15	1.13	1.09	0.61	0.54
Al	0.52	0.16	0.37	0.46	0.15	1.16	0.46	1.20	1.19
Zn	0.81	0.85	0.33	0.80	0.72	1.17	1.16	1.06	1.15

* Potentials originally reported were referred to a 0.1*N* calomel electrode. They are here corrected to the standard hydrogen electrode scale without making correction for the liquid junction potential.

This type of effect has also been observed on Mg corroding in a 3% NaCl solution (20) and is usually found with very active anode metals covered by a protective layer. The positive effect is found in the absence of a protective layer as in the case of Mg dissolving in HCl (21). Similarly, Al anodes show positive difference effects in certain corrosive electrolytes such as NaOH (22) and HF (23) which can dissolve the protective film, while the negative effect shows up in HCl (23) because of the presence of a film on the metal.

Thus one of the difficulties associated with the use of Al and Mg anodes is their poor current efficiencies, especially at low current densities. Moreover, the efficiency at any given current density has been found to decrease with a more intermittent type of discharge. This increase in corrosion on intermittent discharge is attributed to a change in the surface condition of the anode with alteration of current density. An example of this can be seen in Fig. 2, which shows the change in terminal voltage of Mg/$MgBr_2$/MnO_2 and Zn/NH_4Cl-$ZnCl_2$/MnO_2 dry cells as current pulses of 10 and 50 ma are withdrawn (24). It is seen that the Mg-MnO_2 cells undergo a greater instantaneous voltage fluctuation than the conventional Leclanché cells. (Oscillographic measurements of an Al/$AlCl_3$/MnO_2 cell showed a behavior quite similar to that of the Mg cells.) For Mg cells, the large initial drop is believed due to the resistance of the oxide film on Mg, the voltage rising as the oxide layer is being removed, reaching a steady-state value. When the circuit is opened, the cell voltage rises above the original open-circuit value and then gradually returns to its original voltage.

Thus, immediately after decreasing the current or breaking the circuit, the surface of the Mg is seen to be in a more active form than in its steady state under these same conditions. The question is, then, whether this change in the surface condition influences the over-all rate of hydrogen evolution. Presented in Fig. 3 is a comparison of the rate of hydrogen evolution from two magnesium AZ10A alloy samples in 2*N* $MgBr_2$ electrolyte in the absence of an external anodic current. Prior to the measurements, sample A was discharged for an hour at a current density of 5 ma/cm² and then allowed to corrode normally, while sample B was not discharged at all. The difference in corrosion rates of the two samples for the first 3 hr is attributed to a less effective oxide coating for the previously discharged Mg. At the end of 4-5 hr, there is little or no difference in the corrosion rates, and apparently the oxide coating on sample A is just as protective as that on the undischarged Mg, i.e., sample B. It is thus apparent that the change in surface condition with current density influences the rate of hydrogen evolution at a Mg anode. For Zn, no such problem arises, and it functions at high anode efficiencies for normal current drains and discharge tests.

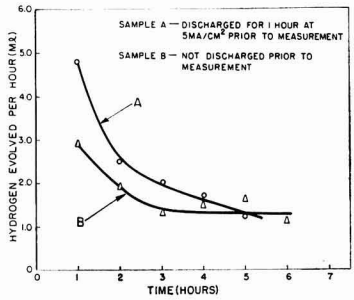

Fig. 3. Corrosion rate of a magnesium AZ10A alloy in 2N $MgBr_2$ electrolyte saturated with $Mg(OH)_2$ (Area 19.6 cm²).

As a consequence of the oxide film, two other problems are encountered in Mg dry cells when current is withdrawn, namely, "delayed action," and impedance. Delayed action is defined as the number of seconds required for the cell voltage to reach a minimum of 1.0 after the circuit is closed. At present this delay is less than 1 sec and apparently is no longer a problem (25). For Al cells using an $AlCl_3$ electrolyte inhibited with potassium chromate, a 1-sec delayed action is found (8).

When a primary cell is considered for use in powering electronic equipment, its impedance values

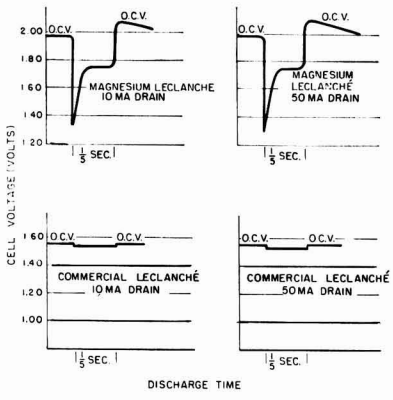

Fig. 2. Oscillographic measurements of change in voltage of AA-size Mg and Zn Leclanche type cells, subjected to 10 and 50 ma constant current drains. [Glicksman and Morehouse (24)].

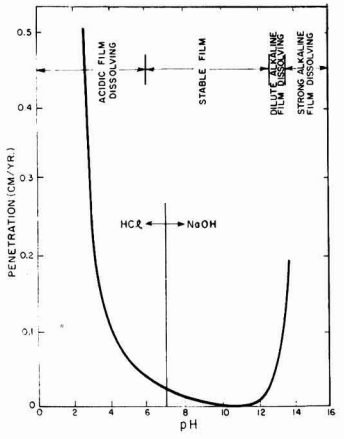

Fig. 4. Effect of pH on the corrosion of Zn by NaOH + HCl [Roetheli, Cox, and Littreal (27)].

under a variety of conditions must also be considered. Impedance measurements (26) for AA-size $Mg-MnO_2$ and $Zn-MnO_2$ cells show that the a-c impedance decreases with increasing current density and increasing frequency. At 400 cps the impedance of Mg cells is similar to that of Leclanché cells, whereas at 30 cps the impedance of the Mg cells becomes much greater than that of Leclanché cells at the lighter current drains. The high impedance of the Mg cells and their instantaneous voltage fluctuations with variations in power output, presents a problem as to the use of these cells in some electronic applications. Similar problems would be expected for Al dry cells.

Effect of Electrolyte

The influence of an electrolyte on the electrode potential and corrosion of a metal anode often depends on the nature of the protective film formed on the metal. In the corrosion process these films serve as barriers for the attack of the metal by the corrosive electrolyte. Frequently they are so effective that rapid corrosion proceeds for only a short time, and when the action of the films becomes a predominantly controlling factor, further corrosion is either prevented or the rate is reduced to a small value. Since the pH of the electrolyte has a marked effect on the solubilities and physical characteristics of this film, it is of great importance in choosing a particular electrolyte.

The influence of pH on the corrosion rate of Zn in mixtures of NaCl with NaOH and HCl (27) is shown in Fig. 4. It is seen that Zn is rapidly corroded by solutions whose pH is less than 6 or greater than 12.5 owing to the high solubility of the corrosion product formed. In solutions having pH values from 6 to 12.5 the low corrosion rates are attributed to the presence of adherent protective corrosion-product films. These films are precipitated probably because of the production of high pH's by the corrosion process in the liquid film adjacent to the metal.

In the Leclanché cell, with its $NH_4Cl-ZnCl_2$ electrolyte, the wasteful corrosion of Zn becomes a problem only on long-time intermittent use. For this electrolyte, which has an initial pH [2] of 4 to 5 depending on the concentration of the NH_4Cl and $ZnCl_2$, the corrosion of Zn can be expressed by

$$Zn + 2NH_4Cl = ZnCl_2 \cdot 2NH_3 + H_2 \qquad [1]$$

which represents the over-all reaction.

In alkaline dry cells, it would be expected that the corrosion of Zn would be much faster as the metal is shifted to more anodic potentials due to the low activity of metallic cations brought about by complex ion formation. For example, Zn exists in a sodium zincate solution as $[ZnO_2]^=$, or if the solution is less alkaline, as $[HZnO_2]^-$. However, in strongly alkaline solutions the Zn anodes owe their stability in large part to the addition of zincate salts to the electrolyte in substantially saturating concentration (4). The presence of the zincate ion decreases the rate of corrosion of the Zn anode by the mass action effect.

[2] The pH of the electrolyte increases during cell discharge, attaining values as high as 8 to 10 during heavy continuous service (28).

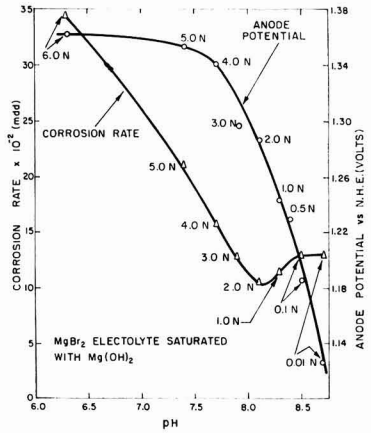

Fig. 5. Effect of pH on the corrosion rate and anode potential of a Mg AZ10A alloy dissolving anodically in various $MgBr_2$ electrolytes [saturated with $Mg(OH_2]$ at a current density of 2.0 ma/cm² [Glicksman (19)].

Aluminum is similar to Zn in that its oxide is soluble in both acid and alkali, and it is attacked by liquids of very high or very low pH value. Analogous curves to that of Zn in Fig. 4 have been obtained for Al, with a minimum near pH 7 (29).

The effect of pH on the corrosion rate of Mg in solutions of NaOH, HCl, and distilled water has been studied by Akimov and Rozenfeld (30). They report that, from pH 3 down, there is a sharp increase in the corrosion rate, while from pH 3 to 11 the corrosion curve slopes smoothly. At pH's of 11 and higher the protective film increases strongly in stability so that corrosion ceases above pH 11.5.

The effect of pH on the corrosion rate and electrode potential of a magnesium AZ10A alloy dissolving anodically in various magnesium bromide electrolytes is shown in Fig. 5 (19). The corrosion rate decreases approximately linearly with increasing electrolyte pH over the range of 6.3 to 8.1 pH units and, at pH's greater than 8.1, approaches a constant value, corresponding to an anode efficiency of 63%. In the weakly acidic solutions the potential varies very slightly with pH, while in the basic pH range the anodic potential falls rapidly with increasing pH and decreasing bromide ion concentration.

These results have been explained in terms of a MgO film on the anode surface, which is more easily penetrable at low pH values because the OH^- ion concentration is too low to maintain an effective oxide film. Thus, at low pH values, high corrosion rates and high anode potentials are observed. At high pH values the OH^- ion concentration controls the precipitation of the Mg^{++} ions produced at the anode, which according to Robinson (16) are precipitated so close to the anode as to stifle the anodic reaction. This results in lower potentials, a decrease in local corrosion, and excessive polarization of the anode.

In an intermediate pH range precipitation of $Mg(OH)_2$ occurs at a sufficient distance from the active anode areas to permit the anodes to function normally. It is in this pH range that other properties

Table III. Electrode potentials of Mg, Al, and Zn in typical electrolytes (potentials referred to a standard hydrogen electrode) [Akimov and Clark (33)]

Metal	3% NaCl		0.1N HCl		0.1N HNO_3		0.1N NaOH	
	1 min	rubbing	1 min	rubbing	1 min	rubbing	1 min	rubbing
Mg	1.418	1.500	1.622	1.596	1.270	1.220	1.086	1.484
Al	0.577	1.221	0.493	0.916	0.320	0.804	1.403	1.386
Zn	0.772	0.818	0.769	0.752	0.688	0.643	1.126	1.123

of the electrolyte, such as the anion present, exert a greater influence over the local corrosion rate and the anode potential.

The effect of the anion present in an electrolyte is often of great importance in dealing with anodes having a protective film. For Al in a solution containing 0.001M K_2CrO_4 and various potassium salts, it was found that small ions show the highest penetration of the oxide film, the order of penetration being Cl^-, Br^-, I^-, F^-, $SO_4^=$, NO_3^-, and $PO_4^{\equiv}$ (31). Evans points out that these differences may be connected not only with size but with solubility and diffusivity as well. What this means in terms of corrosion is seen by the corrosion measurements of Akimov and Glulskova (32) of Al in solutions of NaCl, Na_2SO_4, and $NaNO_3$. Measurements were made over the *p*H range of 0 to 14, and the *p*H being adjusted with NaOH or the acid according to the anion present. In the strongly acid and strongly alkaline regions the rate of corrosion was of the same order, but in neutral or acid solutions the rate of corrosion in the presence of chloride ions was as much as one thousand times greater than in the presence of the sulfate ion.

With metals coated with a protective film, such as Mg and Al, more anodic potentials may be produced by ions which can easily penetrate through this protective film. The fact that aluminum chloride has proved to be the most satisfactory electrolyte for aluminum-manganese dioxide cells (8) is no doubt due to the ability of the chloride ion to penetrate the oxide film and activate the electrode. However, because of their high penetrating power, chlorides are not acceptable for use in conjunction with Mg anodes, and a magnesium bromide electrolyte is used instead.

From an examination of the data in Table II, it is seen that variations in the *p*H of the solution have a pronounced effect on the magnitude of the electrode potential. For the Zn electrode which behaves reversibly except at very high current densities (3), these variations generally follow the Nernst equation. For Al and Mg the influence of *p*H on the electrode potential is essentially due to its effect on the oxide film. Thus, the potential of Al is most anodic in electrolytes of high *p*H in which the oxide film is soluble, but the rate of corrosion is excessive since Al owes its stability in electrolyte to its oxide film.

The influence of protective films on the electrode potentials of Mg and Al is illustrated in Table III (33). Measurements were made by first determining the electrode potentials of the metals in a conventional manner and then during a continuous cleaning of the surface by means of a carborundum rod, which removed much of the original protective film. It is evident that protective films are preserved or formed on metals only when the electrolytes have appropriate characteristics. Thus, a good protecting film is preserved on Al immersed in solutions of NaCl, HCl, and HNO_3, while the film dissolves in NaOH. On the other hand, good protecting films are formed on Mg in NaOH.

Effect of Anode Composition

When hydrogen evolution is the controlling factor in the rate of attack on a metal anode, the effect of low hydrogen overvoltage impurities are important. They produce cathodes from which hydrogen can be evolved rapidly without too much shift in anode potential, so that the conditions for continued corrosion are favorable. The effect of such impurities on the attack of Zn and Al in acid solution is described by Evans (34) while the work of Hannawalt and his co-workers (35) stresses the importance of certain impurities and alloy metals on the corrosion characteristics of Mg alloys in aqueous salt solutions.

For this reason, high-purity Zn (with respect to low hydrogen overvoltage metals) is used in the various zinc-alkaline and Leclanché dry cells. In the case of Mg, although the potential of pure commercial Mg is about 0.04-0.10 v more anodic than the Mg-Al and Mg-Al-Zn alloys, it has been found to be a less efficient anode material than the high-purity alloys (19). It is for this reason that the Mg anodes

Table IV. Electrode potentials* of Al-Zn alloys in various solutions (potentials referred to a standard hydrogen electrode) [Mears and Brown (14)]

Metal	1.0M NaCl	St'd Na_2SO_4	1.0M HCl	1.0M NaOH	1.0M Na_2CO_3	1.0M Na_3PO_4	St'd $Ca(OH)_2$	St'd $CaCO_3$	St'd $CaSO_4$
Al (2S)	0.51	0.16	0.54	1.13	1.01	0.98	1.20	0.70	0.43
Al with 1% Zn (72S)	0.62	0.42	0.68	1.22	1.20	1.19	1.23	0.65	0.36
Al with 5% Zn	0.70	0.48	0.74	1.24	1.16	1.20	1.23	0.71	0.48
Al with 10% Zn	0.71	0.32	0.78	1.24	1.18	1.19	1.24	0.64	0.50
Al with 15% Zn	0.68	0.28	0.78	1.21	1.19	1.15	1.20	0.53	0.46

* Potentials originally reported were referred to a 0.1N calomel electrode. They are here corrected to the standard hydrogen electrode scale without making correction for the liquid junction potential.

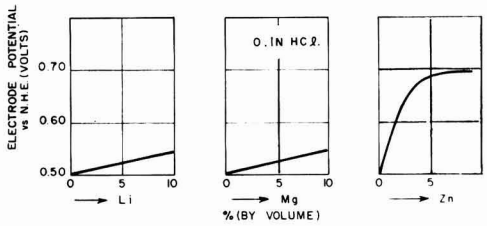

Fig. 6. Electrode potentials of the solid solutions Al-Li, Al-Mg, and Al-Zn. [Akimov and Clark (37)].

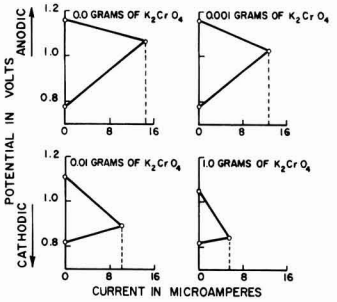

Fig. 7. Effect of concentrations of chromate on local cells on Al in 10% NaCl solution. [Mears and Brown (39)].

used in dry cells have been alloys such as AZ31 and AZ10, the former containing principally 3% Al and 1% Zn, while the latter consists of 1% Al and about 0.5% Zn. The effect of the various alloying ingredients on the anode efficiency of Mg has been reported in detail by Robinson (16). Essentially, the addition of Al permits the removal of the major cathodic impurity, Fe, by precipitation with Mn, while the addition of Zn results in better corrosion distribution and more uniform anode consumption. The latter effect is quite important, for a galvanic anode may operate quite efficiently, but, unless the corrosion is distributed uniformly, segregation losses may be so large as to make operating efficiency a matter of minor concern (36). Recently, it has been found (6) that the addition of small amounts of Ca to the Mg-Al-Zn alloys aids greatly in minimizing "delayed action."

Aluminum dry cells have been fabricated (8) using an Alclad anode which contains an Al 3S alloy on the outside and a 1% Zn-Al alloy on the inside. The effect of Zn is to increase the potential by about 0.1 v. The outer part of the Alclad anode is less anodic than the inner part and serves to prevent pin-hole perforations during normal cell service life and storage. The effect on the electrode potential of alloying Zn to Al has been studied by Mears and Brown (14). They measured the potentials of a series of Al-Zn alloys in various electrolytes and found that in alkaline solutions the potential of Al is high and is not raised greatly by the addition of Zn. However, from the data in Table IV, it is seen that in neutral solutions the addition of Zn raises the potential of Al, and in neutral solutions containing chlorides, the potentials of the Al-Zn alloys approach those of Zn. It was also found by Mears and Brown that, for equal quantities of current supplied by electrodes of such alloys, the Al-base alloys generally lost less than one-third as much weight as did the Zn. Therefore, from the standpoint of metal consumed, the Al-base alloys appear definitely superior to Zn.

Akimov and Clark (37) have made an extensive study of the electrode potentials of solid solutions and have classified them into groups according to the relationship between the potential of a solid solution and its composition. The typical group to which a given system of alloys belongs is defined principally by the nature of (*a*) the components and their interaction, (*b*) the solution, and (*c*) the protective film. They also found that no relationship existed between the potential of a component and the effect on potential produced by this component. Figure 6 presents the influence of three components, Li, Mg, and Zn, on the potential of a corresponding solid solution with Al. It is apparent that Zn shifts the potential of the solid solution in the anodic direction the most and Li the least. This effect is in the reverse relation to the potentials of these three metals.

Corrosion Inhibitors

The corrosion of an anode may be represented as consisting of two parts, an anodic reaction [2], and a cathodic reaction [3].

$$M \rightarrow M^{++} + 2e^- \qquad [2]$$

$$2H^+ + 2e^- \rightarrow H_2 \qquad [3]$$

As long as no external current is present to accept or supply electrons, the two reactions must occur at the same rate. Thus the problem of finding corrosion inhibitors which can retard the corrosion reaction may be accomplished by inhibiting either reaction [2] or [3].

In a dry cell it is desirable that the corrosion of the anode be inhibited by altering the cathodic reaction and not the anodic one, which is necessary for the production of electrical energy in the cell. For example, although organic compounds such as furfural and quinaldine were found to be effective in retarding the corrosion of Zn in dry cell electrolytes, dry cells made with them did not have the expected increase in shelf-life or electrical output (38). The inhibitors either reacted with the paste wall of the cell and decreased its strength or formed a high-resistant film on the Zn. In the latter case, these compounds probably form an insoluble precipitate over the entire surface of the Zn, which stifles not only the undesirable corrosion reaction but also the cell discharge reaction.

The use of soluble chromates, which function as anodic inhibitors, in the electrolyte has proved beneficial for cells during storage. However, they apparently become ineffective when current is drawn from the cell. For Zn the presence of $K_2Cr_2O_7$ in the electrolyte probably passivates the Zn with a very thin chemically resistant film, which, however, breaks down rapidly when current is drawn from the cell. According to Mears and Brown (39) the inhibiting action of sodium chromate on the corrosion of Al in NaCl solution is due to the polarization of local anodes. Chromate functions as an in-

hibitor because it increases anodic polarization in spite of the fact that it decreases cathodic polarization. The latter effect, which is illustrated by the polarization curves in Fig. 7, is to be expected because of the oxidizing properties of the chromate ion.

For Al dry cells which have an aluminum chloride electrolyte, ammonium and alkali chromate inhibitors are used. With potassium chromate a 1-sec delayed action is found, while the Al anode shows no delay with an ammonium chromate inhibitor (8). In general, the concentration of chromate required for protection becomes greater at high chloride concentrations than at low ones and becomes greater still if the temperature is raised (40).

In Mg dry cells, a lithium chromate inhibitor is used in the electrolyte and a small reservoir of an insoluble chromate e.g., barium chromate, is incorporated in the cathode mix to furnish additional soluble chromate as it is used up at the anode. For Mg the lowest chromate concentration which will give adequate corrosion protection is preferred, since delayed action increases with increasing chromate concentration. However, care must be taken since anodic inhibitors like the chromates are dangerous inhibitors when not added to the electrolyte in sufficient quantities. The reason for this is that the area undergoing anodic attack is greatly cut down. If corrosion velocity is controlled exclusively by the anodic reaction, then the anodic attack is cut down in the same ratio, and the intensity of corrosion remains the same. If, however, the velocity is controlled even in part by the cathodic reaction, the corrosion rate will be diminished to a less extent than the corroded area, and the intensity of the attack will be increased (41). In dry cells this localized corrosion causes perforation of the anode can, resulting in loss of electrolyte by leakage and evaporation.

On the other hand, cathodic inhibitors such as mercury are safe in general, as they decrease the total corrosion rate without causing the anodic area to become smaller. For Zn, amalgamation produces an electrochemical couple in which Zn is the anode, but the activation overpotential of hydrogen on mercury is so high as to inhibit the cathodic reaction [3], and thus the corrosion reaction is greatly curtailed. The quantities of mercury than can be used effectively are very limited, seldom exceeding 0.25% because of the embrittlement and loss of strength of the amalgamated metal (1).

For Mg and Al, amalgamation changes both the hydrogen overvoltage and the anodic polarization for the active metal dissolution. The high potentials observed with amalgamated Al and Mg anodes are attributed to the partial removal of the oxide film by amalgamation. For Al this results in a greatly increased rate of corrosion and is therefore undesirable; however, results in this laboratory for Mg dry cells show that the effect of mercurous salts in the electrolyte may be beneficial, especially at low current drains. The use of mercury has a further advantage in that it reduces cell impedance by its interference with the protective oxide coating.

The shelf life of a cell can be considerably increased by storage below ordinary temperatures. The main reasons for this are the lower rates of the corrosion reactions and the increased hydrogen activation overpotential which are associated with decreased temperature. For example, assuming the temperature coefficient of hydrogen activation overpotential at a mercury cathode to be −2.5 mv/°C, Potter (42) calculates that for an amalgamated Zn anode, decreasing the temperature from 40° to 9°C should decrease the current density at the mercury cathode approximately 4.5 times. Thus the shelf life of a cell should be at least 4.5 times as great at 9° as at 40°C. This is in agreement with experimental results.

Cathode Performance

The advantage to the use of a particular anode-electrolyte combination often lies in the effect of the electrolyte on cathode performance. An example of this is illustrated by the coulometric data in Fig. 8 for an electrolytically prepared manganese dioxide.[3] In the more acidic aluminum chloride electrolyte the MnO_2 operates at a potential 0.4-0.5 v higher than in the NH_4Cl-$ZnCl_2$ electrolyte and gives twice the ampere-minute capacity to an end voltage of +0.25 v. This capacity corresponds to a theoretical two-electron change per molecule of MnO_2, indicating that reduction takes place in accordance with the following equation:

$$MnO_2 + 4H^+ + 2e^- = Mn^{++} + 2H_2O \qquad [4]$$

It is also seen that the gain in anode potential derived from the use of a strongly alkaline electrolyte with Zn is offset by the lower operating potential of MnO_2 in this electrolyte. Assuming an end voltage of −0.40 v[4] for MnO_2, the ampere-minute capacity

[3] 85% manganese dioxide.

[4] The potential of Zn is approximately 0.75 v in acidic electrolyte and 1.3 v in strongly basic electrolyte, so that to allow for end voltages of 0.90 v in actual dry cells, half-cell end-potentials of +0.25 and −0.40 v are taken.

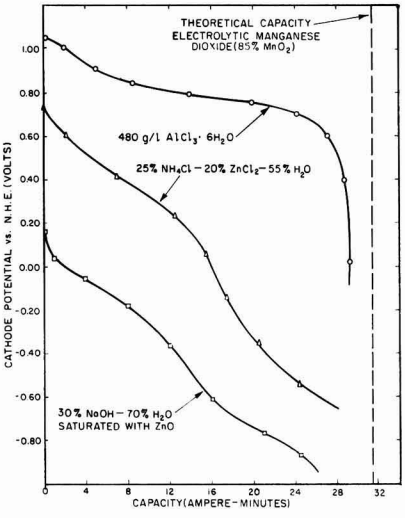

Fig. 8. Effect of electrolyte on the performance characteristics of an electrolytic MnO_2 cathode material.

obtained corresponds to a one-electron change per molecule of MnO_2 in accordance with the following equation:

$$2MnO_2 + H_2O + 2e^- = Mn_2O_3 + 2OH^- \quad [5]$$

It is interesting to note that, under these conditions of discharge, comparable capacities are obtained from MnO_2 in the NaOH and NH_4Cl-$ZnCl_2$ electrolytes. For the use of cathode materials such as mercuric oxide and cupric oxide, however, strongly alkaline electrolytes are necessary because of the solubility of these oxides in acidic solutions.

Conclusions

On the basis of watt-hour capacity per gram, Al and Mg are more attractive anode materials than Zn. The important progress which has been made in the development of Mg dry cells indicates the potential advantages of this anode. However, there are several problems associated with the use of Mg. These are: cost, "delayed action," high impedance, and loss in cell capacity on light intermittent tests. These problems are gradually being solved, and it is predicted that Mg dry cells will achieve commercial significance in the near future. For Al dry cells more research is needed to improve the performance on intermittent tests, as well as to ascertain the shelf life characteristics.

Acknowledgments

The author wishes to express his appreciation to G. S. Lozier and C. K. Morehouse for their helpful suggestions.

Manuscript received Nov. 3, 1958. This paper was prepared for delivery before the Ottawa Meeting. Sept. 28-Oct. 2, 1958.

Any discussion of this paper will appear in a Discussion Section to be published in the December 1959 JOURNAL.

REFERENCES

1. G. W. Heise and N. C. Cahoon, *This Journal*, **99**, 179C (1952).
2. W. S. Herbert, *ibid.*, **99**, 190C (1952).
3. E. A. Schumacher and G. W. Heise, *ibid.*, **99**, 191C (1952).
4. J. M. Booe, *ibid.*, **99**, 197C (1952).
5. P. L. Howard, *ibid.*, **99**, 200C (1952).
6. R. C. Kirk, P. F. George, and A. B. Fry, *ibid.*, **99**, 323 (1952).
7. C. K. Morehouse and R. Glicksman, *ibid.*, **105**, 306 (1958).
8. J. J. Stokes, Jr., Paper presented at ECS Meeting, Pittsburgh, Oct. 10, 1955.
9. E. Willihnganz, *This Journal*, **99**, 234C (1952).
10. U. B. Thomas, *ibid.*, **99**, 238C (1952).
11. G. B. Ellis, H. Mandel, and D. Linden, *ibid.*, **99**, 250C (1952).
12. S. Eidenshon, *ibid.*, **99**, 252C (1952).
13. W. M. Latimer, "Oxidation Potentials," Prentice-Hall, Inc., New York (1952).
14. R. B. Mears and C. D. Brown, *Corrosion*, **1**, 113 (1945).
15. E. Yeager, Abstracts of Papers presented at a Joint Symposium of the Battery and Theoretical Divisions of the ECS, Cleveland, Oct. 1-4, 1956.
16. H. A. Robinson, *Trans. Electrochem. Soc.*, **90**, 485 (1946).
17. A. B. Garrett, Proceedings Tenth Annual Battery Research and Development Conference, p. 4, Power Sources Div., Signal Corps Eng. Labs., Fort Monmouth, N. J.
18. E. C. Potter, "Electrochemistry," p. 370, The Macmillan Co., New York (1956).
19. R. Glicksman, *This Journal*, **106**, 83 (1959).
20. W. O. Kroenig and V. N. Uspenskaja, *Korrosion U. Metallschutz*, **11**, 10 (1935).
21. B. Roald and W. Beck, *This Journal*, **98**, 277 (1951).
22. M. A. Streicher, *J. (and Trans.) Electrochem. Soc.*, **93**, 285 (1948).
23. M. E. Straumanis and Y. N. Wang, *This Journal*, **102**, 304 (1955).
24. R. Glicksman and C. K. Morehouse, *ibid.*, **102**, 273 (1955).
25. R. Kirk, Private communication.
26. G. S. Lozier and C. K. Morehouse, Unpublished work.
27. B. E. Roetheli, G. L. Cox, and W. B. Littreal, *Met. Alloys*, **3**, 73 (1932).
28. N. C. Cahoon, *Trans. Electrochem. Soc.*, **92**, 159 (1947).
29. U. R. Evans, "Metallic Corrosion, Passivity and Protection," p. 213, Longmans, Green and Co., New York (1946).
30. G. V. Akimov and I. L. Rozenfeld, *Doklady Akad. Nauk. S.S.S.R.*, **44**, 211 (1944); *C. A.*, **39**, 0424 (1945).
31. Ref. 29, p. 23.
32. G. V. Akimov and A. J. Glulskova, *Compt. Rend. Acad. Sci. U.R.S.S.*, **49**, 194 (1945); *C. A.*, **40**, 4335 (1946).
33. G. W. Akimov and G. B. Clark, *Trans. Faraday Soc.*, **43**, 679 (1947).
34. Ref. 29, Chap. V.
35. J. D. Hanawalt, C. E. Nelson, and J. A. Peloubet, *Trans. Am. Inst. Mining Met. Eng.*, **147**, 273 (1943).
36. H. A. Robinson, *Corrosion*, **2**, 199 (1946).
37. G. W. Akimov and G. B. Clark, *Trans. Faraday Soc.*, **43**, 685 (1947).
38. C. K. Morehouse, W. J. Hamer, and G. W. Vinal, *J. Research Natl. Bur. Standards*, **40**, 151 (1948).
39. R. B. Mears and R. H. Brown, *This Journal*, **97**, 75 (1950).
40. B. E. Roetheli and G. L. Cox, *Ind. Eng. Chem.*, **23**, 1084 (1931).
41. Ref. 29, p. 545.
42. Ref. 18, p. 365.

Technical Feature

Current Problems in the Production of Magnetic Ceramics

George Economos

Laboratory for Insulation Research, Massachusetts Institute of Technology, Cambridge, Massachusetts

ABSTRACT

Reproducibility of the electrical and magnetic properties while adhering to mechanical tolerances is still the main difficulty in quantity production of magnetic ceramics. This problem is discussed from a developmental viewpoint with suggestions for improving present methods. Older production schemes are compared with newer techniques.

The field of magnetic ceramics has grown by tremendous proportions since its rebirth after World War II. The work by Hilpert (1), Kato (2), Snoek (3), and others came at a time when the need for such materials was not urgent. Television and other high-frequency applications have now brought these materials to the forefront. One of the major difficulties, as in any young industry, is the lack of sufficiently trained technical personnel and of the required "skill in the art." The picture is improving, however, because of the trend in modern ceramics toward a more scientific basis.

The innumerable variables involved in the fabrication of a useful ceramic, from the basic raw materials to a finished electronic component, make it a formidable task to acquire the needed control throughout the production scheme. It must be borne in mind that it is necessary not only to make a product with the proper electrical and magnetic properties, but one that will also meet rather rigid mechanical tolerances of size and shape. The complexity of the problem requires the pooling of many talents. Co-ordination of research and production activities is necessary to utilize the varied skills of the electrical engineer, physicist, chemist, mechanical engineer, ceramist, chemical engineer, crystallographer, and the industrial engineer. There is still considerable inertia in the industry which keeps it from discarding some of the older methods. Present difficulties show the necessity for employing newer and even novel techniques without regard to what is the generally accepted practice.

Achieving reproducibility in the final sintered product necessitates accurate control in all the processing steps. By giving a generalized picture of the various factors involved in the manufacture of these shapes, a critical evaluation of the techniques can be made with suggestions for possible substitutions.

Processing Techniques

General Survey

The "compounding" of ferrites, magnetoplumbites, and other magnetic ceramic materials involves the reaction between various components in the solid state to yield a homogeneous product suitable for forming and sintering into a dense form. A simple outline of the steps required is given below:

1. *Powder preparation*: analysis of the raw materials, weighing the components, mixing, and calcining (reacting).
2. *Ceramic body preparation*: grinding of the calcine, addition of the lubricant and binder, granulating, and drying.
3. *Specimen preparation*: molding, firing (sintering), and testing. An examination of the various steps will give a better insight into the types of problems encountered.

Raw Materials

The choice of raw materials is important in the successful preparation of a homogeneous compound. Extensive information has been compiled on the reactivity between solids (4), which shows that the nature of the reacting species often governs the rate of compound formation. With but few exceptions, the commercial practice is to react the constituent oxides at high temperatures. High-purity oxides are available at relatively low cost, but in using them the manufacturer can defeat one of the prime requisites for high reactivity: high surface area and high-defect crystal structure. Precipitation techniques (5) are available to achieve this end, but they are not competitive at present and find only limited use.

The oxides generally used are products of some decomposition process. Why use the oxide when the original material offers better opportunity for mixing and reacting? This possibility has not been exploited to any extent, even though it could be competitive with the oxides. The result would be a reduction of the calcining temperature and the production of a more friable material for easy grinding.

Comminution Processes

Grinding of the calcine is a major operation in the ceramic body preparation. Ball mills have long been

used, but not until recently have newer type units found extensive use. The attritor and the vibratory ball mill cut the time to a fraction of that needed before. The micronizer (high velocity interparticle impact by air or steam pressure) has not received extensive attention in this field. This unit could accomplish in the dry state what the other methods do in the wet, thus eliminating the expensive dewatering step usually needed.

Dry-Press Body Preparation

The effort expended in the preparation of the dry-press body pays dividends in the behavior of the materials at the presses and in the sintering steps. Lubricants and binders (one or both) are added to the milled material to impart the needed flow properties to this nonplastic material. This is generally done by blending-in these additives in the semi-plastic state. For a given amount of additive, the pressing behavior is related to how well each particle is coated by the blending process. The most obvious method is one in which the additives can be dispersed effectively and brought into intimate contact with the solid material. Emulsions are highly dispersed systems, but a molecular or ionic solution is even more so. Using lubricants and binders which are soluble in a liquid medium permits wetting of the solid particles and, on subsequent evaporation of the solvent, a film of the solute remains on the particles.

A word of caution is needed here. In the evaporation of the solvent, it is essential that agitation be continued until evaporation is complete, otherwise capillary activity brings the solute to the surface and destroys the highly dispersed condition originally present. The most effective method to achieve this is to dry the wet mix quickly in as highly divided state as possible. Spray drying effectively accomplishes this. This unit eliminates the dewatering and the binder-blending step after grinding and produces granules suitable for pressing.

Pressing

Most of the problems in the pressing operation usually can be traced to flaws in one of the previous processes. Proper die design and loading, pressing pressure and speed, and other mechanical effects must be worked out for each shape and composition. Most of the difficulties at this stage of manufacture will be overcome by the proper choice of ceramic body preparation.

Firing

The firing or sintering of the molded shapes can be regarded as a three-stage process: (*a*) heating, (*b*) soaking, and (*c*) cooling. The initial stage of the heating period is the careful removal of the additives by evaporation or by burning. The evaporation is not affected by the furnace atmosphere, whereas the burning requires oxidizing conditions. Obviously, the choice of binder will be critical because the mode of its removal can be detrimental to the body, depending on the composition and its behavior in various furnace atmospheres. This initial portion of the heating cycle progresses at a slower rate compared to the rate which follows, generally at more than 300°C.

The proper regulation of the remainder of the heating cycle, the soak period, and the cooling rate will be governed by the size and shape of the pieces, and by the desired end properties. The usual difficulties, such as cracks due to too rapid burn-out and specimen shattering caused by sharp thermal gradients during heating and cooling, must be overcome. Added to this is concern for the oxygen stoichiometry in the fired piece. No set rule can be made on the optimum firing conditions, because these vary widely with the type of material and its properties. Each composition must be treated separately. Tunnel kilns are most efficient for large volume production; however, for special heating and cooling cycles and atmospheres, batch-type kilns are more suitable.

Comparison of Some Production Schemes

Having considered some of the more critical processes and their associated problems, a few typical production flow sheets may be examined and compared. The "dry-process" (Fig. 1) is the most common (5). Two dewatering steps are required: the first is essential for proper mixing of the component oxides, but the second can be eliminated by using the micronizer. This speeds the process and, in the long run, reduces costs. Figure 2 shows the flow sheet of a "wet-process" plant (5) in which the second wet milling could be replaced also. Use of decomposable salts of the cations can be incorporated at the beginning of both these arrangements.

Highly specialized schemes, such as that using the atomizing burner (6) (Fig. 3), cut down the re-

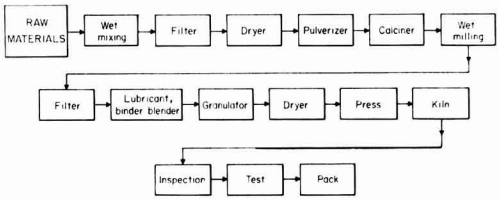

Fig. 1. "Dry-process" flow sheet

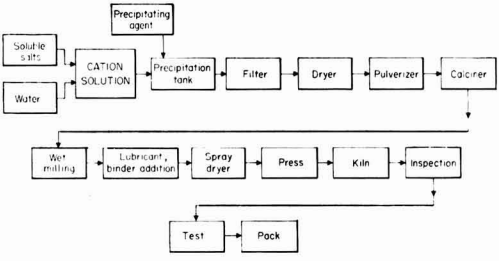

Fig. 2. "Wet-process" flow sheet

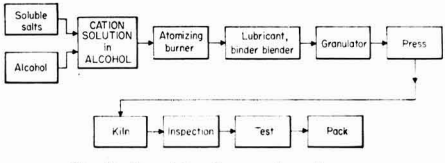

Fig. 3. Atomizing-burner flow sheet

quired number of steps. At present, this technique has found application only where its high cost and low yield can be justified by the special properties of the end product, such as microwave ferrites.

Not to be omitted from this discussion is the present status of the evaluation of the final product. Numerous organizations (Institute of Radio Engineers, Metal Powders Association, American Society for Testing Materials, etc.) have committees which draw up evaluation parameters with acceptable test procedures for these materials. Such factors as shape, size, application, measurement technique, and so on, enter into the picture. Because of the multitude of these factors, no one choice can be expected to win wide acceptance. Some tentative agreements have been reached, but much has to be done before the field is properly covered.

Manuscript received Dec. 1, 1958. This paper was prepared for delivery before the New York Meeting, April 27-May 1, 1958. Work was sponsored by the U. S. Office of Naval Research, the Army Signal Corps, and the Air Force.

Any discussion of this paper will appear in a Discussion Section to be published in the December 1959 JOURNAL.

REFERENCES

1. S. Hilpert, *Ber.*, **42**, 2248 (1909).
2. Y. Kato and T. Takie, *Trans. Am. Electrochem. Soc.*, **57**, 297 (1930).
3. J. L. Snoek, *Philips Tech. Rev.*, **8**, 353 (1946).
4. J. A. Hedwall, "Einführung in die Festkörperchemie," F. Vieweg und Sohn, Braunschweig (1952).
5. G. Economos, *J. Am. Ceram. Soc.*, **38**, 241 (1955).
6. J. F. Wenckus and W. Z. Leavitt, "Preparation of Ferrites by the Atomizing Burner Technique," Papers of the Conference on Magnetism and Magnetic Materials, American Institute of Electrical Engineers, Publication T-91, p. 526 (1957).

Brief Communications

The Ubiquity of Localized Corrosion

R. B. Mears

Applied Research Laboratory, United States Steel Corporation, Monroeville, Pennsylvania

For decades localized corrosion has appeared to be considered more mysterious than uniform or general attack. Many papers have been written pointing out various causes of localized attack, usually implying that uniform corrosion was the expected form and that localized corrosion was exceptional and, therefore, required a special explanation. It now appears that this viewpoint should be changed. Localized corrosion is the form to be expected and uniform corrosion is the form that requires explanation.

Even single crystals of very pure metals contain crystal imperfections. Read and Shockley (1) proposed that localized corrosion (etch pits) occurred at edge dislocations in high-purity aluminum. They stated, "We have proposed that each etch pit originates at a dislocation, where the free energy of the stressed material is somewhat higher than elsewhere; the pit then grows to large size so that it can be observed optically."

Later Vogel, Pfann, Corey, and Thomas (2) showed that etch pits developed in high-purity single crystals of germanium and that the measured spacing of these pits correlated well with spacings predicted from x-ray diffraction. They concluded that individual etch pits are nucleated by single dislocations, with the pit being formed where the dislocation singular line intersects the surface.

Etch pits at dislocation sites have been observed on several other high-purity metals, including iron (3, 4). It now appears that all commercially available metals contain dislocations and that, under appropriate conditions, localized corrosion (etch pits) can develop at dislocation sites. The reason generally given for the formation of these etch pits is still essentially that proposed by Read and Shockley as quoted earlier. However, it should be pointed out that very specific corroding solutions (etchants) must be used to reveal dislocation sites. The majority of corrodents do not give this type of attack. Thus, although following Read and Shockley, we can explain satisfactorily the localized corrosion that occurs in carefully selected etchants, it is much more difficult to explain the more commonly encountered uniform attack.

To complicate matters still further Boswell (3, 4) has pointed out in a private communication that, with the specific etchant he used to reveal dislocation sites in high-purity iron, it was necessary to have between 0.001% and 0.01% carbon in the iron or proper resolution of the dislocation sites did not occur. [Apparently impurity segregation is also necessary for etch pits to be revealed in high-purity Al (5) and Zn (6).]

Metallographers have known for years that grain boundaries, different crystal faces, and dissimilar phases in polycrystalline metals or alloys can be corroded or etched at different rates. Use is made of this "localized corrosion" in examining polished metallic specimens under the microscope.

All metals or alloys used in quantity by industry are polycrystalline and contain dissimilar phases to a greater or lesser extent. The expectation would be, therefore, that all metallic articles when exposed to corrodents would develop localized corrosion.

In addition to these "micro scale" causes for localized corrosion, there are numerous other factors that operate over longer distances. Some 18 of these have been described in an earlier publication (7). All these "macro scale" factors can also cause localized attack under service conditions.

Once localized attack starts at any given area, electrochemical effects usually operate to sustain it at that area and to make it less probable that adjacent areas will corrode.

Thus, the wonder is that all corrosion is not localized and the time has come to develop experimentally supported explanations for the mechanism of uniform corrosion.

Manuscript received Dec. 9, 1958.

Any discussion of this paper will appear in a Discussion Section to be published in the December 1959 JOURNAL.

REFERENCES

1. W. T. Read and W. Shockley, *Phys. Rev.*, **78**, 278 (1950). Based on experimental work by P. Lacombe, Report of Conference on Strength of Solids, Physical Society, London, p. 91 (1948).
2. F. L. Vogel, W. G. Pfann, H. E. Corey, and E. E. Thomas, *Phys. Rev.*, **90**, 489 (1953).
3. F. W. C. Boswell, *Am. Soc. Testing Materials, Proc.*, **57**, 521 (1957).
4. F. W. C. Boswell, *Metal Progr.*, **72**, 92 (1957).
5. G. Wyon and P. Lacombe, *Rept. Conf. on Defects in Crystalline Solids, London*, 1954 (Publ. 1955).
6. J. J. Gilman, *Trans. Am. Inst. Mining Met. Engrs.*, **206**, 998 (1956).
7. R. B. Mears and R. H. Brown, *Ind. & Eng. Chem.*, **33**, 1001 (1941).

The Role of the Metal-Ion Concentration Cell in Crevice Corrosion

G. J. Schafer and P. K. Foster

Department of Scientific and Industrial Research, Dominion Laboratory, Wellington, New Zealand

In a number of publications (1-4) two crevice corrosion mechanisms have been postulated to account for the two types of attack observed, viz., attack inside the crevice, and attack at the crevice mouth. While it is acknowledged that the former is due to differential aeration, the latter has been attributed to "corroding currents which arise in those regions where there is a difference in the metal-ion concentration" (2) and to "metal ion concentration cell action" (1). Although La Que's experiment (5) can be explained on the basis of ionic concentrations, as also can the moto-electric effect as discussed by Evans (6), we wish to point out that these were not long-term experiments and the metal ion concentration cell mechanism is not a valid explanation of steady-state corrosion at the crevice mouth.

It is implied [in Fig. 9-1 of Ref. (2)] that metal ions produced at the crevice mouth (by corrosion) accumulate in the crevice but are removed (by convection and/or diffusion) from the body of the solution adjacent to the crevice mouth. Then since metal in contact with a strong solution of its ions is more noble than the same metal in contact with a weak solution of its ions (other things being equal), the ion-depleted crevice mouth is anodic to the rest of the crevice and corrodes, while the ion-rich crevice is more noble and acts as cathode.

The faults in this mechanism as an explanation of steady-state corrosion are as follows:

1. The anode is the only source of metal ions, and the mechanism requires that the concentration of ions be lower at the source than elsewhere. In a steady-state corroding system, the metal ion concentration must be a maximum at the source as can be seen by considering the heat analogy.

2. No cathodic reaction is suggested. The name "metal-ion concentration cell" (1, 2) also implies cathodic deposition of the metal. Such a cell is not self-sustaining, and current will flow only until the metal ion concentration is equalized throughout the system.

3. The only other obvious cathodic reaction is oxygen depolarization. This is supported, and the differential metal-ion concentration mechanism is vitiated, by the fact that crevice mouth attack is stopped by removal of dissolved oxygen (2). (More generally there is no reason why crevice corrosion should not occur with other cathodic depolarizers as well.)

In view of the above arguments, we suggest that the metal-ion concentration cell cannot be a cause of crevice corrosion, and that crevice mouth attack is a special case of differential aeration. Such variables as electrolyte resistance, polarization curve slopes, dissolved oxygen concentration, and crevice width would be expected to influence the corrosion pattern in a crevice, and there is no obvious reason as yet why, in special cases, the corrosion should not be limited to the mouth of the crevice.

Manuscript received Dec. 29, 1958.

Any discussion of this paper will appear in a Discussion Section to be published in the December 1959 JOURNAL.

REFERENCES

1. E. H. Wyche, L. R. Voigt, and F. L. La Que, *Trans. Electrochem. Soc.*, **89**, 149 (1946).
2. "Corrosion and Wear Handbook for Water-cooled Reactors," chap. 9, McGraw Hill Book Co. (1957).
3. R. V. Jelinek, *Chem. Eng.*, **61**, 125 (1958).
4. "The Mechanism of Corrosion and Its Prevention," A. F. Dunbar and H. A. Stephens, "Corrosion—A Symposium," University of Melbourne, 1956.
5. Discussion on paper by Wyche, Voigt, and La Que *Trans. Electrochem. Soc.*, **89**, 165 (1946).
6. U. R. Evans, "Metallic Corrosion, Passivity, and Protection," p. 232, Arnold & Co. (1937).

H. H. Uhlig Appointed Publication Committee Chairman

Herbert H. Uhlig was appointed Chairman of the Publication Committee by the Board of Directors of The Electrochemical Society in a vote by mail ballot in November 1958. Dr. Uhlig has been active in the affairs of the Society since 1937. He has been a Vice-President and was President in 1955-1956. He also has served as Chairman of the Corrosion Division, of which he was one of the founders, and the Theoretical Electrochemistry Division, as well as of the Gordon Corrosion Conferences and the Intersociety Corrosion Committee. He has written many papers in the field and is Editor of the "Corrosion Handbook," sponsored by the Corrosion Division of the Society. He is past Editor of the JOURNAL.

Fabian Bachrach

Herbert H. Uhlig

Dr. Uhlig received his B.S. degree in chemistry from Brown University in 1929 and his Ph.D. degree in physical chemistry from Massachusetts Institute of Technology in 1932. After a year of electrochemical research at Rockefeller Institute for Medical Research with Dr. Duncan A. MacInnes, he entered the employ of Lever Brothers Co. in Cambridge as research chemist, and later assistant chief chemist. The strong attractions of the fundamental sciences led to an appointment in 1936 as research associate in the Corrosion Lab. at M.I.T. At this time, contributions were made to the theory of pitting in stainless steels and the nature of passivity in corrosion-resistant alloys. In 1940, he joined the staff of the Research Lab. of the General Electric Co. at Schenectady, and returned to M.I.T. in 1946 where at present he is professor of metallurgy, in charge of the Corrosion Laboratory.

Dr. Uhlig's principal researches have been in corrosion and electrochemistry, with particular emphasis on fundamental studies of passivity, metal surface properties, and the chemical and metallurgical behavior of corrosion-resistant alloys.

He is a member of the Advisory Committee for the Prevention of Deterioration Center of the National Research Council, and of the Corrosion Research Council established in 1955 by the Engineering Foundation to promote and sponsor fundamental research in corrosion and to stimulate the training of men in this field. He helped organize, and served as the Society's representative at, the first International Conference on Passivity held at Jugenheim, West Germany, in September 1957. In March 1951 he received the Willis R. Whitney Award of the National Association of Corrosion Engineers for contributions to the science of corrosion. He is a member of the American Academy of Arts and Sciences, and of several other scientific and technical societies.

1959 Gordon Research Conferences

The 1959 Gordon Research Conferences on Corrosion, Physical Metallurgy, and Chemistry and Physics of Metals will be held from June 15 to September 4 at Colby Junior College, New London, N. H.; New Hampton School, New Hampton, N. H.; and Kimball Union Academy, Meriden, N. H.

Attendance at the Conferences is by application. Individuals interested in attending the Conferences are requested to send their applications to the Director at least two months prior to date of the Conference. *All applications must be submitted on the standard application form which can be obtained by writing to the office of the Director.*

Requests for attendance at the Conferences, or for additional information, should be addressed to W. George Parks, Director, Dept. of Chemistry, University of Rhode Island, Kingston, R. I. From June 15 to September 4, mail should be addressed to Colby Junior College, New London, N. H.

Corrosion

July 20-24, 1959
Colby Junior College
New London, N. H.

P. M. Aziz, Chairman
Milton Stern, Vice-Chairman

July 20

The Nature of Metal Surfaces as Revealed by Friction and Wear Measurements

H. A. Liebhafsky, Moderator
E. H. Freitag—Modern Methods of Studying the Structure of Solid Surfaces
A. J. Haltner—Solid Lubricants
L. E. St. Pierre—Reactions at Metal Surfaces
E. H. Freitag—The Friction and Deformation of Metallic Surfaces

July 21

Kinetics of Oxidation Processes

J. E. Draley, Moderator
F. W. Young—Oxide Nuclei and Dislocations

M. Cohen—The Oxidation of Iron at Low Temperatures
A. J. Rosenberg—Oxidation of Intermetallic Compounds
R. K. Hart—Investigation of Metals in Aqueous Environments with Particular Reference to Aluminum

July 22

Kinetics of Electrode Processes
M. Stern, Moderator
B. E. Conway—Corrosion of the Nickel-Nickel Oxide Electrode; Kinetics and Mechanism of Self-Discharge and Oxygen Evolution
J. O'M. Bockris—The Mechanism of the Dissolution of Metals
D. A. Vermilyea—The Role of Crystal Defects in Corrosion Processes

July 23

Inhibition of Corrosion Reactions
N. Hackerman, Moderator
A. C. Makrides—The Inhibition of Metal Dissolution
M. Stern—The Effect of Metal Alloying on Inhibition Processes
J. E. O. Mayne—The Inhibition of the Corrosion of Iron in Neutral and Alkaline Solutions
E. A. Blomgren—The Adsorption of Aromatic Amines on Metal Surfaces

July 24

Inhibition of Corrosion Reactions (cont'd)

General discussion of current theories of inhibition.

Chemistry and Physics of Metals

August 17-21, 1959
Kimball Union Academy
Meriden, N. H.
G. H. Vineyard, Chairman
Warren DeSorbo, Vice-Chairman

August 17

P. M. Marcus—Specific Heats and Vibration Spectra
J. A. Morrison—Present Status of Low-Temperature Specific Heat Measurements
J. A. Krumhansl—Microscopic Theories of Elasticity as Tested in Anisotropic Substances—Graphite

August 18

B. N. Brockhouse—Inelastic Neutron Scattering—Chalk River Results
H. Palevsky—Inelastic Neutron Scattering—Brookhaven Results
M. Lax—Long-Range Forces and Lattice Vibrations in Germanium
E. Burstein—Infrared Observations and Lattice Dynamics

August 19

H. B. Rosenstock—Far Infrared Lattice Absorption
W. C. Overton, Jr.—Vibration Spectra and Critical Points in F.C.C. Lattices with Nearest and Next Nearest Neighbor Interactions
J. Delaunay—Vibration Spectrum Calculations
A. Maradudin—Effects of Defects and Disorder on Vibrational Properties of Crystals

August 20

G. Leibfried—Recent Developments in the Theory of Anharmonic Effects
M. Blackman—Thermal Expansion
R. W. Morse—Acoustic Observations of Phonon-Electron Interactions

August 21

C. Herring—Phonon-Drag Effects
M. Walsh—Spin-Phonon Interactions

Division News

Electrodeposition Division

Papers are being solicited for the October Meeting of the Division in Columbus. In addition to the general sessions, the Division is planning two symposia: 1—Electrode Reactions in Nonaqueous Media, and 2—Electro- and Chemical-Polishing.

The symposium on Electrode Reactions in Nonaqueous Media is being sponsored jointly by the Electrodeposition, Theoretical Electrochemistry, and Electro-Organic Divisions of the Society. It is hoped that this symposium will stimulate interest and activity in this neglected field of electrochemistry. The papers submitted may deal with the study of the mechanism of electrode reactions, identification of the products formed, current efficiencies, polarization, and heat effects. Questions concerning the symposium should be addressed to Abner Brenner, National Bureau of Standards, Washington 25, D. C.

All inquiries and suggestions concerning the Electro- and Chemical-Polishing symposium should be sent to Don Foulke, Hanson-Van Winkle-Munning Co., Matawan, N. J. Papers are wanted on such topics as: 1—Electro- and chemical-polishing of metals and semiconductors, 2—Metallographic techniques, 3—Adhesion and corrosion of electroplated coatings on electro- or chemically-polished surfaces, and 4—Theoretical studies—role of mass transfer, polarization, etc. It is not necessary that the papers be concerned only with theoretical matters. However, they should not be simply a review of operating conditions or a compilation of formulas.

Triplicate copies of abstracts *(not exceeding 75 words in length)* must be received at Society Headquarters, 1860 Broadway, New York 23, N. Y., *by June 1, 1959* to be considered for the Fall Meeting.

Section News

Indianapolis Section

The Indianapolis Local Section of the Society holds its second technical meeting of the current season on February 16, 1959, at Butler University in Indianapolis. The speaker was Dr. J. W. Faust from the Westinghouse Research Labs. His subject was "Semiconductor Devices—Problems and Fabrication."

Dr. Faust first presented a review of the basic characteristics of semiconductor materials and the various types of devices which have been made from them. Then he discussed the different types of semiconductors, both elemental and intermetallic, and related their inherent functional parameters to their use in different applications and in different environments. Following this, he covered the different techniques which are currently being employed in material purification, crystal growth, doping, cutting, surface preparation and assembly, etc. Dr. Faust emphasized the particularly critical nature of certain operations and the over-all importance of cleanliness during all phases of the manufacturing process. After the formal presentation, he answered various questions relative to certain specific techniques and problems.

During the accompanying business meeting, the Chairman, Mr. Leon Deer, announced his resignation—resulting from a change in position and relocation in Huntsville, Ala. This action was accepted, with the regrets and best wishes of the Indianapolis Section members. The following Nominating Committee also was appointed to prepare a slate of officers for the next year to be voted on at the next meeting: J. M. Booe, Chairman; B. R. Haueisen, R. E. Ralston.

T. C. O'Nan,
Secretary-Treasurer

Philadelphia Section

At the January 7 meeting of the Philadelphia Section, the speaker was Dr. Ralph Roberts, research coordinator for chemistry in the Office of Naval Research. Dr. Roberts presented an impressive review of the research projects sponsored by the ONR.

The speaker at the March 4 meeting was Mr. Wayne McRae, director of research for Ionics, Inc. Mr.

McRae discussed the properties and applications of ion exchange membranes.

The following have been re-elected officers of the Section for another term:

Chairman—G. W. Bodamer, Rohm & Haas Co., 5000 Richmond St., Philadelphia 37, Pa.

Vice-Chairman—K. A. Krieger, Harrison Lab. of Chemistry, University of Pennsylvania, Philadelphia 4, Pa.

Treasurer—A. A. Ware, Ware Bros. Co., 317 No. Broad St., Philadelphia 7, Pa.

Secretary—H. C. Mandell, Jr., Pennsalt Chemicals Corp., P. O. Box 4388, Philadelphia 18, Pa.

G. W. Bodamer, *Chairman*

New Members

In March 1959, the following were elected to membership in The Electrochemical Society by the Admissions Committee:

Active Members Sponsored by a Sustaining Member

T. S. Dewoody, Jr., Diamond Alkali Co., Painesville, Ohio (Industrial Electrolytic)

V. V. Hughey, Basic, Inc., P. O. Fostoria, Ohio (Electrodeposition)

Michael Rivera, Vacuum Equipment Div., New York Airbrake Co., 1325 Admiral Wilson Blvd., Camden, N. J. (Electrothermics & Metallurgy)

A. G. Stanley, Philco Corp., C & Tioga Sts., Philadelphia 34, Pa. (Electronics)

Active Members

Antonios Antoniou, National Research Council; Mail add: 442 Talbot St., Ottawa 2, Ont., Canada (Corrosion, Theoretical Electrochemistry)

P. M. Aziz, Aluminium Labs., Ltd., P. O. Box 84, Kingston, Ont., Canada (Corrosion)

J. P. Badger, Electric Auto-Lite Co.; Mail add: Elmwood Park, Genoa, Ohio (Battery)

Adolph Blicher, RCA Semiconductor Div., Rt. 202, Somerville, N. J. (Electronics)

E. C. Brown, Canadian Industries Ltd., P. O. Box 10, Montreal, Que., Canada (Theoretical Electrochemistry)

J. C. Bovankovich, Monsanto Chemical Co., R. & E. Div., 800 No. Lindbergh Blvd., St. Louis 66, Mo. (Corrosion)

Leo Bulvanoski, American Smelting & Refining Co.; Mail add: 1001 Main St., Fords, N. J. (Electrodeposition)

B. D. Cahan, Electric Storage Battery Co.; Mail add: 7310 Shelbourne St., Philadelphia 11, Pa. (Battery, Theoretical Electrochemistry)

Pei-Yen Chao, Hughes Aircraft Co.; Mail add: 4038 W. 105 St., Inglewood 2, Calif. (Electrothermics & Metallurgy)

E. J. Clugston, Jr., Reading Metals Refining Corp.; Mail add: Box 1111, Reading, Pa. (Electrodeposition)

John Dasher, Central Research Lab., Crucible Steel Co. of America, 234 Atwood St., Pittsburgh 13, Pa. (Electrodeposition, Electrothermics & Metallurgy, Industrial Electrolytic)

V. R. Erdelyi, Hughes Products, P. O. Box 90427, Los Angeles 45, Calif. (Electronics, Electrothermics & Metallurgy)

D. S. Glass, National Carbon Co.; Mail add: 2083 Newark Ave., Westfield, N. J. (Industrial Electrolytic)

C. V. Gopal Rao, Paranthon Chemicals Corp., Jaffna District, Ceylon, India (Corrosion, Industrial Electrolytic)

W. O. Groves, Monsanto Chemical Co., R. & E. Div., Dayton 7, Ohio (Electronics)

Gerard Hallie, Bibliotheek, Staatsmijnen in Limburg, Centraal Laboratorium, Geleen, The Netherlands (Corrosion, Electro-Organic)

R. D. Hancock, Pacific Semiconductors, Inc.; Mail add: 646 Via Miradores, Redondo Beach, Calif. (Electronics)

R. W. Hardy, Battelle Memorial Institute, 505 King Ave., Columbus, Ohio (Electrodeposition, Electro-Organic)

Vladimir Hospadaruk, International Nickel Co.; Mail add: 28 Meadowbrook Village, Plainfield, N. J. (Corrosion, Electrodeposition, Theoretical Electrochemistry)

R. W. Hull, General Instrument Corp.; Mail add: 107 Calberson Rd., Basking Ridge, N. J. (Electronics)

R. C. Jacobsen, Hydro-Electric Power Commission of Ontario; Mail add: 32 Lowther Ave., Toronto 5, Ont., Canada (Corrosion)

W. C. M. Klein, American Smelting & Refining Co.; Mail add: 145 Thomas St., Menlo Park, N. J. (Electrodeposition, Electronics, Industrial Electrolytic)

M. H. Little, Gould-National Batteries, 2630 University Ave. S. E., Minneapolis 14, Minn. (Battery)

Ludwig Luft, General Electric Co.; Mail add: 10044 Princeton Rd., Cincinnati 41, Ohio (Corrosion, Electrodeposition, Electrothermics & Metallurgy, Theoretical Electrochemistry)

D. C. MacWilliams, Dow Chemical Co.; Mail add: 1101 Baldwin St., Midland, Mich. (Electro-Organic, Theoretical Electrochemistry)

H. F. Mataré, 1 Emilian Strasse, Nurnberg, Germany (Electronics)

B. J. Patton, International Resistance Co.; Mail add: 528 Inman Terrace, Willow Grove, Pa. (Electronics)

C. S. Peet, Jr., Battelle Memorial Institute; Mail add: 3074 Hamilton Ave., Columbus 24, Ohio (Electronics)

J. F. Pruett, Varian Associates, Inc., 611 Hansen Way, Palo Alto, Calif. (Electrodeposition)

J. W. Rhyne, Jr., American Machine & Foundry Co.; Mail add: 1210 Moore Dr., Raleigh, N. C. (Battery)

J. A. Roberts, Texas Instruments Inc.; Mail add: 612 Northill, Richardson, Texas (Electronics)

H. U. Ross, Dept. of Metallurgical Engineering, University of Toronto, Toronto 5, Ont., Canada (Electrothermics & Metallurgy)

R. L. E. Seifert, Dept. of Chemistry, Indiana University, Bloomington, Ind. (Theoretical Electrochemistry)

J. T. Smith, Catalyst Research Corp.; Mail add: 1305 Warwick Dr., Lutherville, Md. (Battery)

P. H. Stephens, Texas Instruments Ltd.; Mail add: 29 Silverdale St., Kempston, Bedford, England (Electronics)

Victor Van Vinckenroy, Centre D'Information du Cobalt; Mail add: 35 Rue des Colonies, Brussels 4, Belgium (Battery, Electrodeposition)

J. E. Wright, Radio Corp. of America; Mail add: 95 Anderson St., Raritan, N. J. (Electronics)

J. C. Zemlin, Trancoa Chemical Corp.; Mail add: 23 Granger Ave., Reading, Mass. (Industrial Electrolytic)

By action of the Board of Directors of the Society, all prospective members must include first year's dues with their applications for membership.

Also, please note that, if sponsors sign the application form itself, processing can be expedited considerably.

Student Associate Member

Walter Zloczower, New York University; Mail add: 114-06 Queens Blvd., Forest Hills 75, N. Y. (Electronics)

Associate Members

E. D. Parent, Jr., Sylvania Electric Products Inc.; Mail add: 25 Prospect Ave., Newtonville 60, Mass. (Electrodeposition)

Harlow Freitag, International Business Machines Corp.; Mail add: 30 Parkwood Blvd., Poughkeepsie, N. Y. (Theoretical Electrochemistry)

Reinstatement to Active Membership

Hamilton Maze, W. H. Maze Co.; Mail add: South Fruit St., Peru, Ill. (Corrosion, Electrodeposition)

Transfer from Associate to Active Membership

R. E. Edgington, Good-All Electric Mfg. Co.; Mail add: 614 Student Dr., Ogallala, Neb. (Electrodeposition, Electronics, Theoretical Electrochemistry)

News Items

Clyde Williams Awarded James Douglas Gold Medal

Dr. Clyde Williams, noted metallurgist and president of Clyde Williams and Co., industrial research and management advisory firm, Columbus, Ohio, is the recipient of the James Douglas Gold Medal of the American Institute of Mining, Metallurgical, and Petroleum Engineers. Regarded as one of the most distinguished honors in the field of metallurgical science, it was presented to Dr. Williams at the annual national banquet of the AIME in San Francisco on February 18, 1959.

The Medal, established in 1922, bears the name of James Douglas, twice president of the AIME. It "recognizes distinguished achievement in nonferrous metallurgy, including both beneficiation of ores and alloying and utilization of nonferrous metals."

This specific citation goes to Dr. Williams "for outstanding contributions in nonferrous metallurgy particularly through stimulating research and interest in the basic metallurgy and use of both common and less common metals."

New Sustaining Member

The General Physics Research Dept., General Electric Co., Schenectady, N. Y., recently became a Sustaining Member of The Electrochemical Society.

ECS Membership Statistics

The following three tables give breakdown of membership as of Apr. 1, 1959. The Secretary's Office feels that a regular accounting of membership will be very stimulating to membership committee activities. In Table I it should be noted that the totals appearing in the right-hand column are *not* the sums of the figures in that line since members belong to more than one Division and, also, because Sustaining Members are not assigned to Divisions. But the totals listed are the total membership in each Section. In Table I, Sustaining Members have been credited to the various Sections.

Table I. *ECS Membership by Sections and Divisions*

Section	Division: Battery	Corrosion	Electric Insulation	Electrodeposition	Electronics	Electro-Organic	Electrothermics & Met.	Industrial Electrolytic	Theoretical Electrochem.	No Division	Total as of 1/1/59	Total as of 4/1/59	Net Change
Boston	18	27	6	38	64	7	25	14	27	6	151	152	+ 1
Chicago	14	30	3	39	28	9	13	10	22	15	132	125	— 7
Cleveland	53	32	2	51	38	10	30	32	36	14	198	195	— 3
Columbus, Ohio	3	15	0	14	7	2	25	3	8	3	49	53	+ 4
Detroit	11	18	4	49	9	6	8	6	21	18	91	90	— 1
India	8	6	2	18	8	6	8	11	15	3	35	35	0
Indianapolis	11	8	5	13	11	4	6	3	7	2	39	43	+ 4
Midland	9	15	0	5	2	3	7	13	11	1	43	41	— 2
Mohawk-Hudson	4	12	13	7	14	1	8	1	16	4	54	57	+ 3
New York	88	105	26	141	140	31	71	69	103	42	517	516	— 1
Niagara Falls	13	26	1	24	9	5	81	67	31	20	183	182	— 1
Ontario-Quebec	11	26	1	16	7	3	38	27	10	13	82	86	+ 4
Pacific Northwest	5	10	0	8	3	1	10	10	9	10	44	43	— 1
Philadelphia	29	30	4	36	70	10	24	19	50	30	185	191	+ 6
Pittsburgh	3	45	3	25	8	6	41	17	35	9	133	129	— 4
San Francisco	8	13	1	18	18	4	17	20	16	4	71	70	— 1
S. Calif.-Nevada	17	22	3	29	36	5	17	15	27	10	105	113	+ 8
Washington-Baltimore	37	37	7	38	23	3	11	9	33	6	129	130	+ 1
U. S. Non-Section	62	90	12	86	79	43	63	75	114	28	408	401	— 7
Foreign Non-Section	46	63	7	65	37	32	42	60	77	89	262	272	+10
Total as of Jan. 1, 1959	441	638	103	723	621	190	549	486	656	329	2911		
Total as of Apr. 1, 1959	450	630	100	720	631	191	545	481	668	325		2924	
Net Change	+9	—8	—3	—3	+10	+1	—4	—5	+12	—4			

Table II. *ECS Membership by Grade*

	Total as of 1/1/59	Total as of 4/1/59	Net Change
Active	2538	2446	— 92
Faraday (Active)	30	31	+ 1
Deutsche Bunsen Gesellschaft (Active)	15	17	+ 2
Delinquent	70	177	+107
Active Representative Patron Members	10	10	0
Active Representative Sustaining Members	99	103	+ 4
Total Active Members	2762	2784	+ 22
Life	17	17	0
Emeritus	49	49	0
Associate	31	22	— 9
Student	46	46	0
Honorary	6	6	0
Total	2911	2924	+ 13

The figures pertaining to Patron and Sustaining Member Representatives, and Faraday and Deutsche Bunsen Gesellschaft members subscribing to the JOURNAL, have been added to reflect reclassifications and changes in membership status.

Table III. *ECS Patron and Sustaining Membership*

	Total as of 1/1/59	Total as of 4/1/59	Net Change
Patron Member Companies	5	5	0
Sustaining Member Companies	148	151	+ 3

Stoughton Award Presented to Lehigh University Metallurgy Professor

Dr. Joseph F. Libsch, professor of metallurgy at Lehigh University, Bethlehem, Pa., has been named recipient of the Stoughton Award of the Lehigh Valley Chapter of the American Society for Metals. At Lehigh since 1946, he was cited for his contributions to the field of metallurgy. The award is named after Dr. Bradley Stoughton, professor emeritus of metallurgy at Lehigh University, and Past President of The Electrochemical Society.

Dr. Libsch, a native of Rockville, Conn., received the $2000 award from the American Society of Metals for outstanding contributions to the teaching of metallurgy in 1954. He is a graduate of the Massachusetts Institute of Technology. During World War II, he served as captain in the Army Ordnance Dept., assigned to the Springfield Armory for metallurgical research and development.

Symposium on Corrosion of Iron and Tin in Contact

A symposium dealing with the corrosion of iron and tin in contact will be held on Friday, November 6, 1959, at the Southeastern Regional Meeting of the American Chemical Society to be held in Richmond, November 5-7. Papers are now being accepted for presentation at the meeting and will be accepted until August 1.

Papers on such topics as effect of metal ions on the corrosion of iron and tin, polarization curves for iron and tin, oxide films on iron and tin, corrosion inhibition of iron and tin, and the theory of the corrosion of metals in contact would be particularly appropriate topics.

Further information can be obtained from the Chairman of the symposium, Dr. Henry Leidheiser, Jr., Virginia Institute for Scientific Research, 2820 Grove Ave., Richmond 21, Va.

Fourth Annual Appalachian Underground Corrosion Short Course Program Arranged

The program for the Appalachian Underground Corrosion Short Course to be held June 2, 3, and 4, 1959, at West Virginia University, Morgantown, W. Va., has been arranged. There will be 64 classes and field demonstrations covering eight categories as follows: Basic, Intermediate Pipe, Intermediate Cable, Advanced, Water, Coatings, Instruments, and Special.

Basic, June 2-4

Fundamentals of Corrosion
Mud Tub Demonstration
Electrochemical Principles
Fundamental Analysis of Stray Current Corrosion
Electrolysis Currents Related to a Distribution System
Soil Bacterial Corrosion
General Corrosion Control Practices

Intermediate Pipe, June 2-4

Field Practices
Fundamentals of Plant Testing for Underground Corrosion
Construction Practices
Protection of Gas Service Lines in Non-Stray Current Areas
Demonstration of a Theory of Cathodic Protection
Application of Cathodic Protection
Intermediate Analysis of Stray Current Corrosion
Safe Operating Practices Related to Electrical Current Flows upon Natural Gas Pipe Line Structures

Intermediate Cable, June 2-4

Some Fundamentals of Lead Cable Corrosion
Instrumentation and Equipment
Fundamentals of a Corrosion Survey
Interpretation of Survey Data in a Stray Current Area
The Interpretation of Survey Data in the Non-Stray Current Area
Electrolysis Currents Related to a Power Cable System
Corrosion Surveys and Mitigative Measures of Power Cables in Non-Stray Current Areas
Bonding and Grounding (Power) (Intermediate—Cable)

Advanced, June 2-4

Expendable Anodes
Expendable Anode Applications
Pipe Type Cables
Rectifier Installations and Protection
Rectifier Units for Cathodic Protection
Practical Interference Testing
Design and Installation of Cathodic Protection

Water, June 2-4

Corrosion Resistance of Cast Iron Pipe
Carbonate Deposits for Pipe Protection
Water Pipeline—Exterior Corrosion Control
Corrosion and Its Control in Public Water Systems
Elements of Water Transmission Corrosion
Cold Water Corrosion of Copper—Related Problems
Reference Electrodes
Corrosion Problems in the Chemical and Metallurgical Industries

JUST PUBLISHED!

A definitive new work on principles, phenomena, materials . . .

SEMICONDUCTORS

ACS Monograph No. 140
Edited by N. BRUCE HANNAY
Bell Telephone Laboratories
Murray Hill, New Jersey

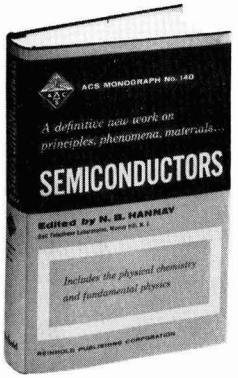

1959, 792 pages, $15.00

Here is an unrivaled, indispensable reference on the fundamental physics and physical chemistry of semiconductors, with detailed analyses of important semiconducting materials. The emphasis throughout is on basic principles and phenomena.

Semiconducting materials are treated individually, with the amount of attention given each material being in direct relation to the degree of understanding of that material which exists.

Each chapter, whether it be on principles, crystal growing, or specific materials is preceded by an introduction placing that chapter in perspective with semiconduction as a whole.

By virtue of its organization, thoroughness and authorship, this work will stand for many years to come as the standard book on semiconductors.

CONTENTS: Semiconductor Principles; Survey of Semiconductor Chemistry; Semiconductor Crystal Growing; Control of Composition in Liquid-Solid Systems; The Chemistry of Some Compound Semiconductors; Defect Interactions in Semiconductors; Diffusion and Precipitation in Germanium and Silicon; Group IV Semiconductors; Other Elemental, and Intermetallic, Semiconductors; Compound Semiconductors; Compounds of the Transition Metals; Organic Semiconductors; Recombination, Trapping and Luminescence; Light Absorption in Semiconductors; Semiconductor Surfaces; Electrochemical Reactions at Interfaces; Bibliography; Index.

Send for your on-approval copy today from—

REINHOLD PUBLISHING CORPORATION

Dept. M-442, 430 Park Avenue
New York 22, N. Y.

Coatings, June 2-4

Asphalt Coatings
The Use of Wax Coating for Protecting Underground Pipe
Plastic Coated Pipe
Hot Applied Tapes
Cold Applied Tapes
Coal Tar Epoxy Coatings
Review of Properties of Coal Tar Coatings
Duties of a Coating Inspector

Instruments, June 2-4

Corrosion Testing Instruments
A New Concept in Recording Voltmeters
Instruments Used in Soil Resistivity Measurements
Electrical Holiday Detectors
Earth Current Meter
Pipe Locators

Special, June 2-4

Polyvinyl Chloride Pipe
Corrosion Resisting Characteristics of Aluminum Alloys
Cathodic Protection of Casings in Gas Storage Wells
Weather Versus Cathodic Protection
Microbiological Corrosion of Underground Structures
A Report on the Effectiveness of Armored Gaskets in Couplings for Cathodic Protection of Gas Distribution Lines
New Coupling Developments to Speed Field Joining and Protection of Pipe
Wrought Iron, Its Production, Properties, and Performance

Field Demonstration, June 4

Soil Resistivity—Survey
Pipe to Soil Potentials—Survey
Surface Potentials—Survey
Line Current Measurements
Magnesium Anode Installation
Cathodic Protection with Rectifier
Other Underground Structures

Fourth International Symposium on Free Radical Stabilization

The Fourth International Symposium on Free Radical Stabilization will be held at the National Bureau of Standards, August 31 to September 2, 1959. In accordance with the theme of the meeting, "Trapped Radicals at Low Temperatures," emphasis will be placed on the properties of solids containing trapped radicals, and the chemical and physical interactions involving trapped radicals at low temperatures.

Activities tentatively scheduled for the first day of the symposium include a discussion of "The Organization and Aims of the NBS Free Radicals Program," a session on "Low Temperature Chemistry," and a banquet in the evening. On the following day, "Methods of Production of Trapped Radicals and Physical Properties of Radical-Trapping Solids" and "Identity and Concentrations of Trapped Radicals" will be discussed. The evening activities will include a round-table discussion of "Future Trends in Free Radical Stabilization." The final session of the symposium, "Interaction of Free Radicals with Solids," will be held the morning of September 2. That afternoon, tours of the laboratories of the Bureau's Free Radicals Program will be conducted.

Although the program of presented papers is for the most part already complete, time has been set aside in the various discussion periods for brief reports. These short communications will be listed in the program, but need not be submitted in manuscript form. Notification of the nature of a proposed communication should be made before August 1.

The Bureau has arranged for accommodations at Dunbarton College, which is located within a few minutes' walking distance of the Bureau. Dormitory facilities at $5.00 (single) or $3.50 (double or multiple) per night are available from August 30 to September 5. As rooms are being assigned at the college in the order of receipt, pre-registration is urged.

Further information can be obtained by writing Dr. A. M. Bass, National Bureau of Standards, Washington 25, D. C.

Carborundum Co. to Build New Pilot Plant at Niagara Falls

The Carborundum Co. will build a new ¾-million-dollar pilot plant for its Research and Development Div. in Niagara Falls, it has been

In electrotyping, plating rotogravure rolls, electroforming, "Plus-4" Copper Anodes cut plating costs

Electrotypers have discovered that, in addition to eliminating the use of bags and diaphragms, they can place "Plus-4" (Phosphorized Copper) Anodes closer to the cathodes to speed up the plating cycle 30% or more with the same power input—and still obtain a smooth deposit. As an alternate, power can be reduced by one third with an equal reduction in resistance and generation of heat to obtain finished electros in the same plating time. This is an important advantage when thermoplastic plates or molds are used and tanks must run no higher than 95 F.

Makers of rotogravure rolls have found that "Plus-4" Anodes provide a much finer, smoother surface for polishing and etching, and retain the quality of the light tones in runs of over one million impressions on a single set of design cylinders.

In addition, they report significant reductions in cost. One publisher found that he produces superior rolls with less labor, and a reduction of 18 to 20% for materials required in the plating process. Another reports he gets a dividend of eight extra rolls for each tank load of "Plus-4" Anodes. And still another has found a 15% saving in over-all costs.

In electroforming operations, "Plus-4" Anodes—by eliminating the most prevalent acid-copper plating difficulties—have made it practical to produce many new products. Their ability to provide a smooth, dense deposit relatively free from growths and blemishes made possible relatively thick shells for molds used in making rubber and plastic articles, and in intricate precision parts for electronic use. Electroformers report operating economies similar to those found in the graphic arts field.

WRITE FOR INFORMATION on how you can obtain a test quantity to supply one tank. Address: The American Brass Company, Waterbury 20, Conn. In Canada: Anaconda American Brass Ltd., New Toronto, Ontario. 59104

ANACONDA®

"PLUS-4"® ANODES Phosphorized Copper

Made by The American Brass Company

announced by General Clinton F. Robinson, president of the company. Nine to twelve months will be required for the construction of the building, procurement and installation of the equipment.

Carborundum's Research and Development Div. is turning out new products which require ultra-high-temperature processing techniques not available at present in the main operating divisions of the company. The new R&D Pilot Plant will provide the special equipment necessary to bring these new products through their R&D development stages to a point where they can be allocated to present divisions for production and sale, or form the basis for new operating divisions of the company.

The pilot plant will be operated by the New Products Branch of the Research and Development Div., headed by Mr. Donald G. Sturges, manager of the branch.

Ammonium Perchlorate Expansion Second for Pennsalt in Four Months

Pennsalt Chemicals Corp., which completed its first ammonium perchlorate plant last October, recently announced approval of plans for a major expansion of the plant at Portland, Ore. The new plant will expand capacity by several thousand tons. Ammonium perchlorate is the most widely used oxidizer for high-energy solid-state missile propellants.

Coincident with this expansion will be a 25% increase in capacity for the adjacent sodium chlorate unit which provides the principal raw material for ammonium perchlorate. Sodium chlorate is also used in pulp bleaching and weed killing. Upon completion, total investment in this expansion will amount to approximately $2,000,000.

Pennsalt Chemicals has been producing sodium chlorate at Portland since 1942. The company's electrolytic process and equipment were designed and developed by Pennsalt chemists and engineers. The unit has been expanded several times to meet growing demands in traditional markets and to supply the needs of the ammonium perchlorate expansions.

In addition to its interest in solid missile fuels, Pennsalt is also active in the propellant field through fluorine, perchloryl fluoride, and other fluorine derivatives, as well as organic nitrogen compounds.

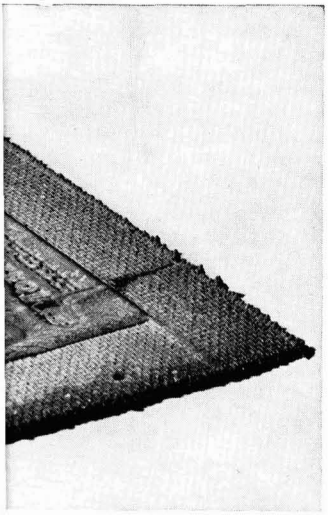

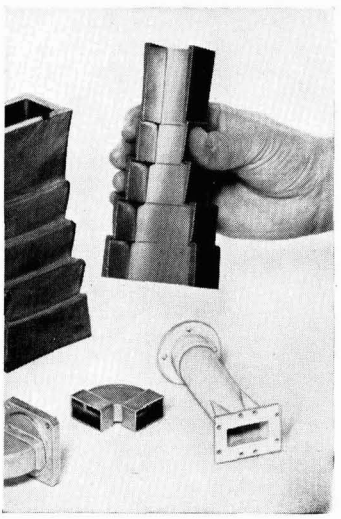

ECS Volumes Available

A set of TRANSACTIONS of The Electrochemical Society from 1924 to 1945, comprising 43 volumes, is available at a reasonable price. Anyone interested in obtaining them should contact Mr. G. D. Mallory, Technical Adviser, Dept. of Trade and Commerce, Ottawa, Ont., Canada.

Volumes 79 (1941) through 94 (1948) of the TRANSACTIONS of The Electrochemical Society also are available for purchase through Miss Betsey Packard, Librarian, International Minerals & Chemical Corp., P. O. Box 2537, Mulberry, Fla.

Book Reviews

Semiconductor Abstracts, Volume IV (1956), compiled by Battelle Memorial Institute. Edited by E. Paskell. Sponsored by The Electrochemical Society; published by John Wiley & Sons, Inc., New York City, 1959. 456 pages; $12.00.

With this volume, The Electrochemical Society continues its ambitious program of providing, for those who work in the general area of semiconductor science, a convenient and comprehensive set of abstracts of papers in their field. This volume contains over 1400 abstracts, two-thirds of which cover literature originally appearing in 1956, with most of the rest coming from the preceding year. Many of the entries are taken verbatim from the abstract of the original article, or, in the case of short communications at meetings of professional societies, from the society bulletins. Author

Lepel

HIGH FREQUENCY INDUCTION HEATING UNITS

BRAZING SOLDERING BOMBARDING MELTING HARDENING ANNEALING

The Lepel line of induction heating equipment represents the most advanced thought in the field of electronics as well as the most practical and efficient source of heat yet developed for numerous industrial applications.
If you are interested in induction heating you are invited to send samples of the work with specifications. Our engineers will process and return the completed job with full data and recommendations without any cost or obligations.

FLOATING ZONE FIXTURE FOR METAL REFINING AND CRYSTAL GROWING

A new floating zone fixture for the production of ultra-high purity metals and semi-conductor materials. Purification or crystal growing is achieved by traversing a narrow molten zone along the length of the process bar while it is being supported vertically in vacuum or inert gas. Designed primarily for production purposes, Model HCP also provides great flexibility for laboratory studies.

Features

- A smooth, positive mechanical drive system with continuously variable up, down and rotational speeds, all independently controlled.
- An arrangement to rapidly center the process bar within a straight walled quartz tube supported between gas-tight, water-cooled end plates. Placement of the quartz tube is rather simple and adapters can be used to accomodate larger diameter tubes for larger process bars.
- Continuous water cooling for the outside of the quartz tube during operation.
- Assembly and dis-assemby of this system including removal of the completed process bar is simple and rapid.

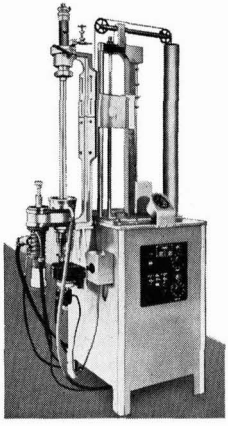

Model HCP

Electronic Tube Generators from 1 kw to 100 kw.
Spark Gap Converters from 2 kw to 30 kw.

WRITE FOR THE NEW LEPEL CATALOG . . . 36 illustrated pages packed with valuable information.

All Lepel equipment is certified to comply with the requirements of the Federal Communications Commission.

LEPEL HIGH FREQUENCY LABORATORIES, INC.
55th STREET and 37th AVENUE, WOODSIDE 77, NEW YORK CITY, N. Y.

and subject indexes are provided. The coverage in terms of subject matter is satisfactorily wide, running all the way from the measurement of transistor parameters to band theory. Judging from the particular fields with the literature of which I am fairly familiar, the coverage seems to be pretty good—better, as one might expect, for the American literature than for the West European, and better for that than for the Russian. The accuracy is good but not perfect.

Perhaps my only serious comment is that the volume has appeared rather too late for its full usefulness to be served. A delay of three years seems excessive for an abstract service in a fast-moving field. Against this, one must set the convenience of the arrangement of entries, which makes this volume handier to use (for someone working in the field) than, for example, "Physics Abstracts."

C. G. B. Garrett

Soviet Research in Fused Salts—1956, Part II. Chemistry Collection Series. Published by Consultants Bureau, Inc., New York City, 1959. 268 pages; $20.00.

This set of translations of 19 articles which appeared in Russian journals during 1956 is the second half of the second set of papers of this sort. (The first set dealt with papers appearing between 1949 and 1955.) The translation seems to be smooth with few awkward or ambiguous phrases. The printing and binding are of barely acceptable quality, considering the substantial price.

As in the previous sets, the papers deal primarily with technology. Thus, there are six on electrowinning (aluminum, magnesium, and thorium), three on corrosion of metals, four on slags, and six on assorted physical properties. The research itself is workmanlike and straightforward—techniques and equipment tend to be simple but adequate. Russian re-

Notice to Members and Subscribers
(Re Changes of Address)

To insure receipt of each issue of the JOURNAL, please be sure to give us your old address, as well as your new one, when you move. Our records are filed by states and cities, not by individual names. The Post Office does not forward magazines.

search in this field compares fairly well with its American equivalent of 1956. However, nothing comparable to the high-quality academic papers appearing here in increasing numbers is yet evident in Russian publications.

Benson R. Sundheim

Atoms for Power: United States Policy in Atomic Energy Development. Edited by P. C. Jessup. Published by The American Assembly, Columbia University, New York City, Dec. 1957. 159 pages; $1.00.

It is usually the fate of conference reports to be filed and forgotten, and this present publication from Columbia's American Assembly will probably be no exception. This, of course, would be a great pity, for the participants in this Assembly conference—held October 17-20, 1957—included some of the world's foremost authorities on atomic energy. Anyone wanting a concise yet reasonably detailed account of where the world stands today on atomic power (for nothing significant has changed since these papers were delivered) should read this 159-page publication.

It opens with an admirable historical review of the U. S. atomic energy effort, by Robert Oppenheimer, written as only he could write it. Speaking of the unending stream of rosy forecasts made about the atomic future, he says quite frankly ". . . most of the warm and glowing pronouncements about the hopes of atomic energy would have read more true had they been written with 'science and technology' replacing 'atomic energy,' or with a more modest 'atomic energy as a part of science and technology.'"

Walter H. Zinn, one of the world's top reactor experts, summarizes the AEC's reactor program and compares it with that of the United Kingdom. He suggests that the U. S. has paid inadequate attention to natural (i.e., unenriched) uranium reactors and to gas-cooled reactors—the types the British are pushing vigorously.

Klaus Knorr, professor of economics at Princeton, analyzes U. S. foreign policy and the atom and finds that President Eisenhower's "Atoms for Peace" speech of 1953 ". . . promised, however vaguely, more than the U. S. was prepared to deliver" and that ". . . *Atoms for Peace* as a global program, unrelated to real needs and abilities, was perhaps a rash venture."

Sir John Cockcroft, the eminent British physicist, provides an illuminating review of what his country is doing and how very much it hopes to achieve within less than two decades. The U. K. expects nuclear power to reach cost parity with coal power by about 1963 and to be about 30% cheaper than coal by 1970. By 1975, Britain may be getting half of all its power from the atom.

Finally, Max Kohnstamm, who headed the committee that drafted *A Target for Euratom,* describes the exigencies that make atomic power important to the six nations that constitute Euratom and the General Common Market. Euratom's ambitious target: 15 million kw of nuclear capacity by 1967 (vs. 6 million-or-so for Britain). It was the sense of the American Assembly participants that the U. S. should do everything in its power to help Euratom reach its goal.

Francis Bello

JOURNAL ELECTROCHEMICAL SOCIETY

Wanted to Buy.
Back sets, volumes, and issues of this JOURNAL and TRANSACTIONS.
Especially volumes 1, 3 and from volume 60 to date.
We pay good prices.
Buy also Technical and Scientific Periodicals.
E. O. ASHLEY, 27 E. 21 St., New York 10, N. Y.

Employment Situations

Positions Available

Engineers (Aeronautical, Electrical, Electronic, Industrial, General, Mechanical, and Power Plant), **Electronic Scientists, Metallurgists, Physicists, Technologists**—Vacancies exist for professional personnel in the above positions. Starting salaries range from $4490 per annum to $10,130 per annum. The Naval Air Material Center is currently engaged in an extensive program of aeronautical research, development, experimentation, and test operations for the advancement of Naval aviation. Experimental work also is being conducted in the guided missile field. Personnel are needed for work on projects involving modification, overhauling, and testing of aeronautical equipment, materials, accessories, power plants, launching and arresting devices, and for modification and structural testing of aircraft. Also, for work involving the basic design of catapults, launchers, arresting gear and their component parts; test and development work at shore stations and on board U. S. Navy ships; evaluation of new equipment and establishment of performance parameters, and applied research on the many problems relevant to this field.

Interested persons should file an Application for Federal Employment, Standard Form 57, with the Industrial Relations Dept., Naval Air Material Center, Naval Base, Philadelphia 12, Pa. Applications may be obtained from the above address or information as to where they are available may be obtained from any first or second class post office.

Chemists, Physicists, Metallurgists—New R&D Lab. needs qualified personnel to handle projects in electrochemical, lead acid, and related areas. Latest equipment—fine working conditions—fringe benefits. Must relocate to Twin Cities. Send résumés to: T. W. Murphy, Personnel Dept., Gould-National Batteries, Inc., E. 1326 First National Bank Bldg., St. Paul 1, Minn.

Executive Research and Development—Pioneer manufacturer of precious metals salts and solutions for industrial and decorative electroplating requires electrochemist for staff research and development. Opportunity to work with recognized authorities in this field, and for advancement to key position for mature, responsible applicant. Ph.D. preferred, M.S. with good practical experience acceptable. Salary commensurate with qualifications. Location: Metropolitan New York area. Send complete résumé indicating past earnings to *Box No. A-280,* c/o The Electrochemical Society, Inc., 1860 Broadway, New York 23, N. Y.

Advertiser's Index

The Electrochemical Society

Patron Members

Aluminum Co. of Canada, Ltd.,
Montreal, Que., Canada
International Nickel Co., Inc.,
New York, N. Y.
Olin Mathieson Chemical Corp.,
Niagara Falls, N. Y.
Industrial Chemicals Div., Research
and Development Dept.
Union Carbide Corp.
Divisions:
Union Carbide Metals,
New York, N. Y.
National Carbon Co., New York, N. Y.
Westinghouse Electric Corp., Pittsburgh, Pa.

Sustaining Members

Air Reduction Co., Inc.,
New York, N. Y.
Ajax Electro Metallurgical Corp.,
Philadelphia, Pa.
Allen-Bradley Co., Milwaukee, Wis.
Allied Chemical & Dye Corp.
General Chemical Div., Morristown, N. J.
Solvay Process Div., Syracuse, N. Y.
(3 memberships)
Allied Research Products, Inc.,
Detroit, Mich.
Alloy Steel Products Co., Inc., Linden, N. J.
Aluminum Co. of America,
New Kensington, Pa.
American Machine & Foundry Co.,
Raleigh, N. C.
American Metal Co., Ltd.,
New York, N. Y.
American Potash & Chemical Corp.,
Los Angeles, Calif. (2 memberships)
American Zinc Co. of Illinois,
East St. Louis, Ill.
American Zinc, Lead & Smelting Co.,
St. Louis, Mo.
American Zinc Oxide Co., Columbus, Ohio
M. Ames Chemical Works, Inc.,
Glens Falls, N. Y.
Auto City Plating Company Foundation,
Detroit, Mich.
Basic Inc., Maple Grove, Ohio
Bell Telephone Laboratories, Inc.,
New York, N. Y. (2 memberships)
Bethlehem Steel Co., Bethlehem, Pa.
(2 memberships)
Boeing Airplane Co., Seattle, Wash.
Burgess Battery Co., Freeport, Ill.
(4 memberships)
C & D Batteries, Inc., Conshohocken, Pa.
Canadian Industries Ltd., Montreal, Que.,
Canada
Carborundum Co., Niagara Falls, N. Y.
Catalyst Research Corp., Baltimore, Md.
Chrysler Corp., Detroit, Mich.
Ciba Pharmaceutical Products, Inc., Summit,
N. J.
Columbian Carbon Co., New York, N. Y.
Columbia-Southern Chemical Corp.,
Pittsburgh, Pa.
Consolidated Mining & Smelting Co. of
Canada, Ltd., Trail, B. C., Canada
(2 memberships)
Continental Can Co., Inc., Chicago, Ill.
Cooper Metallurgical Associates, Cleveland,
Ohio
Corning Glass Works, Corning, N. Y.
Crane Co., Chicago, Ill.
Diamond Alkali Co., Painesville, Ohio
(2 memberships)
Dow Chemical Co., Midland, Mich.
Wilbur B. Driver Co., Newark, N. J.
(2 memberships)
E. I. du Pont de Nemours & Co., Inc.,
Wilmington, Del.
Eagle-Picher Co., Chemical Div., Joplin, Mo.
Eastman Kodak Co., Rochester, N. Y.
Electric Auto-Lite Co., Toledo, Ohio
Electric Storage Battery Co.,
Philadelphia, Pa.
Englehard Industries, Inc., Newark, N. J.
(2 memberships)
The Eppley Laboratory, Inc., Newport, R. I.
(2 memberships)
Erie Resistor Corp., Erie, Pa.
Fairchild Semiconductor Corp., Palo Alto,
Calif.
Federal Telecommunication Laboratories,
Nutley, N. J.
Food Machinery & Chemical Corp.
Becco Chemical Div., Buffalo, N. Y.
Westvaco Chlor-Alkali Div., South
Charleston, W. Va.
Ford Motor Co., Dearborn, Mich.
General Electric Co., Schenectady, N. Y.
Chemistry & Chemical Engineering
Component, General Engineering
Laboratory
Chemistry Research Dept.

(Sustaining Members cont'd)

General Electric Co. (cont'd)
General Physics Research Dept.
Metallurgy & Ceramics Research Dept.
General Motors Corp.
Brown-Lipe-Chapin Div., Syracuse, N. Y. (2 memberships)
Guide Lamp Div., Anderson, Ind.
Research Laboratories Div., Detroit, Mich.
General Transistor Corp., Jamaica, N. Y.
Gillette Safety Razor Co., Boston, Mass.
Gould-National Batteries, Inc., Depew, N. Y.
Grace Electronic Chemicals, Inc., Baltimore, Md.
Great Lakes Carbon Corp., New York, N. Y.
Hanson-Van Winkle-Munning Co., Matawan, N. J. (3 memberships)
Harshaw Chemical Co., Cleveland, Ohio (2 memberships)
Hercules Powder Co., Wilmington, Del.
Hill Cross Co., Inc., New York, N. Y.
Hoffman Electronics Corp., Evanston, Ill.
Hooker Chemical Corp., Niagara Falls, N. Y. (3 memberships)
Houdaille Industries, Inc., Detroit, Mich.
Hughes Aircraft Co., Culver City, Calif.
International Business Machines Corp., Poughkeepsie, N. Y.
International Minerals & Chemical Corp., Chicago, Ill.
Jones & Laughlin Steel Corp., Pittsburgh, Pa.
K. W. Battery Co., Skokie, Ill.
Kaiser Aluminum & Chemical Corp.
Chemical Research Dept., Permanente, Calif.
Div. of Metallurgical Research, Spokane, Wash.
Kennecott Copper Corp., New York, N. Y.
Keokuk Electro-Metals Co., Keokuk, Iowa
Libbey-Owens-Ford Glass Co., Toledo, Ohio
P. R. Mallory & Co., Indianapolis, Ind.
McGean Chemical Co., Cleveland, Ohio
Merck & Co., Inc., Rahway, N. J.
Metal & Thermit Corp., Detroit, Mich.
Metals and Controls Corp., Attleboro, Mass.
Minnesota Mining & Manufacturing Co., St. Paul, Minn.
Monsanto Chemical Co., St. Louis, Mo.
Motorola, Inc., Chicago, Ill.
National Cash Register Co., Dayton, Ohio
National Lead Co., New York, N. Y.
National Research Corp., Cambridge, Mass.
National Steel Corp., Weirton, W. Va.
New York Air Brake Co., Vacuum Equipment Div., Camden, N. J.
Northern Electric Co., Montreal, Que., Canada
Norton Co., Worcester, Mass.
Olin Mathieson Chemical Corp., Niagara Falls, N. Y.
High Energy Fuels Organization (2 memberships)
Pennsalt Chemicals Corp., Philadelphia, Pa.
Phelps Dodge Refining Corp., Maspeth, N. Y.
Philco Corp., Philadelphia, Pa.
Philips Laboratories, Inc., Irvington-on-Hudson, N. Y.
Pittsburgh Metallurgical Co., Inc., Niagara Falls, N. Y.
Poor & Co., Promat Div., Waukegan, Ill.
Potash Co. of America, Carlsbad, N. Mex.
Radio Corp. of America, Harrison, N. J.
Ray-O-Vac Co., Madison, Wis.
Raytheon Manufacturing Co., Waltham, Mass.
Reynolds Metals Co., Richmond, Va. (2 memberships)
Schering Corporation, Bloomfield, N. J.
Shawinigan Chemicals Ltd., Montreal, Que., Canada
Speer Carbon Co.
International Graphite & Electrode Div., St. Marys, Pa. (2 memberships)
Sprague Electric Co., North Adams, Mass.
Stackpole Carbon Co., St. Marys, Pa.
Stauffer Chemical Co., New York, N. Y.
Sumner Chemical Co., Div. of Miles Laboratories, Inc., Elkhart, Ind.
Sylvania Electric Products Inc., Bayside, N. Y. (2 memberships)
Tennessee Products & Chemical Corp., Nashville, Tenn.
Texas Instruments, Inc., Dallas, Texas
Titanium Metals Corp. of America, Henderson, Nev.
Udylite Corp., Detroit, Mich. (4 memberships)
Universal-Cyclops Steel Corp., Bridgeville, Pa.
Upjohn Co., Kalamazoo, Mich.
Victor Chemical Works, Chicago, Ill.
Western Electric Co., Inc., Chicago, Ill.
Wyandotte Chemicals Corp., Wyandotte, Mich.
Yardney Electric Corp., New York, N. Y.

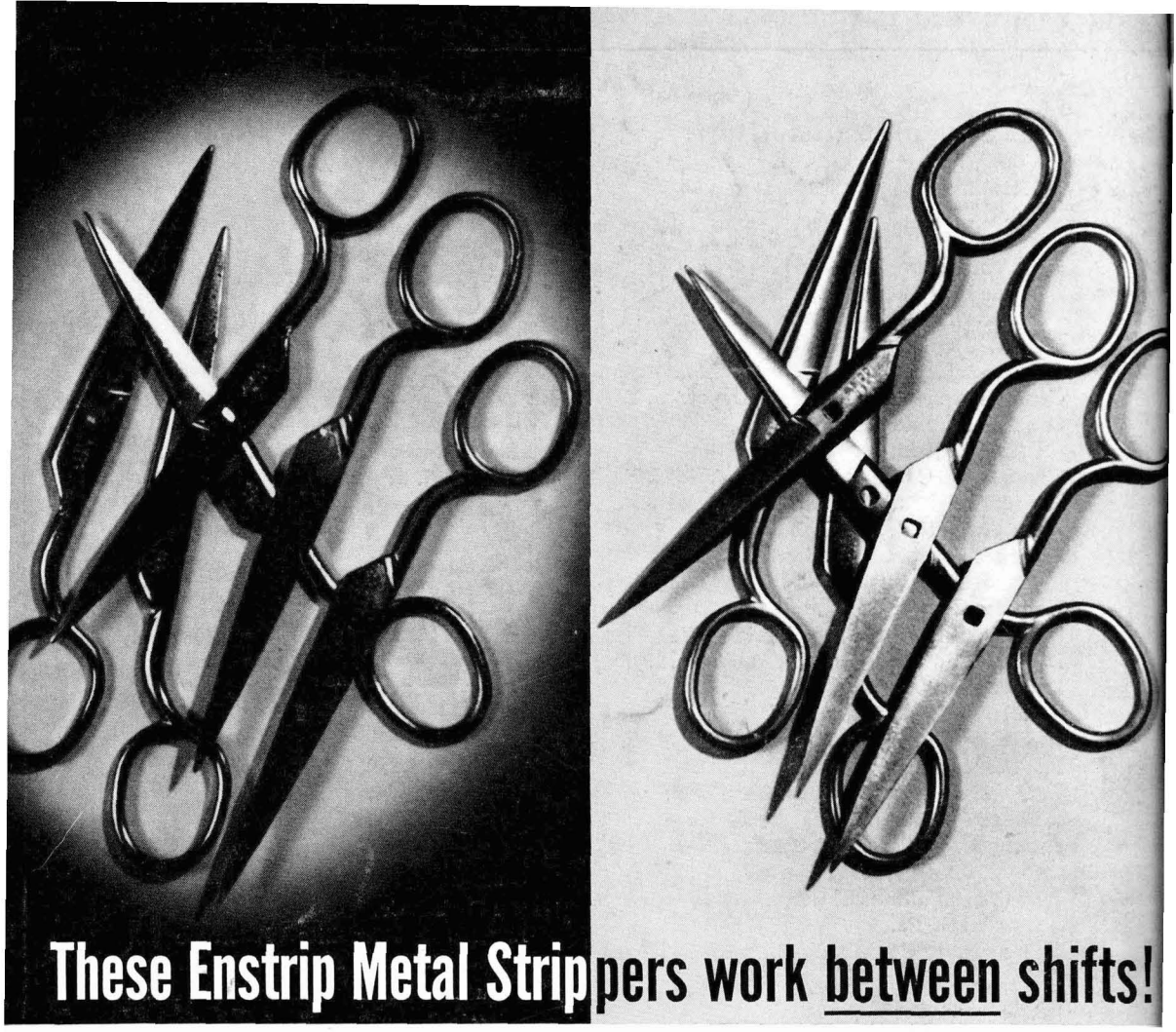

These Enstrip Metal Strippers work between shifts!

Nickel plated scissors on left were immersed overnight in an Enstrip A solution and left without supervision. Next morning (see right) they were down to bare steel ready for replating.

How would you like to dump your rejected plated parts into a stripping solution and "forget" them? Next morning, there they are, completely stripped and ready for replating! That's what Enstrip S and Enstrip A can do for you. These patented products of Enthonics research are alkaline solutions that dissolve nickel, copper, brass, silver, zinc and cadmium plate without attacking steel basis metals. Even when parts remain in the bath for hours after completion of stripping, the base metal remains as bright and shiny as it was prior to original plating.

Enstrip S and Enstrip A solutions operate at room temperature. No temperature, voltage or current to control. No electrical contacts to keep tight. Never any need to "rescue" the work upon completion of stripping. If you want rapid stripping, Enstrip S and Enstrip A solutions, operated at elevated temperatures, will dissolve .0015" of nickel or .0030" of copper per hour!

Write for the handy Enstrip Selection Chart which gives complete information about these new Enstrips, along with Enstrip 165 S (to dissolve nickel from copper and brass); Enstrip T-L (to dissolve soft solder, tin, and lead from steel and copper base alloys); Enstrip L-88 (to anodically remove copper, nickel, and chromium from zinc base die castings in a single operation), and many others. Ethone Incorporated, 442 Elm Street, New Haven, Connecticut.

ASARCO

ANOTHER PRODUCT OF Enthonics RESEARCH

ENTHONE

A Subsidiary of American Smelting and Refining Company